1-1-2007

The effects of corrosion on the performance of reinforced concrete beams

Roger W. Smith
Ryerson University

THE EFFECTS OF CORROSION
ON THE PERFORMANCE OF
REINFORCED CONCRETE BEAMS

By: Roger W. Smith

Bachelor of Engineering in Civil Engineering Ryerson
University, Toronto, Canada, 2004

A thesis presented to Ryerson University
in partial fulfillment of the requirements
for the degree of Master of Applied Science
in the program of Civil Engineering

Toronto, Canada, 2007

© Roger Smith, 2007

AUTHOR'S DECLARATION

I herby declare that I am the sole author of this thesis.

I authorize Ryerson University to lend this thesis to other institutions or individuals for the purpose of scholarly research.

Roger W. Smith

I further authorize Ryerson University to reproduce this thesis by photocopying or by other means, in total or in part, at the request of other institutions or individuals for the purpose of scholarly research.

Roger W. Smith

BORROWERS' PAGE

Ryerson University requires the signatures of all persons using or photocopying this thesis.
Please sign below and provide address and date.

Name	Address	Signature	Date

ABSTRACT

Thesis Title:	The Effects of Corrosion on the Performance of Reinforced Concrete Beams
Degree:	Master of Applied Science
Year of Convocation:	2007
Name:	Roger W. Smith
Program:	Civil Engineering
University:	Ryerson University

This report presents the results of a laboratory investigation into the effects of corrosion on the structural behaviour of reinforced concrete (RC) beams. Twelve RC beams (156 × 176 × 1150 mm) were constructed, ten of which were corroded to various levels by impressed current while the remaining two were set aside as the control beams. Each beam was tested using non-destructive methods and then by four-point loading and the corresponding loads and deflections were recorded. Following the mechanical testing, the tensile steel was retrieved and cleaned in order to assess the mass loss. The results of this experiment clearly indicated a dramatic shift in the nature of the failure of corroded RC beams. Specifically, it was observed in the present study that as corrosion increased the failure mode of the beams shifted from predictable ductile flexure failures at mid-span, to more brittle failures near the support. Based on the data collected, several new corrosion-dependant empirical relationships were established to model the altered responses of RC beams (i.e. stiffness, deflection ratio, ductility, and toughness). In addition to beam tests, a pullout study was conducted in an effort to identify the relationship between the reduction of load-carrying capacity and the residual bond strength of the tensile steel. Other behavioural changes examined are initial cracking load, flexural crack development and the evolution of the failure mode. It was found that the overall

behaviour of the beam specimens tested conforms to that reported in the literature, with reductions in the ultimate capacity, deflection capacity and stiffness upon increasing corrosion. Also, the results of this experiment clearly indicated a dramatic shift in the nature of the failure of corroded RC beams. Specifically, it was observed that as corrosion increased, the failure mode of the beams shifted from predictable ductile flexure failures at mid-span, to more brittle failures near the support.

TABLE OF CONTENTS

LIST OF TABLES

TABLE OF FIGURES

LIST OF SYMBOLS

a	=	depth of equivalent rectangular stress block, mm.
A	=	atomic weight, g.
A_s	=	the area of the tensile steel reinforcement, mm^2.
b_c'	=	the concrete cover to reinforcing steel, mm.
B	=	relative capacity of a beam, %.
c	=	depth of neutral axis measured from top face of beam, mm.
cor	=	corroded stage
C_L	=	corrosion level used by Fang et al., %.
C_n	=	relative number of flexural cracks, %.
C_r	=	resultant of compression force, N or kN.
C_{sp}	=	relative spacing of flexural cracks, %.
$C_\%$	=	percent corrosion calculated by Equation 4-4, %.
b	=	width of concrete section, mm.
d	=	depth of tensile steel reinforcement measured top face of beam, mm.
d_{corr}	=	diameter after corrosion, mm.
d_b	=	the diameter of the bar, mm.
d_i	=	diameter prior to corrosion, mm.
d_x	=	nominal diameter of a corroded bar $= d - 2x$, mm.
Δd	=	change in diameter, mm.
D	=	diameter of specimen, mm.
Dc	=	relative beam ductility, %.
Dr	=	deflection ratio, %.
E_D	=	dynamic modulus of elasticity (kN/mm2)
f_c'	=	specified compressive strength of concrete, MPa.
f_s	=	stress in tension reinforcement, MPa.
f_t	=	splitting tensile strength, MPa.
F	=	Faraday's constant, 96500 C/mol.
G	=	weight of bar after the removal of corrosion products, N.
g_0	=	weigh per unit length of the bar, N/mm.
G_0	=	initial weight of the un-corroded bar, N.
i_{corr}	=	corrosion current density, $\mu A/cm^2$.
jd	=	lever arm = distance between the resultant compressive force and the resultant tensile force at a section, mm.
k	=	relative beam stiffness (i.e. slope of load-deflection curve), %.
l	=	the bond length, mm
L	=	is the length of the specimen, mm
m	=	mass, g.

m_{corr}	=	mass after corrosion, g.
m_i	=	mass prior to corrosion, g.
$m_{\%}$	=	mass reduction, %.
M_f	=	factored moment resistance, N·mm or kN·m.
M_r	=	moment due to the factored loads, N·mm or kN·m.
ML	=	percent mass loss, %.
n	=	valence of the reaction.
P	=	value of applied load, N or kN.
P_{avg}	=	average half-cell potential, mV.
r^2	=	coefficient of determination
R		rate of corrosion, mm/year; reduction factor to account for corrosion.
R_c	=	concrete cover measured from the centre of the bar to the closest surface, mm.
t	=	time after corrosion initiation, years.
Δt	=	time for compression wave to pass through concrete, sec.
T	=	relative beam toughness (i.e. area under the load-deflection curve), %.
T_r	=	resultant factored tensile force, N or kN.
V	=	Velocity of compression wave, km/s.
V_i	=	volume prior to corrosion, mm^3.
V_{corr}	=	volume after corrosion, mm^3.
w_{corr}	=	largest corrosion crack width, mm.
y	=	perpendicular distance from neutral axis of section, mm.
α_1	=	ratio of average stress in rectangular compression stress block to specified strength of concrete.
β_1	=	ratio of depth of rectangular compression stress block to distance from extreme compression fibre to neutral axis.
ε	=	normal strain, mm/mm.
ϕ	=	curvature of beam = the angle change over a defined length.
ϕ_c	=	resistance factor for concrete.
ϕ_s	=	resistance factor for reinforcing steel.
$\varnothing$	=	diameter of reinforcing bar, mm.
τ	=	the bond strength, MPa.
τ_{avg}	=	average bond stress, MPa.
τ_{max}	=	maximum bond strength, MPa.
τ_{rel}	=	relative bond stress, %.
τ_{res}	=	residual bond stress, MPa.
ρ	=	density (kg/m^3).
υ	=	dynamic Poisson's ratio.

ACKNOWLEDGEMENTS

Chapter 1

INTRODUCTION

1.1 The Problem of Corrosion

Reinforced concrete (RC) is a widely used construction material in the world today and is generally very durable, yet there have been many occurrences of failures of such structures due to the corrosion of its reinforcement, as shown in Figure 1-1. One American study estimated that in 2001, there were approximately 235,000 RC bridges in that country, and over 21,000 of those were rated as structurally deficient and the leading cause of deterioration for many of these deficient bridges is attributed to chloride-induced corrosion (Koch et al., 2001).
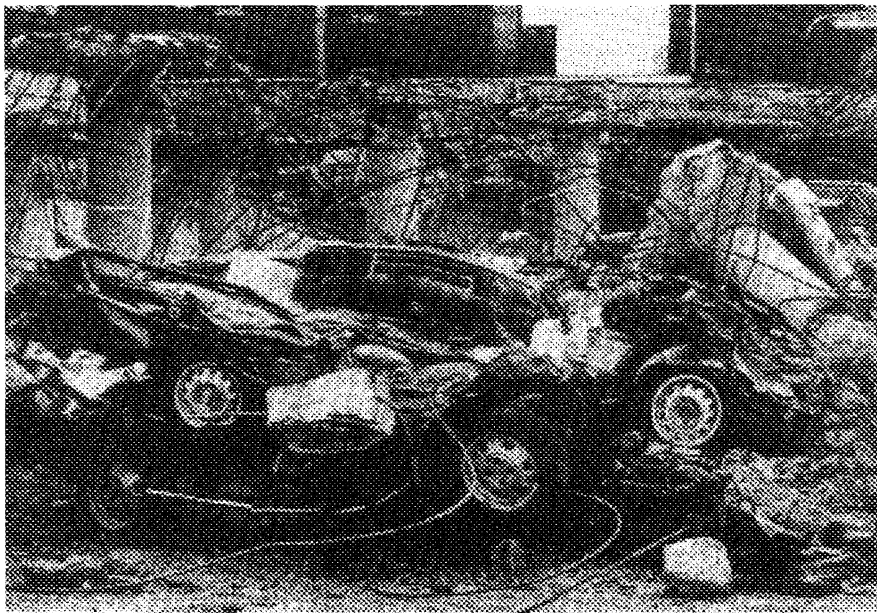
Figure 1-1: Parking garage failure due to corrosion (Feld and Carper, 1997).

The depassivation of the reinforcing steel can be attributed to either the ingress of chlorides or carbonation and leads to rapid corrosion. The corrosion of steel in concrete is one of the leading causes of deterioration of RC. The corrosion of steel results in the reduction of the cross-sectional area of the rebar, which in turn reduces the steels ductility and strength. The products of corrosion occupy roughly 3 to 6 times the original volume of steel, which exert tensile forces within the concrete causing the concrete to crack and spall, resulting in a reduction of the steel-concrete bond.

Corrosion in RC structures poses a real problem with serious consequences. These include the degradation of the aesthetics and/or serviceability of a structure and the structural performance and its safety, all of which involve costly repairs.

Corrosion is possibly the most pressing durability query of RC. Currently, there is no suitable method by which to predict the behaviour and more importantly, the load-carrying capacity for beams deteriorated by corrosion of the reinforcing steel. Furthermore, partial steel-to-concrete bond loss due to corrosion is not accounted for in conventional codes of practice. A better understanding of the effects of corrosion on RC would no doubt aid in the development of new models to predict the residual strength of RC beams.

1.2 Objective and Scope

The objective of this project is to study how progressive corrosion affects reinforced concrete beams. Specifically, the aim is to investigate both qualitatively and quantitatively the changes in flexural crack development, mode of failure, stiffness, ductility, toughness, and load-carrying capacity of RC beams. The intention is to add to the body of knowledge and broaden the understanding concerning the global behaviour of corroded RC beams in order

2

to facilitate the development of a numerical model to predict the behaviour of RC beams with corroded reinforcement that considers the effect of a partial loss of bond, which will be the focus of future work.

To this end, existing research on the subject of bond strength of corroded reinforcement is reviewed with the goal of establishing a numerical relationship between bond strength and load-carrying capacity. Experimental studies have indicated that bond properties should be studied and modeled, as bond directly affects ductility, which is associated with the mode of failure and ultimate capacity (Coronelli and Gambarova, 2004).

1.3 Thesis Layout

This thesis contains eight chapters, starting with a brief introduction and an examination of the literature. The experimental program is then outlined along with a description of the methods of testing. The results of each test program are then presented separately followed by a discussion and analysis section where comparisons and correlations are established. The report is then summarized and concluded.

The following is a more detailed overview of each chapter.

First, chapter 1 sets the stage with an introduction to the problem of corrosion, which illustrates the need for continued research into its effects. The introduction also specifies the objectives and scope of the project.

Chapter 2 is dedicated to presenting some essential background information that includes the fundamentals of corrosion, flexure theory, and bond strength.

The literature review is presented in chapters 3 and 4. Chapter 3 highlights some of the works concerning the effects of corrosion on RC beams. Chapter 4 examines studies of the way in which corrosion affects bond strength and presents some numerical models for the calculation of residual bond strength.

Following this, chapter 5 introduces the experimental program to the reader and provides details concerning specimen identification; materials used; the procedures for constructing, curing, and accelerating corrosion; and the test methods used to study various phenomena.

Chapter 6 presents the findings and observations from the various tests performed throughout the experiment. The results for each test are reported separately in this chapter followed by an analysis of the data in chapter 7, where the findings are observed and studied as a whole, making comparisons and correlations.

Chapter 8 ends the thesis with a summary and conclusions. Included in this chapter is a discussion regarding recommendations for future research in an attempt to answer the question of where we go from here.

Chapter 2

CORROSION BASICS

2.1 Introduction

Corrosion is one of the most, if not the most, pressing durability queries of RC. The following sections report on the fundamentals of some aspects of corrosion, including the conditions that lead to corrosion and factors that influence the rate of corrosion, with the focus on corrosion initiated by chloride ions, as this was the mechanism used to initiate corrosion for the experimental work.

2.2 Conditions for Corrosion

Corrosion of steel in concrete occurs only when both anodic and cathodic reactions are possible. An anodic reaction requires the depassivation of the steel bar, while oxygen must be available at the surface of the steel bar for a cathodic reaction. For these reactions to be possible, there must be conditions that allow a flux of ions and electrons between the anode and cathode. Ions are transported through the environment or electrolyte, while electrons migrate via a metallic connection (Hunkeler, 2005).

2.3 Electrochemical Process

Corrosion is an electrochemical reaction wherein electrons flow from the anodic to the cathodic sites in the presence of both water and oxygen. Equation 2-1 and Equation 2-2

represent the anodic and cathodic reactions respectively and these reactions are illustrated in Figure 2-1. The Addition of Equation 2-1 to Equation 2-2 results in Equation 2-3. The product of Equation 2-3 is ferrous hydroxide, which forms on the surface of the iron. At the outer surface of this oxide layer, oxygen reacts with the ferrous hydroxide to form hydrous ferric oxide or ferric hydroxide, as represented by Equation 2-4. Ferric hydroxide then becomes hydrated ferric oxide as represented by Equation 2-5. These reactions are illustrated in Figure 2-2. The majority of ordinary rust consists of hydrous ferric oxide and is orange to red-brown in colour (Roberge, 2000).
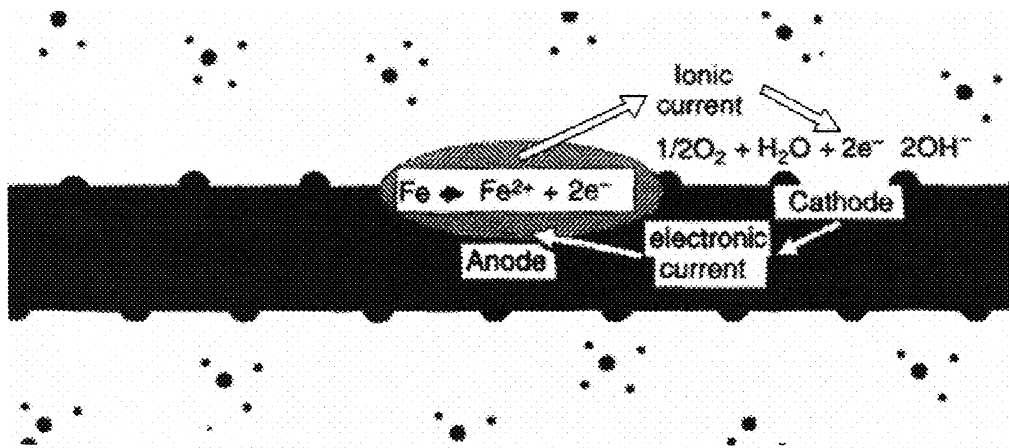
Figure 2-1: The anodic and cathodic reactions (Broomfield, 1997).

Equation 2-1 $\qquad Fe \rightarrow Fe^{2+} + 2e^{-}$ $\qquad$ (Anode)

Equation 2-2 $\qquad \frac{1}{2}O_2 + H_2O + 2e^{-} \rightarrow 2(OH)^{-}$ $\qquad$ (Cathode)

Equation 2-3 $\qquad Fe^{2+} + 2OH \rightarrow Fe(OH)_2$ $\qquad$ (Ferrous hydroxide)

Equation 2-4 $\qquad Fe(OH)_2 + O_2 + H_2O \rightarrow 4Fe(OH)_3$ $\qquad$ (Ferric hydroxide)

Equation 2-5 $\qquad 2Fe(OH)_3 \rightarrow Fe_2O_3 \cdot H_2O + 2H_2O$ $\qquad$ (Hydrated ferric oxide)

6
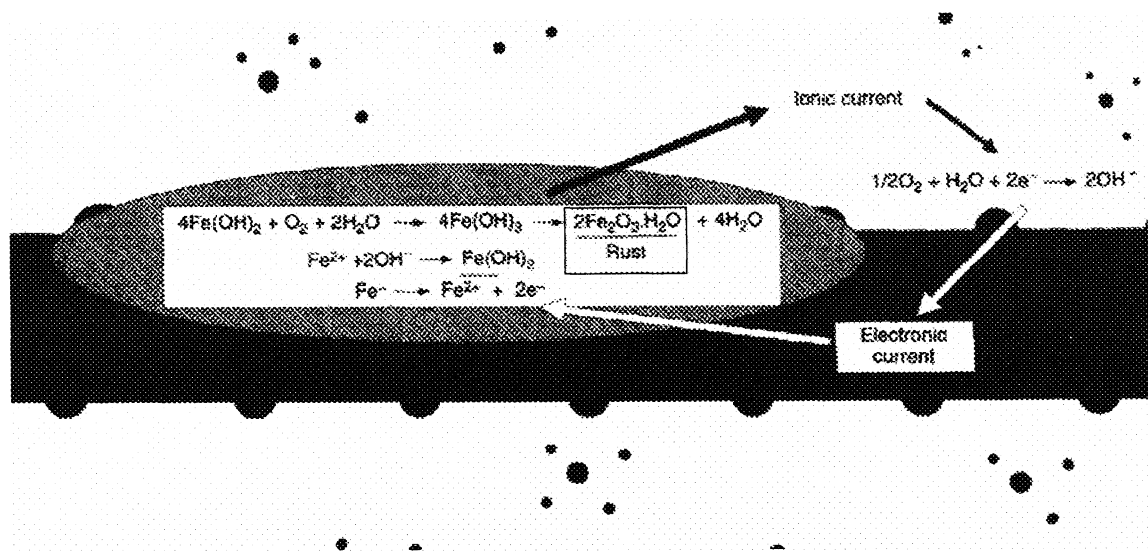
Figure 2-2: Anodic and Cathodic reactions on steel (Broomfield, 1997).

2.4 Concrete's Defence against Corrosion

Reinforced concrete can be a very durable building material with many inherent qualities to protect the reinforcing steel from the initiation of corrosion. These qualities include its resistive nature, a microstructure that serves as a physical barrier against transport processes, and a high alkaline pore solution.

2.4.1 Resistivity of Concrete

The resistivity of concrete is an important factor in the corrosion process and is determined by the moisture content and pore structure of the concrete and the composition of the water in its pores. The conduction inside concrete occurs mainly through the movement of ions in the pore solution. These ions include, $Na+$, $K+$, $OH-$, $SO42-$, and $Ca++$ (Gu et al., 2001).

The value of the electrical resistivity of the pore solution in cement paste typically ranges from 25 to 35 Ωcm. On the other hand, the resistivity of standard aggregates used in concrete ranges from 105 to 1014 Ωcm, making them good insulators.

Moisture content greatly affects the electrical resistivity of concrete such that the resistivity of air-dried concrete and moist concrete ranges from 0.6 to 1.2 MΩcm and from 2.5 to 4.5 kΩcm respectively (Gu et al., 2001).
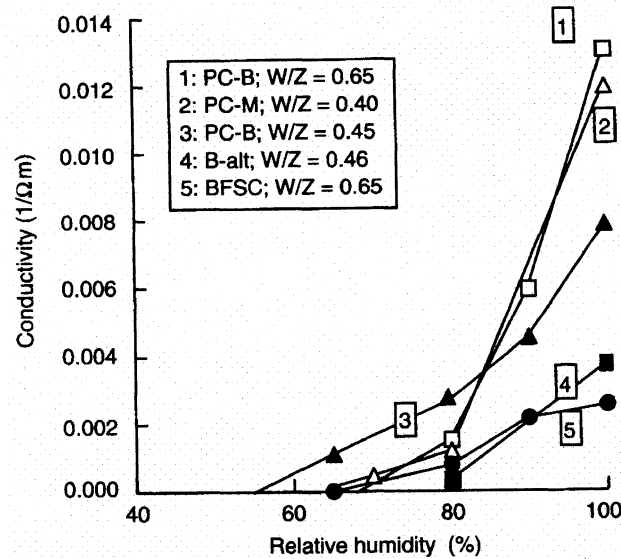
Figure 2-3: Conductivity as a function of relative humidity (Hunkeler, 2005).

Resistivity can be understood by studying its reciprocal, which is the conductivity of concrete. Figure 2-3 plots the relationship between conductivity and relative humidity, showing that the conductivity is zero when the relative humidity is between 40 and 80% (Hunkeler, 2005).

2.4.2 Transport Processes in Concrete

The corrosion process not only requires the movement of electrons, but also the transport of gases (O_2, CO_2), ions (CL-), and water. Good quality concrete will physically impede the movement of these substances and protect the reinforcing steel against corrosion. The transport of the gases, ions and water depends on the transport mechanism, the concrete properties, the binding between the substance being transported and the hydrated cement

paste, and the microclimate at the surface of the concrete. This is summarized in Figure 2-4 (Bertolini et al., 2004).
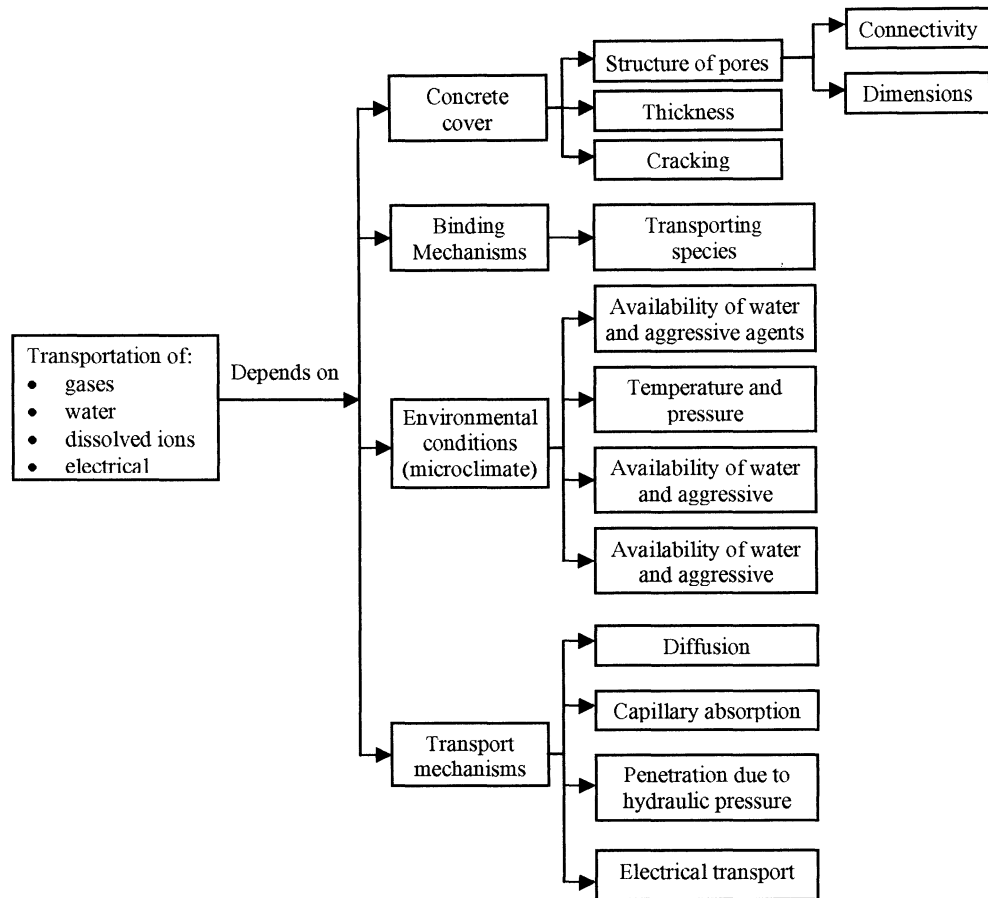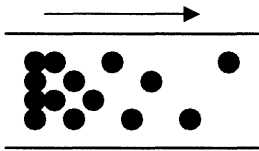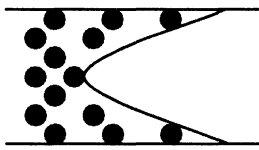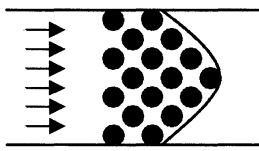
Figure 2-4: Primary factors involved in the transport process in concrete (Bertolini et al., 2004).

The motivation of these substances is caused by *permeation* (gradients of pressure), *diffusion* (gradients of concentrations), *capillary forces* (inside the cement paste), and *migration* (resulting from electrical potential gradients). This is outlined in Table 2-1 (Bertolini et al., 2004).

Table 2-1: Transport processes in concrete (Hunkeler, 2005).

Type	Driving Force	Pores
Diffusion (gases and ions)	Concentration gradient dc Partial pressure difference dp	Filled with air or water
Capillary suction (liquids)	Surface tension s Contact angle q	Filled with air
Permeation (gases and liquids)	Absolute pressure difference dp	Filled with air or water

According to Malhotra and Carino (2004), there are five key principles that must be understood when describing the movement of aggressive substances through concrete; these principles are described below:

Adsorption – The process by which molecules are attracted to the internal surfaces of concrete. This can be from either chemical bonds or the forces of adhesion (i.e. van der Waals force).

Absorption – The process by which the concrete pores are filled with a liquid by capillary suction. The rate at which liquid is taken in is known as absorptivity or sorptivity.

Diffusion – The process by which liquids, gases, or ions are motivated through concrete by way of a molar concentration gradient. This process is described by a diffusivity value or a diffusion coefficient.

Permeability – An inherent concrete property that describes the resistance of a fluid penetration that is motivated by way of a pressure gradient. This is often confused with porosity.

Porosity – This is the proportion of the total volume that is occupied by pores, usually expressed as a percentage.

2.4.3 Passive Layer

Another important characteristic of concrete is the high alkalinity of the pore solution, which is comprised of mainly sodium and potassium hydroxides, with a pH ranging from 12.6 to 13.8. At this pH level, a protective (or passive) film is spontaneously formed during the early stages of cement hydration. This passive film may grow to a thickness of the order of 10^{-3} to 10^{-1} μm and contains hydrated iron oxides. The theory of the existence of this passive layer is based only on indirect evidence of anodic polarization measurement. There is still much to be learned concerning this passive film, such as the conditions of its formation, and its chemical and mineralogical composition. It is possible that this passivating film consists of several phases (Ramachandran, 2001).

2.5 Chloride-Induced Corrosion

The steel can be depassivated by chloride ions or the process known as carbonation[1]. The introduction of chlorides into concrete can occur by way of contamination or additives in the original mix or through environmental exposure (e.g. de-icing salt). Chlorides introduced to the original mix initiate corrosion immediately, whereas chlorides introduced from an external source accumulate over time, eventually leading to a condition where corrosion is initiated (Gu et al., 2001).

According to Hunkeler (2005), the negative effect of chlorides on RC is fourfold:

- A reduction of the solubility of $Ca(OH)_2$ resulting in a lowered pH of the pore water.

- An increase in the moisture content of the concrete due to the hydroscopic nature of salts (e.g. $NaCl$, $CaCl_2$).

- A rise in the electrical conductivity of the concrete.

- The destruction of the passive layer making corrosion possible.

2.6 Mechanisms of Chloride Attack

The way in which chloride ions depassivate reinforcing steel is currently under speculation. According to Gu et al. (2001), there are three modern theories that propose the mechanisms of the chloride attack on reinforcing steel. A short summary of each theory is provided below:

---

[1] Carbonation of concrete is caused by the chemical reaction of atmospheric carbon dioxide (CO_2) and the alkaline components of the cement paste (e.g. NaOH, KOH, $Ca(OH)_2$ and calcium-silicate hydrates) in the presence of water which tend to neutralize the alkalinity of the concrete (Hunkeler, 2005).

The Oxide Film Theory – The oxide film is thought to be responsible for the passivity of the steel. As chloride ions can penetrate the oxide film easier than other ions (such as SO_4^{2-}), they eventually form colloids and disperse the oxide film, making it more susceptible to corrosion.

The Adsorption Theory – This theory holds that chloride ions in competition with oxygen or hydroxyl ions are adsorbed to the reinforcing steel. The chloride ions promote the hydration of iron ions, facilitating corrosion.

The Transitory Complex Theory – This theory states that chloride ions become incorporated in the passive film, replacing some hydroxides. This process increases the conductivity and solubility of the passive layer, thus reducing its protective qualities.

2.7   Deterioration Process

The deterioration process of RC beams can be divided into four stages:

Stage I – Marked by the initiation of corrosion when the reinforcing steel is depassivated by either a chloride or a carbonation attack.

Stage II – Denoted by the propagation of corrosion, which leads to the cracking of the concrete and rust staining on the surface.

Stage III – Indicated by cracking and delaminating of the concrete, accelerating the rate of corrosion due to the increased accessibility of moisture and chloride ions.

Stage IV – Typified by spalling of the concrete cover, exposing the reinforcing steel to the full impact of the corrosive environment.

These four stages are illustrated in Figure 2-5 (Higgins et al., 2003).
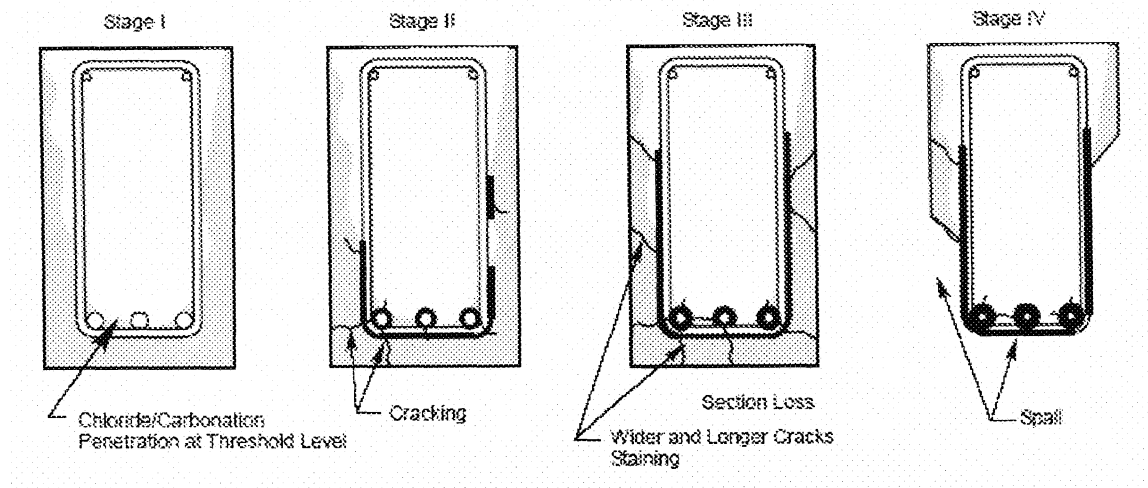
Figure 2-5: Illustration of the four stages of the deterioration of RC beams (Higgins et al., 2003).

The structural consequences of corrosion, such as a reduction in the rebar cross-sectional area and the mechanical properties of the steel, are shown in Figure 2-6. The products of corrosion cause tensile stresses in the concrete that produce cracks, spalling, and/or delamination, resulting in the deterioration of the steel-concrete bond. These effects are initiated by corrosion and their severity increases over time (Bertolini et al., 2004).
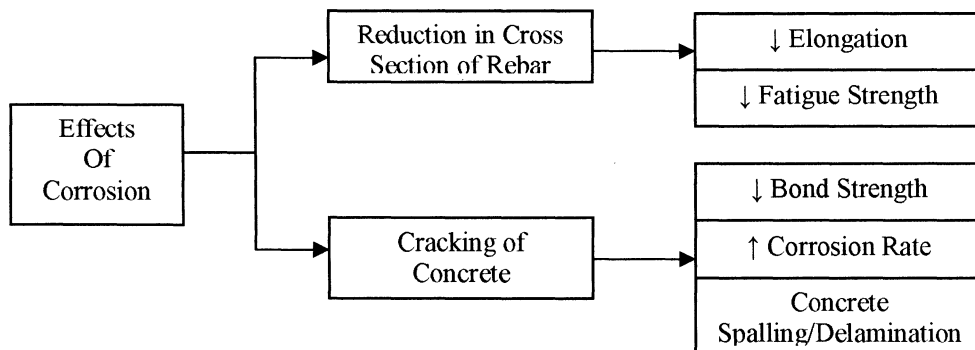
Figure 2-6: The effects of corrosion on RC structures (Bertolini et al., 2004).

14

These consequences of corrosion can ultimately lead to the failure of a structure. A disaster of this nature can be extremely costly to society due to the loss of time, revenue and property upon the removal and disposal of the debris and replacing of the structure. More importantly, there is a potential for loss of life in the event of a structural failure (MacGregor and Bartlett, 2000).

In order to avoid a catastrophic failure, engineers must be able to determine when a deteriorated structure requires repair or replacement. The strength of a RC member with corroded reinforcement cannot be determined by conventional cross-section analysis due to the loss in both the bond strength and bond rigidity, as well as the reduction of the mechanical properties of the reinforcing steel (Lee et al., 2002).

Currently, there is no suitable method to assess the reduction in the load-carrying capacity of a corroded RC beam. Therefore, a new method of evaluating the strength of RC members damaged by reinforcement corrosion is needed. This method should consider the reduction of the bond and mechanical properties of the corroded steel.

Chapter 3

THE EFFECTS OF CORROSION ON REINFORCED CONCRETE BEAMS

3.1 Introduction

It is known that the load-carrying capacity of reinforced concrete (RC) beams is reduced with increasing corrosion. Numerous published papers have focused on measuring this reduction as well as analysing changes to the structural response of RC beams. This section provides an overview of the fundamentals of conventional flexural theory and highlights a selection of research papers discussing corroded RC beams.

3.2 Flexural Theory

The basic design requirement of RC beams simply states that the factored resistance must be greater than or equal to the effect of factored loads (i.e. $M_r \geq M_f$, where M_r represents the factored moment resistance of the cross-section and M_f represents the moment due to the factored loads).

For conventional RC beam analysis and design, two requirements must be satisfied. The first is that at any given point, the stress must correspond with the strain (except in the case of short, deep beams). This is also known as stress and strain compatibility. The second requirement is that the internal forces must be in equilibrium. The stresses and forces in a rectangular beam are illustrated in Figure 3-1 (MacGregor and Bartlett, 2000).

16

a) Cross-section   b) Actual Stress Distribution   c) Equivalent Rectangular Stress Distribution

In the figure: $\phi_c \alpha_1 f_c'$, $C_r = \phi_c \alpha_1 \beta_1 f_c' b c$, $a = \beta_1 c$, $jd = d - \dfrac{a}{2}$, $\phi_s f_s$, $T_r = \phi_s A_s f_s$
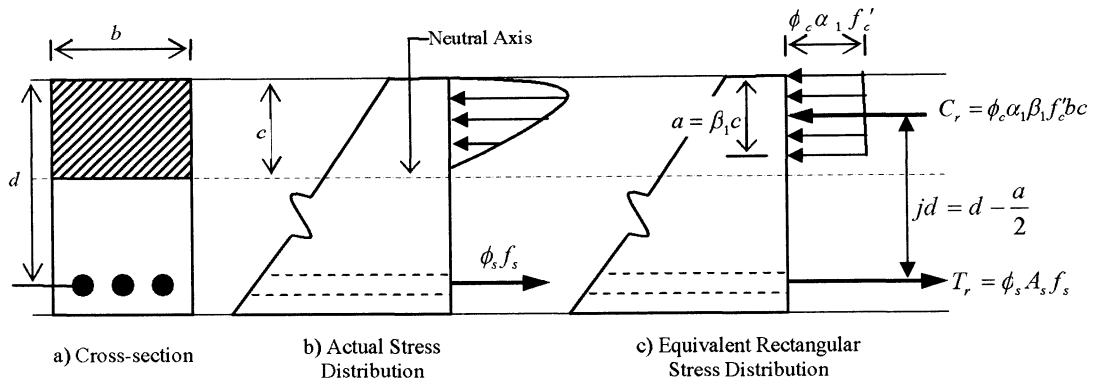
Figure 3-1: Stresses and forces in a singly RC rectangular beam[2] (MacGregor and Bartlett, 2000).

When a simply supported beam is loaded and the stresses at the bottom reach the tensile strength of the concrete, the beam cracks and its curvature increases. At this point, the tensile force is transferred to the reinforcing steel, reducing the stiffness of the beam. The curvature ϕ of the beam is the angle change over a defined length and is calculated by Equation 3-1, where ε is the strain at distance y from the neutral axis (MacGregor and Bartlett, 2000).

Equation 3-1
$$\phi = \frac{\varepsilon}{y}$$

This curvature can be plotted with its corresponding load level in what is known as a moment-curvature diagram. A simply supported RC beam is typically assumed to reach its maximum capacity when the slope of the moment-curvature diagram equals zero (MacGregor and Bartlett, 2000).

---

[2] Please Note: The symbols used in Figure 3-1 are summarized in Appendix A.

3.3 Selected Research

3.3.1 Uomoto and Misra

Uomoto and Misra (1988) investigated the influence of longitudinal cracking on beams and columns. The reinforcement was corroded by adding chlorides in the concrete mix and impressing a current ranging from 280 to 380 $\mu A/cm^2$ over a 7 to 14 day period. The beams tested had dimensions of 200 x 100 x 2100 mm and were reinforced with 2-6 mm diameter top bars and 2-16 mm diameter bottom bars.

These beams failed when the compression-concrete crushed and the top bars buckled. Uomoto and Misra found that a weight loss in the tension reinforcement ranging from 1 to 2.4% resulted in a 4 to 17% reduction in the load-carrying capacity. These researchers attributed this reduction in the capacity of the beams to a decrease in the reinforcement area and concrete cracking (Uomoto and Misra, 1988).

3.3.2 Al-Sulaimani et al.

Al-Sulaimani et al. (1990) conducted tests to determine the manner in which cracking and reinforcement corrosion affect the behaviour of the steel-concrete bond. For this purpose, tests were performed on pullout specimens and 24 beam specimens having dimensions of 150 x 150 x 1000 with a 12 mm diameter bottom-reinforcing bar.

Corrosion was induced by the application of a constant current density of 2 mA/cm^2. The behaviour of the beams was observed at four stages of corrosion: no corrosion, pre-cracking corrosion, corrosion at the appearance of the first visible cracks, and post-cracking corrosion (Al-Sulaimani et al., 1990).

Table 3-1: Test results for beams failing in flexure (series IV) (Al-Sulaimani et al., 1990).

Beam	Cross-section Loss (%)	Ultimate Load (kN)
1	0.00	47.0
2	0.00	47.2
3	0.65	47.0
4	1.50	47.3
5	2.43	46.8
6	3.50	46.1
7	4.94	46.3
8	6.30	45.6
9	7.10	44.0
10	9.35	42.1
11	8.93	42.5
12	10.36	42.2

For the beams designed to fail in flexure (series IV), adequate development length and shear stirrups were provided to prevent bond or shear failures. The results of this portion of the experimental work are shown in Table 3-1. The ultimate load at 0% corrosion was found to be 47.0 kN and 47.2 kN. Figure 3-2 summarizes the findings of Al-Sulaimani et al. and graphically illustrates how the ultimate load is affected by steel cross-section loss (Al-Sulaimani et al., 1990).

For each beam tested, the average bond stress over the embedded length was found to be well below the ultimate bond stress observed in pullout tests for bars with similar corrosion. This observation confirmed that the failure of the beams in series IV was due to the yielding of steel and was not a bond failure (Al-Sulaimani et al., 1990).

Furthermore, since the bond stress was less than the ultimate bond stress, Al-Sulaimani et al. (1990) concluded that the reduction in beam capacity was not due to a decrease in bond stress but rather, it could be attributed primarily to the reduced area of the reinforcing steel. As this conclusion was reached many years ago, it is contradicted by many researchers today (Mangat and Elgarf, 1999; Al-Negheimish and Al-Zaid, 2004; Castel et al., 2000b).
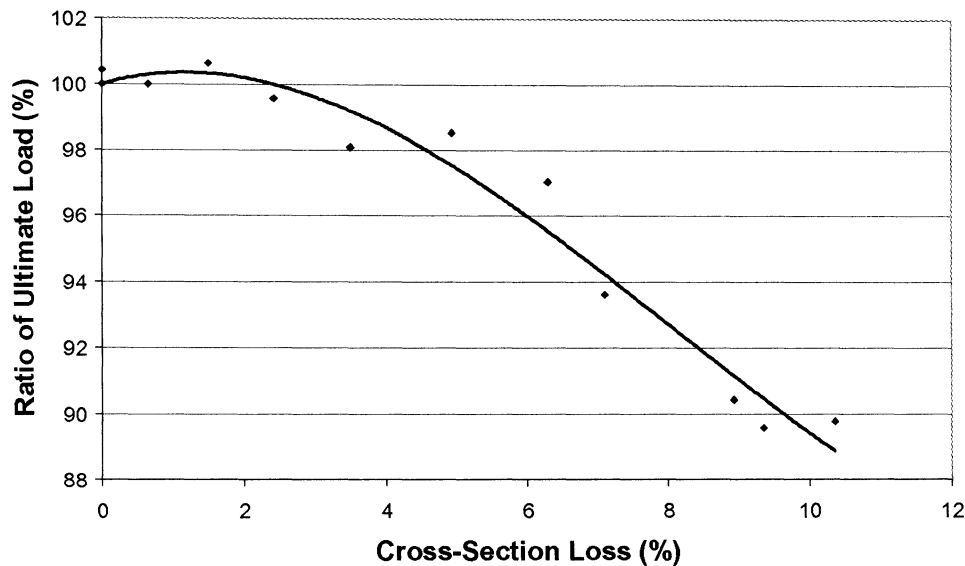
Figure 3-2: Reduction of ultimate load in terms of cross-section loss (Al-Sulaimani et al., 1990).

3.3.3 Cabrera and Ghoddoussi

Cabrera and Ghoddoussi (1992) researched the effects of corrosion on beams of 160 x 125 x 1000 mm, reinforced with 2-10 mm diameter bars at the top, 2-12 mm diameter bars at the bottom and 8 mm diameter stirrups. The main tensile reinforcing bars were corroded by applying an unknown current density. The maximum reduction in the steel cross-sectional area was 9%, which resulted in a 20% reduction in the ultimate bending moment and a 40% increase in deflection at the service load (Cabrera and Ghoddoussi, 1992).

3.3.4 Eyre and Nokhasteh

Eyre and Nokhasteh (1992) examined the behaviour of concrete beams with exposed reinforcement. In the tests performed, the concrete-steel interface was assumed to have zero bond over various lengths of the beam and the capacity of the beam was observed to reduce with smaller bond lengths. Moreover, after a critical un-bonded length, the beams failed by the concrete crushing, regardless of steel ratio.

20

This led Eyre and Nokhasteh to propose an algebraic method for predicting the ultimate strength of corroded RC beams. However, according to Maaddawy et al. (2005a), this method assumes that concrete acts as a linear-elastic material and thus does not properly reflect the stress-strain behaviour of concrete, and presumes a total loss of bond, which does not reflect actual conditions.

3.3.5 Huang and Yang

Huang and Yang (1997) carried out tests that illustrate the relationship between the corrosion of RC beams and load-carrying capacity. Beams of 150 x 150 x 500 mm, reinforced with two 6 mm bottom bars were corroded by immersing them in sea water and applying a current of 5 A/cm². The two specimen types used were beams without cracks (type S) and beams with a middle surface crack (type K), and the two concrete mix designs used were mix A and mix B, having a water to cement ratio (w/c) of 0.4 and 0.3 respectively.

Figure 3-3 and Figure 3-4 show the relationship of corrosion to stiffness and ultimate moment for concrete types A and B. The reduction in load-carrying capacity as corrosion thickness increased was more significant in beams with a low w/c or predetermined cracks (mix B or type K). Huang and Yang concluded that this behaviour was a result of the chloride ions having easier access to the reinforcing steel in cracked beams than in uncracked ones (Huang and Yang, 1997).

The fact that the beams made with a lower w/c (which makes for a higher strength concrete), displayed a less favourable response seemed to be counter-intuitive. The authors addressed this and explained the behaviour by saying that, "... lower water/cement ratio concretes have smaller pores, which show lower energy-absorbing capacity", and that after

cracking, beams made of high strength concrete may fail before ones of low strength concrete (Huang & Yang, 1997).

W/C = 0.4
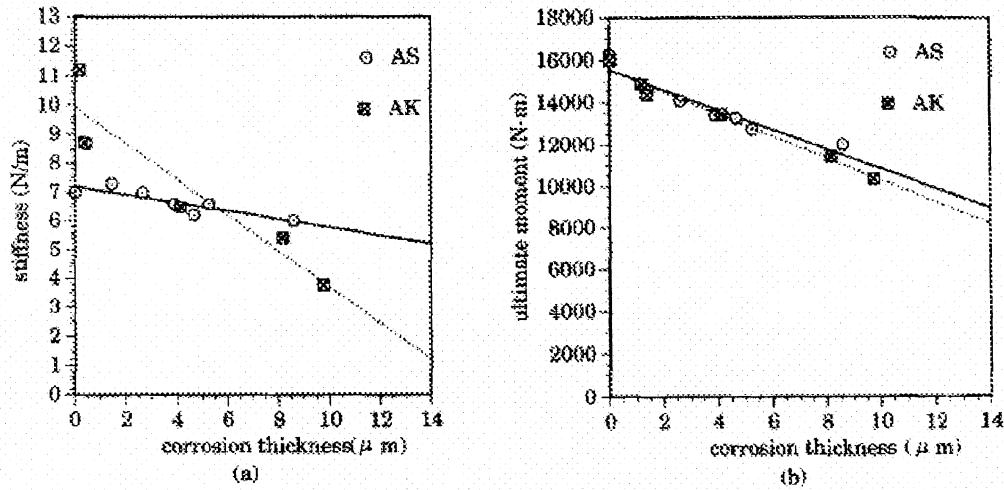
Figure 3-3: (a) Effect of corrosion on stiffness and (b) effect of corrosion on ultimate moment
(AS – beams without cracks and AK – beams with a middle surface crack)
(Huang &Yang, 1996).

W/C = 0.3
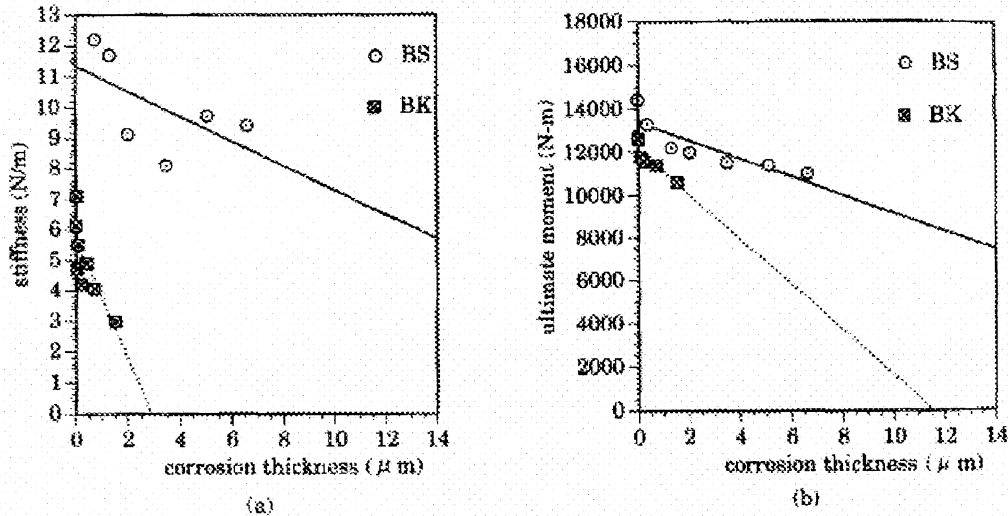
Figure 3-4: (a) Effect of corrosion on stiffness; (b) effect of corrosion on ultimate moment
(BS – beams without cracks and BK – beams with a middle surface crack)
(Huang &Yang, 1996).

In terms of pore size, a supplementary explanation is available. That is, concrete that has smaller pores cannot accommodate voluminous rust products as well as concrete with larger pores. This is because the existence of larger pores allows the oxides to migrate more easily into the matrix of the concrete, thus reducing the expansive tensile stresses. Conversely, concrete with smaller pores is more greatly influenced by rust products and experiences larger internal stresses, resulting in a more rapid deterioration of the concrete (Amleh, 2005).

3.3.6 Rodriguez et al.

Rodriguez et al. (1997) completed experimental work on 31 beams with dimensions of 200 x 150 x 2300 mm and 200 x 150 x 2050 mm. In order to study the interaction between corrosion and loading, Rodriquez et al. varied the corrosion and the detailing of the reinforcement. Corrosion was accelerated by adding 3% calcium chloride by weight to the mixing water. After 28 days of curing, a current of 100 μA/cm^2 was applied for 100 to 200 days.

The study revealed that corrosion increases deflections and crack widths at the service load, decreases strength at the ultimate load, and causes an increase in both the spacing and width of transverse cracking due to bond deterioration. It was also observed that corrosion could change the type of failure experienced by RC beams with typical reinforcement ratios. In this case, un-corroded beams failed mostly by bending and corroded beams failed mostly by shear.

Figure 3-5 depicts the types of failures that were observed by Rodriguez et al. (1997) when testing corroded beams, as detailed below:

Type 1 – occurred in both corroded and un-corroded beams with a low tensile reinforcement ratio.

Type 2 – was produced in beams with un-corroded tensile reinforcement of a high ratio and most corroded beams with a high ratio of shear reinforcement.

Type 3 – occurred in nearly all beams having a high ratio of corroded tensile bars and large stirrup spacing.

Type 4 – was found in corroded and un-corroded beams with curtailed tensile reinforcement.

1) Failure by bending (yielding of tensile reinforcement).
2) Failure by bending (crushing of concrete).
3) Failure by shear.
4) Failure by both shear and bond splitting.
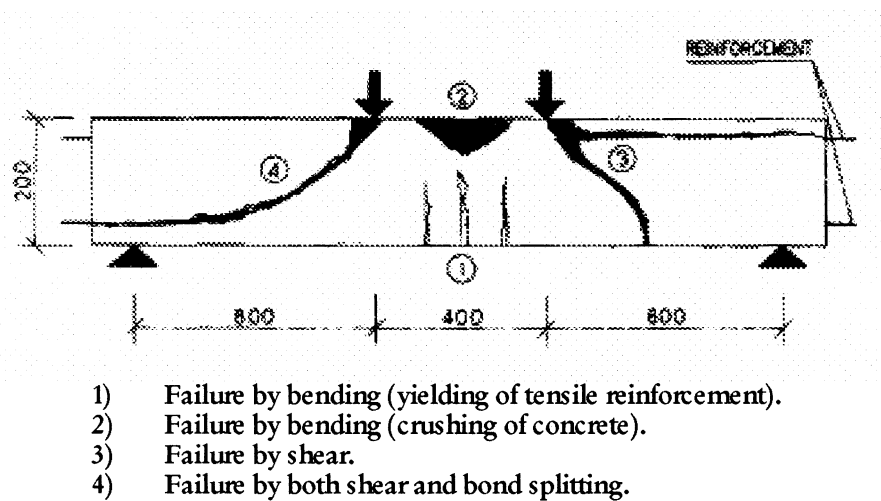
Figure 3-5: Illustration of types of failures of beams with corroded reinforcement
(Rodriguez et al., 1997).

Moreover, Rodriguez et al. (1997) concluded that by using the reduced sections of steel and concrete with conventional RC models, conservative values of the ultimate moment and shear force can be calculated for RC members damaged by corrosion. However, this method of calculating the strength of damaged members is deficient in that it fails to consider the reduction of bond.

3.3.7 Mangat and Elgarf

Mangat and Elgarf (1999a) carried out an extensive research program on 111 under-reinforced concrete beams in order to study their residual flexural capacity after being subjected to various levels of corrosion. Corrosion was induced at four different rates by applying a current of either 1, 2, 3, or 4 mA/cm². Nine groups of beams were fabricated, having dimensions of 100 x 150 x 910 (Mangat and Elgarf, 1999a).

Load-deflection relationships were then developed, showing that when the degree of corrosion is greater than 2.5%, load-deflection curves become dependant on the rate of corrosion. In light of this, the researchers suggested that when accelerated corrosion testing is necessary, the lowest practical corrosion rates should be used to induce corrosion, particularly when the desired degree of corrosion is high (Mangat and Elgarf, 1999a).

The rate of corrosion was also found to have an affect on the flexural load capacity. When corrosion is less than 3.75%, the rate of corrosion has little influence on the residual strength. Conversely, when corrosion is greater than 5%, an increase in the rate of corrosion greatly reduces the flexural strength of RC beams (Mangat and Elgarf, 1999a).

Regression analysis of the experimental data led to the proposal of a numerical relationship between residual flexural strength and the level of corrosion, as seen in Equation 3-2, where B is the percent flexural load capacity, R is the rate of corrosion in mm/year, and t is the elapsed time in years after corrosion initiation. The expression $2Rt/d_b$ in Equation 3-2 is the formula for the degree of corrosion as a percentage reduction in bar diameter. This equation is plotted in Figure 3-6 (Mangat and Elgarf, 1999a).

Equation 3-2

$$B = \left[1 - \sin^2\left(7\frac{2Rt}{d_b}\right)\right]100\%$$

Mangat and Elgarf (1999a) were able to write Equation 3-2 in terms of corrosion current density i_{corr}, deriving Equation 3-3. The researchers claim that this equation can be used to create nomograms for determining the residual strength of beams with corroded reinforcement (Mangat and Elgarf, 1999).
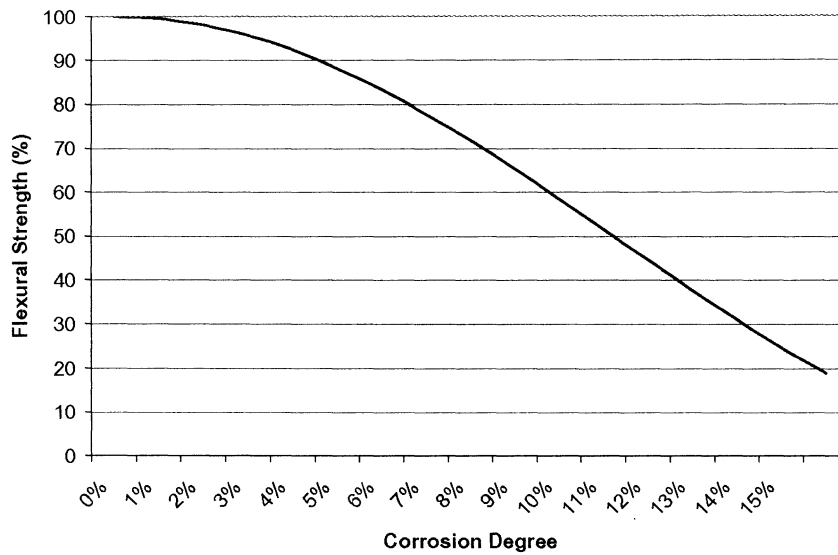
Figure 3-6: Relationship between degree of corrosion and flexural strength (Equation 3-2).

Equation 3-3

$$B = \left[1 - \sin^2\left(2.312\frac{t}{d}i_{corr}\ln(i_{corr})\right)\right]\cdot100\%$$

Figure 3-7 plots Equation 3-3 for 20 mm bars and rates of 60, 70, 90, and 100 $\mu A/cm^2$. An error seems to occur when i_{corr} equals 100 $\mu A/cm^2$ where the predicted flexural strength increases to correspond with 70 $\mu A/cm^2$. Another problem with this equation arises when i_{corr} equals 1 $\mu A/cm^2$. In this instance, the result will always be equal to 100% since $\ln(1) = 0$.

The effect of the curing time prior to the initiation of corrosion was also investigated in this study. A number of beams were cured for periods of 16 days, 28 days, 6 months, and 1 year and then corroded to 5% corrosion (at 3 mA/cm²). The residual strengths for all of these beams were close to 70% of the control beams. This finding allowed Mangat and Elgarf (1999a) to conclude that the curing period before corrosion (up to 1 year) has no bearing on flexural strength (Mangat and Elgarf, 1999a).
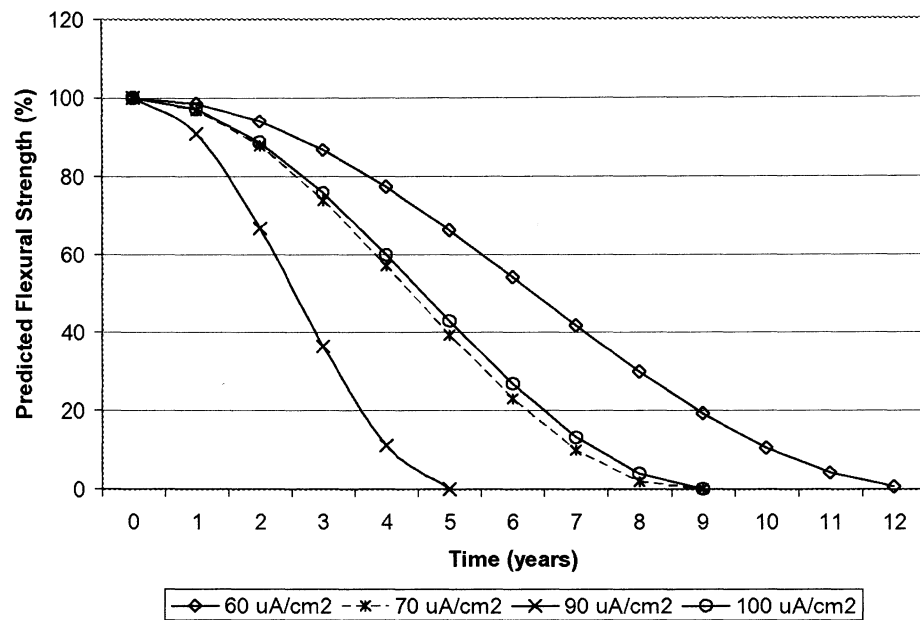
Figure 3-7: Plot of Equation 3-3, where $d = 20$; and $i_{corr} = 60, 70, 90,$ and 100 $\mu A/cm^2$

It was also determined that corrosion has a significant effect on the deflection and capacity of RC beams and the reduction in steel cross-sectional area due to corrosion has an insignificant effect on the residual flexural strength of beams. This reduction of the flexural capacity is attributed to the reduced steel-concrete bond (Mangat and Elgarf, 1999a), which is in direct opposition to the position taken by Al-Sulaimani et al. (1990).

3.3.8 Castel et al.

Castel et al. (2000a & 2000b) conducted long-term experimental research to investigate the mechanical behaviour of RC beams with corroded reinforcement and published their findings in two separate parts.

In the first part, four beams with dimensions of 150 x 280 x 3000 mm were studied. These beams were naturally corroded in a salt fog environment for 14 years in an attempt to emulate actual field conditions. They were then subjected to three-point loading to determine their ultimate strength. The average reported degree of corrosion was 10% and the reduction in flexural strength was 20% with a 70% reduction in ductility (Castel et al., 2000a).

Several assumptions were formulated, including the idea that concrete cracks resulting from compression reinforcement corrosion have an insignificant effect on the global behaviour of RC beams. The authors did acknowledge, however, that other researchers have established that this type of cracking can reduce the flexural capacity by causing compressive concrete splitting (Castel et al., 2000a).

The researchers also proposed that the decrease in stiffness was due to the reduction of both the steel cross-sectional area and bond strength. This was attributed to the fact that the average maximum cross-section loss near the centre of the beam was 20%, which would theoretically result in a stiffness decrease of 15%. However, the total stiffness loss for one of the beams tested was 35%. Thus, there was a 20% difference in loss that was unaccounted for, which the researchers suspected to be the result of bond deterioration (Castel et al., 2000a).

Additionally, the reduction of ultimate strength was found to correspond to the average maximum steel cross-section loss (20%). Therefore, Castel et al. (2000a) concluded that the reduction in steel-concrete bond had an insignificant effect on the ultimate behaviour and thus the residual capacity can be determined by considering the reduction of steel alone.

The purpose of the second part of this study was to further explore the separate and coupled affects of bond stress and a decrease in steel cross-sectional area. Beams with similar dimensions to those in the first part of the study were used to facilitate this second part. Bond loss was simulated by notching the concrete and exposing the reinforcing bar, while a corrosion-pitting attack was simulated by using a grindstone to create local indentations on the steel surface (Castel et al., 2000b).

Upon analyzing the data, the researchers hypothesized that pitting corrosion located between flexural cracks has little influence on the global behaviour of RC beams when bond strength is not modified. Conversely, when both bond strength and steel cross-section were reduced in their study, the global behaviour of RC beams was greatly altered. This was attributed to the increase in steel stress at the crack location, due to the reduction of both steel cross-sectional area and tensile concrete contribution (Castel et al., 2000b).

In sum, these researchers concluded that the corrosion of RC beams is always a, "... coupling phenomenon between steel cross-section reduction... and loss of bond strength." For this reason, both effects must be considered when attempting to predict the residual strength or non-fragile behaviour (Castel et al., 2000b).

3.3.9 Wang et al.

Wang et al. (2000) tested beams having dimensions of 100 x 150 x 1170 mm, reinforced with one 19 mm diameter bottom bar. The reinforcement was corroded by exposing the beams to a NaCl solution and impressing current. The beams were simultaneously corroded and loaded, using either sustained or previous (cyclic) loading. Details concerning specimen names and their loading type are summarized in Table 3-2.

Table 3-2: Specifications of beams tested by Wang et al. (2000).

Specimens	Flexural Loading (% of Ultimate Load*)	Ponding (Stage I)	External Current (Stage II)
AP00	0 % load	No	No
NP45	45% previous load	3% NaCl	~ 50 days after ponding
NP75	75% previous load	3% NaCl	~ 50 days after ponding
NS45	45% sustained load	3% NaCl	~ 50 days after ponding
NS75	75% sustained load	3% NaCl	~ 50 days after ponding

* The ultimate flexural load = 41 kN.

The researchers found that at higher loading levels, the corrosion initiation time was reduced while corrosion propagation was more severe. In addition, sustained loading had a more significant effect on the rate of corrosion than did cyclic loading and the rate of corrosion was increased with higher load levels for both types of loading (Wang et al., 2000).

These findings can be explained in terms of the access chloride ions had to the reinforcing steel. At higher loading levels, crack widths are wider and thus allow for an easier ingress of chloride ions. Additionally, these cracks are continuously open and widening with sustained loading, facilitating the migration of the chloride ions. In contrast, cyclic loading causes these cracks to constantly open and close giving chlorides intermittent access, which results in a relatively slower rate of corrosion (Amleh, 2005).

Figure 3-8 graphs the residual flexural capacities of the beams tested. Wang et al. (2000) reported that the residual strength of the beams subjected to sustained loading was lower than that of the beams subjected to cyclic loading, and the remaining capacity of the beams subjected to 75% of the ultimate load was lower than that of the beams exposed to 45%. The researchers also observed that as the rate of corrosion increased, the mode of failure shifted from shear to bond splitting.
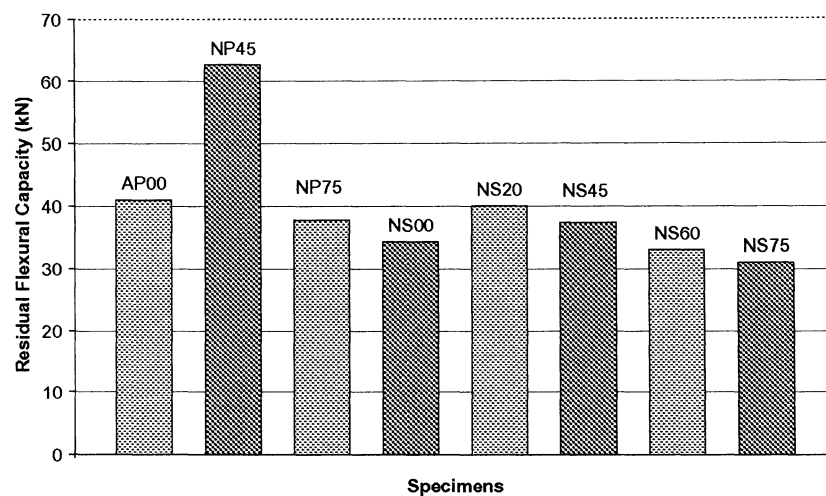
Figure 3-8: Remaining flexural capacities of beams (Yoon et al., 2000)[3].

It is worth pointing out that the residual strength of the corroded beam NP45 was found to be significantly stronger than the undamaged beam AP00, which may indicate a possible error in this experiment (Amleh, 2005). Although the researchers did not provide an explanation for this, they did mention that a second AP00 specimen that was tested with the use of external stirrups achieved an increased ultimate load of 70 kN. However, according to Amleh (2005), 70 kN cannot be used to reference the other test specimens unless the experiment is repeated with the same external reinforcement applied to all the beams.

---

[3] The research by Wang et al. was also published under Yoon et al.

31

3.3.10 Ballim and Reid

Ballim and Reid (2003) tested beams having dimensions of 160 x 100 x 1500 mm, reinforced with a single 16 mm diameter bottom bar and a pair of 8 mm diameter top bars. Corrosion was initiated through carbonation and was accomplished by placing the beams in a CO_2 filled pressure chamber (that was kept at 80 kPa) and supplying a current of 400 $\mu A/cm^2$. The beams were simultaneously corroded and loaded to either 23% or 34% of the ultimate load (P_u).
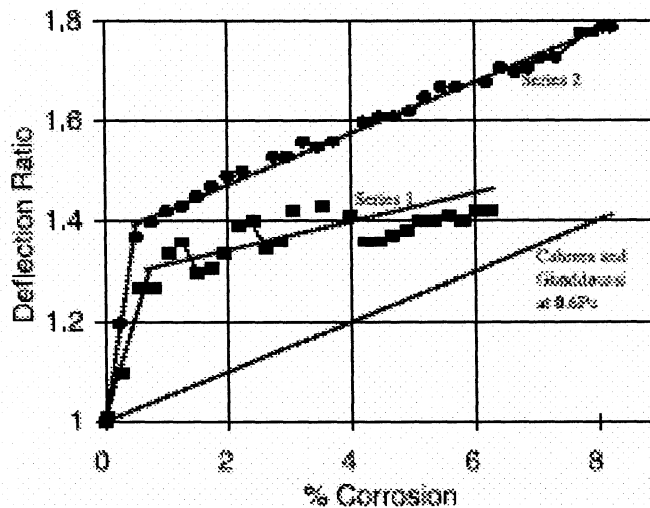
Figure 3-9: Effect of corrosion on the deflection ratio of RC beams. Series I - loaded to 0.23Pu. Series II - loaded to 0.34Pu (Ballim & Reid, 2003).

Figure 3-9 summarizes the deflection ratios that were observed by Ballim and Reid (2003), which were calculated by dividing the average deflections of the corroded beams with those of the control beams. This graph indicates that the deflection increased as corrosion propagated, particularly at the early stages. The researchers attributed this initial increase in deflection to early crack formation, as the crack creation and widening progressed at a slower rate after a certain point (Ballim and Reid, 2003).

3.3.11 Maaddawy et al.

Maaddawy et al. (2005a) published a report on determining the flexural behaviour of corroded RC beams, the main objective of which was to model the deflection of RC beams. In this study, deflection was not determined from the curvatures of beam sections, but rather from the elongation of the steel reinforcement between flexural cracks. Their research led Maaddawy et al. to propose a model that accounts for reductions in both bond strength and steel cross-sectional area.

This model assumes beams to be comprised of a series of elements with a length equal to the mean crack spacing, which are subjected to a constant pure bending moment and have a single crack (initiated when the applied moment exceeds the cracking moment) located at the middle. The stress and strain of the tensile steel are the highest at this crack location. Some of this stress and strain are transferred to the concrete via the concrete-steel bond, thus reducing the steel strain and elongation, which in turn decreases the beam deflection (Maaddawy et al., 2005a).

The model also assumes that the bond stress distribution is uniform over the length of each element and its direction is reversed at the centre of the element. The maximum bond stress is estimated by considering the contributions of both concrete and stirrups to the bond strength and a reduction factor is employed to account for corrosion (Maaddawy et al., 2005a).

This factor is based on experimental work (conducted by Saifullah and Clark[4]), yet it may be suitable only for laboratory situations. This is because the reduction factor is dependent upon the current density applied to induce corrosion, which does not occur in the field. Therefore,

---

[4] The publication year is not provided in Maaddawy et al. (2005).

while this bond model might be acceptable for the experimental work in this case, a different model should be considered for the assessment of beams with un-accelerated corrosion.

This model uses bond strength to establish the mean crack spacing and steel elongation for RC beams. Beam deflection is then based on the calculated steel elongation and thus the prediction of deflection is dependant on bond strength. On the other hand, the way in which the maximum capacity of the beam is determined does not consider bond strength. Specifically, it is calculated using conventional strain compatibility equations once the strain in the extreme fibre of concrete reaches the limiting compressive strain.

Since the maximum capacity is determined using the limiting compressive strain, its value will be affected by reductions in compressive strength of the concrete in the compressive zone. Yet, this model fails to take into account the reduction of concrete compressive strength resulting from micro-cracking due to corrosion.

In sum, the model proposed by Maaddawy et al. (2005a) is suitable for determining the load-deflection curve of a corroded beam and the reduction of load-carrying capacity (the load at which the steel yields) can then be inferred from this curve. However, indirectly determining the ultimate capacity in this manner may by inaccurate since the reduction in bond strength is not directly considered. It is important not to ignore bond strength, since its reduction can cause an anchorage failure and the forces transferred from the concrete to the tensile steel may not be sufficient to cause the steel to yield.

Chapter 4

BOND BETWEEN CONCRETE AND REINFORCING STEEL

4.1 Introduction

Conventional flexural theory of RC beams presumes a complete transfer of tensile stresses from the concrete to the reinforcing steel. This transfer is only possible by way of the steel-to-concrete bond, and therefore, a reduction in bond strength will result in a decrease of flexural capacity. This relationship marks the vital role bond strength plays in the development of the ultimate load-carrying capacity of corroded RC beams.

4.2 Bond Basics

The primary mechanism of bond is the mechanical interlocking between concrete and bar deformations. The strength of the bond is greatly influenced not only by the deterioration of the ribs on the reinforcing steel, but also by the reduced cohesion and adhesion at the surface of the steel due to the widening of splitting cracks caused by corrosion products. Specifically, bond strength at the steel-concrete interface rapidly decreases when the corrosion level increases. This is particularly the case when there is highly localized corrosion, which causes a major reduction of the interlocking forces between the ribs and concrete keys (Amleh and Mirza, 1999).

4.3 Selected Research

Many researchers are working towards the development of an accurate model to predict bond strength with respect to corrosion. Both residual and ultimate steel-concrete bond strengths have been the subject of many published papers, a few of which are discussed below.

4.3.1 Amleh and Mirza

Amleh and Mirza (1999) concluded that as the level of corrosion increases, the number of transverse cracks decrease until they become negligible. In addition, these researchers found that a 4% weight loss of steel resulted in transverse cracks and a bond loss of 9%. Conversely, a weight loss of 17.5% corresponded to a 92% loss of bond with no transverse cracks. As the level of corrosion increased, the widths of these transverse cracks also increased, indicating a reduction of steel-concrete bond.

4.3.2 Al-Negheimish and Al-Zaid

Al-Negheimish and Al-Zaid (2004) conducted research on the manner in which the manufacturing process of deformed bars affects bond behaviour. Their investigation included an assessment of the bond characteristics of hot-rolled and quenched bars, which showed consistent ultimate bond strength trends. That is, increasing corrosion resulted in an initial decrease, followed by a gradual increase and then a rapid loss of bond strength at the end. Al-Negheimish and Al-Zaid (2004) also observed that for a mass loss of approximately 1.5%, all of the bars tested showed similar final bond strength reductions of approximately 10%. While the quenched bars experienced the greatest mass loss, this did not adversely affect the bond behaviour.

4.3.3 Romagnoli et al.

Romagnoli et al. (2002) reported that an increasing water to cement ratio resulted in a decrease in bond strength between the steel and concrete mortar, which was attributed to the increasing porosity of the cement paste. This is because as the porosity increases, a greater number of locations that lack binding material exist on the surface of the steel.

4.3.4 Fang et al.

Fang et al. (2004) performed pullout tests in order to evaluate the influence of corrosion on bond in RC. It was found that specimens with deformed bars that had stirrups responded minimally to corrosion. That is, at 6% corrosion, the bond strength was reduced by only 12%. The researchers explained this by stating that the confinement supplied was sufficient to enable the retention of bond strength.

Conversely, they reported that bond strength was very sensitive for specimens with deformed bars having no stirrups, such that when the corrosion level C_L was 9%, the bond strength was reduced by 66%. The corrosion level was calculated using Equation 4-1, where G_0 is the initial weight of the un-corroded bar, G is the weight of the bar after the removal of corrosion products, g_0 is the weight per unit length of the bar, and l is the bond length (Fang et al., 2004).

Equation 4-1
$$C_L = \frac{G_0 - G}{g_0 l} 100\%$$

4.3.5 MacGregor and Bartlett

According to MacGregor and Bartlett (2000), the average bond stress τ_{avg} at failure in a beam is calculated by Equation 4-2, where R_c is measured from the centre of the bar to the closest surface, d_b is the diameter of the bar, and f'_c is the compressive strength of concrete. This equation is intended for a pristine beam and assumes no corrosion.

Equation 4-2
$$\tau_{avg} = 0.5\sqrt{f'_c} \cdot \left(\frac{R_c}{d_b} - \frac{1}{2} \right)$$

4.3.6 Cabrera

Cabrera (1996) investigated the manner in which the rate of corrosion affects cracking and bond behaviour and developed a numerical model to predict the bond stress. The test specimens consisted of RC slabs, RC beams, and concrete cubes with a centrally located bar. Corrosion was accelerated by the application of various currents and was followed by either flexural or pullout tests. This yielded experimental data with a trend line represented by Equation 4-3, where τ is the bond strength in MPa and $C_\%$ is the percent corrosion.

Equation 4-3
$$\tau = 23.478 - 1.313 \cdot C_\%$$

The level of corrosion $C_\%$ for this relationship (and later Equation 4-11 and Equation 4-12) is taken as the percent mass loss and is computed using Equation 4-4, where m denotes mass and the subscripts i and $corr$ represent the initial and corroded stages respectively.

Equation 4-4
$$C_\% = \frac{m_i - m_{corr}}{m_i} \cdot 100\%$$

4.3.7 Stanish et al.

Stanish et al. (1999) conducted research on one-way slabs measuring 350 mm (width) by 150 mm (thickness) with a span of 1300 mm. Based on the experimental program and subsequent mathematical analysis, the peak bond strength at various corrosion levels was estimated.

The bond strength was normalized (or divided by the square root of the 28 day compressive strength $\sqrt{f_c'}$ of the concrete) and plotted against the percent mass loss $m_\%$ for all specimens. After a linear regression analysis was performed with a 95% confidence limit, the mean predictor equation (Equation 4-5) and the lower 95% confidence level equation (Equation 4-6) were obtained, where the bond strength τ and f_c' are both in MPa (Stanish et al., 1999).

Equation 4-5 $$\frac{\tau}{\sqrt{f_c'}} = 0.77 + 0.027m_\%$$ (Mean Predictor Equation)

Equation 4-6 $$\frac{\tau}{\sqrt{f_c'}} = 0.63 + 0.041m_\%$$ (Lower 95% Confidence Limit)

The mass reduction percentage $m_\%$ is determined by Equation 4-7, where V denotes volume. In terms of residual bar diameter, Equation 4-7 simplifies to Equation 4-8, where Δd is the change in bar diameter, d_{corr} is the diameter after corrosion, and d_i is the diameter prior to cracking.

Equation 4-7 $$m_\% = \frac{m_{cor}}{m_i} \cdot 100\% = \frac{V_{cor}}{V_i} \cdot 100\%$$

Equation 4-8
$$m_{\%} = \left(1 - \frac{d_{cor}^2}{d_i^2}\right) \cdot 100\% \cong 2 \cdot \frac{\Delta d}{d_i} \cdot 100\%$$

By substituting Equation 4-8 into Equation 4-5 and Equation 4-6, the mean predictor equation becomes Equation 4-9 and the lower 95% confidence level equation becomes Equation 4-10 (Stanish et al., 1999).

Equation 4-9
$$\frac{\tau}{\sqrt{f_c'}} = 0.77 - 2.7\left(1 - \frac{d_{corr}^2}{d_i^2}\right) \cong 0.75 - 5.4\frac{\Delta d}{d_i}$$
(Mean Predictor Equation)

Equation 4-10
$$\frac{\tau}{\sqrt{f_c'}} = 0.63 - 4.1\left(1 - \frac{d_{corr}^2}{d_i^2}\right) \cong 0.63 - 8.2\frac{\Delta d}{d_i}$$
(Lower 95% Confidence Limit)

4.3.8 Lee et al.

Lee et al. (2002) examined bond properties between concrete and reinforcement by performing pullout tests. The concrete specimens were corroded to 0, 3, 15, 20, or 30% corrosion by applying a direct current of 1 ampere (A). Using finite element analysis Equation 4-11 was developed to calculate the maximum bond strength τ_{max}, where $C_{\%}$ is the level of corrosion (as per Equation 4-4).

Equation 4-11
$$\tau_{max} = 5.21 \cdot e^{-0.0561 \cdot C_{\%}}$$

4.3.9 Chung et al.

Chung et al. (2004) carried out experimental research in order to determine the way in which corrosion affects bond strength and development length. Concrete slab specimens having one steel reinforcing bar were corroded to either 1, 2, 3, 5, 7, 10, or 15%, with and induced

current of 12 A at 12 volts direct current. After the analysis of flexural tests, a correction factor for the ACI development length provisions was suggested. This correction factor is shown as Equation 4-12, which is an empirical formula for predicting bond strength.

Equation 4-12
$$\tau = 2.09 \cdot C_\%^{-1.06} \qquad (C_\% > 2\%)$$

Chung et al. (2004) concluded that the empirical equations previously proposed by Cabrera (in section 4.3.6), Stanish et al. (Equation 4-5), and Lee et al. (Equation 4-11), "... do not properly capture the gradual bond strength reduction behaviour after 2% corrosion level." This is because these equations predict the reduction in bond strength to be a linear function of increasing corrosion, which was challenged by Chung et al.

Chapter 5

EXPERIMENTAL PROGRAM

5.1 Methodology of Research

The present study involves the construction, corrosion, and mechanical testing of twelve reinforced concrete beam specimens. For each beam specimen, a pullout specimen was constructed and exposed to the exact same conditions. Corrosion was initiated and propagated by impressing a direct current to the tensile steel. The specimens were then tested at various levels of corrosion. The results from these tests are used to study the changes in flexural behaviour of corroded reinforced concrete (RC) beams with increasing corrosion.

5.2 Test Specimens

5.2.1 Beam Test Study

To study the relationship between corrosion and flexural strength, a total of twelve beam specimens (BS) were constructed, the dimensions of which are shown in Figure 5-1. These specimens had a cross-section of 156 × 176 mm and a clear span of 1000 mm. The concrete cover of the stirrups (b_c') was 30 mm. All twelve beams had two No. 15 reinforcing bars at the bottom and two No. 10 bars at the top with 6 mm double-leg stirrups along the shear span at 40 mm spacing.

Figure 5-1: Geometry of a typical beam specimen (BS) used in this study.

The system for identifying the steel bars closely follows the specimen naming scheme. The six faces of each beam are named top, bottom, left, right, front, or back, as shown in Figure 5-2. The bar on the right hand side of the beam with respect to front face is denoted by the specimen name followed by "- R", and the bar on left hand side by "- L", as shown in Figure 5-3.

Figure 5-2: Illustration of beam face names.

B   S   0   8   -   R

B = Beam   Specimen number   R = Right
                                                 L = Left

Figure 5-3: Reinforcing steel designation.

Precautionary steps were taken in an attempt to limit corrosion to the reinforcing steel in the clear span of the beams. One such step was to protect the ends of the reinforcing bars that

protruded out of the ends of the beams, which were exposed to the electrolyte solution when the corrosion was accelerated. This was accomplished by epoxy coating and duct taping the first 60 mm of the bar tips. These tips were also covered with silicone before they were corroded.

Another measure taken was to protect against the corrosion of the shear reinforcement, as it was important to prevent the possibility of the beams failing in shear. This was accomplished by wrapping the bottom corners of the stirrups where they made contact with the tensile reinforcement with electrical tape in order to electrically isolate each stirrup. This also served to prevent unwanted corrosion in the top bars.

5.2.2 Pullout Tests Study

In order to correlate the residual strength of the reinforced concrete beams to residual bond strength, 12 pullout specimens (PS) were constructed. It is possible to obtain a close estimate of the ultimate bond stress of the tensile steel using a mathematical model found in the literature. However, this pullout study was conducted using the same materials and exposure conditions as in the beam study in order to establish the relationship more accurately.

The details of the pullout specimens are shown in Figure 5-4. Each specimen had a pre-weighed No. 15 steel bar embedded in a concrete cylinder having a diameter of 100 mm and a height of 200 mm.

The tensile force applied to the reinforcing steel and the area of the embedded length of the bar are used to calculate the average ultimate bond stress τ_{avg}. This is shown in Equation 5-1, where P is the maximum tensile force applied, l is the embedded length the reinforcing steel, and the d_b is the diameter of the steel bar.
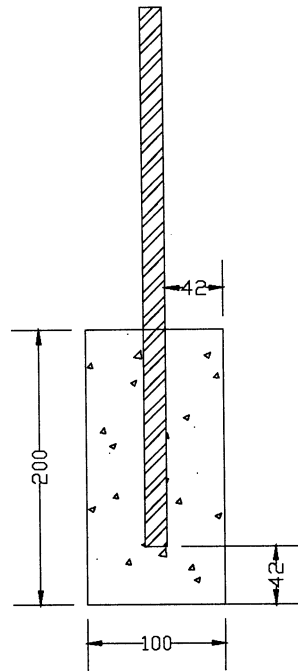
Figure 5-4: Typical pullout specimen (PS).

Equation 5-1
$$\tau_{avg} = \frac{P}{\pi d_b l}$$

It should be noted that this investigation focuses on the beam study rather than the pullout study. The objective of the pullout test is only to obtain the bond to corrosion relationship of the material used given the exposure conditions.

5.2.3   Specimen Designation

The naming of the test specimens is demonstrated in Figure 5-5. The specimens are referred to using four characters. The first letter indicates whether the specimen is a beam or a pullout while the third and fourth characters denote the specimen number ranging from 1 to 12.

<div align="center">

B   S   0   8

BS = Beam Specimen

PS = Pullout Specimen   Specimen number

Figure 5-5: Specimen designation legend
</div>

5.3 Material Properties

5.3.1 Reinforcing Steel

All deformed reinforcements used for the construction of the beam and pullout specimens were obtained locally and conformed to the CSA Standard G30.18. All of the steel bars were deformed with the exception of the 6 mm stirrups, which were plain. These stirrups were selected for the shear reinforcement due to the small cross-section of the beam, as larger deformed bars would not meet the requirement for the minimum bend diameter. To determine the mechanical properties of the 15M tensile reinforcing bars used for this study, tension tests were performed on six randomly selected bars. These tests returned an average experimental yield strength and ultimate strength of 550 and 691 MPa respectively.

5.3.2 Concrete

Throughout this experiment, CSA Type 10 or the ASTM Type I normal Portland cement was used. The properties of the fine and coarse aggregates that were used are

summarized in Table 5-1 and Table 5-2. Due to the close spacing of the reinforcement, the course aggregate selected was pea gravel, having a nominal maximum size of 10 mm. The aggregates and the cement used throughout this experiment were manufactured and/or supplied by LaFarge Canada.

<div align="center">46</div>

Table 5-1: Sieve analysis and other properties of fine aggregate.

SIEVE SIZE		FRACTION	FRACTIONAL	CUMULATIVE	CUMULATIVE
mm	No.	MASS (g)	% RETAINED	% RETAINED	% PASSING
10	3/8 in.	0.00	0.00	0.00	100.00
5.00	4	20.40	4.08	4.08	95.92
2.50	8	50.45	10.09	14.17	85.83
1.25	16	71.70	14.34	28.51	71.49
630um	30	96.30	19.26	47.77	52.23
315um	50	130.50	26.10	73.87	26.13
110um	100	95.05	19.01	92.88	7.12
Pan		35.60	7.12	100.00	0.00

FINENESS MODULUS	2.61
ORIGINAL OVEN DRY MASS OF SAMPLE	501 g
SUM OF FRACTIONAL MASS RETAINED	500 g
PERCENT LOSS	0.25 %
BULK RELATIVE DENSITY	2485.90 kg/m³
BULK RELATIVE DENSITY (SSD)	2516.11 kg/m³
APPARENT RELATIVE DENSITY	2563.31 kg/m³
ABSORPTION	1.21 %

Table 5-2: Sieve analysis and other properties of coarse aggregate.

SIEVE SIZE		FRACTION	FRACTIONAL	CUMULATIVE	CUMULATIVE
mm	No.	MASS (g)	% RETAINED	% RETAINED	% PASSING
20	3/4 in	0.00	0.00	0.00	100.00
14.00	1/2 in	17.00	0.46	0.46	99.54
10.00	3/8 in	948.00	25.89	26.35	73.65
5.00	4	2495.00	68.13	94.48	5.52
2.36	8	101.00	2.76	97.24	2.76
Pan		101.00	2.76	100.00	0.00

NOMINAL MAXIMUM OF AGGREGATE	10 mm
ORIGINAL OVEN DRY MASS OF SAMPLE	3658 g
SUM OF FRACTIONAL MASS RETAINED	3662 g
PERCENT GAIN	0.10 %
DRY RODDED DENSITY	1821.16 kg/m³
BULK RELATIVE DENSITY	2620.40 kg/m³
BULK RELATIVE DENSITY (SSD)	2656.50 kg/m³
APPARENT RELATIVE DENSITY	2718.46 kg/m³
ABSORPTION	0.38 %

5.4 Mixing, Casting and Curing

The concrete mix used for every specimen was based on the mix design previously used by Yoon et al. (2001). The properties of the concrete are summarized in Table 5-3. The weight proportion of the concrete mixture was 1 (cement): 2 (coarse aggregate): 2 (fine aggregate): 0.5 (water), giving a water to cement ratio (w/c) of 0.5. The concrete was mixed in the laboratory using a 4 cubic foot portable electric mixer. The dry constituents of the concrete were mixed for 3 minutes, followed by the addition of water over a 2-minute period, and then mixed for another 3 minutes after the water was added.

Table 5-3: Concrete properties.

UNIT WEIGHT	2277.63 kg/m³
CEMENT	414.11 kg/m³
AIR	2 %
W/C	0.5
SLUMP	200 mm

The workability of the concrete was very high with a slump of 200 mm and an air content of 2.5 %. The properties of hardened concrete were studied by performing 28-day tests, the average 28-day compressive strength and splitting tensile strength were tested to be 39 and 3.2 MPa respectively. Specifically, compressive strength tests in accordance with ASTM C39 and indirect tensile strength tests in accordance with ASTM C496 were done on cylinders having a diameter and height of 100 mm and 200 mm respectively. The splitting tensile strength was calculated by Equation 5-2 where, f_t is the splitting tensile strength [MPa], P is the maximum applied load [N], L is the length of the specimen [mm], and D is the diameter of the specimen [mm].

Equation 5-2 $$f_t = \frac{2P}{\pi LD}$$

For the beam specimens, the concrete was cast horizontally in wooden moulds and compacted using an electric poker vibrator. The pullout specimens were cast vertically in plastic moulds and compacted using a vibrating table. After casting, the test specimens remained in their respective moulds and were placed in a moist curing room at 23 ± 2 degrees Celsius and 100% relative humidity. The specimens were removed from their forms after 48 hours and kept under the same conditions for 80 days.

5.5 Corrosion Acceleration

After curing the specimens for 80 days, they were partially immersed in a 5% saltwater solution (by weight). Subsequent to this, the specimens were subjected to accelerated galvanic corrosion by the impression of a direct current density of 3 mA/cm^2. In the case of the beam specimens, the applied current was based on the surface area of the tensile reinforcing steel. As specimens 1 and 2 were the control specimens, they were not exposed to any accelerated corrosion.

5.5.1 Voltage Monitoring

Since the current used to corrode the beam and pullout specimens was constant, the voltage had to be regulated to compensate for changes in the resistivity of the circuit. Corrosion of the specimens causes increased concrete cracking, which in turn results in a reduced resistance. Therefore, observing the fluctuations in voltage can be useful when determining initial cover cracking, analysing the deterioration process, or comparing the corrosion of

individual specimens. For this reason, the voltage was recorded daily as part of the accelerated corrosion monitoring in this study.

5.5.2 Development of Various Corrosion Levels

Each specimen remained in the corrosion tank until the desired level of corrosion was reached. For this study, the degrees of corrosion were categorized in terms of longitudinal corrosion crack widths and were identified as stages I, II, III and IV. A description of each stage is provided below:

Stage I – this level is reserved for the designated control specimens (01 and 02), which were not exposed to any accelerated corrosion. These specimens were considered to be in pristine condition.

Stage II – this level represents the early stages of a chloride attack. At this point, chloride penetration and the depassivation of the reinforcing steel are complete. The formation of corrosion cracks typified the achievement of this level. The crack width chosen to identify the upper limit of this classification was 0.2 mm.

Sage III – the propagation of corrosion is well under way at this point with rust products starting to appear at the surface and the development of visible corrosion cracks. This intermediate group was defined by corrosion cracks greater than 0.2 mm, but less than or equal to 0.5 mm.

Sage IV – this degree is characterized by wider and longer corrosion cracks with heavy rust staining synonymous with significant section loss of the reinforcing steel. The crack width chosen to identify the lower limit of this classification was 0.5 mm.

It should be noted that other methods to define targeted levels of corrosion have been successfully used in previous studies. A common method employed is based on Faraday's Law, which prescribes the relationship between the mass of iron consumed (M_s) and the amount of current (I_{corr}), which is passed through the corrosion cell. Faraday's Law is shown in Equation 5-3 where, A is the atomic weight of the ion being dissolved [g/mol], F is Faraday's constant and equals 96500 C/mol, and n is the valence of the reaction and is usually taken as 2. In the case of iron (Fe), the atomic weight is 55.85 g/mol (Higgins et al., 2003).

Equation 5-3
$$\frac{dM_s}{dt} = \frac{I_{corr} \cdot A}{n \cdot F}$$

5.5.3   Experimental Setup for Accelerated Corrosion

5.5.3.1   *Beam Specimens*

Each beam specimen was corroded simultaneously with its corresponding pullout specimen using an accelerated galvanic method. Kenwood PAC30-3R regulated DC (direct current) power supplies with a maximum output of 3 amperes (A) at 30 volts (V) were used. A separate power supply was used for each length of tensile reinforcement to accurately control and monitor the current passing through each bar. The two power supplies were integrated by a steel mesh at the bottom of the tank, which served as the common ground. The positive terminals on each power supply were connected to either the right (R) or the left (L) reinforcing steel.

The components of the system included a plastic tank, electrolyte solution, a steel mesh at the bottom of the tank (cathode), and the reinforcing steel (anode). The electrolyte solution

was comprised of 5% de-icing salt (sodium chloride) by the weight of water and was changed every 48 hours to maintain a constant pH and NaCl concentration.

It is important to note that although precautions were taken to prevent corrosion in the stirrups, it was later found that the corrosion setup initially employed produced this very effect. Consequently, a second setup was opted for that split the specimens into categories of series I and series II. Series I is comprised of beam specimens BS03, BS04, BS05, and BS06, and series II of BS07, BS08, BS09, BS10, BS11, and BS12.

For series I, the beams were placed in the tank with the top face-up and the electrolyte solution just above the height of the bottom bars so that the beams were almost fully submerged. For series II, the beams were about half submerged to just above the height of the tensile reinforcement with the bottom face down. Figures 5-6 and 5-7 each show a representative cross-section illustrating one side of the electrical system used for series I and II beam specimens respectively.
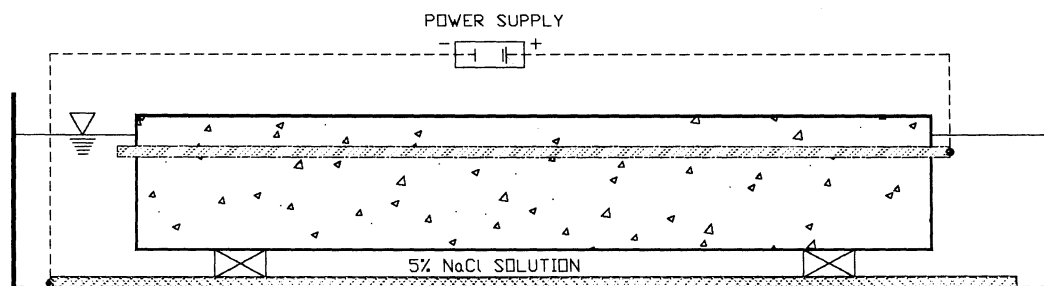
Figure 5-6: Representative cross-section showing current-induced corrosion setup for BS03, BS04, BS05, and BS06 (series I).
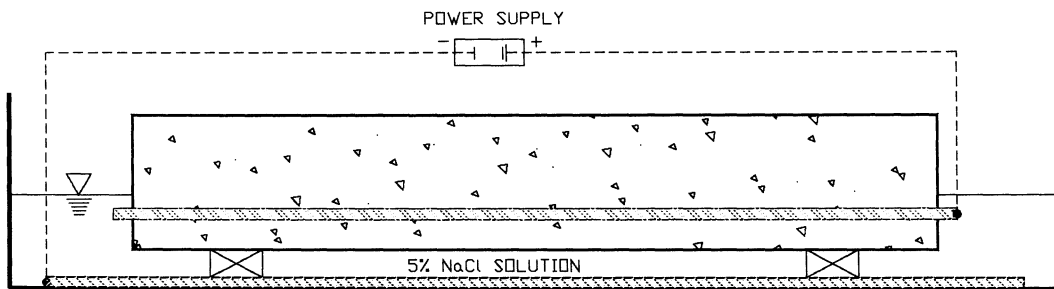
Figure 5-7: Representative cross-section showing current-induced corrosion setup for BS07, BS08, BS09, BS10, BS11, and BS12 (series II).

5.5.3.2 Pullout Specimens

The electrical system used for the pullout specimens required the use of one power supply for two specimens. The positive terminal of the power supply was connected in parallel to each protruding rebar to act as an anode, while the negative terminal was connected to the steel mesh resting on the bottom of the tank, which served as a cathode. The electrolyte solution (5% NaCl) covered two thirds of the concrete portion of the pullout specimens, as illustrated in Figure 5-8.
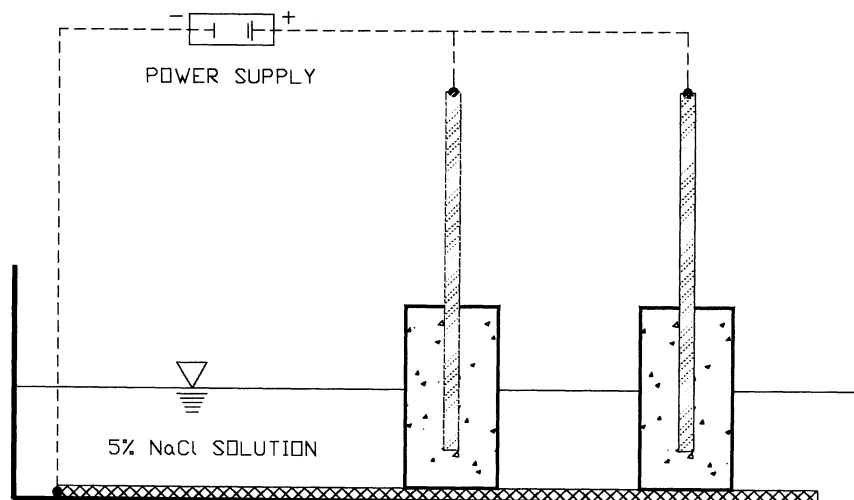
Figure 5-8: Representative cross-section showing current-induced corrosion setup for pullout specimens.

5.6 Methods of Testing

Following the accelerated corrosion stage, visual observations were performed to gain an overview of the degree of damage to each specimen. Crack maps were drawn for each beam specimen indicating the length and location of each corrosion crack in order to categorize the level of deterioration.

Non-destructive tests were performed to investigate the internal state of deterioration of each specimen. These tests include the ultrasonic pulse velocity and half-cell potential (i.e. corrosion potential) tests.

Thereafter, the beams were loaded in four-point bending until failure and the mid-span deflections were measured. The flexural and failure cracks were mapped in order to study the changes in the failure mode and flexural crack development.

Finally, the specimens were broken open to retrieve the reinforcing steel and the mass loss was determined.

5.6.1 Visual Survey

The first stage in any condition assessment is generally a visual survey, which is a valuable method of determining the nature of the deterioration. This type of survey can aid in identifying areas that require further testing and/or a more detailed analysis. In this laboratory experiment, the deterioration is deliberately caused and is clearly the corrosion of the reinforcing steel. As a result, this stage serves not to investigate the cause of the deterioration, but to monitor and document its extent.

A visual survey for all specimens was conducted before, during, and after the corrosion stage and any defects or cracks were noted before the specimens entered the corrosion tank. During corrosion, a visual inspection was performed every 48 hours until the desired level of corrosion was obtained.

5.6.1.1 *Corrosion Crack Survey*

Following this stage, the specimens were visually inspected and a detailed crack survey was performed on the beam specimens.

The crack survey entailed the recording and plotting of all corrosion cracks. This task was performed by tracing a scaled digital image using AutoCAD.

5.6.2   Non-Destructive Testing

Ultrasonic pulse velocity and half-cell potential tests were performed prior to mechanical testing.

5.6.2.1 *Ultrasonic Pulse Velocity Method*

The ultrasonic pulse velocity method is described in ASTM C 597-02 and indicates the state of deterioration by detecting changes in concrete, such as internal cracking and other defects.

The pulse velocity method rests on the premise that the velocity of a pulse of compressional waves passing through a medium is dependant upon the elastic properties and density of the medium, as shown in Equation 5-4 below:

V = compression wave velocity (km/s)

$$K = \frac{(1-\upsilon)}{(1+\upsilon)\cdot(1-2\upsilon)}$$

E_D = dynamic modulus of elasticity (kN/mm²)

ρ = density (kg/m³), and

υ = dynamic Poisson's ratio

Equation 5-4 $$V = \sqrt{\frac{K \cdot E_D}{\rho}}$$

The basic circuitry of a typical pulse velocity testing unit is shown in Figure 5-9. A compressional wave is sent through the concrete by the transmitting transducer and is received at a distance d_x by the receiving transducer. The testing equipment displays the time (Δt) it takes the wave to pass through the concrete. The velocity (V) of the compressional wave is shown in Equation 5-5 (Malhotra and Carino, 2004).

Equation 5-5 $$V = \frac{d_x}{\Delta t}$$

There are three possible arrangements in which the transducers may be placed (see Figure 5-10). These configurations are (A) direct, (B) semi direct, and (C) indirect. The direct transmission positioning was the arrangement used in this experiment. This is the most desirable configuration in that it transmits the maximum amount of energy to the receiving transducer (Malhotra and Carino, 2004).
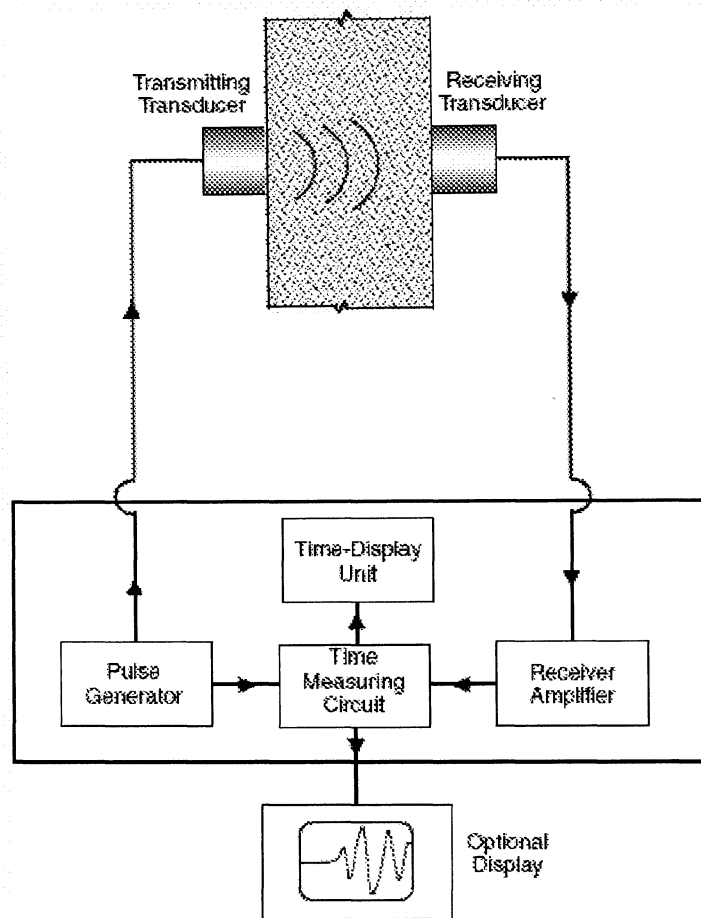
Figure 5-9: Schematic of a typical pulse velocity test circuit (Malhotra and Carino, 2004).

As the velocity of the compressional waves is affected by the matter through which it passes, it is important when conducting this test that the waves only be affected by the subject concrete. Effects that alter the pulse velocity relating to concrete characteristics include aggregate size, grading, type, and content; cement type; water-cement ratio; admixtures; and the age of the concrete. However, there also exist other factors that are unrelated to concrete characteristics, such as the quality of the transducer contact; temperature, moisture and curing conditions of the concrete; path length; size and shape of the specimen; level of stress in the specimen; and the presence of reinforcing steel (Malhotra and Carino, 2004).
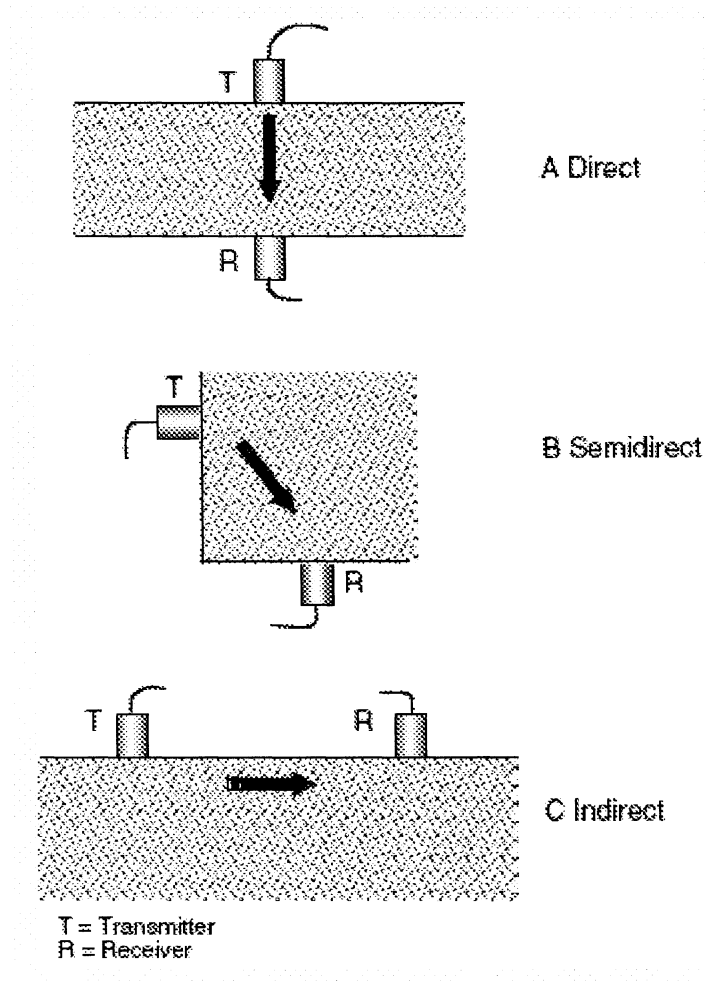
Figure 5-10: Pulse velocity test configurations: (A) direct, (B) semi direct, and (C) indirect (Malhotra and Carino, 2004).

Ultrasonic pulse velocity readings were taken on all of the beam specimens. After the beams were removed from the corrosion tanks, they were allowed a minimum of one week to air-dry before this test was performed. Due to the high concentration of reinforcing steel, only two pulse velocity readings were taken in the centre of each beam: one horizontally and one vertically (see Figure 5-11). This test was not performed on the pullout specimens due to their cylindrical shape and the location of the reinforcing steel.
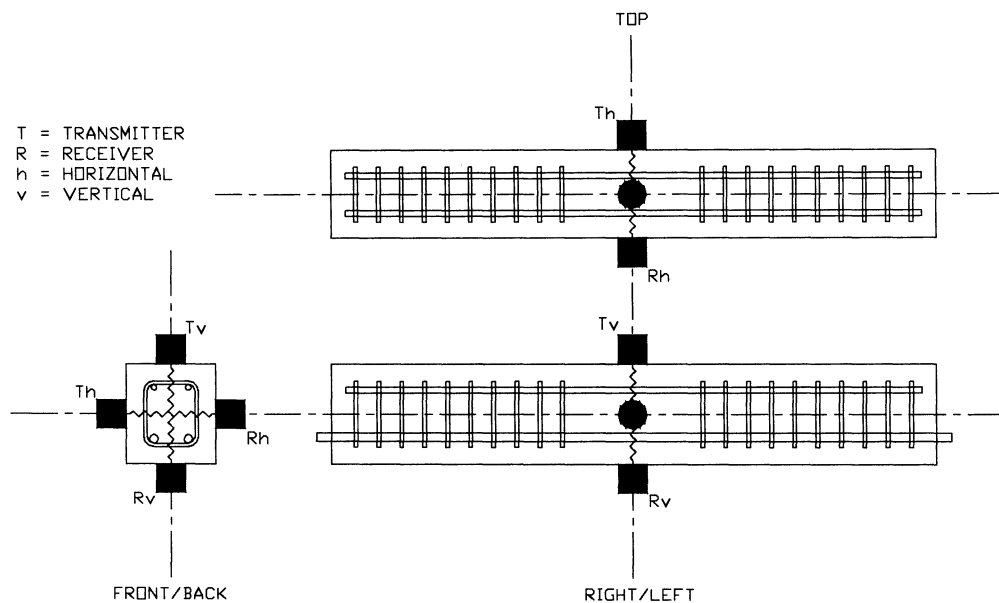
Figure 5-11: Schematic of pulse velocity test locations on beam specimens.

5.6.2.2 Half-cell Potential Test

ASTM C876-91 describes the standard test method for measuring half-cell potentials of uncoated reinforcing steel in concrete. The half-cell potential test assesses the possible extent of the corrosion activity of the reinforcing steel embedded in the concrete.

Figure 5-12 illustrates the Daniell cell, which can be used to understand the chemistry behind the half-cell potential test. This cell is composed of two half-cells: zinc in zinc sulphate and copper in copper sulphate. In each half-cell, the metal is dissolved and ions are precipitated, with the copper being more resistant to this reaction than the zinc. When the two cells are connected by a porous partition[5] and the metals are connected by a wire, the copper from the copper sulphate solution is deposited on the copper electrode and the zinc dissolves (Broomfield, 1997).

---

[5] A semi-permeable membrane that allows charges to be exchanged but does not permit ions to pass.
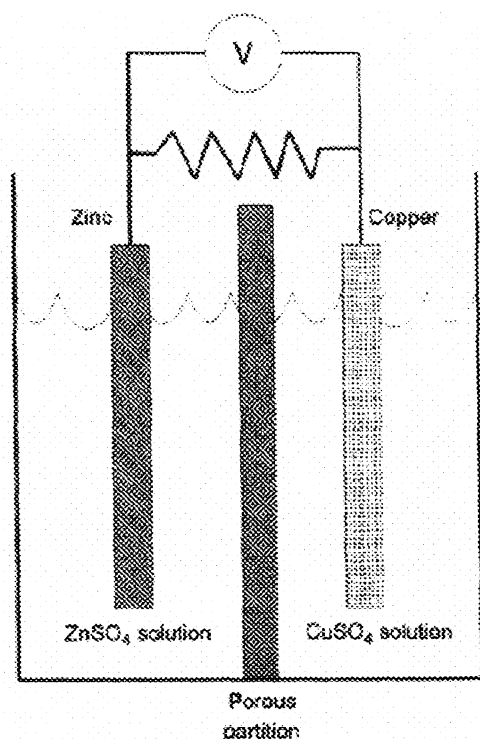
Figure 5-12: The Daniel cell (Broomfield, 1997).

The voltage of a cell is determined by the metals used and by the properties and composition of the solutions. The concentration of the solution is also a factor in determining the potential of half-cells. Generally, a more concentrated solution is more corrosive than a diluted solution. Therefore, a cell comprised of a single metal in a solution of different concentrations will produce current potential. Table 5-4 lists the standard[6] half-cell potentials that are commonly used to evaluate corrosion problems. For instance, the cell voltage of the Daniell cell is equal to +0.34 minus -0.76 or +1.10 V (Broomfield, 1997).

Table 5-4: Half-cell potentials (Broomfield, 1997).

$Zn \rightarrow Zn^{2+} + 2e^-$	-0.76 V
$Fe \rightarrow Fe^{2+} + 2e^-$	-0.44 V
$Cu \rightarrow Cu^{2+} + 2e^-$	+0.34 V

---

[6] The voltage of any cell referenced to a standard hydrogen electrode.

The risk of corrosion can be measured by introducing an external half-cell on the surface of the concrete, as shown in Figure 5-13. If the half-cell is moved along the steel, the measured potential will fluctuate, since the potential is dependant on the iron in its pore water environment. In anodic areas, iron can easily go into solution, much like the zinc in the Daniell cell. In cathodic areas, the steel resists dissolution. This results in higher voltages in anodic areas and lower voltages in cathodic areas (Broomfield, 1997).
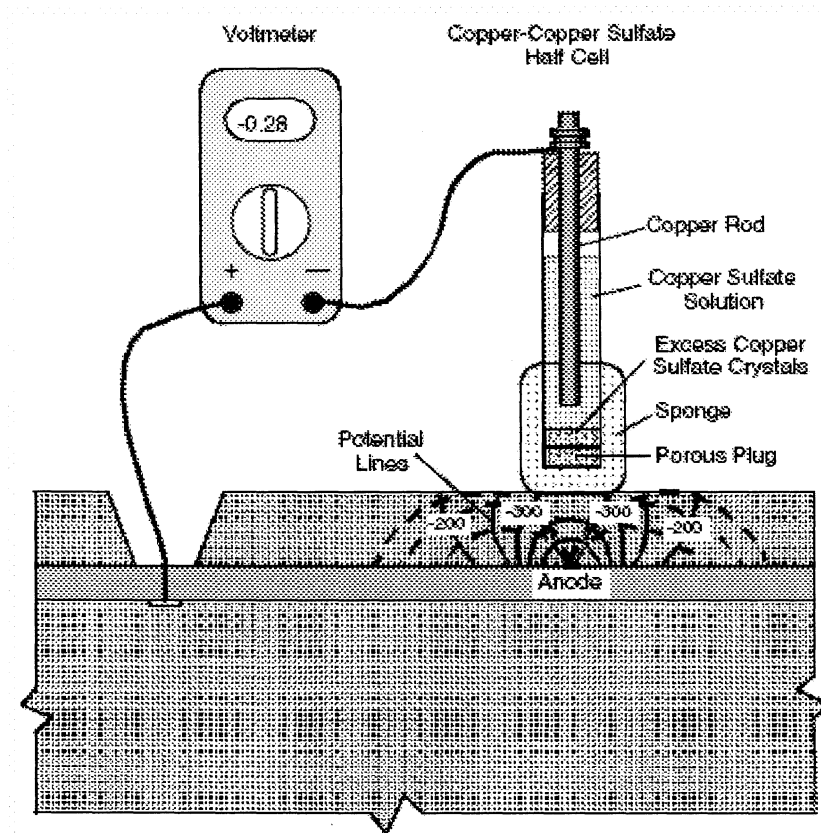
Figure 5-13: Half-cell measurement of corrosion potential (Malhotra and Carino, 2004).

Figure 5-14 shows the grid layout used for each half-cell potential survey on the beam specimens. Columns 1 through 11 are spaced at 100 mm between the clear span and rows A, B, C, and D are directly over the steel bar. Rows B and C are on the bottom face of the beam while rows A and D are on the left and right faces. The interpretation of the potential

readings for this study follows the convention standardized in ASTM 876, which is summarized in Table 5-5.

It is important to note that half-cell potentials are entirely a function of corrosion. Factors that may affect half-cell potentials include concrete cover depth and resistivity, the availability of oxygen, water content (saturation), and carbonation.
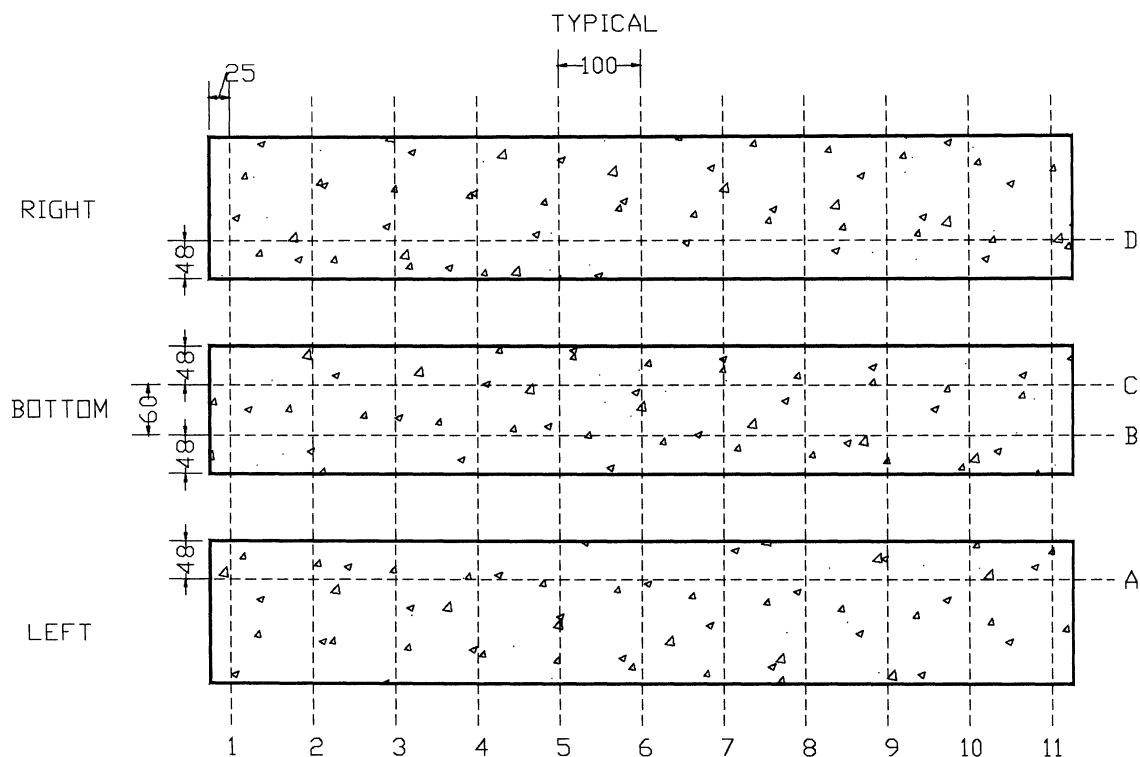
Figure 5-14: Grid layout for the half-cell potential test.

Table 5-5: Interpretation of half-cell potential readings using a copper/copper sulphate half-cell.

Corrosion Potential	Corrosion Condition
>-200 mV	Low. 10% risk of corrosion
-200 to -350 mV	Intermediate corrosion risk
-350 to -500 mV	High. 90% risk of corrosion
<-500 mV	Severe corrosion

5.6.3 Mechanical Testing

After each beam specimen had reached the targeted level of corrosion, it was removed from the corrosion cell along with its counterpart pullout specimen and was mechanically tested.

5.6.3.1 *Beam Test*

Ultimate load tests were performed in the laboratory to determine the load-carrying capacity of the beam specimens. The load arrangement used was four-point loading, as shown in Figure 5-15. This arrangement allows for a central region having virtually constant moment without any shear force.
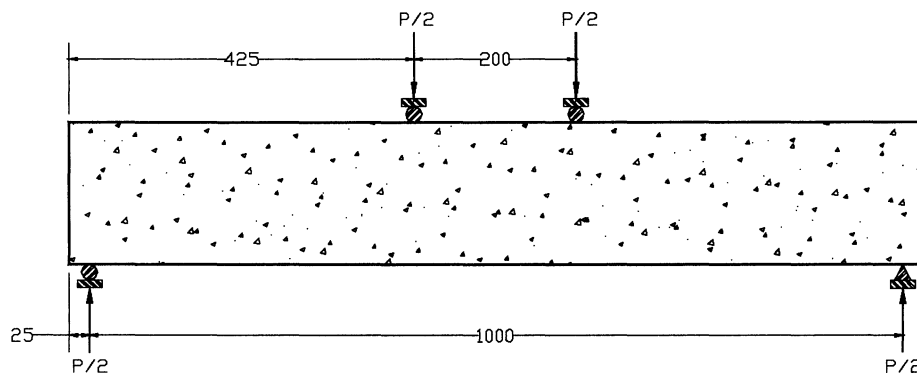
Figure 5-15: Illustration showing placement of loads for beam test (dimensions are in mm).

An increment of 5 kN applied load was used until failure, at an approximate rate of 1 kN per second. At each 5 kN increment, the paths of each crack were traced using a permanent marker to enhance their visibility and then photographically recorded. Crack widths were measured using a hand-held, illuminated optical microscope and an unmagnified comparator scale viewed under a high-powered magnifying glass. The load and deflection was constantly recorded using a data acquisition program that was connected to the load cell and a linear variable differential transformer located at mid-depth and mid-span.

5.6.3.2 *Pullout Test*

The pullout specimens were tested in order to determine the maximum bond stress at each level of corrosion. Each pullout specimen was mounted in a specifically designed test frame and subjected to a standard pullout test, where the embedded reinforcing steel is tensioned until it is completely pulled out. For each test, the applied load was recorded using a data acquisition program.

5.6.4 Post Test Evaluations

After the completion of the beam tests, a second crack survey was completed and the actual steel mass loss due to corrosion was determined for both the beam and pullout specimens.

5.6.4.1 *Flexural Crack Survey*

This second crack survey plotted the flexural and failure cracks that occurred during the beam tests. This survey was performed by tracing a scaled digital image using AutoCAD.

5.6.4.2 *Mass Loss Determination*

Following the structural and subsequent destructive tests, the tensile reinforcement was removed from each beam and pullout specimen and the corrosion products were cleaned using a wire brush. The corroded reinforcing bars were characterized by percent mass loss (ML), which was calculated by Equation 5-6 where m denotes mass and the subscript i represents the initial or reference mass and $corr$ represents the residual mass. The reference mass of reinforcement was measured using non-corroded (pristine) reinforcement.

Equation 5-6
$$ML = \frac{m_i - m_{corr}}{m_i} \times 100$$

Chapter 6

RESULTS OF THE EXPERIMENTAL PROGRAM

6.1 Introduction

The purpose of this chapter is to report the results gathered from the accelerated corrosion process, non-destructive testing, destructive testing, and post-test examinations.

6.2 Corrosion Cell Configuration

An unexpected complication that arose during this experiment was unwanted corrosion in the shear reinforcement due to the initial electrochemical cell configuration. This was discovered during the ongoing visual surveys of the beam specimens that were conducted during the accelerated corrosion phase. As a result, the corrosion cell setup used for the beam specimens was redesigned shortly after the corrosion phase started.

Figures 5-6 and 5-7 show two different corrosion configurations; the former configuration had the beam almost fully submerged and inverted in the tank, while the latter had the beam in an upright position partially submerged to just above the height of the tensile steel.

The initial setup (series I) was opted for in order to facilitate the daily visual surveys, the rationale being that the tensile portion of the beam would be more easily accessed by only having to slightly elevate it out of the salt solution. However, the corrosion of the stirrups necessitated the employment of series II, thus preventing the stirrups from becoming

submerged in the salt solution. This required that the beams be completely removed from the tank and inverted 180 degrees to be monitored.

After the first two beams (BS03 and BS04) were corroded, the impending problem with the configuration of series I was not yet evident as the corrosion level was too low. When the second pair of beams (BS05 and BS06) nearly completed the corrosion phase, the occurrence of cracking and the accumulation of corrosion products in places other than in the area of the tensile reinforcement were observed.
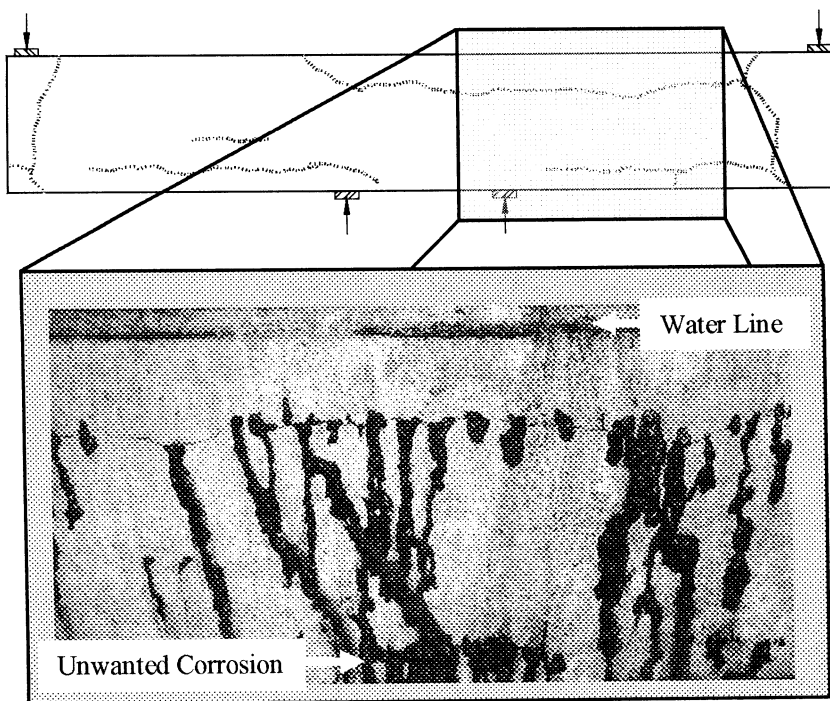
Figure 6-1: Photograph showing portion of BS06 (left face) after corrosion phase.

Figure 6-1 is a photograph of the left side of BS06 immediately after it was removed following 126 hours in the accelerated corrosion tank. The top of the photo is where the left face meets the bottom face, while the bottom clearly shows corrosion products in the compression zone of the beam, indicating the corrosion of either the top bars or the stirrups.

This phenomenon occurred despite the measures taken to electrically isolate the bottom bars from the rest of the reinforcement cage. Based on the evidence observed and considering that electrons will take the path of least resistance, it can be hypothesized that while in the corrosion tank, current moved from the tensile reinforcement to the stirrups through the ionic medium. When the electrons departed from the stirrups to move toward the cathode, they effectively became anodic and corrosion occurred. This phenomenon is know as stray current corrosion and is most commonly associated with electric powered streetcars (Broomfield, 1997).

In an attempt to correct this problem, the corrosion cell arrangement was changed to the setup depicted in Figure 5-7. The six remaining beams (BS07 to BS12) were corroded in this fashion, with the beams placed in the tank with the top face-up and the electrolyte solution just above the height of the bottom bars.

The visible damage to the exterior of these beams prior to the corrosion program suggested that the corrosion activity was more concentrated to the tensile region when compared to the previous setup. Due to this change in the corrosion cell setup almost midway through the corrosion program, the corrosion stages were restarted and therefore, the maximum level of corrosion induced was far below what had been anticipated.

6.3   Accelerated Corrosion Monitoring

Corrosion was accelerated by impressing a current density of 3 mA/cm², with respect to the tensile reinforcement. This method of corrosion was employed to reach advanced stages of deterioration in a relatively short time. The details of this corrosion program for the beam specimens are summarized in Table 6-1.

Table 6-1: Summary of the accelerated corrosion program for beam specimens.

Specimen	Setup Configuration	Rate of Corrosion	Exposure Time (Hrs)	Degree of Corrosion
BS03	Series I		47	Stage II
BS04	Series I		47	Stage II
BS05	Series I		100	Stage III
BS06	Series I		126	Stage IV
BS07	Series II	3 mA/cm^2	45	Stage II
BS08	Series II		45	Stage II
BS09	Series II		103	Stage III
BS10	Series II		103	Stage III
BS11	Series II		170	Stage IV
BS12	Series II		170	Stage IV

6.3.1 Voltage Readings

As mentioned earlier, the fluctuations in the voltage of the corrosion cell can be useful when comparing the corrosion of individual specimens. After 80 days of curing, each specimen (except for the control) was subjected to accelerated galvanic corrosion. The current and voltage that was supplied was recorded on a daily basis. These readings for all of the beams corroded are supplied in Appendix A.

Since the current was constant, the voltage was continuously regulated to compensate for the changing resistance. The average voltages for series I and series II corrosion cells are shown in Figure 6-2 (refer to Figure 5-3 for the naming of the rebar). As mentioned earlier, each rebar was assigned its own power supply incorporated by common ground for each beam. The average voltages during the accelerated corrosion phase for series I and II beam specimens were approximately 17V and 27V respectively.
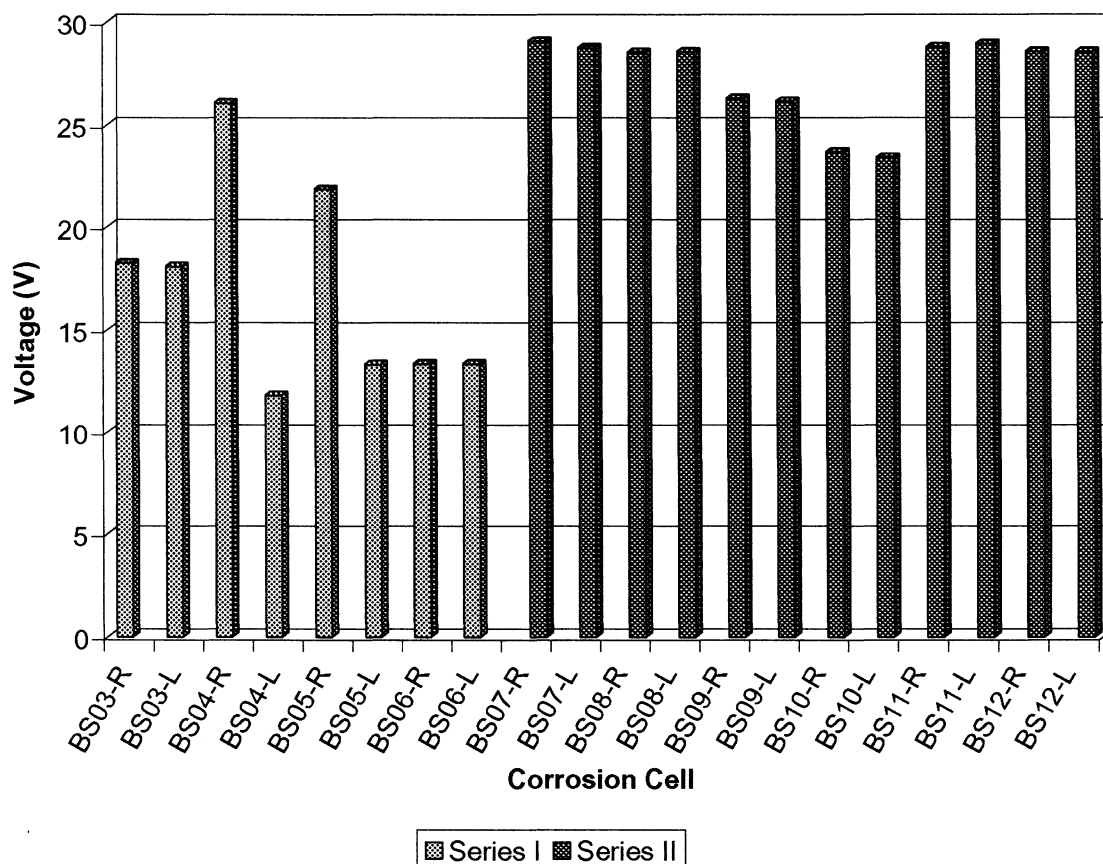
Figure 6-2: Average voltage readings for series I and II beam specimens.

This disparity in the voltage readings between series I and II specimens is due to the increased electrical resistance of the series II circuit. Since only the tensile steel and the lower portion of the stirrups were submerged in the electrolyte solution, the area in which the electron exchange process took place was reduced, making the movement of the electrons through the circuit more difficult.

Figure 6-3 and Figure 6-4 plot the voltage readings taken during the accelerated corrosion phase for both series I and II. The general trend in Figure 6-3 (series I beams) shows that the voltage had undergone an initial increase within the first 24 hours, which was followed by a gradual decrease. Given that voltage is directly proportional to resistance when current is

constant (i.e. a decrease in resistance would require a reduction in voltage), it can be concluded that there was mounting electrical resistance initially, followed by a progressive reduction.
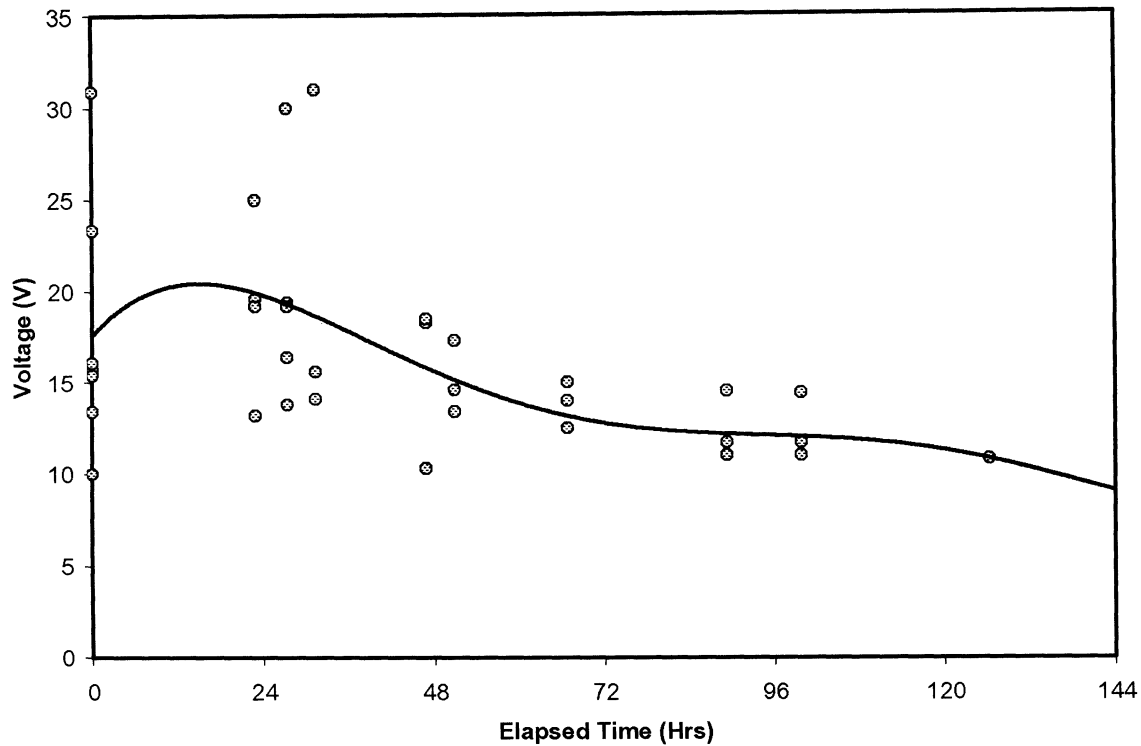
Figure 6-3: Voltage readings for series I beam specimens..

Figure 6-4 on the other hand, tells an incomplete story. Although this plot also shows a decreasing trend, the initial increase is absent. The reason for this difference in behaviour is that the power supplies used was limited to providing a maximum output of 31 volts, which is evident by the numerous readings at this threshold. This capping of the voltage not only eliminated the initial increasing trend that is clearly observed in Figure 6-3, but it also disabled some of the beams in series II from receiving the full 3 mA/cm^2 within the first 96 hours.
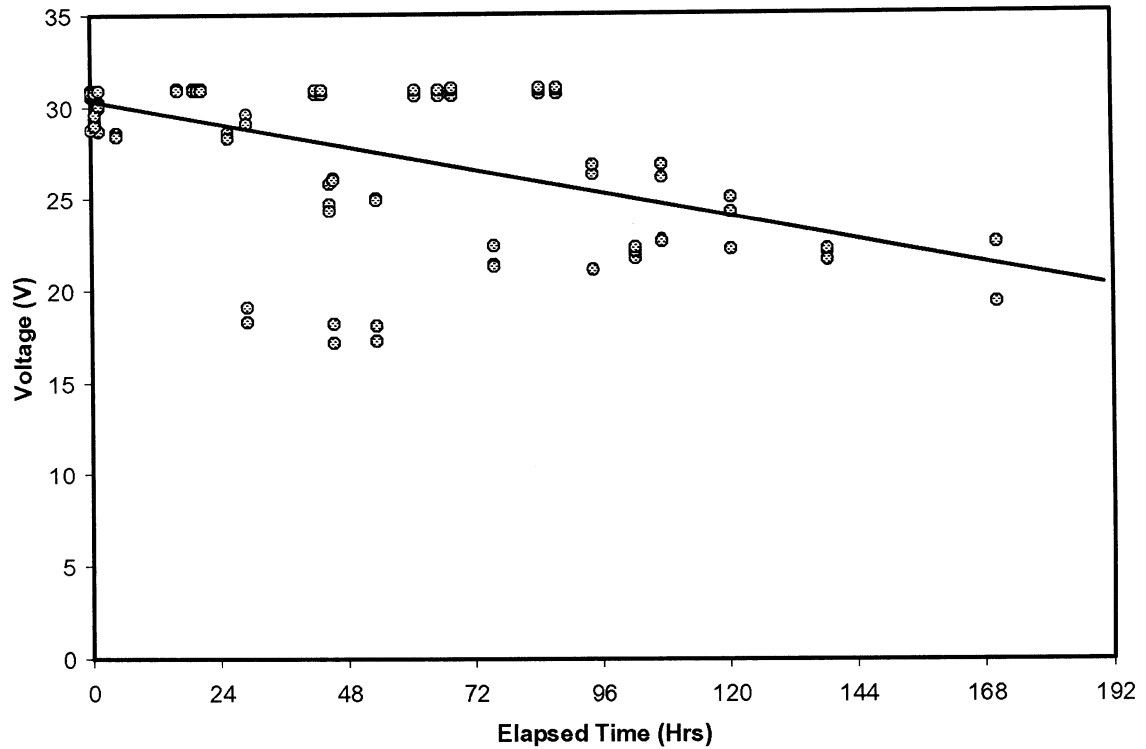
Figure 6-4: Voltage readings for series II beam specimens.

The six readings in Figure 6-4 that hover below the sample population are of BS10 and these uncharacteristically low voltages are due to faulty insulation of the electrical connection within the electrolyte solution. This resulted in a 'short' of the electrical circuit and lowered the voltage required to maintain a constant current flow.

Figure 6-5 is a prime example of the diminishing of the current caused by the limitations of the power supply. This graph shows both the voltage and current readings with respect to time for rebar BS11-L; the letters 'V' and 'A' following the rebar name denote voltage and current respectively.

71
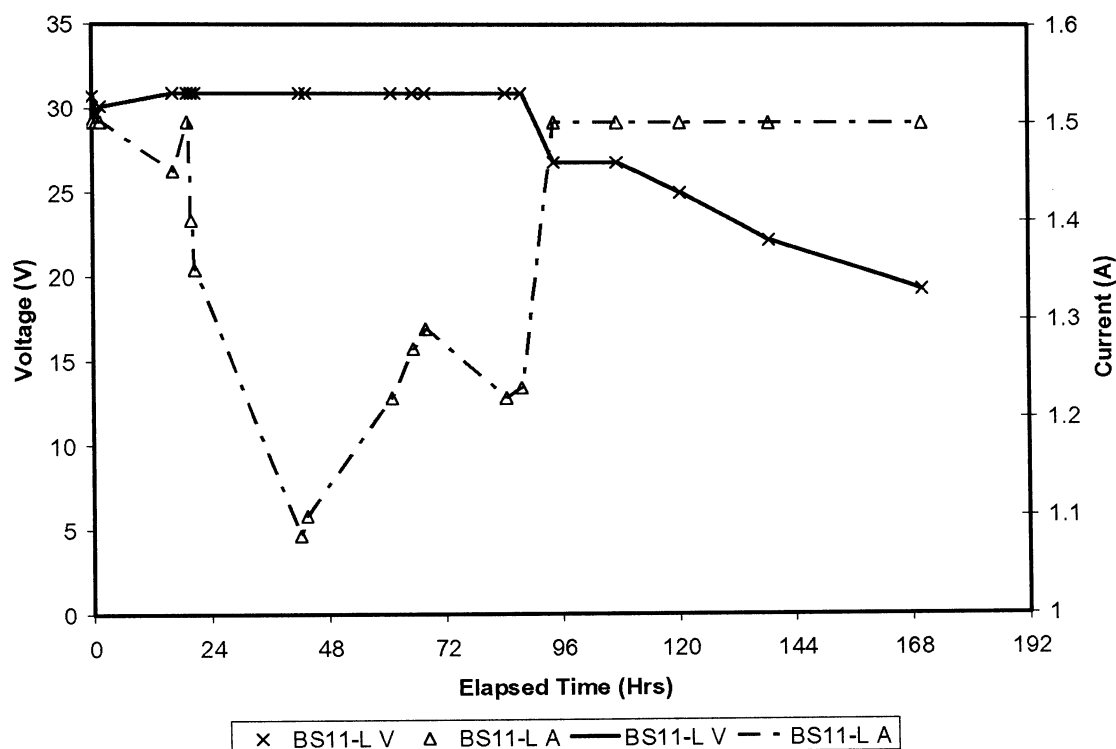
Figure 6-5: Voltage and current readings for BS11-L.

Both the increase in the voltage observed for series I and the reduction in the current observed for series II are due to the fluctuation of resistance in the system. It is clear from these observations that there is an initial increase of resistance within the system, which is followed by a decreasing trend. This phenomenon can be attributed to the initial build up of corrosion products that occupy the pores of the concrete, thus blocking the movement of ions and increasing the electrical resistance. Eventually, the tensile stresses developed within the concrete caused by the expanding corrosion products crack the concrete, making a corridor for the transport of ions and escaping corrosion products, which results in the subsiding of resistance.

The voltage readings from the pullout specimens show this trend more clearly, as seen in Figure 6-6. The reason for this clarity is that this type of specimen has only one rebar embedded within it and thus there are no resistance fluctuations due to stray current.
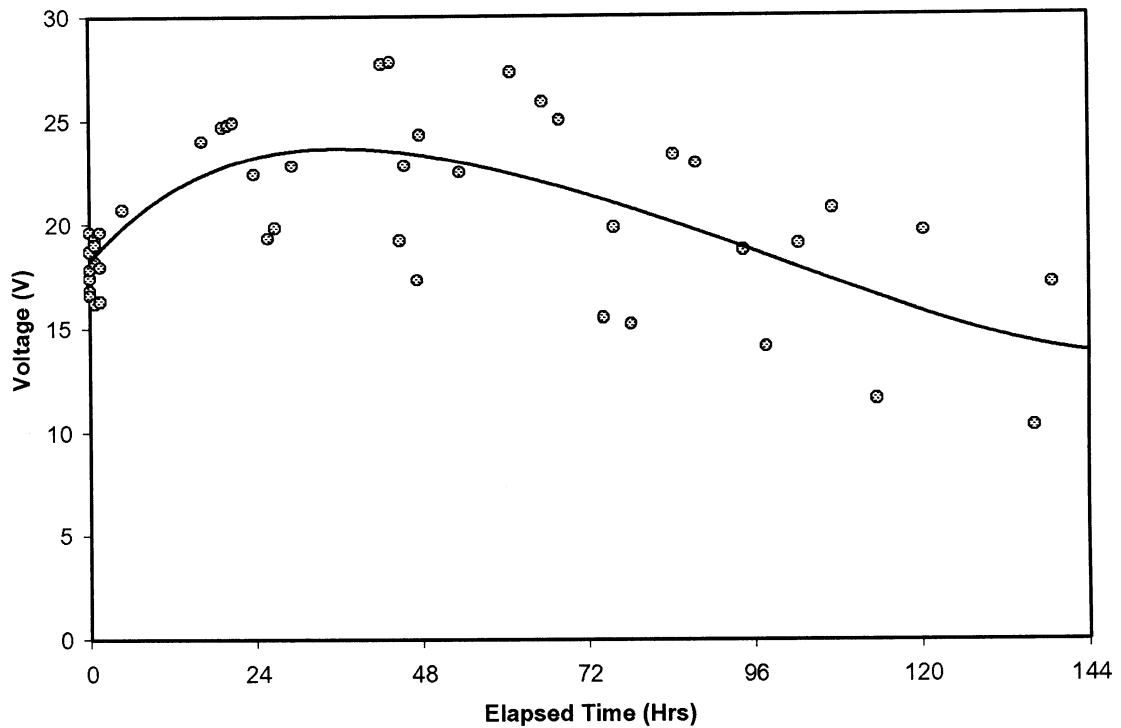
Figure 6-6: Voltage readings for pullout specimens.

6.3.2 Crack Development

Observations from the accelerated corrosion program revealed that for series II, the evolution of corrosion crack width followed a linear progression with respect to time, as shown in Figure 6-7. The crack width growth rate for these beams was measured at 5.4 μm/hr.
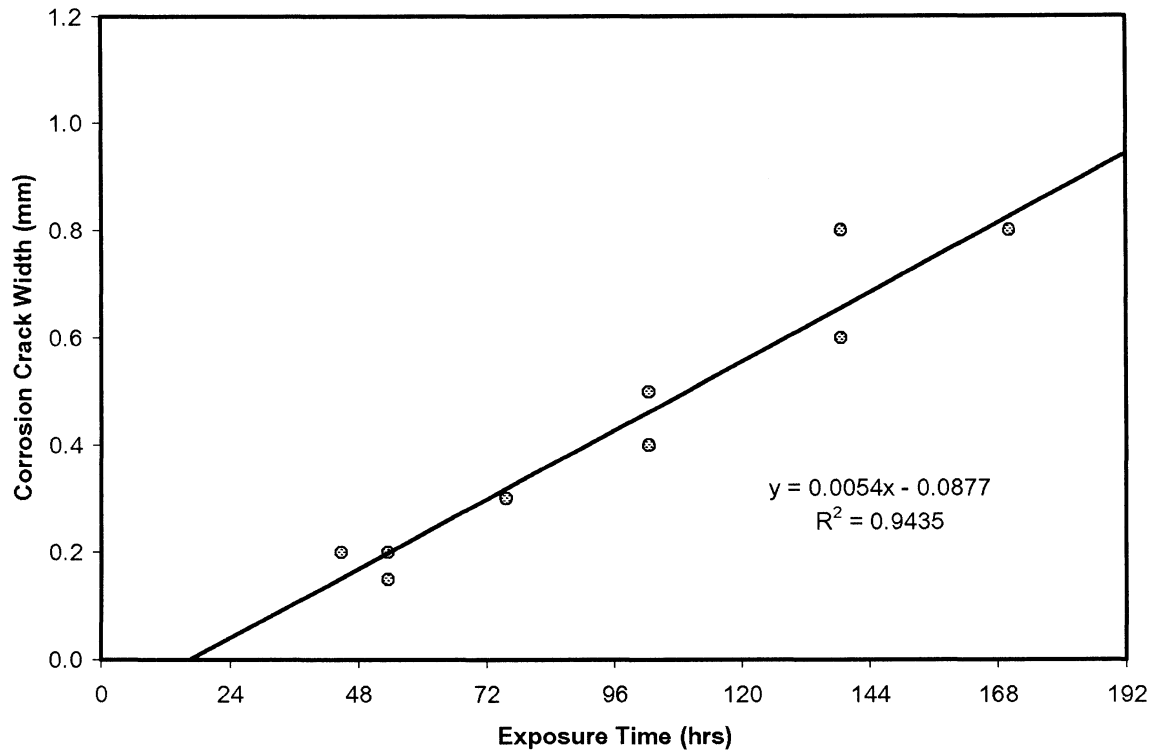
Figure 6-7: Evolution of corrosion crack width for series II beam specimens.

On the other hand, the crack width measurements observed for series I specimens were quite scattered, showing large residual errors when linearly regressed. This is due to the variability of corrosion location and propagation inherent with stray current corrosion. Nevertheless, a corrosion-crack expansion rate of approximately 2.4 μm/hr was estimated.

Since the current density applied to all of the beams was constant, the difference in the above rates can be explained in terms of the area of steel corroded. The entire reinforcing cage for series I was submerged in the electrolyte solution, and thus the area of the steel corroded was greater, which in turn reduced the rate of corrosion.

6.3.3 Corrosion Crack Survey

Following the removal of the beams from the corrosion tank, corrosion crack maps were drawn. These maps are presented in Appendix B where they show the location and width in mm for all visible surface corrosion cracks. For each figure, corrosion cracks are identified by a dotted line, and the beam faces illustrated (starting from the top) are right face, bottom face, and left face. An example corrosion crack survey is shown in Figure 6-8.
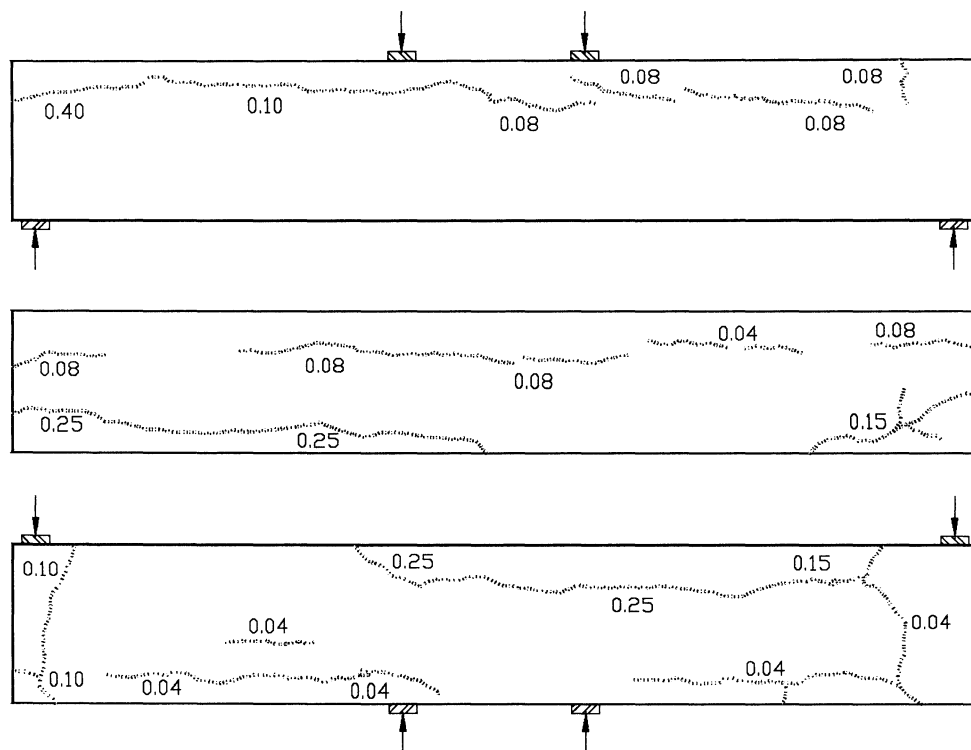
Figure 6-8: Example corrosion crack survey.

According to the convention outlined in Figure 5-2, the edge on the left hand side of the representations is the *front* face; this is where the electrical connection was provided. It should also be noted that BS01, BS02, and BS04 are intentionally excluded from the figures in Appendix B, as BS01 and BS02 were not corroded and BS04 was in the pre-cracking stage after the completion of the accelerated corrosion.

6.4 Non-Destructive Testing

Following the accelerated corrosion stage, the beam specimens were allowed to dry for one week before they were non-destructively tested. The results of the half-cell potential and pulse velocity tests are presented below.

6.4.1 Half-Cell Potential Readings

Half-cell potential readings were taken every 100 mm along the tensile reinforcement on the bottom and the two side faces of each beam specimen (as shown in Figure 5-14), giving a total of 44 readings per beam. These readings for all twelve beams are provided in Appendix C with an example shown in Figure 6-9. The half-cell potential readings are divided into seven categories, as shown in Table 6-2. These categories range from "A" to "G", where "A" and "G" represent the highest and the lowest risk of corrosion respectively. This system of designation allowed for more contrast and clarity when analyzing the potential readings.

RIGHT | D   D   C   C   C   D   D   D   C   D   D | RIGHT
BOTTOM | D   D   D   D   D   D   D   D   D   D   D | BOTTOM
 | C   C   C   C   C   B   C   C   C   C   C |
LEFT | C   B   B   B   B   B   B   C   C   C   C | LEFT
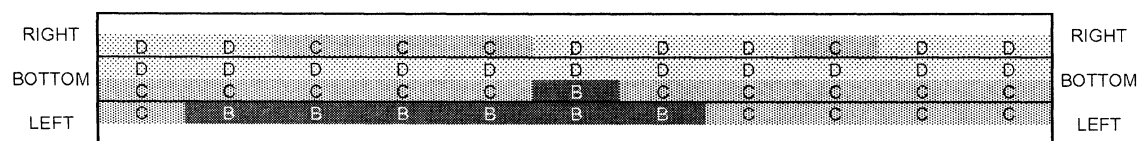
Figure 6-9: Example half-cell potential survey.

Table 6-2: Classification of half-cell potentials.

Designation	Readings Less Than	Legend
A	-0.42 mV	
B	-0.35 mV	
C	-0.28 mV	
D	-0.21 mV	
E	-0.14 mV	
F	-0.07 mV	
G	0.00 mV	

Figure 6-10 graphs the average half-cell potential reading for each beam and Table 6-3 lists these values along with the corrosion condition, according to ASTM 876 (provided in Table 5-5). The half-cell potentials were as expected, yielding increasing negative values with more severely corroded elements.
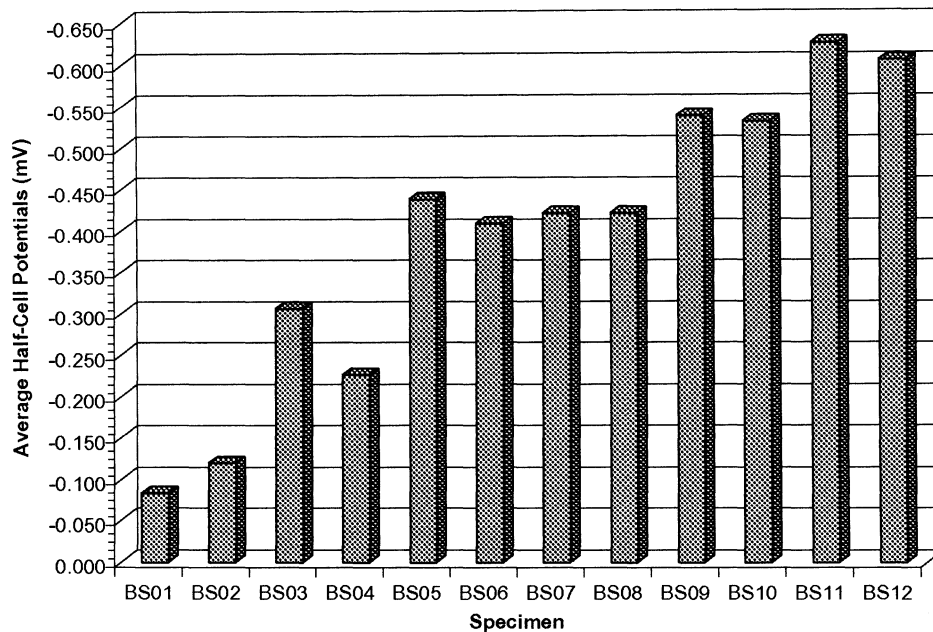
Figure 6-10: Average half-cell potential readings for beam specimens.

Table 6-3: Summary of half-cell potential readings.

Specimen	Avg. HCP Reading (mV)	Category	Corrosion Condition	Total Mass Loss (%)
BS01	-0.083	F	Low: 10% Risk of Corrosion	0.00%
BS02	-0.120	F	Low: 10% Risk of Corrosion	0.00%
BS03	-0.306	C	Intermediate Corrosion Risk	0.00%
BS04	-0.227	D	Intermediate Corrosion Risk	0.25%
BS05	-0.438	A	High: 90% Risk of Corrosion	1.13%
BS06	-0.409	B	High: 90% Risk of Corrosion	3.03%
BS07	-0.422	A	High: 90% Risk of Corrosion	2.45%
BS08	-0.422	A	High: 90% Risk of Corrosion	0.89%
BS09	-0.540	A	Severe Corrosion	7.14%
BS10	-0.532	A	Severe Corrosion	5.15%
BS11	-0.626	A	Severe Corrosion	11.56%
BS12	-0.606	A	Severe Corrosion	10.25%

Avg. = Average
HCP. = Half-Cell Potential

Interestingly, the half-cell potentials for those beams of series I and II that were exposed to the same current for approximately the same amount of time are noticeably different. Specifically, series I beams BS03 and BS04 were exposed to 46.75 hours of corrosion, while series II beams BS07 and BS08 were exposed to 44.75 hours of corrosion, and yet the latter showed a higher corrosion potential. Figure 6-11 and Figure 6-12 are frequency diagrams of the half-cell potential readings for these beams. Since all of the beams were identical and the impressed current was the same, it can be deduced that the different corrosion potentials are a direct result of the configuration of the corrosion setup. Figure 6-11 and Figure 6-12 illustrate that the potential for corrosion was much lower for series I, implying that the rate of corrosion was lower and supporting the notion of stray current occurrence.
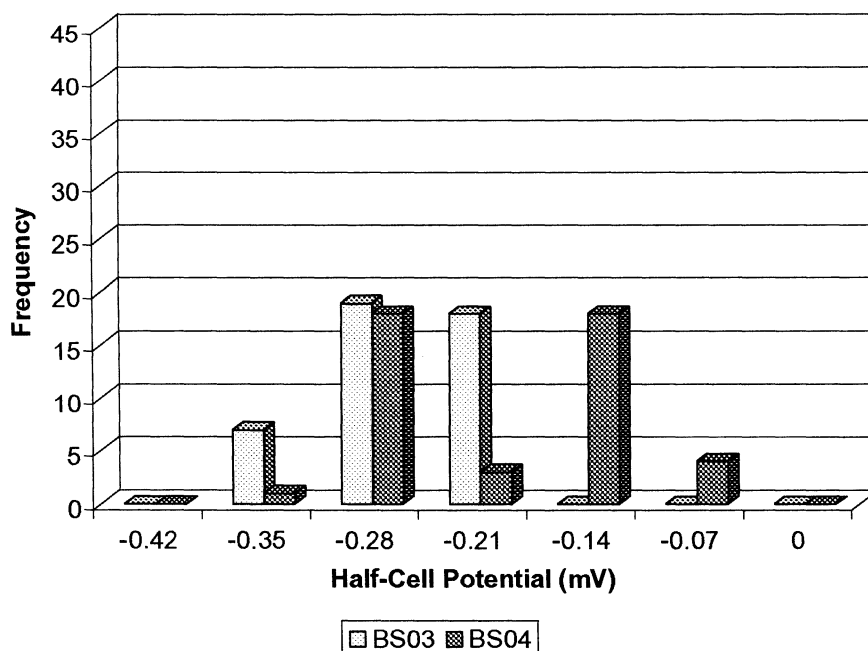
Figure 6-11: Frequency diagram of the half-cell potential readings for BS03 and BS04.

45
40
35
30
25
20
15
10
5
0

Frequency

-0.42   -0.35   -0.28   -0.21   -0.14   -0.07   0

Half-Cell Potential (mV)

BS07 BS08
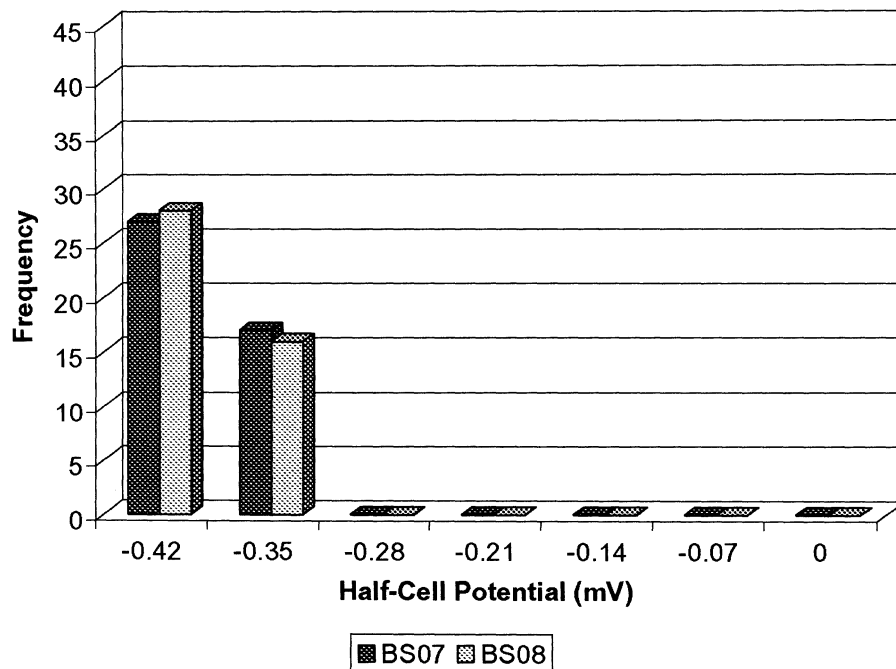
Figure 6-12: Frequency diagram of the half-cell potential readings of BS07 and BS08.

6.4.2 Ultrasonic Pulse Velocity Readings

Table 6-4 provides the ultrasonic pulse velocity readings for each beam specimen, where the x-axis is the horizontal width and the y-axis is the vertical height (see Figure 5-11 for schematic of test locations). This method, which is described in ASTM C 597-02, provides an indication of the state of concrete deterioration by detecting changes in the concrete matrix such as internal cracking. The average pulse velocities for each beam with respect to corrosion time are summarized in Figure 6-13.

These results showed a difference between the pulse velocities of series I and series II specimens. There was a reduction in the average pulse velocities for the series I beams, particularly in the case of specimens BS05 and BS06, which were the most corroded. This is due to the increased concrete cracking from the corrosion that was induced in both the stirrups and tensile reinforcement.

Table 6-4: Ultrasonic pulse velocity readings.

Specimen	Time (μsec)		Distance (mm)		Velocity (km/sec)		Average Velocity (km/sec)	Total Mass Loss (%)
	x-axis	y-axis	x-axis	y-axis	x-axis	y-axis		
BS01	33.9	37.9	156	176	4.602	4.644	4.623	0.00%
BS02	33.1	37.7	156	176	4.713	4.668	4.691	0.00%
BS03	33.9	37.9	156	176	4.602	4.644	4.623	0.00%
BS04	34.1	38.1	156	176	4.575	4.619	4.597	0.25%
BS05	38.2	41.3	156	176	4.084	4.262	4.173	1.13%
BS06	38.0	42.5	156	176	4.105	4.141	4.123	3.03%
BS07	36.6	39.4	156	176	4.262	4.467	4.365	2.45%
BS08	37.2	40.2	156	176	4.194	4.378	4.286	0.89%
BS09	36.5	38.1	156	176	4.274	4.619	4.447	7.14%
BS10	36.5	39.6	156	176	4.274	4.444	4.359	5.15%
BS11	38.2	39.3	156	176	4.084	4.478	4.281	11.56%
BS12	36.2	39.0	156	176	4.309	4.513	4.411	10.25%
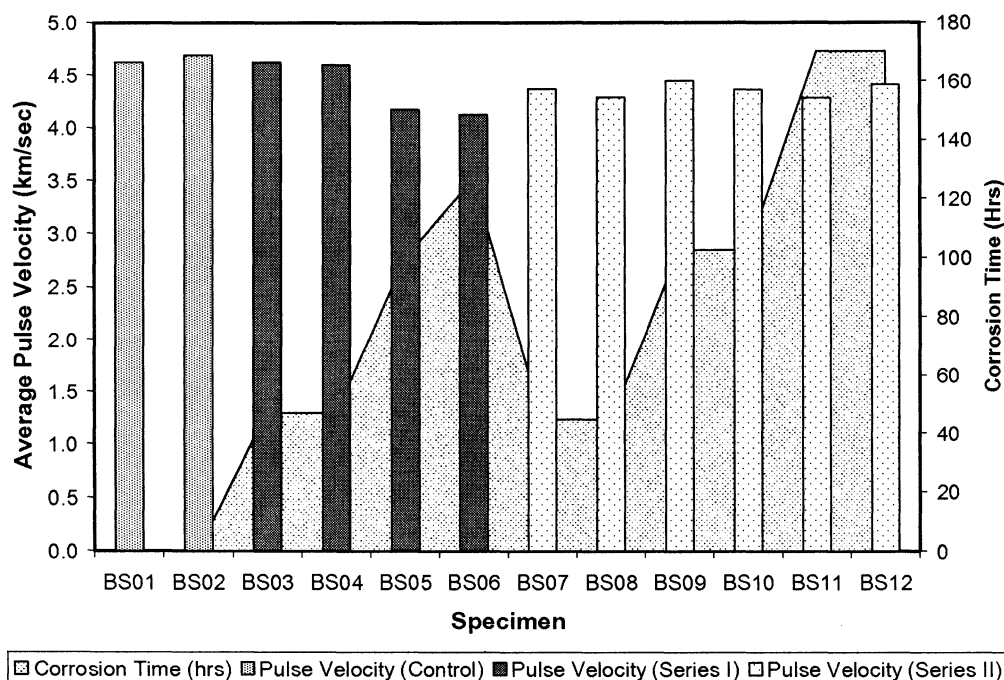
Figure 6-13: Average ultrasonic pulse velocities.

In contrast, while the pulse velocity readings of the series II beam specimens (BS07 to BS12) were all reduced when compared to the control beams, there was no decreasing trend with increasing corrosion time as with series I. This can be explained by the fact that the series II beams had considerably more chlorides deposited above the water line, where the pulse velocities were measured. Since salt is hydroscopic, it can be speculated that the local

moisture content was slightly higher, causing an increase in the pulse velocity and a longer corrosion time resulted in the accumulation of more salt.

6.5 Beam Tests

After the non-destructive testing was completed, the beams were loaded in four-point bending until failure (see Figure 5-15 for set-up details) and the corresponding load and mid-span deflections were measured.

It is very important to note that the frame used to test the beam specimens proved defective midway through the experiment, requiring that the test be relocated to a second frame for the remaining beams. The problem resulted from the buckling of the I-beam above the hydraulic piston used to apply the load, which skewed the direction of the load. This misalignment of the load was discovered after the control specimen BS02 failed in shear (as shown by the flexural crack survey in Appendix F), which prompted an investigation into the behaviour. It was found that the applied load was slightly rotated towards the front face and the misalignment got progressively worse with increasing load.

Due to this discovery, the results of the beams tested under these conditions were deemed as compromised and unreliable. Consequently, the beam test results of BS02 and all of the series I beams (BS03 to BS06) have been excluded from the report and will not be discussed in the analysis section.

6.5.1 Load-Carrying Capacity

Table 6-5 summarizes the results of the beam tests that are discussed in this report. This table lists the ultimate load (P) that each beam was able to support, along with the

corresponding relative capacity, initial cracking load, and deflection capacity (or mid-span deflection). In this study, a decrease in deflection capacity is regarded as an indication of reduced ductility.

Table 6-5: Summary of beam tests.

Specimen	Ultimate Load, P (kN)	Relative Capacity (%)	Initial Crack, P (kN)*	Deflection Capacity (mm)	Total Mass Loss (%)
BS01	140.25	100.00%	35	4.39	0.00%
BS07	117.40	83.70%	30	3.72	2.45%
BS08	115.86	82.61%	30	3.50	0.89%
BS09	100.81	71.88%	30	3.17	7.14%
BS10	101.27	72.21%	30	3.15	5.15%
BS11	96.47	68.78%	40	3.07	11.56%
BS12	96.08	68.51%	40	3.08	10.25%

* = Approximate Value

As expected, the beam tests show a reduction in both the load-carrying capacity and the deflection capacity with this increase in corrosion level. This is due to the known effects of reductions in steel-concrete bond, reinforcing steel cross-sectional area, and concrete contribution.

6.5.2 Load-Deflection Behaviour

Load-deflection curves (LDCs) reveal much information concerning the behaviour of RC beams and they are notably altered with the progression of corrosion. As predicted, results show that a higher corrosion level results in decreased stiffness, increased deflection and reduced ultimate load. The ultimate deflections, however, were reduced with increasing corrosion. These phenomena are a result of the combination of the deteriorated bond between the steel and the concrete, the reduction in the cross-sectional area of the reinforcing steel, and the cracking and delamination of the concrete.

The load-deflection curves for BS01 and BS07 to BS12 are depicted in Figure 6-14. These load-deflection plots are generalized, showing the linear trend until the yielding of the tensile steel in the case for BS01 or failure for all of the corroded beams.

The slope of the LDC before failure or the yielding of the reinforcing steel can indicate the stiffness of RC beams, while the area under the LDC can indicate the toughness or absorbed energy. The calculated slopes and areas of the above LDCs are summarized in Table 6-6.

The slope of a line is given by m, when the equation of a line is in the slope-intercept form $(y = mx + b)$. The slope of the LDCs was determined by m of the equation of the straight-line portion of each LDC, in the section of the curve before the yielding of the reinforcing steel or the collapse of the beam, whichever came first. The area under the LDC was obtained by finding the definite integral of the best fitting trend line(s) of the LDC. Appendix D shows the trend lines of the LDCs for beam specimens BS01 and BS07 to BS12. These plots also give the equations of the trend lines and the deflection values used to calculate the area under the curve.

The slope of the LDC, the area under the LDC and the deflection capacity all decrease with increased corrosion intensity, implying a reduction in the stiffness, toughness and ductility. These reductions suggest a rise in brittleness, which is precisely what was observed during the beam tests performed for this study.
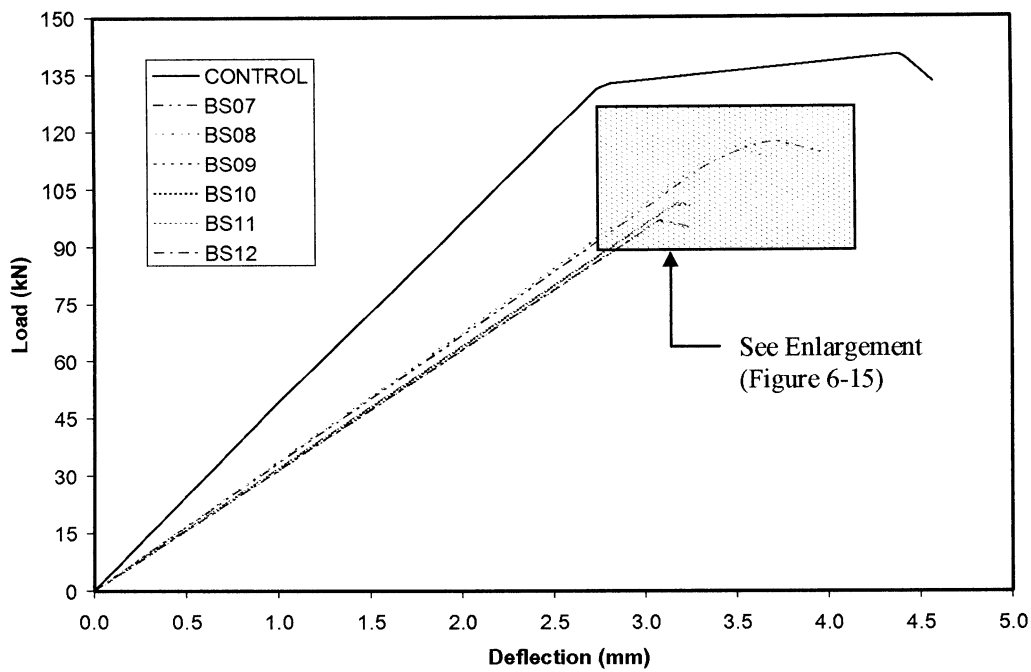
Figure 6-14: Load-deflection behaviour for series II beam specimens.
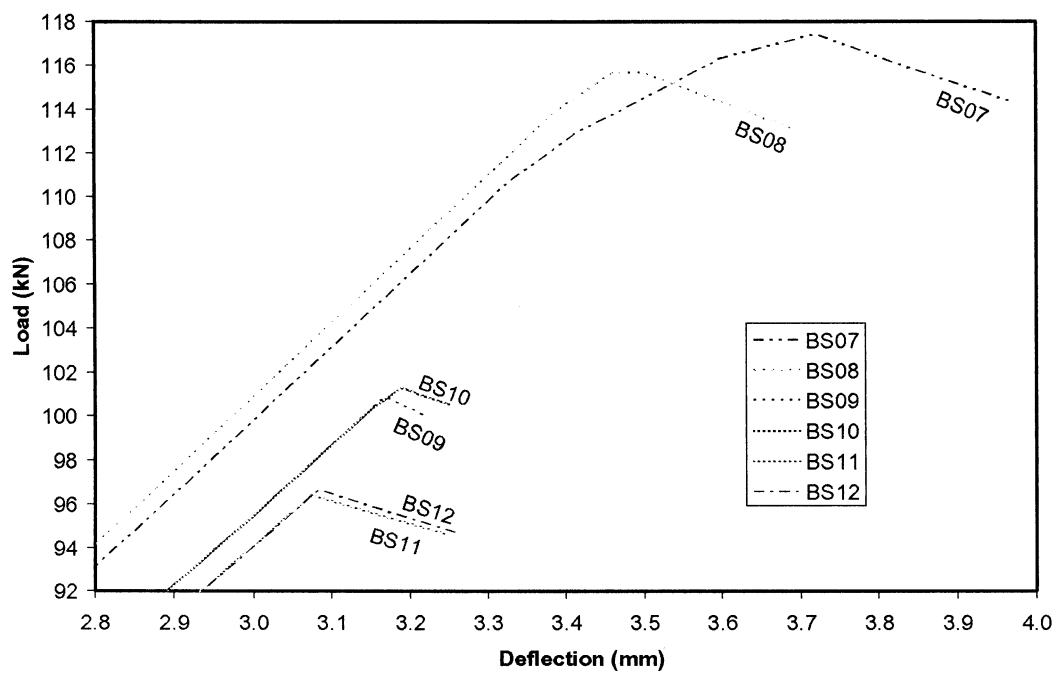
Figure 6-15: Enlargement of highlighted area in Figure 6-14.

Table 6-6: Slopes and areas of the load-deflection curves.

Specimen	Slope of LDC	Relative Slope of LDC (%)	AU LDC (kN·mm)	Relative AU LDC (%)	Total Mass Loss (%)
BS01	47.07	100.00%	402.74	100.00%	0.00%
BS07	33.26	70.66%	229.06	56.88%	2.45%
BS08	33.62	71.42%	205.69	51.07%	0.89%
BS09	31.83	67.62%	159.99	39.73%	7.14%
BS10	31.82	67.60%	158.00	39.23%	5.15%
BS11	31.36	66.63%	148.21	36.80%	11.56%
BS12	31.35	66.60%	149.01	37.00%	10.25%

AU = Area Under
LDC = Load-Deflection Curve

As corrosion increased, the failure mode of the beams shifted from predictable ductile flexure failures at mid-span, to more brittle bond-shear failures near the support. Severely corroded beams displayed extremely brittle failures at the support, with no forewarning and only one primary fracture line.

Photographs of the failure zone of each beam specimen were taken immediately after the beam tests and are shown in Appendix E. Figure E-1 depicts the failure zone for the control beam BS01, which experienced a balanced flexural failure with yielding of the reinforcement and crushing of the concrete. Figure E-2 illustrates the failure zone for the control beam BS02, which experienced an unexpected shear failure due to a faulty test frame that transferred a disproportionate load to one side of the beam.

The pictures in Figure E-3 to Figure E-6 portray the failure zones for series I beam specimens BS03 to BS06. Although these beams were all tested in the faulty test frame and thus their results have been excluded, the photographs are still presented since they show an evolution of the failure mode. Series II beam specimens BS07 to BS12, on the other hand, experienced no such complications during beam testing and their results are discussed in the analysis section. The failure zones for these beams are pictured in Figure E-7 to Figure E-12.

6.6 Post-Test Examinations

Following the completion of the beam tests, a second crack survey was conducted and the actual mass loss of the reinforcing steel due to corrosion was determined.

6.6.1 Flexural Crack Survey

While the first crack survey documented corrosion cracks that resulted from the accelerated corrosion stage, this second survey recorded flexural cracks that developed due to the mechanical testing. These flexural crack maps are provided in Appendix F, and Figure 6-16 is an example. The faces illustrated in these crack maps (starting from the top) are right, bottom, and left. Therefore, according to the convention outlined in Figure 5-2, the edge on the left hand side of the representations is the front face; this is where the electrical connection was made. The numbers on the right face indicate the maximum width of each flexural crack before failure. Figure F-1 is a legend distinguishing each crack type.
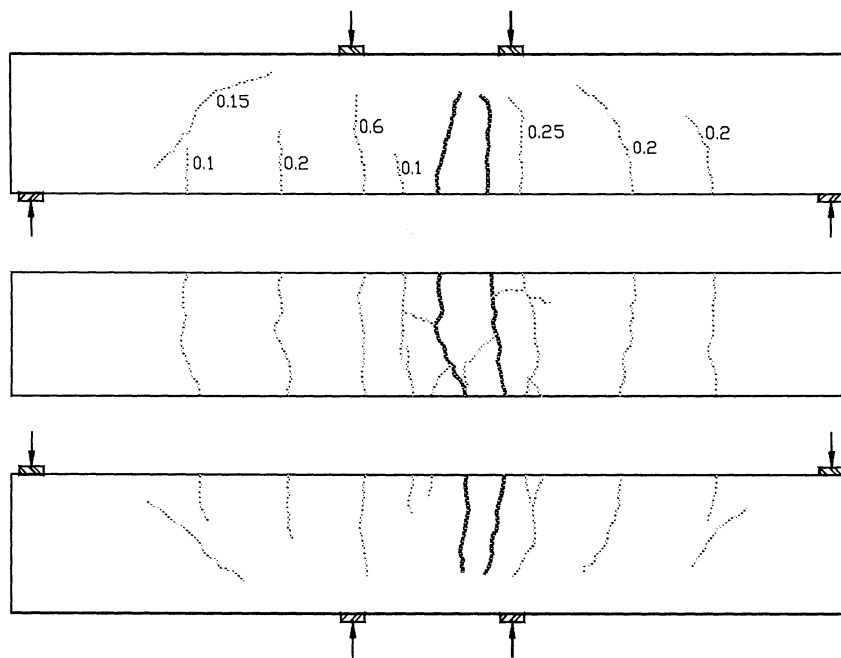
Figure 6-16: Example flexural crack survey.

6.6.2 Flexure Crack Development

The crack survey discussed above was used to study flexural crack development. Specifically, the average number and the average spacing of transverse flexural cracks were both considered. For example, in Figure 6-17 showing the right face of BS11, there are four flexural cracks and the average crack spacing in millimetres is equal to: (132+89+140)/3. This procedure was carried out for both the left and right faces of each beam, referencing the cracks from the bottom edge of these faces between the supports. Table 6-7 summarizes the average number and the average spacing of these cracks for beam specimens BS01 and BS07 to BS12.
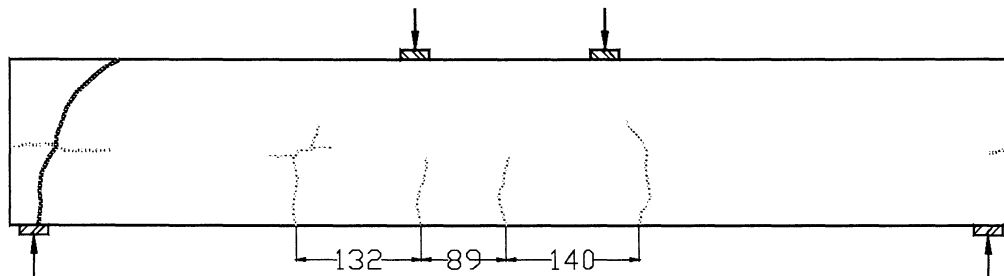
Figure 6-17: Typical flexural crack study.

Table 6-7: Flexural crack patterns.

Specimen	Avg. No. of Cracks	Rel. No. of Cracks (%)	Avg. Crack Spacing (mm)	Rel. Crack Spacing (%)	Total Mass Loss (%)
BS01	10.0	100%	72.4	100%	0.00%
BS07	5.5	55%	137.6	190%	2.45%
BS08	5.5	55%	134.7	186%	0.89%
BS09	4.5	45%	159.4	220%	7.14%
BS10	5.0	50%	167.8	232%	5.15%
BS11	4.0	40%	138.7	191%	11.56%
BS12	3.5	35%	169.4	234%	10.25%

Avg. = Average
Rel. = Relative
No. = Number

6.6.3 Mass Loss Determination

Following the mechanical testing, the beams were pulverised with a jackhammer to retrieve the reinforcing steel. Once obtained, the tensile bars were trimmed to a standard length of 1 metre, cleaned to remove all corrosion products and concrete, and then weighed. The mass loss was then calculated relative to a predetermined benchmark called the control mass.

Table 6-8: Samples used to calculate the control mass.

Bar	Mass (g)
Sample 1	1542.93
Sample 2	1548.05
Sample 3	1540.11
Sample 4	1540.95
Sample 5	1540.15
Sample 6	1548.31
Average	**1543.42**

Table 6-9: Mass loss calculation for each corroded bar.

Bar	Mass	Mass Loss (g)	% Mass Loss
BS03-R	1545.03	0.00	0.00%
BS03-L	1548.88	0.00	0.00%
BS04-R	1539.57	3.85	0.25%
BS04-L	1553.75	0.00	0.00%
BS05-R	1531.23	12.19	0.79%
BS05-L	1538.23	5.19	0.34%
BS06-R	1537.17	6.25	0.40%
BS06-L	1502.93	40.49	2.62%
BS07-R	1513.86	29.56	1.92%
BS07-L	1535.20	8.22	0.53%
BS08-R	1536.28	7.14	0.46%
BS08-L	1536.84	6.58	0.43%
BS09-R	1488.94	54.48	3.53%
BS09-L	1487.68	55.74	3.61%
BS10-R	1485.29	58.13	3.77%
BS10-L	1522.10	21.32	1.38%
BS11-R	1474.46	68.96	4.47%
BS11-L	1433.98	109.44	7.09%
BS12-R	1475.21	68.21	4.42%
BS12-L	1453.49	89.93	5.83%

The control mass was calculated by taking the average of six un-corroded (1 metre) sample bars, as shown in Table 6-8. Table 6-9 lists the mass for each corroded tensile bar and its corresponding relative mass loss. Next, the average and the total mass losses of the left and right bars were calculated for each beam specimen. These values are found in Table 6-10.

Table 6-10: Average and total mass loss for beam specimens.

Specimen	Average Mass Loss (%)	Total Mass Loss (%)
BS03	0.00%	0.00%
BS04	0.12%	0.25%
BS05	0.56%	1.13%
BS06	1.51%	3.03%
BS07	1.22%	2.45%
BS08	0.44%	0.89%
BS09	3.57%	7.14%
BS10	2.57%	5.15%
BS11	5.78%	11.56%
BS12	5.12%	10.25%

6.6.4 Corrosion Damage to Tensile Reinforcement

The type of corrosion found in the more severely corroded bars can be classified as generalized. It was observed that corrosion of the steel typically started with the formation of pits that increased in number and expanded until they eventually connected, resulting in generalized corrosion. This progression of rebar deterioration is depicted in Figure 6-18. According to Broomfield (1997), this sequence is characteristic of reinforcing bars exposed to carbonation or chlorides.
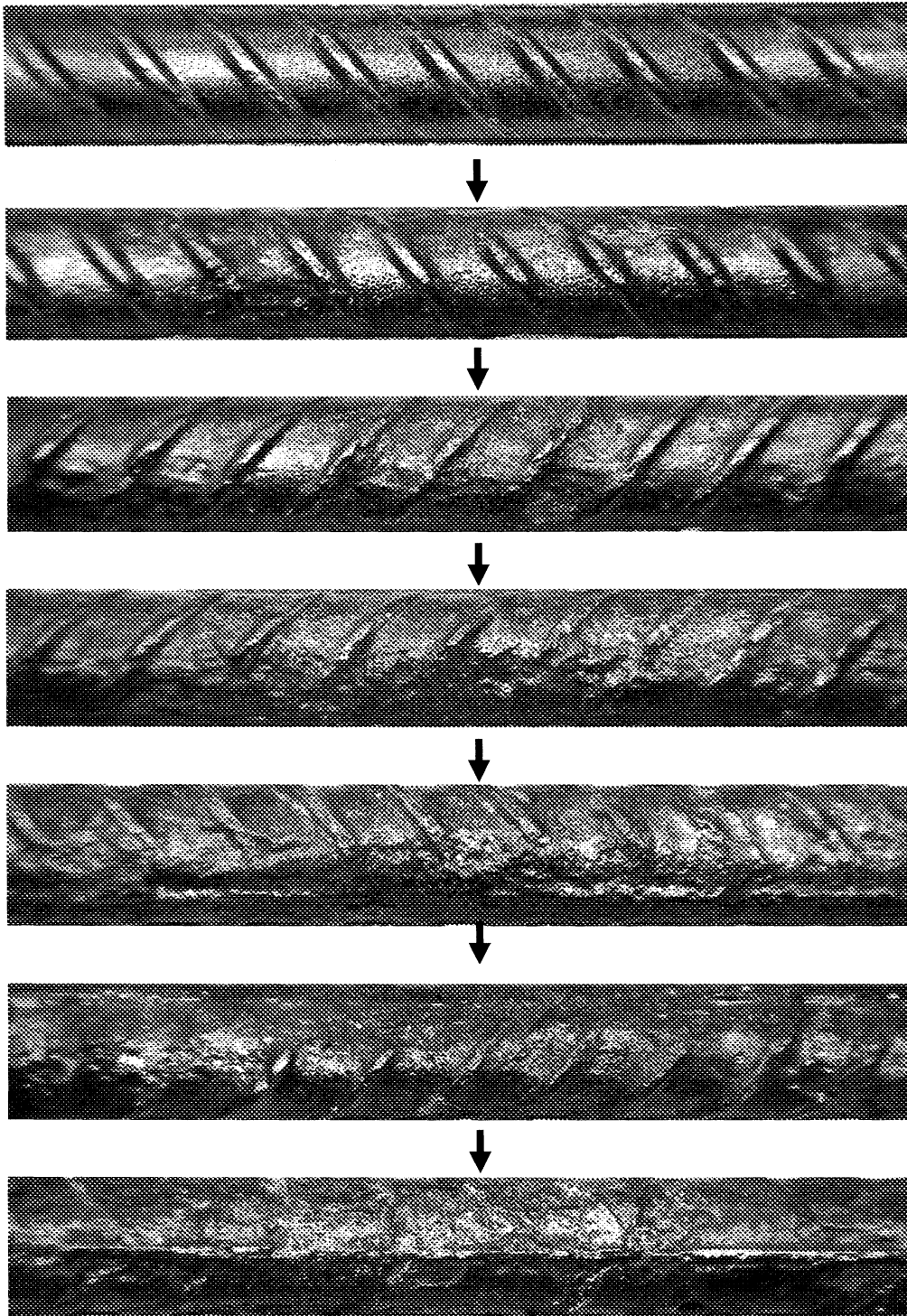
Figure 6-18: Diagram of the progression of rebar deterioration.

6.7 Pullout Study

As mentioned previously, twelve pullout specimens (PS) were constructed, corroded, and tested in order to determine the relationship between bond strength and the capacity of corroded RC beams.

6.7.1 Half-cell potentials

After the pullout specimens were corroded, the half-cell potentials were measured in two locations and averaged. These averages are shown in Table 6-11 along with the category of each specimen (as prescribed in Table 6-2) and the corrosion condition (according to ASTM 876's criteria provided in Table 5-5).

Table 6-11: Average half-cell potentials and categories for pullout specimens (mV = millivolts).

Specimen	Avg. HCP Reading (mV)	Category	Corrosion Condition	Total Mass Loss (%)
PS01	-0.158	E	Low: 10% Risk of Corrosion	0.00%
PS02	-0.144	E	Low: 10% Risk of Corrosion	0.00%
PS03	-0.279	D	Intermediate Corrosion Risk	0.00%
PS04	-0.256	D	Intermediate Corrosion Risk	0.25%
PS05	-0.261	D	Intermediate Corrosion Risk	1.13%
PS06	-0.278	D	Intermediate Corrosion Risk	3.03%
PS07	-0.178	E	Intermediate Corrosion Risk	2.45%
PS08	-0.151	E	Intermediate Corrosion Risk	0.89%
PS09	-0.298	C	Intermediate Corrosion Risk	7.14%
PS10	-0.301	C	High: 90% Risk of Corrosion	5.15%
PS11	-0.354	B	High: 90% Risk of Corrosion	11.56%
PS12	-0.394	B	High: 90% Risk of Corrosion	10.25%

Avg. = Average
HCP. = Half-Cell Potential

6.7.2 Average Bond Stress

The results of the pullout tests are provided in Table 6-12. The maximum load that each specimen was able to withstand before the pulling out of the reinforcing steel was used in

Equation 5-1 to calculate the ultimate bond stress developed. The relative bond stress was then calculated using the average bond stress between PS01 and PS02.

Table 6-12: Results of the pullout test.

Pullout Specimen	Load (kN)	Bond Stress (Mpa)	Relative Bond Sress	Mass Loss (%)
PS01	58.83	5.85	100.00%	0.00%
PS02	55.64	5.53	100.00%	0.00%
PS03	44.81	4.46	78.33%	0.84%
PS04	36.98	3.68	64.64%	1.06%
PS05	24.64	2.45	43.08%	7.11%
PS06	29.52	2.94	51.60%	4.89%
PS07	46.63	5.87	103.13%	0.24%
PS08	64.00	8.06	141.54%	0.38%
PS09	30.18	3.00	52.75%	2.08%
PS10	36.01	3.58	62.96%	3.51%
PS11	26.80	2.67	46.85%	7.09%
PS12	30.55	3.04	53.41%	7.27%

6.7.3 Mass Loss

Once the mechanical testing of the pullout specimens was completed, the bars were cleaned of any remaining concrete and corrosion products, trimmed to a standard length and weighed. The percent mass loss for each of the 12 bars was then calculated using Equation 5-6, the results of which are given in Table 6-13. The average weight of the PS01 and PS02 bars provided the control mass.

Table 6-13: Total mass loss for pullout specimens.

Pullout Specimen	Mass (g)	Mass Loss (%)
PS01	303.01	0.00%
PS02	303.62	0.00%
PS03	300.78	0.84%
PS04	300.11	1.06%
PS05	281.74	7.11%
PS06	288.49	4.89%
PS07	302.59	0.24%
PS08	302.15	0.38%
PS09	297.00	2.08%
PS10	292.67	3.51%
PS11	281.82	7.09%
PS12	281.26	7.27%

6.8   Summary of Results

The results of the experimental program employed for this study are summarized in Table 6-14. The upper portion of this table is dedicated to the beam specimens, while the lower portion pertains to the pullout specimens. As previously indicated, beam test results for specimens BS02 to BS06 have been excluded due to a faulty test frame.

Table 6-14: Results of the experimental program.

	Phenomena	01	02	03	04	05	06	07	08	09	10	11	12
	Specimen Number												
Beam Specimens (BS)	Ultimate Load (kN)	140.25		Results Disregarded				117.40	115.86	100.81	101.27	96.47	96.08
	Relative Capacity	100%						83.7%	82.6%	71.9%	72.2%	68.8%	68.5%
	Initial Crack Load (kN)*	35						30	30	30	30	40	40
	Avg Number of Cracks	10.0						5.5	5.5	4.5	5.0	4.0	3.5
	Relative Number of Cracks	100%						55.0%	55.0%	45.0%	50.0%	40.0%	35.0%
	Avg Crack Spacing (mm)	72.4						137.6	134.7	159.4	167.8	138.7	169.4
	Relative Crack Spacing	100%						190%	186%	220%	232%	191%	234%
	Slope of LDC	47.07						33.26	33.62	31.83	31.82	31.36	31.35
	Relative Stiffness	100%						70.7%	71.4%	67.6%	67.6%	66.6%	66.6%
	Deflection at UL (mm)	4.39						3.72	3.50	3.17	3.15	3.07	3.08
	Relative Ductility	100%						84.7%	79.6%	72.1%	71.7%	70.0%	70.2%
	AU LDC (kN·mm)	402.74						229.06	205.69	159.99	158.00	148.21	149.01
	Relative Toughness	100%						56.9%	51.1%	39.7%	39.2%	36.8%	37.0%
	Average Mass Loss	0.00%	0.00%	0.00%	0.12%	0.56%	1.51%	1.22%	0.44%	3.57%	2.57%	5.78%	5.12%
	Total Mass Loss	0.00%	0.00%	0.00%	0.25%	1.13%	3.03%	2.45%	0.89%	7.14%	5.15%	11.56%	10.25%
	Corrosion Time (hrs)	0.00	0.00	46.75	46.75	99.75	126.25	44.75	44.75	102.50	102.50	170.25	170.25
	Corrosion Crack Width (mm)	0.00	0.00	0.15	0.00	0.25	0.25	0.20	0.25	0.35	0.50	0.60	0.80
	Avg Half Cell Potential (mV)	-0.083	-0.120	-0.306	-0.227	-0.438	-0.409	-0.422	-0.422	-0.540	-0.532	-0.626	-0.606
	Pulse Velocity (km/h)	4.62	4.69	4.62	4.60	4.17	4.12	4.36	4.29	4.45	4.36	4.28	4.41
	Resistivity (kΩ·cm)	13.2	15.0	21.6	20.3	12.4	15.6	18.5	19.9	12.1	11.1	15.7	14.2
Pullout Specimens (PS)	Ultimate Load (kN)	58.83	55.64	44.81	36.98	24.64	29.52	46.63	64.00	30.18	36.01	26.80	30.55
	Bond Stress (Mpa)	5.85	5.53	4.46	3.68	2.45	2.94	5.87	8.06	3.00	3.58	2.67	3.04
	Relative Bond Stress	100%	100%	78.3%	64.6%	43.1%	51.6%	103.1%	141.5%	52.8%	63.0%	46.8%	53.4%
	Mass Loss	0.00%	0.00%	0.84%	1.06%	7.11%	4.89%	0.24%	0.38%	2.08%	3.51%	7.09%	7.27%
	Avg Half Cell Potential (mV)	-0.158	-0.144	-0.279	-0.256	-0.261	-0.278	-0.178	-0.151	-0.298	-0.301	-0.354	-0.394

Avg = Average
LDC = Load Deflection Curve
UL = Ultimate Load
AU = Area Under
* = Approximate Value

94

Chapter 7

ANALYSIS OF RESULTS

7.1 Introduction

This chapter qualitatively and quantitatively discusses the results from the experimental program and focuses on the manner in which progressive corrosion affects reinforced concrete (RC) beams. Specifically, the changes in flexural crack development, mode of failure, stiffness, ductility, toughness, and load-carrying capacity of RC beams are examined.

7.2 Analysis of Half-Cell Potentials

As the half-cell potential test is a qualitative test that indicates the probability of corrosion of the reinforcing steel embedded within the concrete, caution must be exercised when using absolute potential values quantitatively. In fact, several studies have shown that numerous variables can alter absolute half-cell potential values, while keeping the degree of corrosion at the steel surface constant and thus quantitative interpretation based on absolute potential values can be misleading (RILEM TC 154-EMC, 2003; Grimaldi et al., 1986).

Nevertheless, Sarveswaran et al. (2000) used half-cell potentials to develop an empirical relationship for the prediction of section loss in RC beams due to the corrosion of both the main reinforcement bars and the shear links. This empirical relationship was used as part of a methodology to assess the reliability of deteriorated RC beams.

In light of this, while the half-cell potential measurements obtained in this study are not given undue emphasis, they are included in this discussion due to the remarkable correlations found. That is, the average half-cell potentials of the beam specimens related very well to both the total mass loss and the relative beam capacity.
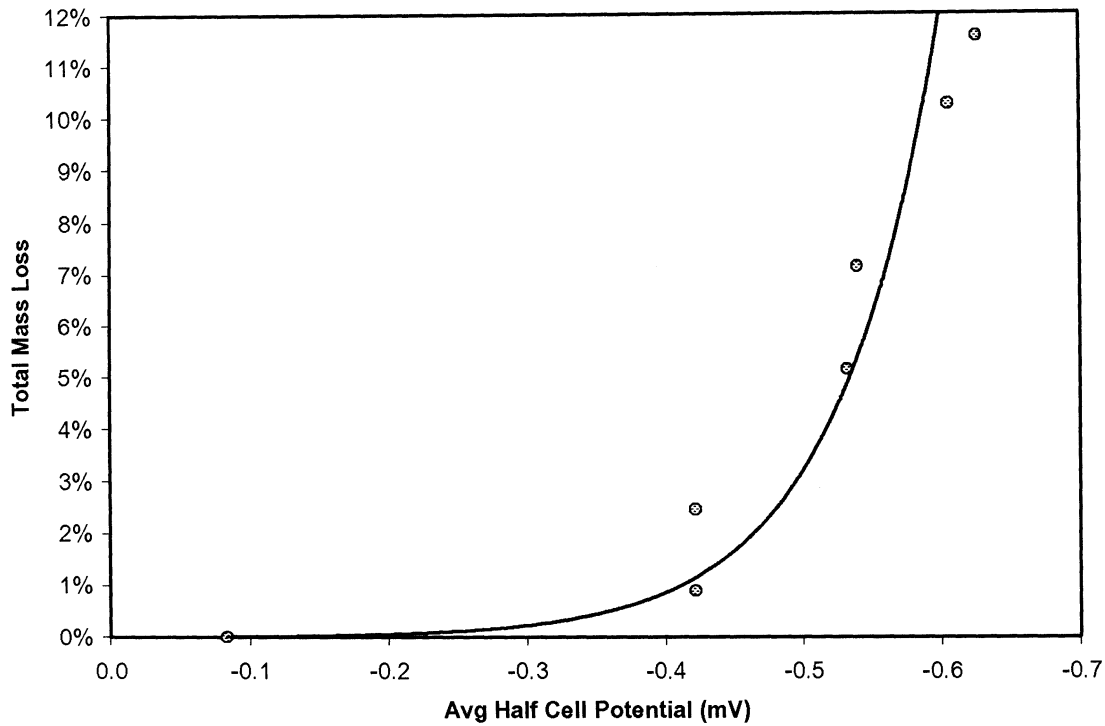
Figure 7-1: The relationship between total mass loss and the average half-cell potentials.

Figure 7-1 plots the average measured half-cell potentials against the total mass loss for the beam specimens, as well as an exponential correlation representing the best-fit line through all the data. Equation 7-1 is the numerical relationship of this line, where ML is the mass loss of the tensile steel, P_{avg} is the average half-cell potential of the beam, and r^2 is the coefficient of determination.

Equation 7-1 $$ML = 4.24 \cdot 10^{-0.5} \cdot e^{-13.25 \cdot P_{avg}}$$ $(r^2 = 0.97)$
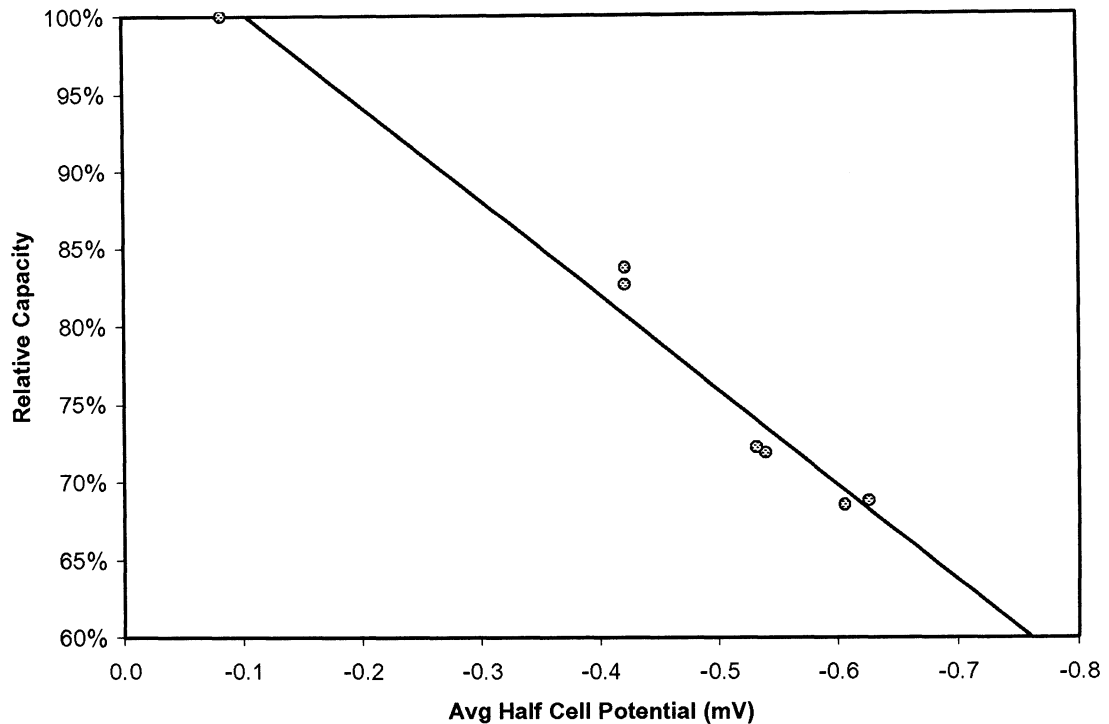
Figure 7-2: The relationship between the relative beam capacity and average half-cell potentials.

The average half-cell potentials were also plotted against the relative capacities of the beam specimens, along with a linear correlation representing the best-fit line through all the data, as shown in Figure 7-2. Equation 7-2 is the numerical relationship of the linear regression, where B is the relative capacity of the beam, P_{avg} is the average half-cell potential of the beam, and r^2 is the coefficient of determination.

Equation 7-2 $$B = 0.61P_{avg} + 1.06 \qquad (r^2 = 0.97)$$

Admittedly, Equation 7-1 and Equation 7-2 are quantitative interpretations based on qualitative results. As mentioned previously, half-cell potential readings may be misleading and an over-reliance on them to make any sort of predictions can be risky. However, half-cell

potentials can be used in conjunction with other tests and data as part of a systematic probabilistic assessment program.

7.3 Effect of Corrosion on Initial Cracking Load

In the literature reviewed, the effect of corrosion on the initial cracking load is not frequently addressed. However, two recent papers did arrive at contrasting conclusions concerning this effect. While Maaddawy et al. (2005) argued that corrosion has almost no effect on the cracking load, Fan et al. (2004) proposed that the cracking load decreased sharply with increasing corrosion.
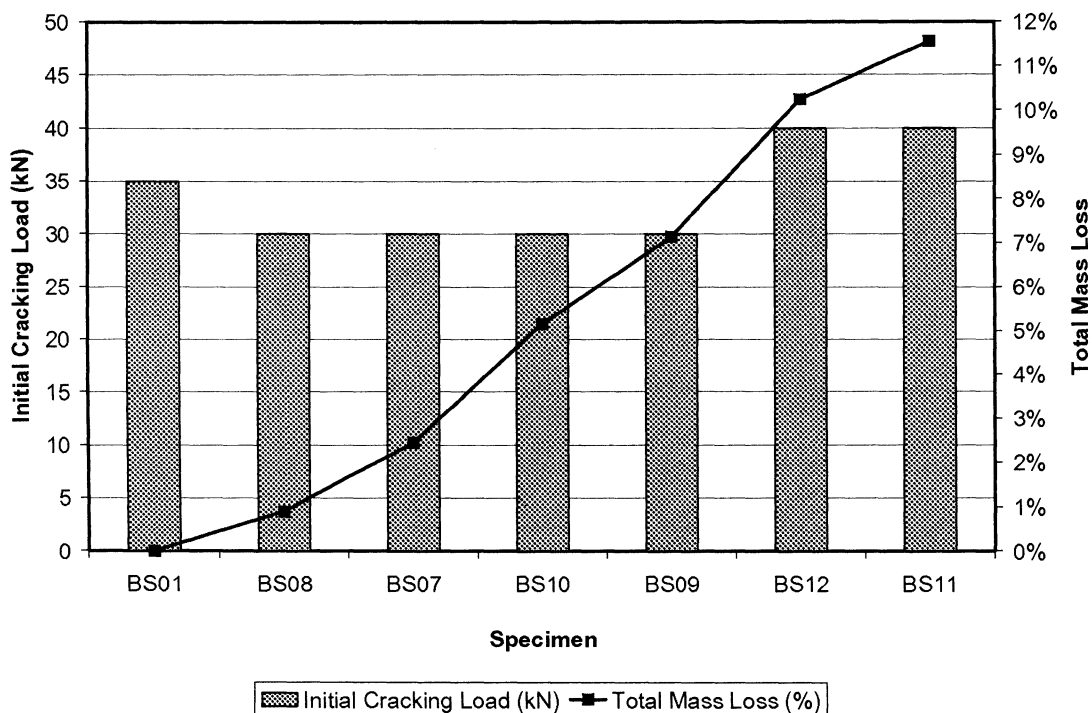
Figure 7-3: Effect of corrosion on the initial cracking load.

The findings of the present study do not support either of the above ideas; it was observed that the initial cracking load decreased at low levels of corrosion and remained constant, with

a final increase at a mass loss of approximately 10%. Figure 7-3 shows the observed initial cracking loads and the corresponding total mass loss for each beam.

The initial cracking load for the control beam was recorded at P = 35 kN. The lowest stage of corrosion yielded a mass loss of 0.89% and at this level, the initial cracking load decreased slightly to P = 30 kN. The first cracking load remained constant at 30 kN until the mass loss reached 10.25%, where it exceeded the original cracking load at P = 40 kN.

The decrease in the initial cracking load at lower levels of corrosion is likely due to internal corrosion cracks and micro-cracks that have weakened the concrete matrix, thus lowering the initial cracking load. Although the occurrence and severity of these internal cracks increases as corrosion progresses, the initial cracking load does not decrease due to the loss in concrete-steel bond strength. As bond strength is reduced and internal cracking is increased, the forces transferred from the reinforcement to the encircling concrete are diminished and thus the initial cracking load is increased at higher levels of corrosion.

7.4 Effect of Corrosion on Crack Development

A key characteristic of bond performance is its influence on crack development. The tensile concrete between the flexural cracks is largely responsible for the balancing of tensile stresses within the beam (Castel et al., 2000b). This phenomenon is known as tension stiffening. As corrosion propagates, there are reductions in bond strength and tension stiffening due to cover cracking and delamination (Coronelli and Gambrova, 2004).
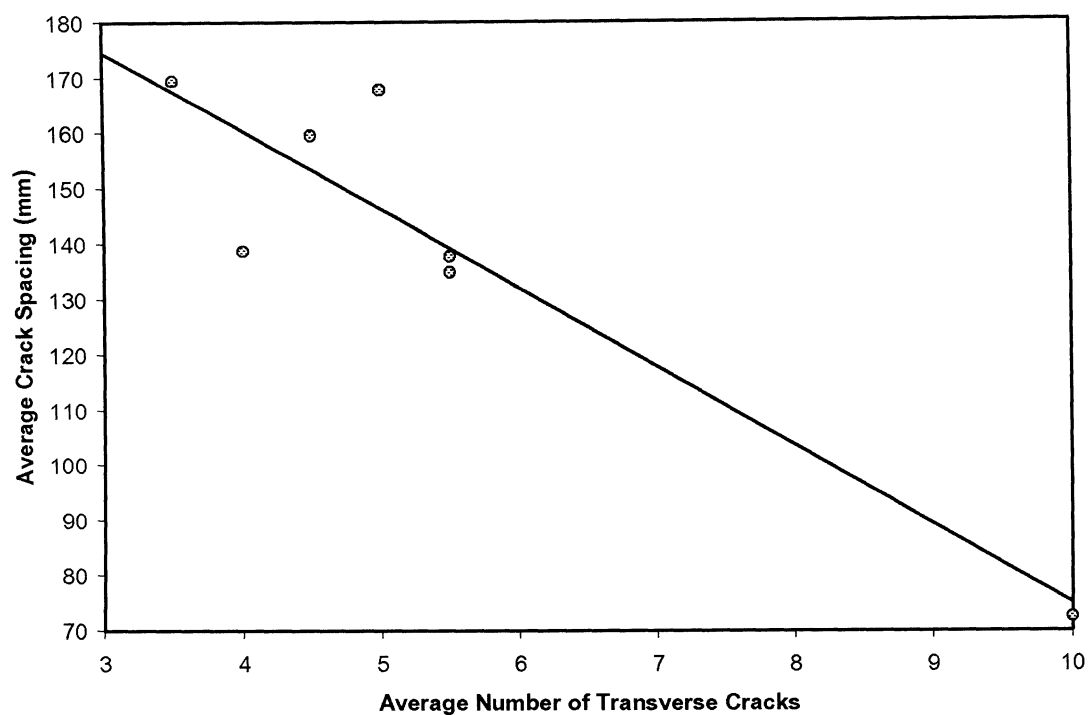
Figure 7-4: The relationship between the average number of transverse cracks
and the average crack spacing.

Amleh and Mirza (1999) found that the association between a decrease in the tension
stiffening and an increase in the corrosion level signifies the initiation of bond breakdown,
which is highly influenced by the surface conditions of the bar and the level of its adhesion
and cohesion to the surrounding concrete.

In terms of flexure or transverse cracks, it is evident that with higher levels of corrosion,
there is an increase in crack spacing and a decrease in the average number of cracks, as
shown in Figure 7-4. These observations of decreased crack numbers are consistent with the
findings of Amleh (2000), who studied tension specimens[7]. The author attributed the fewer
transverse cracks in corroded specimens relative to the control specimens to the effect of loss
of bond strength and/or internal cracking of the concrete surrounding the steel bars. As

---

[7] Concrete cylindrical specimens, 1000 mm long by 125 mm diameter and reinforced with a single 20M
deformed bar.

bond strength is reduced and internal cracking is increased, the forces transferred from the reinforcement to the encircling concrete are diminished (Amleh, 2000). It was also noted that, "In order to form a new crack between two existing cracks, the tensile force which causes cracking of the concrete should be introduced into the concrete by this bond at the steel-concrete interface" (Amleh, 2000).

On the other hand, while Amleh (2000) observed an increase in maximum crack widths as corrosion progresses, this was not exhibited by the specimens tested for this study. Granted, the testing of tension specimens is an excellent method of studying both bond behaviour and the mechanics that occur in the tension face of RC beams experiencing pure flexure. However, at high levels of corrosion, their behaviour can only be applied to RC beams that can produce like steel stresses in the reinforcing steel.

Conditions that support the transfer of stresses from the concrete to the steel include the state of the surrounding concrete, adequate anchorage, and sufficient development length. It is likely that for the beam specimens tested for this study, these conditions were lost due to the corrosion of the tensile steel. The reason that corroded tension specimens produce wider cracks at high levels of corrosion is that the embedded rebar is mechanically tensioned, thus directly stressing the steel. Conversely, in the case for loaded beams, the forces must be transferred to the tensile steel in order to produce these stresses.

After testing RC beams with un-bonded tensile bars at the shear span having adequate anchoring at their ends, Nokhasteh and Eyre (1992) observed fewer, but wider flexural cracks. This behaviour was also exhibited by the severely corroded beams tested by Rodriguez et al. (1997), particularly beam type 11. This beam had a cross-section of 150 x 200 mm, which is similar to those tested for this study, but with twice the development

length. The former case had adequate anchorage, whereas the latter had sufficient development length, both of which are required for the transfer of stresses to the steel, as stated above.

Therefore, the fact that the beams tested in this study did not experience wider flexural cracks at severe corrosion levels suggests a loss of anchorage, which prevented the transfer of the forces required to introduce and widen cracks. In terms of bond mechanics, the interlocking that occurs between the bar ribs and concrete keys was deteriorated as corrosion levels increased and slippage of the rebar occurred.

7.5 Widening of Flexural Cracks

Coronelli and Gambarova (2004) modelled beam type 11 from the above-mentioned study by Rodriguez et al. (1997), and proposed that arch action (which is indicative of wider flexural cracks) was activated when the tensile steel suffered complete bond loss along the mid-span while being well anchored at the ends by two mechanisms. The first of these mechanisms was support-induced confinement and the second was the compression of the concrete in the tension face near the support. The notion of the latter mechanism was taken from Cairns and Zhao (1993), who observed this phenomenon when studying RC beams with anchored ends but exposed tensile steel in the mid-span.

The following data analysis is provided in an attempt to make a comparison between beam type 11 and those in this study, with respect to support-induced confinement. The most corroded type 11 beam (# 116) suffered a mass loss of roughly 26% and the reaction at each support was 11.9 kN, whereas the most deteriorated beam in this study (BS11) had a mass loss of 11.56% and the reaction at each support was 48.2 kN. These numbers indicate that

beam # 116 had roughly 2.2 times the corrosion, while BS11 had reactions that were 4 times larger.

As the width of the beams is comparable[8] and the compressive strength of the concrete is similar[9], the other factor to consider when comparing confinement pressure is bar size. Beam type 11 had two 10 mm bars and the beams tested for this study had two 16 mm bars, giving a size ratio of 1.6 and an area ratio of 2.56 (i.e. 1.6^2). This means that for every kN at the support, 10 mm bars experience 2.56 times the confinement pressure as 16 mm bars. Assuming that the reactions at the support are directly proportional to the confining pressure (1:1), BS11 experienced 1.58 times (i.e. 48.2/[2.56*11.9]) the pressure of beam # 116.

Considering all of the above, the question arises as to why the beams tested by Rodriguez et al. (1997) produced wider flexural cracks as corrosion progressed, while those tested for this study did not. In other words, why did beam BS11, which had half the corrosion and 1.58 times the confining pressure of # 116, fail to experience wider flexural cracks?

One possible explanation is that this failure is due to the difference in reinforcement ratio, since beam # 116 had a ratio of 0.52%, while BS11 had a ratio of 1.46%. However, Rodriguez et al. (1997) tested beams with reinforcement ratios ranging from 0.52 % to 1.51 % and observed wider cracks in all cases. Since the reinforcement ratio of the beams tested in this study was less than 1.51%, and they did not produce wider flexural cracks, it is clear that it is not the determining factor in this case.

The difference in beam span is another possible reason for the lack of wider flexural cracks in the beams tested for this study, as it was half that of the beams tested by Rodriguez et al.

---

[8] 150 mm for type 11 and 156 mm for this study
[9] 34 MPa for type 11 and 39 MPa for this study

(1997). A longer span causes three main effects. The first is that a beam with a longer span deflects more than one with a shorter span and a greater deflection means wider cracks. The second effect is a longer development length, which increases the area in which the transfer of stresses from the concrete to the steel takes place. The problem with these two factors is that in both cases, sufficient bond is required to cause the widening of cracks, and yet Coronelli and Gambarova (2004) claimed a complete loss of bond between the supports of beam type 11.

The third effect and most plausible explanation for these cracks is that the greater shear span of beam type 11 allowed for a longer length of concrete in the tension face to shift into compression, as in the research by Cairns and Zhao (1993). When the concrete surrounding the bars in the shear span is in compression, the confinement of the bars is enhanced and the bond stress is improved.

From this reasoning, it can be concluded that for the beams tested by Rodriguez et al. (1997), the widening of flexural cracks has more to do with the length of the shear span than with support-induced confinement and reinforcement ratio. Moreover, the (1.58 times) greater confining pressure and the considerably less corrosion of the beams tested in this study implies that the bar ends were well anchored allowing for arch action, albeit flexural cracks never widened.

7.6 Evolution of Failure Mode

The failure mode of undamaged RC beams depends upon the reinforcing ratio. Lightly reinforced beams fail in a ductile manner by the yielding of the reinforcement prior to the crushing of concrete, while moderately reinforced beams may fail by the crushing of concrete

with adequate ductility. The failure of over-reinforced RC beams is by the crushing of concrete, which precedes the yielding of the reinforcement.

It is clear from the literature that the failure mode of RC beams tends to change after corrosion due to the loss of both concrete and steel sections and the decay of the concrete-steel bond. For instance, Rodriguez et al. (1997) found that un-corroded beams that are designed to fail by bending actually tend to fail by shear when corroded. In addition, Wang et al. (2000) reported that as corrosion increased, the failure mode shifted from shear to bond splitting, with the longitudinal reinforcement pulled out.

In contrast, Capozucca and Cerri (2003) investigated the influence of corrosion on the compressive zone and found that while un-corroded beams failed by the yielding of the tensile reinforcement, corroded beams failed by the crushing of the concrete and had wider flexural cracks. These researchers also concluded that corrosion damage to reinforcement in the compressive zone results in a reduction in the compressive strength of the concrete in the direction along the bar.

In the case for simply supported beams with high bond deterioration, Coronelli and Gambarova (2004) proposed two possible failure scenarios. The first failure mode is a bond failure located close to flexural cracks that is accompanied by excessive slip and high-localized bond stresses. Plizzari et al. (1996) suggested that these bond stresses may cause concrete splitting along the bar, where the radial splitting cracks propagate throughout the cover until bond failure occurs. The second mode is an anchorage failure of the tensile reinforcing steel. Using their reliability theory, Sarveswaran et al. (2000) demonstrated that this type of failure is the most critical.

Although the beams tested for the present study were simply supported and were deemed in section 7.4 to have high bond deterioration, the failure modes did not conform to either of the two scenarios mentioned above. Specifically, after the onset of corrosion, there was a shift from predictable and ductile flexure failures at mid-span, to more brittle bond-shear failures near the support with the failure crack inclined at approximately 45 degrees (from the horizontal). As corrosion progressed, both the brittleness and the angle of the failure crack increased. Severely corroded beams displayed extremely brittle failures at the support, with no forewarning and only one primary failure crack, which was nearly vertical (Figure 7-5).

BS07 (2.45% ML)   BS09 (7.14% ML)   BS12 (10.25% ML)
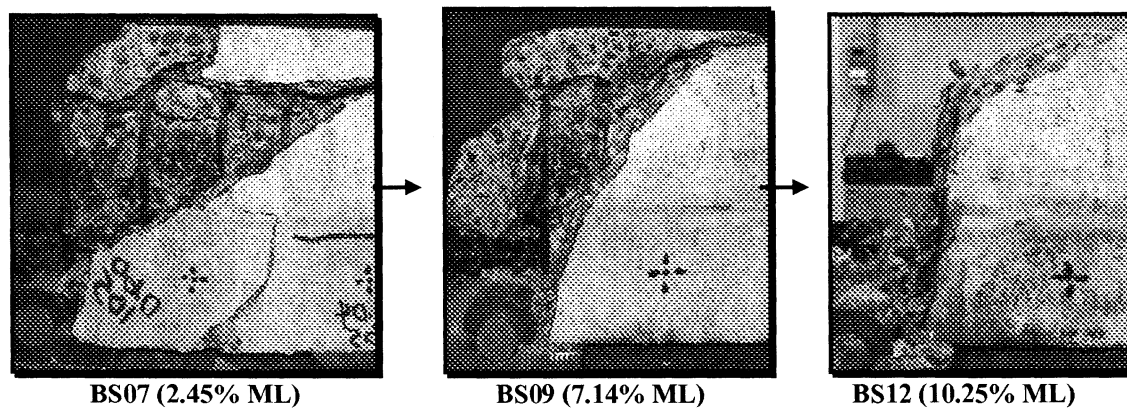
Figure 7-5: Evolution of failure mode.

This shift in the type of failure is also illustrated by the crack surveys of beam specimens BS01, BS07, and BS11 in Figure 7-6, Figure 7-7, and Figure 7-8 respectively. The right and left beam faces are illustrated on the top and the bottom of these three figures.
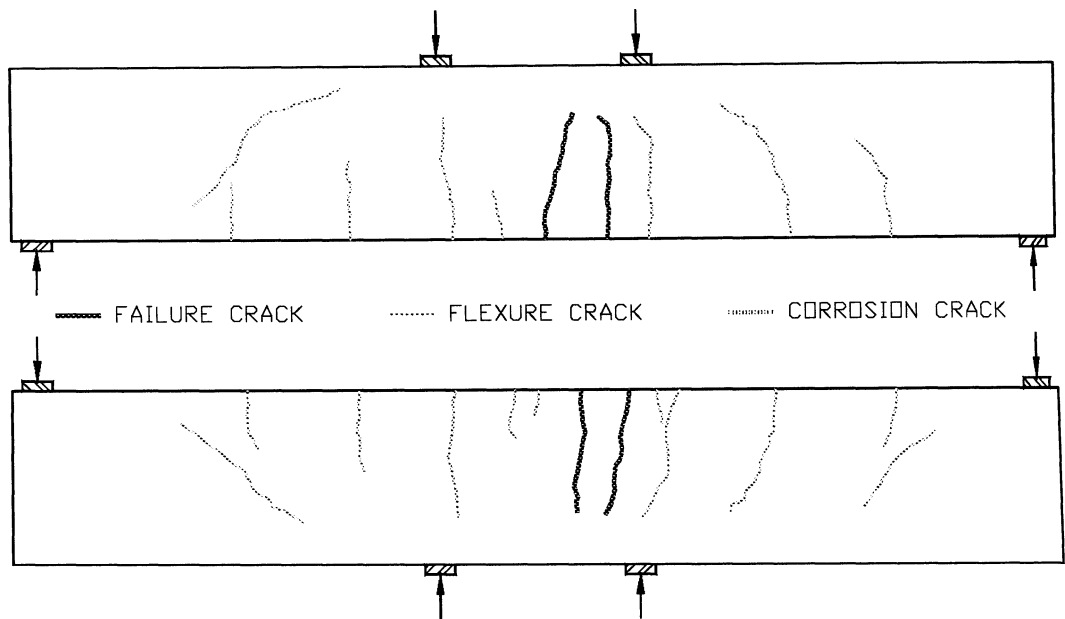
Figure 7-6: Illustration showing crack survey of BS01 (ML = 0%).
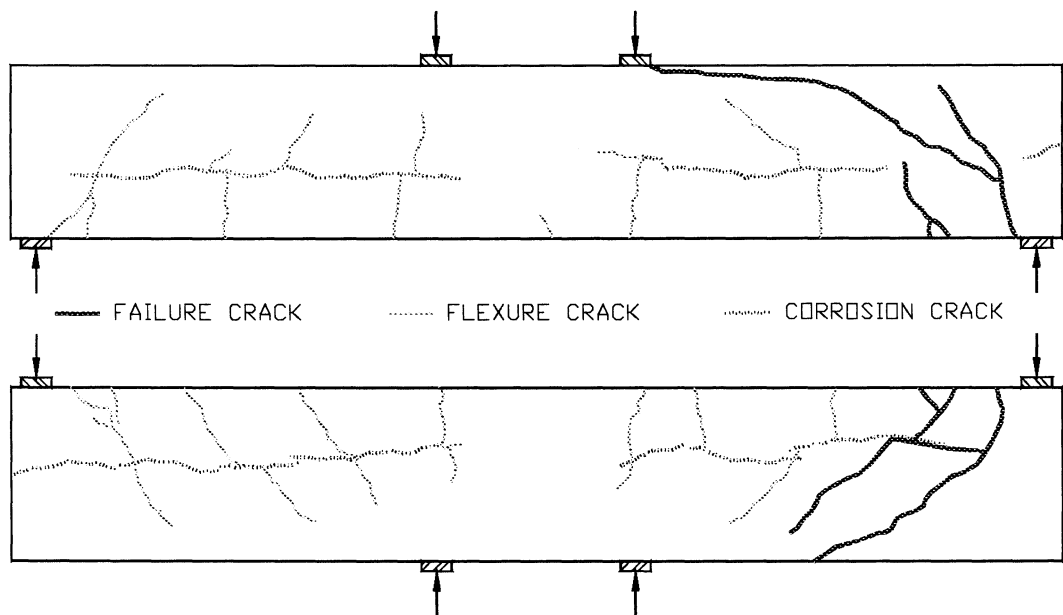
Figure 7-7: Illustration showing crack survey of BS07 (ML = 2.45%).
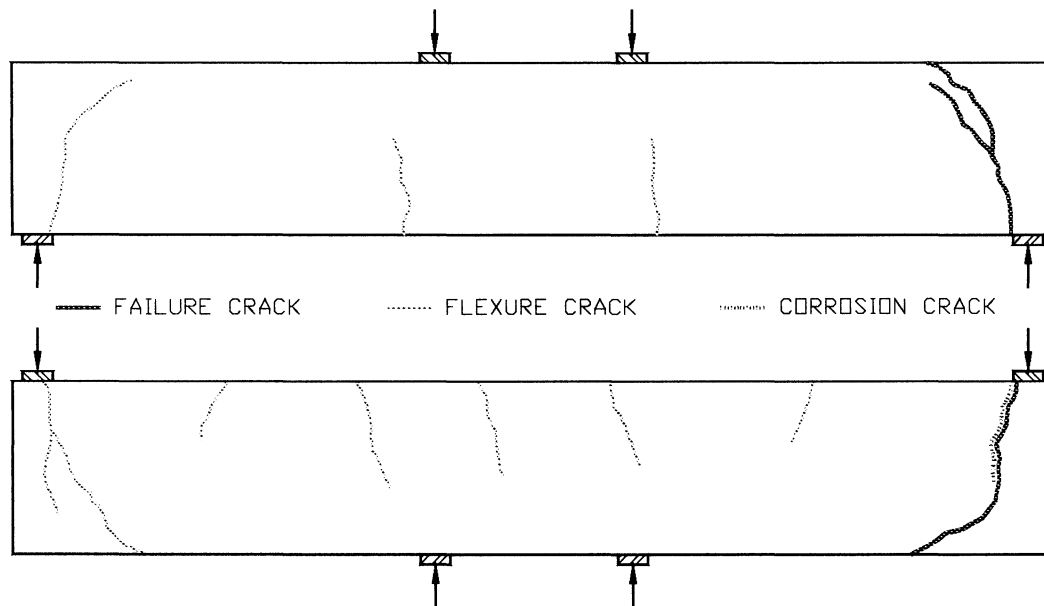
Figure 7-8: Illustration showing crack survey of BS12 (ML = 10.25%).

Figure 7-6 shows the crack survey for BS01, a control specimen that was not exposed to any accelerated corrosion. This beam had an ultimate capacity of 140.25 kN and its failure was as expected: balanced with the yielding of the tensile steel and the crushing of concrete. The average number of flexural cracks and their spacing was measured at 10 and 72.4 mm respectively.

This predicted type of failure was considerably altered when the RC beam specimens were even slightly corroded, as seen in Figure 7-7 showing the crack survey for BS07. This beam suffered a total mass loss (ML) of 2.45% and consequently, the ductile flexure failure of the control beam shifted from the centre towards a more brittle bond-shear failure near the support and was ultimately only able to carry 83.7% of the average control load. Furthermore, the flexural cracking pattern changed so that the average number of cracks dropped 45% and the average crack spacing increased by a factor of 1.90.

As corrosion increased, this shift in behaviour became more pronounced. For instance, the failure of BS12 was extremely brittle and occurred abruptly at the support, with only one primary fracture line. This beam had the second highest level of corrosion with a total ML of 10.25% and was able to carry 68.5% of the control load. The cracking pattern for BS12 also changed dramatically, as shown in Figure 7-8, with the number of flexure cracks decreasing by 65% and the average crack space increasing by a factor of 2.34.

The results of this experiment as well as the literature reviewed clearly indicate a dramatic shift in the nature of the failure of corroded RC beams. However, due to the many inbuilt differences in beams (e.g. the layout and ratio of reinforcement, size and placement of stirrups, intensity and location of corrosion, slenderness, and span), predicting the nature of the failure that a corroded beam will experience is an area that requires further research.

7.7 Effect of Stirrup Corrosion

The purpose of the stirrups in the present study is to ensure that the shear strength of a beam equals or exceeds its flexural strength. Likewise, the beam specimens had extra shear reinforcement, which ensured a flexural failure of the control beam and prevented a shear failure of any of the corroded ones.

Although the stirrups did fulfil their function, they corroded in spite of the precautions taken. The effects of stirrup corrosion include the weakening of the surrounding concrete by micro-cracking, and the cracking and delamination of the concrete cover, both of which were observed in this study. The latter effect lessened the effective depth and width of the concrete in the shear span of the beams.

Figure 7-9 displays the failure zone of BS07, a beam with a corrosion level of 2.45%, and demonstrates how the concrete split into separate layers. The photo on the left shows the complete failure zone and provides the context for the enlargement photo on the right. The white arrow in this photo points to one of the stirrups that was exposed after the beam collapsed and the areas darkened by corrosion products signify corrosion. In addition, the rust staining on the concrete between the stirrups confirms that the concrete between each of the stirrups was cracked in the plane of the stirrups below the cover.

Figure 7-9: (Left) Photograph of the failure zone of BS07 - 2.45% ML,
(Right) Enlargement of exposed stirrups.

Although the crack survey of BS12 (Figure 7-8) recorded two vertical flexural cracks at the supports, the failure crack coincided with a vertical corrosion crack that was likely caused by the corrosion of the end stirrup. This indicates that the corrosion of the stirrups may have determined the location of the failure. Figure 7-10 is a photograph of this area, illustrating that the failure crack coincided with the rust stained corrosion crack.

Figure 7-10: Photograph of the failure zone of BS12 (10.25% ML).

7.8 Effect of Corrosion on Deflection Ratio

Many researchers, including Dekoster et al. (2003) and Maaddawy et al. (2005), concur that there is a significant increase in mid-span deflections with increasing corrosion. Similarly, Ballim et al. (2001) found that for beams simultaneously subjected to load and accelerated corrosion, time-dependant deflections increase with greater corrosion.

The rise in mid-span deflections can be explained by a loss of bond between the tensile steel and the surrounding concrete. When bond strength is reduced, tensile stresses in the re-bars are significantly increased (Castel et al., 2000b). Indeed, Castel et al. (2000b) and Cabrera

(1996) both attributed the increase of in-service mid-span deflections to loss in bond strength.

Cabrera (1996), who developed a numerical relationship between deflection ratio[10] and corrosion, reported that when the corrosion level reached 9%, beam deflections increased by 1.5 times that of the non-corroded beam. Similarly, the present study found that at a corrosion level of 10.25%, beam deflections increased by a factor of 1.54 times.

The distribution of the results obtained by this study, however, was quite different. As shown in Figure 7-11 the deflection ratio that was attained from the findings of the present study is a logarithmic increase in the deflection ratio, while the deflection ratio that was observed by Cabrera (1996) is a simple linear relationship. The trend found in this study is very similar to that observed by Ballim and Reid (2003), who reported that deflections increased as corrosion propagated, with the largest increase near the early stages of corrosion.

Equation 7-3 is the numerical expression established by way of logarithmic regression analysis[11], where Dr is the deflection ratio, ML is the total percent mass loss, and r^2 is the coefficient of determination.

Equation 7-3 $$Dr = 0.076 \ln ML + 1.72 \qquad (r^2 = 0.97)$$

---

[10] calculated by dividing the average deflections of corroded beams with those of the control beams
[11] Since ln(0) is not possible, the regression analysis was conducted with the ML of the control beam taken as 0.0001.
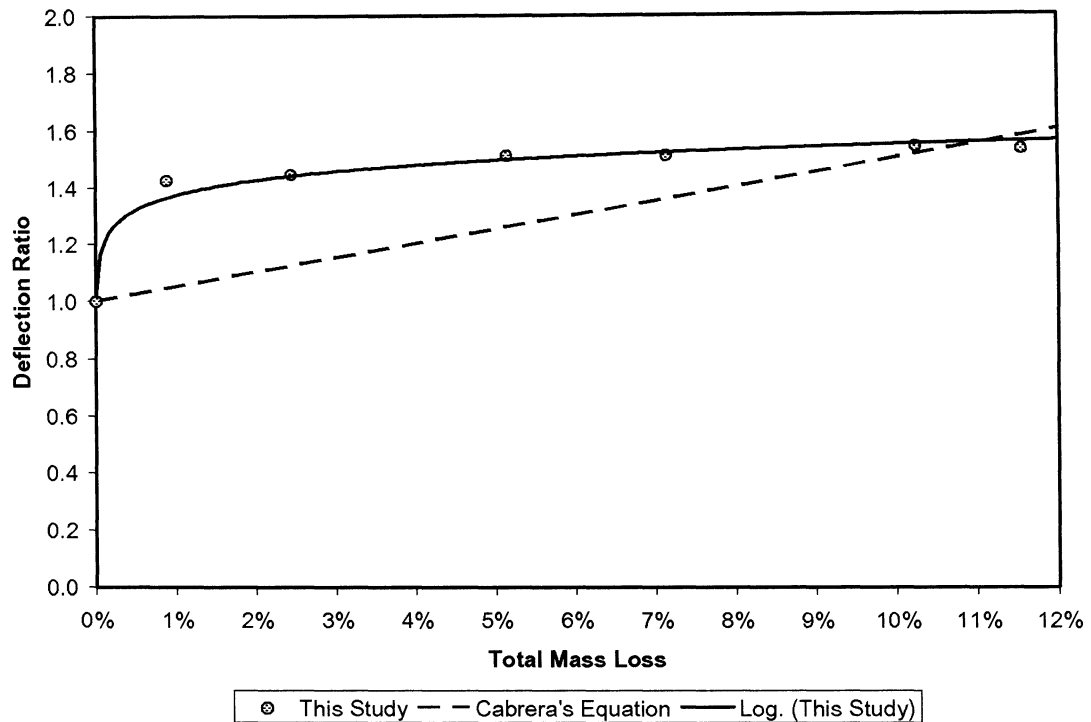
Figure 7-11: The deflection ratio versus total percent mass loss.

7.9 Effect of Corrosion on Ductility

The rise in corrosion intensity not only causes mid-span deflections to increase, but also causes deflection capacities[12] to decrease significantly. This notion of the reduction in deflection capacity is substantiated by a number of researchers, including Dekoster et al. (2003) and Maaddawy et al. (2005). In this study, deflection capacity is regarded as an indication of ductility or flexibility.

Coronelli and Gambrova (2004) stated that changes in the ductility of concrete beams are caused by the notch effect of pitting corrosion of the tensile steel bars. As the cross-section of the steel bars is diminished, ductility is reduced. Castel et al. (2000b) postulated that this

---

[12] Deflection capacity is the deflection corresponding to the ultimate load.

113

loss in ductility appears to be controlled by the mere presence of the notch rather than its depth.

Castel et al. (2000b) concluded that as corrosion increases, the ductility of RC beams decreases exponentially and then stabilizes at a loss of approximately 75% of the original. The results from the present study are consistent with this finding, showing a very similar trend with an exponential decrease and stabilization at around 70% of the original ductility. Figure 7-12 graphs the observed relationship between steel mass loss and the relative deflection capacity and Equation 7-4 is the numerical relationship obtained by power regression analysis[13], where Dc is the relative ductility, ML is the total percent mass loss, and r^2 is the coefficient of determination.
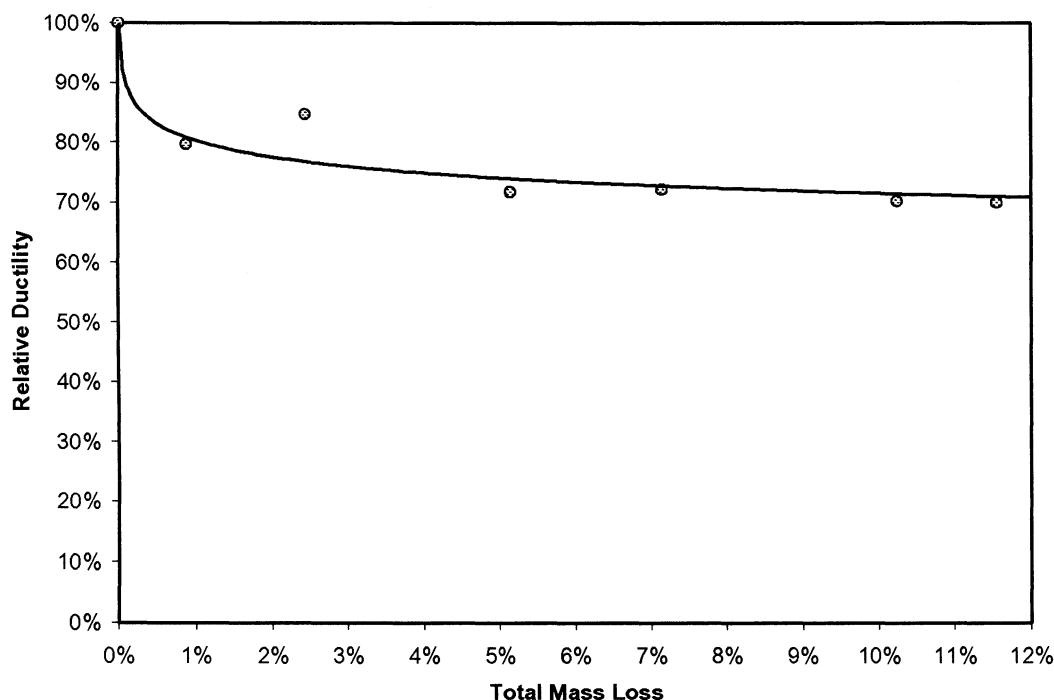
Figure 7-12: Relative ductility versus total percent mass loss.

[13] Since zero raised to the power of a negative number is not possible, the regression analysis was conducted with the ML of the control beam taken as 0.0001.

Equation 7-4 $$Dc = 0.64ML^{-0.05}$$ $(r^2 = 0.89)$

7.10 Effect of Corrosion on Stiffness

Corrosion also has an effect on stiffness, which is related to deflection. In fact, several researchers have reported a marked reduction in the stiffness of corroded beams (Perno et al., 2005; Dekoster et al., 2003; Castel et al., 2000b). On the other hand, Maaddawy et al. (2005) found that the stiffness of beams that are corroded under sustained loading is higher than that of virgin beams when loaded to failure.

Castel et al. (2000a) found that the loss of beam stiffness is attributed to a decrease in strengths of both the rebar cross-sectional area and the local steel-concrete bond of the tensile bars. A reduction in the stiffness of a beam is also caused by the formation of cracks, as reported by Chung et al. (2004) and Yoon et al. (2000).

As mentioned earlier, bond breakdown is related to concrete cracking, both of which cause a decrease in tension stiffening. Considering this, it follows that stiffness decay is due to impaired tension stiffening (Coronelli and Gambarova, 2004). Based on the findings of the research discussed, it can be concluded that changes in stiffness occur whenever there is a redistribution of internal stresses.

The slope of the load-deflection curve (LDC) can be used to indicate the stiffness of an element, as in the work by Huang and Yang (1997). In the present study, a relationship between the stiffness and the total percent mass loss (ML) of RC beams was derived from the findings of the experimental program, as shown in Figure 7-13. This figure demonstrates that as corrosion increases, stiffness decreases exponentially and then stabilizes at a loss of

approximately 70% of the original stiffness (much like ductility). Equation 7-5 provides the

numerical relationship obtained by power regression analysis[14], where k is the relative

stiffness, ML is the total percent mass loss, and r^2 is the coefficient of determination.

Equation 7-5 $$k = 0.57ML^{-0.058}$$ $(r^2 = 0.96)$
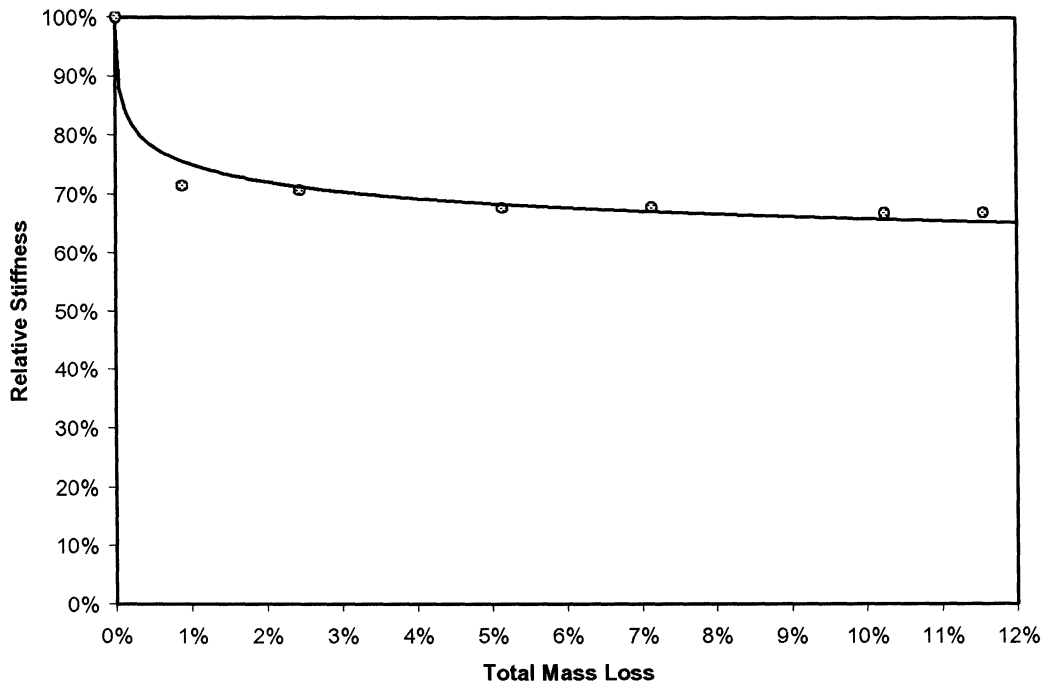
Figure 7-13: The relationship between stiffness and mass loss.

7.11 Effect of Corrosion on Toughness

Toughness, which is related to stiffness and ductility, is another measurable characteristic of

RC beams. The toughness of a material is defined as the energy absorbed per unit volume,

and is measured by the area under the stress-strain curve up to fracture. A ductile fracture

occurs when a material experiences appreciable plastic deformation and energy absorption

---

[14] Since zero raised to the power of a negative number is not possible, the regression analysis was
conducted with the ML of the control beam taken as 0.0001.

prior to fracture. Conversely, a brittle fracture results when a material experiences little or no energy absorption prior to fracture (Illston and Domone, 2001).

The area under the LDC up to failure has been used to assess the absorbed energy of RC beams (i.e. toughness), as in the research by Uomoto and Misra (1988) and Azher (2005). Although the literature reviewed contains limited information concerning the manner in which corrosion affects the area under the LDC of RC beams, it is established that toughness is typically reduced with increasing corrosion (Azher, 2005).

Using data from the experiment conducted for the purpose of this study, a relationship between toughness and the level of corrosion was established, as seen in Figure 7-14. The data acquired reveals a trend similar to that of the reduction in stiffness and ductility. Specifically, as corrosion increased, the energy absorbed by the beams decreased exponentially followed by a levelling off.
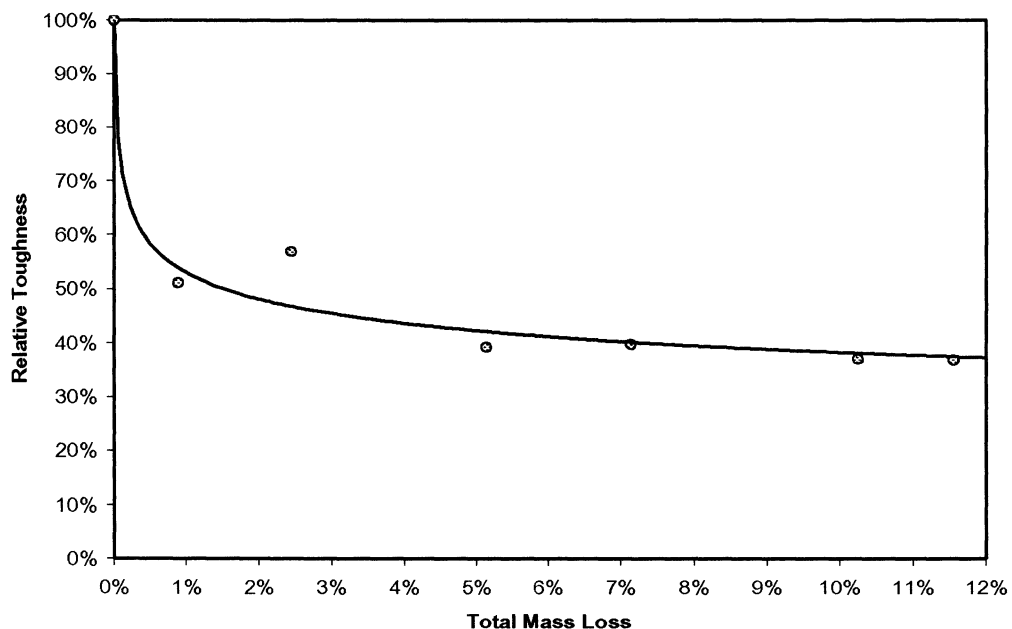
Figure 7-14: The relationship between the area under the LDC and ML.

The difference in this case, however, is that the stabilization occurred at the lower value of approximately 40% of the original. Equation 7-6 shows the numerical relationship obtained by power regression analysis[15], where T is the relative toughness, ML is the total percent mass loss, and r^2 is the coefficient of determination.

Equation 7-6 $$T = 0.28ML^{-0.14}$$ $(r^2 = 0.94)$

The absorption of energy by RC beams causes visible and measurable external responses, such as more frequent cracking of the tensile concrete and greater deflections, both of which intensify as the applied load increases. When this load is applied to the beam, it is primarily supported by internal moments and shears, and its effects are shear forces and bending moments that can be determined using the laws of statics.

At any section in the beam, the internal resisting shear and moment are necessary to equilibrate the applied shear force and bending moment. This internal resisting moment induces compressive and tensile forces within the beam. Cracking occurs when these tensile forces cause the stresses at the bottom of the beam to exceed the tensile strength of the concrete (MacGregor and Bartlett, 2000).

Changes in the cracking pattern are indicative of an altered absorbed energy. Indeed, the results of the beam tests revealed that a reduction in the absorbed energy due to increasing corrosion intensity was proportional to the number of flexural cracks and inversely proportional to the spacing of the flexural cracks. This relationship between toughness and flexural crack development is shown in Figure 7-15.

---

[15] Since zero raised to the power of a negative number is not possible, the regression analysis was conducted with the ML of the control beam taken as 0.0001.
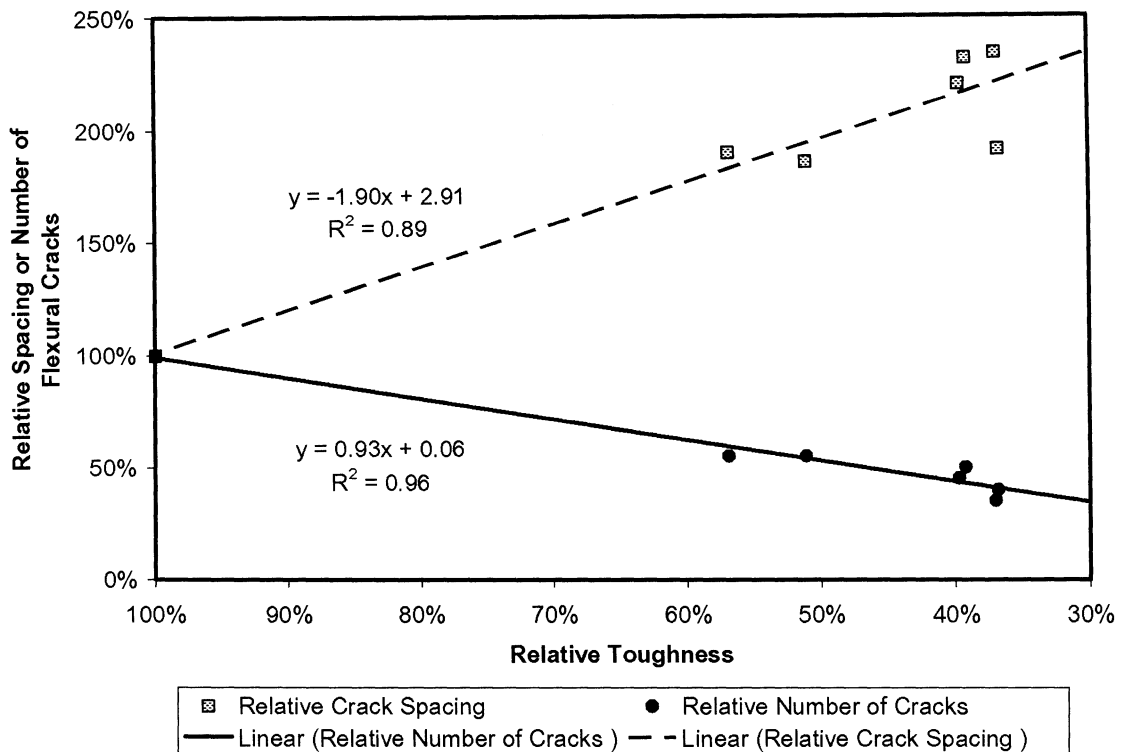
Figure 7-15: The relationship between the area under the LDC and flexural crack development.

After cracking, the internal tensile forces of a beam are redistributed into the reinforcing steel, resulting in reduced stiffness and/or increased deflections. These changes in stiffness and ductility also suggest an altered absorbed energy. Since stiffness is measured using the slope of the LDC and ductility is indicated by the maximum deflection, their reductions imply a decrease in the area under the curve (i.e. toughness) as well. In fact, it was observed from the results of the beam tests that a reduction in the absorbed energy was proportional to both the stiffness and ductility of corroded RC beams, as seen in Figure 7-16.

119
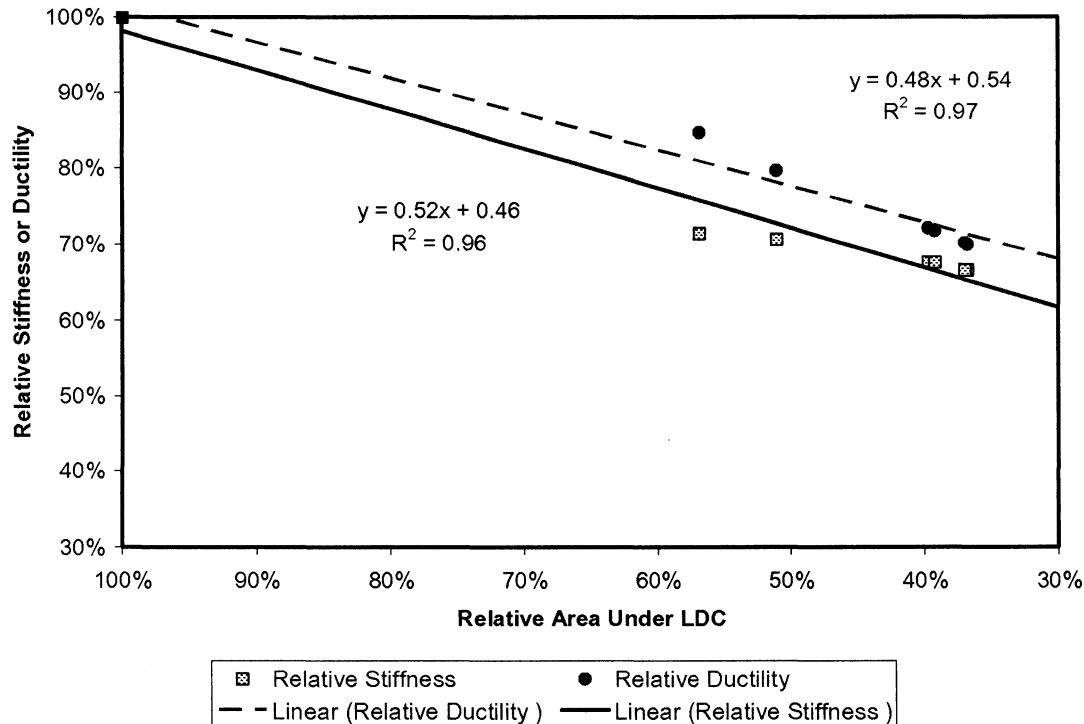
Figure 7-16: The relationship between the area under the LDC and beam deflections.

7.12 Ductility, Stiffness, and Toughness Compared

As mentioned previously, ductility is indicated by the deflection capacity, stiffness by the slope of the LDC, and toughness by the area under the LDC (up to failure). All three of these properties are related, in that they are revealed by the load-deflection behaviour. Toughness is the most connected, since the area under the LDC is greatly influenced by both the slope of the curve (i.e. stiffness) and the deflection that corresponds to the ultimate load (i.e. ductility).

Interestingly, the data obtained from the experimental study for all three of these properties was best numerically modelled (i.e. yielding the highest coefficient of determination) by

power regression analysis. These equations are provided in Equation 7-4 for ductility [Dc], Equation 7-5 for stiffness [k], and Equation 7-6 for toughness [T].

When these numerical relationships are compared, it is clear that for the beams tested, the relative stiffness is approximately equal to the relative ductility, which are both roughly twice the relative toughness.

That is,
$$0.57ML^{-0.058} \approx 0.64ML^{-0.05} \approx 2 \times 0.28ML^{-0.14}$$

Which is roughly,
$$0.6ML^{-0.058} \approx 0.6ML^{-0.050} \approx 0.6ML^{-0.141}$$

Or,
$$k \approx Dc \approx 2T$$

7.13 Effect of Corrosion on Beam Capacity

The effect of corrosion on the ultimate load-carrying capacity is the final behavioural phenomenon of beams investigated in this study. Figure 7-17 is a plot of the relative beam capacity versus the total mass loss of each beam tested. The capacities of the beam specimens rapidly decreased and tapered off at approximately 75% of the control strength. Equation 7-7 is the numerical expression developed to find the relative beam capacity (B) that was obtained by logarithmic regression analysis[16], where ML is the total percent mass loss and r^2 is the coefficient of determination.

---

[16] Since ln(0) is not possible, the regression analysis was conducted with the ML of the control beam taken as 0.0001.
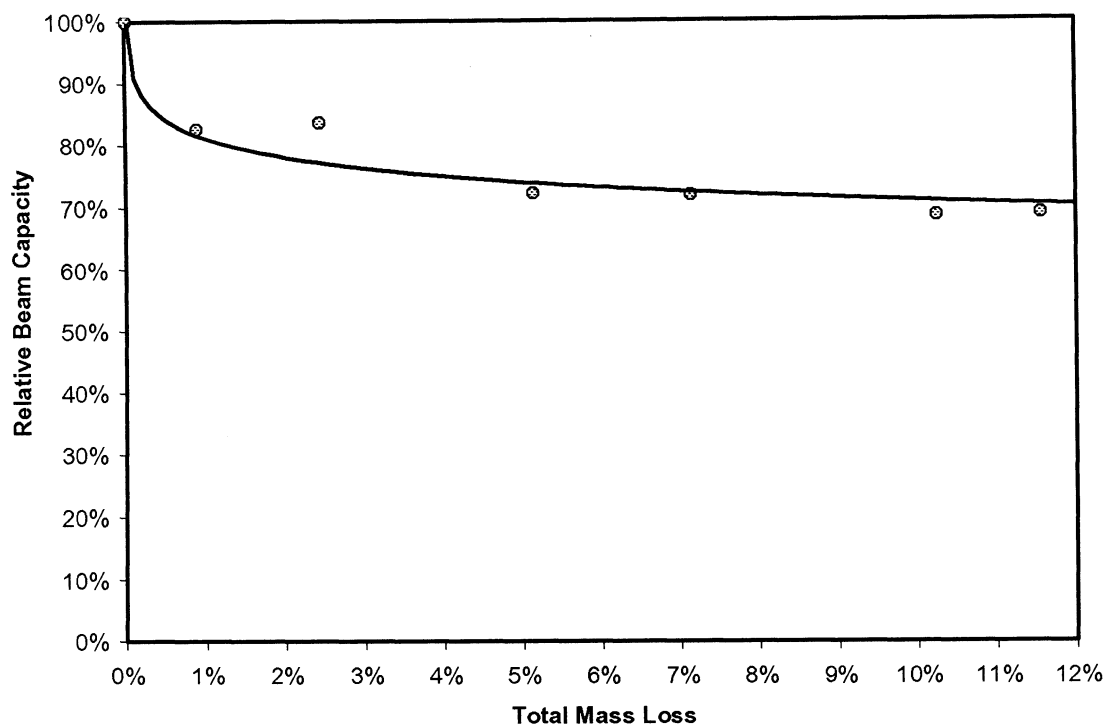
Figure 7-17: Relationship between mass loss and the relative beam capacity.

Equation 7-7 $$B = -0.044 \ln ML + 0.61 \qquad (r^2 = 0.93)$$

For the purpose of this study, the results of over 100 corroded-beam tests conducted by other researchers were reviewed. When the results of the present study are compared to those found in the literature, the reduction in capacity proves to have a more rapid loss that occurs sooner, as shown in Figure 7-18. In this figure, the results of the current tests are denoted by dark circular points, while the previous test results are represented by grey

122

diamonds. The sources and some pertinent details concerning the data used to generate this graph are provided in Appendix G.
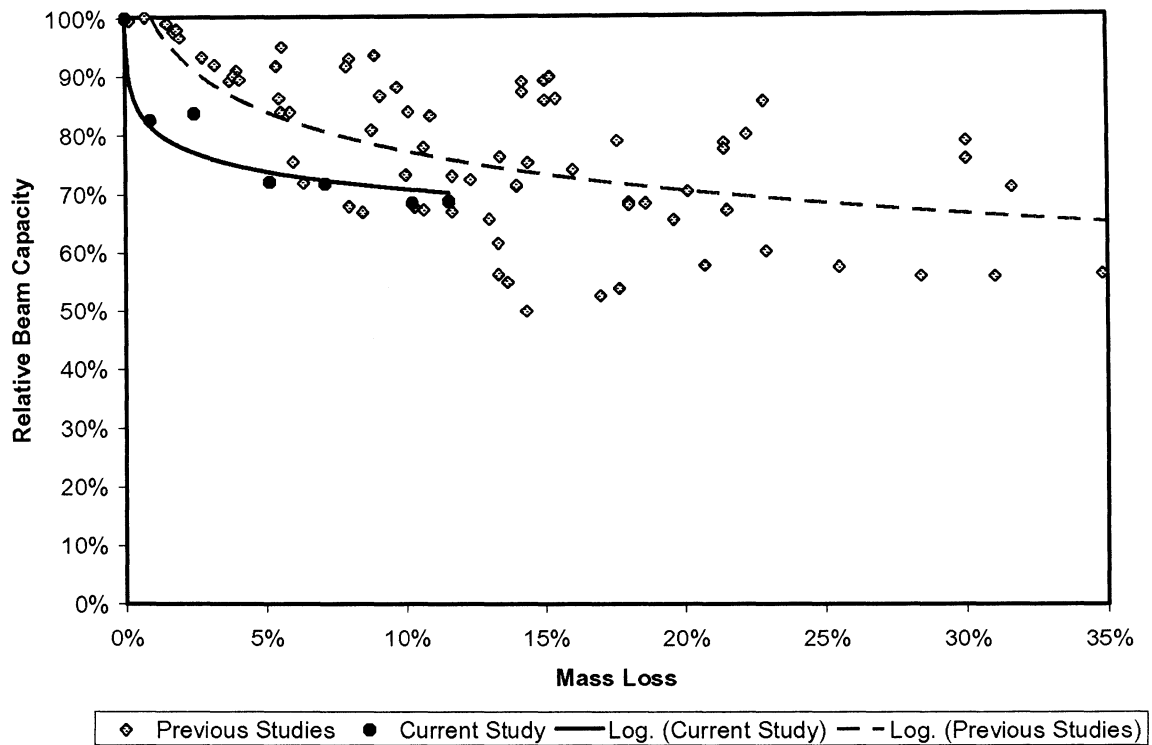
Figure 7-18: Comparison between the relative capacities of previous beam tests
and those of the present study.

The earlier and quicker strength loss exhibited by the beams tested here can be attributed to the 3 mA/cm² rate of corrosion used on these specimens, while the average rate for the other beams in Figure 7-18 is 1.35 mA/cm². This idea is supported by the findings of Mangat and Elgarf (1999a), who studied the effect of corrosion rates on the flexural load capacity of beams. These researchers found that beam capacity decreases with increasing corrosion rates and this effect is enlarged with higher degrees of corrosion.

The data collected from the beam tests in the literature encapsulates a wide range of factors, including beam sizes, reinforcement detailing, levels and rates of corrosion, and material

properties. For instance, the spans of these beams range from 900 to 3000 mm and steel bar sizes range from 8 to 19 mm.
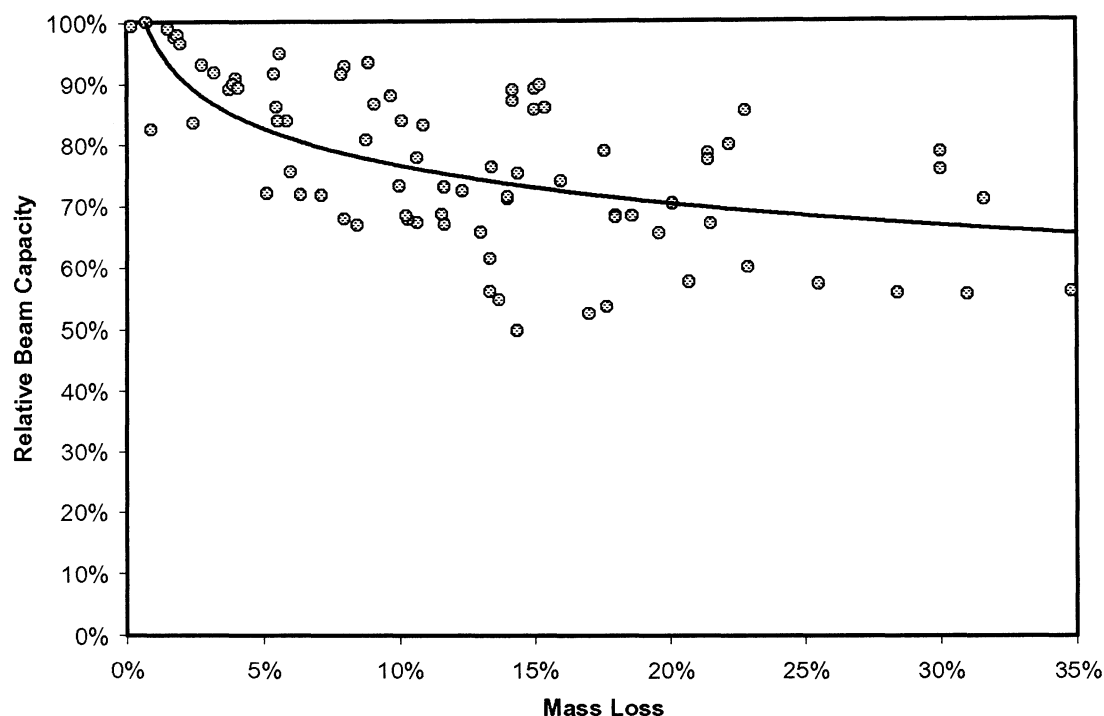
Figure 7-19: Generalized trend of capacity loss of RC beams.

Due to this diversity in the sample population, a generalized trend for the capacity loss of RC beams with increasing corrosion is generated by means of logarithmic regression analysis. Figure 7-19 is a plot containing all of the current and previous data with the logarithmic trend line and Equation 7-8 is the numerical expression of the trend, where B is the relative beam capacity, ML is the total percent mass loss, and r^2 is the coefficient of determination.

Equation 7-8 $$B = -0.089\ln(ML) + 0.56 \qquad (r^2 = 0.41)$$

124

Granted, the coefficient of determination in this case is quite low ($r^2 = 0.41$), but a large scattering of data is expected in a general case such as this. In order to gain a clearer and more specific picture, the sample size must be enlarged and categorized according to different parameters, such a bar diameter, tensile and compressive reinforcement ratio, cover thickness, bar yield strength, and concrete compressive strength.

7.14 Importance of Bond Strength

The load-carrying capacity of RC beams with corroded reinforcement has been studied by many researchers and those consulted for this study have all concluded that ultimate strength decreases with increasing corrosion (Higgins and Farrow, 2006; Maaddawy et al., 2005b; Pemo et al., 2005; Dekoster et al., 2003). However, there has been much speculation regarding the causes of this effect and the general consensus appears to have shifted. While earlier studies neglected to consider reductions in bond strength as a factor, recent works have focused on the importance of bond strength when considering ultimate capacity.

Uomoto and Misra (1988) attributed a decrease in the load-carrying capacity of corroded RC beams to both the reduction in the reinforcement area and the cracking of the concrete. In contrast, Al-Sulaimani et al. (1990) concluded that the decrease was primarily caused by the reduced area of the reinforcing steel, stressing that it was *not* due to a reduction in bond stress. Meanwhile, Rodriguez et al. (1997) surmised that pitting of the reinforcing steel had the greatest impact on load-carrying capacity. Despite their differing views, these researchers all recognized the deterioration of the concrete cover as being relevant but did not consider bond strength to be a factor.

On the contrary, Mangat and Elgarf (1999a) more recently proposed that, "... the reduction in reinforcing bar section due to corrosion has an *insignificant* effect on the residual flexural strength of beams." In fact, they hypothesized that a reduction in flexural strength is mainly related to the deterioration of the bond at the steel-concrete interface. Furthermore, Mangat and Elgarf (1999b) observed in another study that when a bond failure occurs, the tensile stress in the reinforcement is less than its yield stress. This indicates that bond strength plays a key role in reducing ultimate capacity.

Moreover, Castel et al. (2000a; 2000b) carried out a two-part study in order to investigate the mechanical behaviour of corroded RC beams, wherein the effect of bond strength was only considered in the latter half. The results of this study demonstrate that if the influence of bond strength is acknowledged, it will have a positive correlation with ultimate strength. If bond strength is ignored, on the other hand, the loss of rebar cross-sectional area will be the only factor determining residual strength. Thus, these researchers argued that bond strength should be taken into account when studying the residual capacity of RC beams.

For this reason, the present study was designed to include pullout tests in an attempt to find the relative bond strength of the tensile steel at different levels of corrosion and relate this to relative beam capacities.

7.15 Effect of Corrosion on Bond Strength

Previous research work has found that as corrosion progresses, there is generally an initial increase in bond strength prior to a decrease. While Amleh (2000) reported this decrease as gradual, Chung et al. (2004) described it as rapid. The latter characterization is consistent with the results observed in the present study, where there was an initial increase in bond strength

followed by a rapid decrease. The relationship between the losses in relative bond strength and bar mass (ignoring the initial increase) is portrayed in Figure 7-20, which plots the findings of the pullout study.
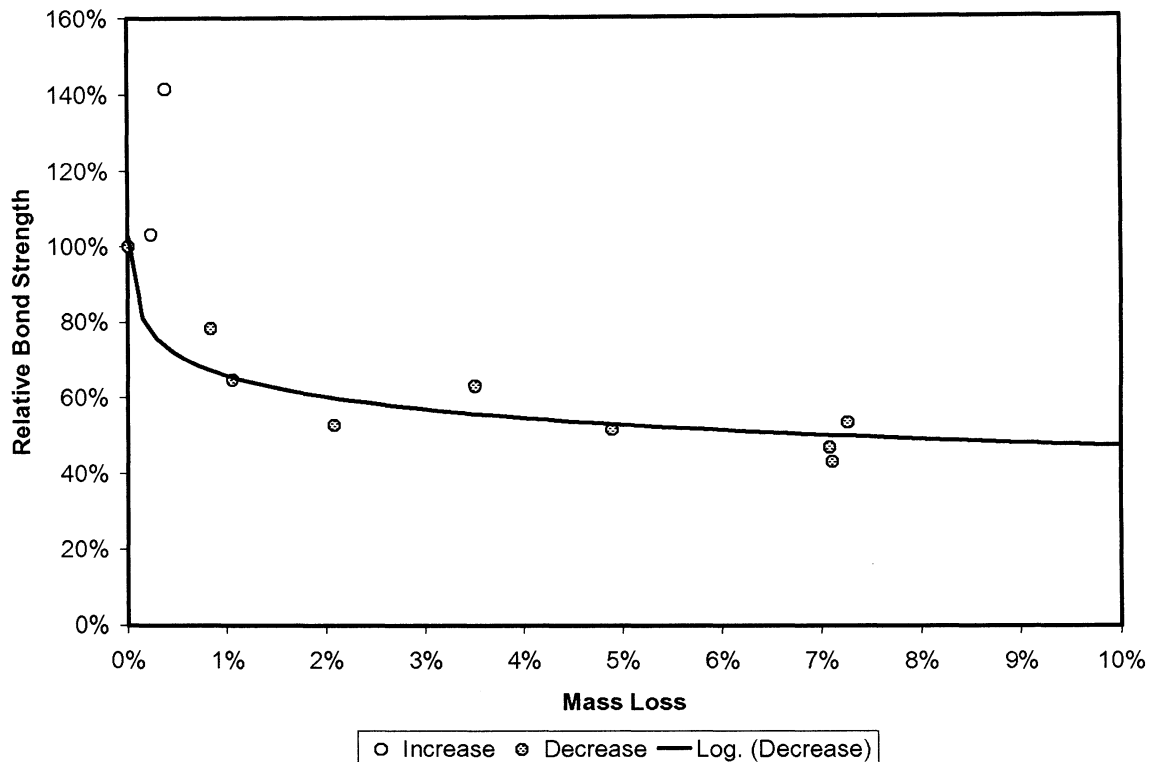
Figure 7-20: Relative bond strength versus mass loss.

A numerical relationship to calculate the reduction in bond strength in terms of bar mass loss was obtained by performing logarithmic regression analysis[17] on instances showing a decrease in the relative bond strength. Equation 7-9 gives this correlation, where τ_{rel} is the relative bond strength, *ML* is the total percent mass loss (in decimal form), and r^2 is the coefficient of determination. This nonlinear relationship between bond stress and corrosion supports the findings of Chung et al. (2004).

---

[17] Since ln(0) is not possible, the regression analysis was conducted with the ML of the control beam taken as 0.0001.

Equation 7-9 $$\tau_{rel} = -0.08 \ln ML + 0.29 \qquad (r^2 = 0.88)$$

Using Equation 7-9 as a reduction factor and multiplying it with Equation 4-2 yields Equation 7-10, where τ_{res} is the average residual bond strength, R_c is measured from the centre of the bar to the closest surface, d_b is the diameter of the bar, and f_c' is the compressive strength of concrete.

Equation 7-10 $$\tau_{res} = \left[0.5\sqrt{f_c'} \cdot \left(\frac{R_c}{d_b} - \frac{1}{2} \right) \right] \cdot \left[0.29 ML^{-0.19} \right]$$

However, Equation 7-9 is only able to provide a close estimate of the bond strength at the rebar surface in the beam specimens tested for this study. The actual bond strength cannot be calculated using this equation for two main reasons. Firstly, the cover of the tensile bars in the beam was 36 mm, while the cover in the pullout specimens was 42 mm. Secondly, the bars in the beam specimens had the benefit of the confinement provided by the stirrups, whereas pullout specimens did not.

7.16 Relationships with Beam Capacity

Some researchers have proposed models for predicting the residual strength of corroded RC beams, claiming good correlation with their own and/or other available experimental data (Azher, 2005; Mangat and Elgarf, 1999a; Rodriquez, 1997; Eyre and Nokhasteh, 1992; and Cairns and Zhao, 1993). While these models may provide greatly needed insight into beam capacity reductions, many have been criticized by Maaddawy et al. (2005) for oversimplification since they fail to take into account the coupled effects of the reductions in both the steel cross-sectional area and bond strength.

Improved ultimate strength models can be developed with further study, as well as a better understanding of the holistic nature and behaviour of RC beams suffering from corrosion. A discussion of the relationships between beam capacity and a variety of phenomena, as established in the present study is essential. Figure 7-21 is a diagram illustrating these relationships.
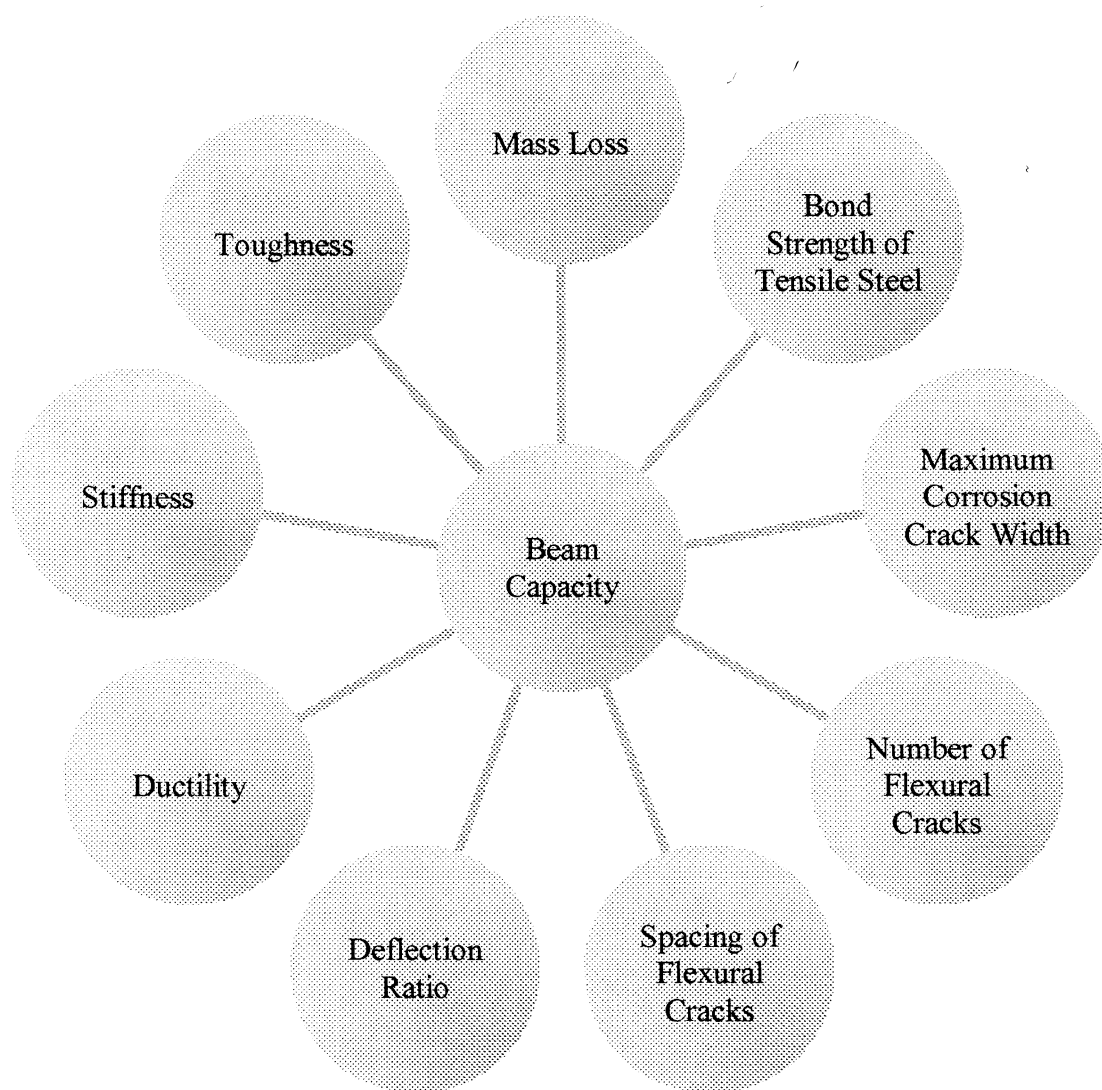
Figure 7-21: Phenomena that related well to the relative beam capacity.

Specifically, relative beam capacity was found to have good correlations with the total mass loss (see section 7.12), bond strength of the tensile steel, maximum corrosion crack width, number and spacing of flexural cracks, deflection ratio, ductility, stiffness, and toughness.

7.16.1 Beam Capacity and Bond Strength

As corrosion increased, the reduction in bond strength was found to exceed the reduction in beam capacity. This is evident in Figure 7-22, which graphs Equation 7-9 (for bond strength) and Equation 7-7 (for beam capacity). Adding these equations together yields the numerical relationship (see Equation 7-11) between bond strength and beam capacity, where τ_{rel} is the relative bond strength, B is the relative beam capacity, and r^2 is the coefficient of determination. This new relationship is plotted in Figure 7-23.
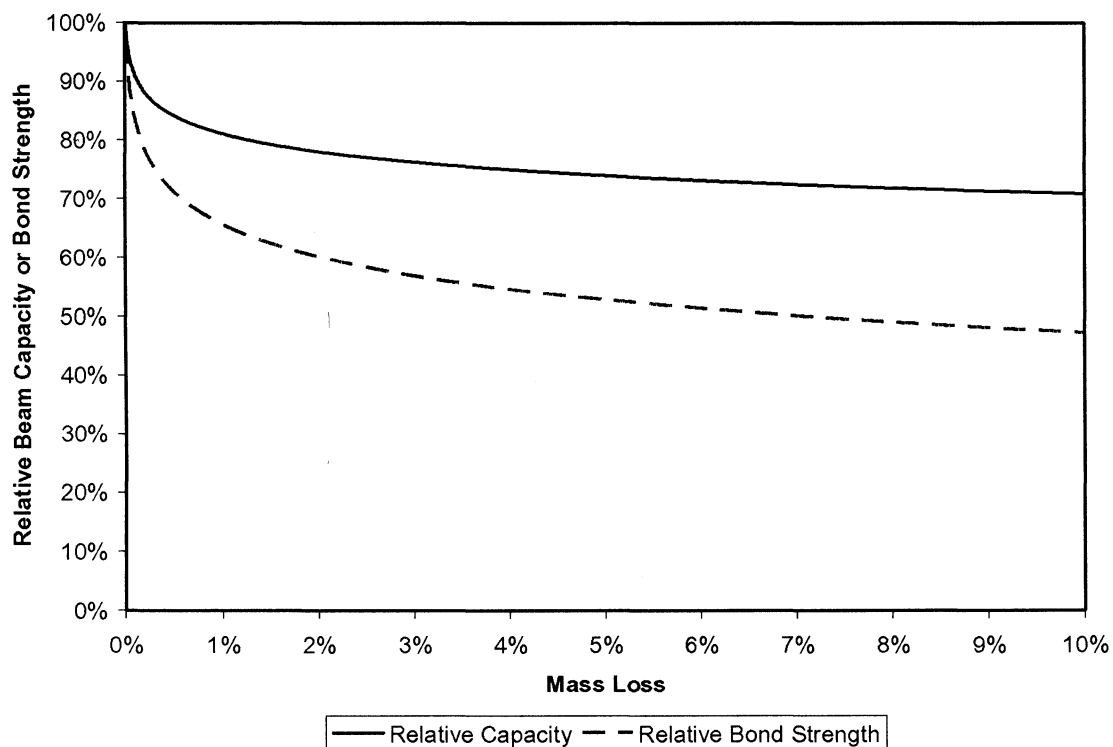
Figure 7-22: Comparison between the reductions in beam capacity and bond strength.

130

Equation 7-11 $$B = 0.55\tau_{rel} + 0.45$$
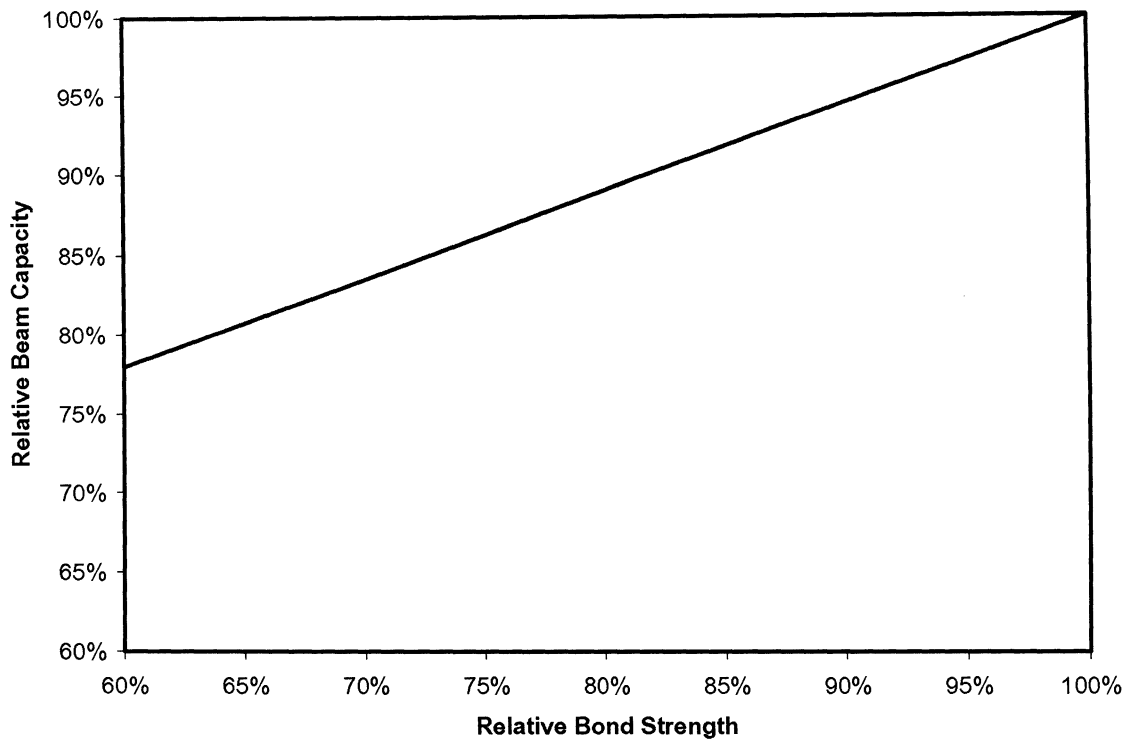
Figure 7-23: Relationship between beam capacity and bond strength.

Traditional flexure theory (as described in 3.2) relies on the composite action of the tensile steel and concrete and presupposes complete bond between the two, implying that the resisting moment is proportional to the bond strength between them. However, this proportionality can only occur when the applied loads are equilibrated exclusively by beam action.

Yet, it has been proven that after the de-bonding of the tensile steel in the shear span, arch action is initiated and the forces are transferred to the supports via an inclined compressive strut (as discussed in 7.4). In the present study, beam action cannot be used to reconcile the capacities observed, due to the relatively low residual bond strength. It can therefore be

argued that in this case, beam action was replaced with an alternative force equilibrating mechanism such as arch action.

7.16.2 Beam Capacity and Maximum Corrosion Crack Width

Corrosion cracks, which are induced by expanding rust products, contribute to a reduction in both bond strength and beam capacity. Accordingly, the data obtained from the present study reveals that the capacity of the beam specimens tested is related to the maximum corrosion crack width of the concrete surrounding the tensile reinforcing steel.

Figure 7-24 plots this relationship and Equation 7-12 is its numerical expression, obtained by power regression analysis, where w_{corr} is the largest corrosion crack width in mm, B is the relative beam capacity, and r^2 is the coefficient of determination.
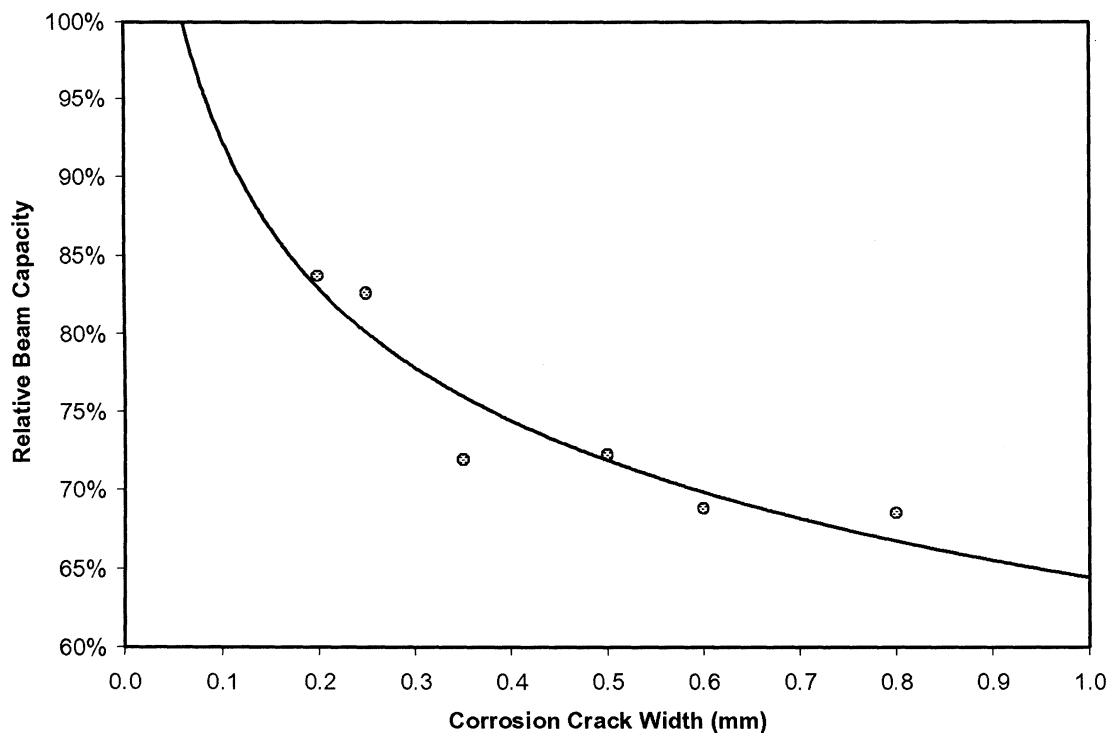
Figure 7-24: Relationship between beam capacity and maximum corrosion crack width.

Equation 7-12 $$B = 0.64 w_{corr}^{-0.16}$$ $(r^2 = 0.87)$

7.16.3 Beam Capacity and Number of Flexural Cracks

The manner in which RC beams develop flexural cracks is greatly affected by their level of corrosion. In addition, the results of the present laboratory study indicate a definite relationship between flexural crack development and beam capacity. Specifically, the average number of flexural cracks was found to decrease linearly with capacity, as graphed in Figure 7-25.
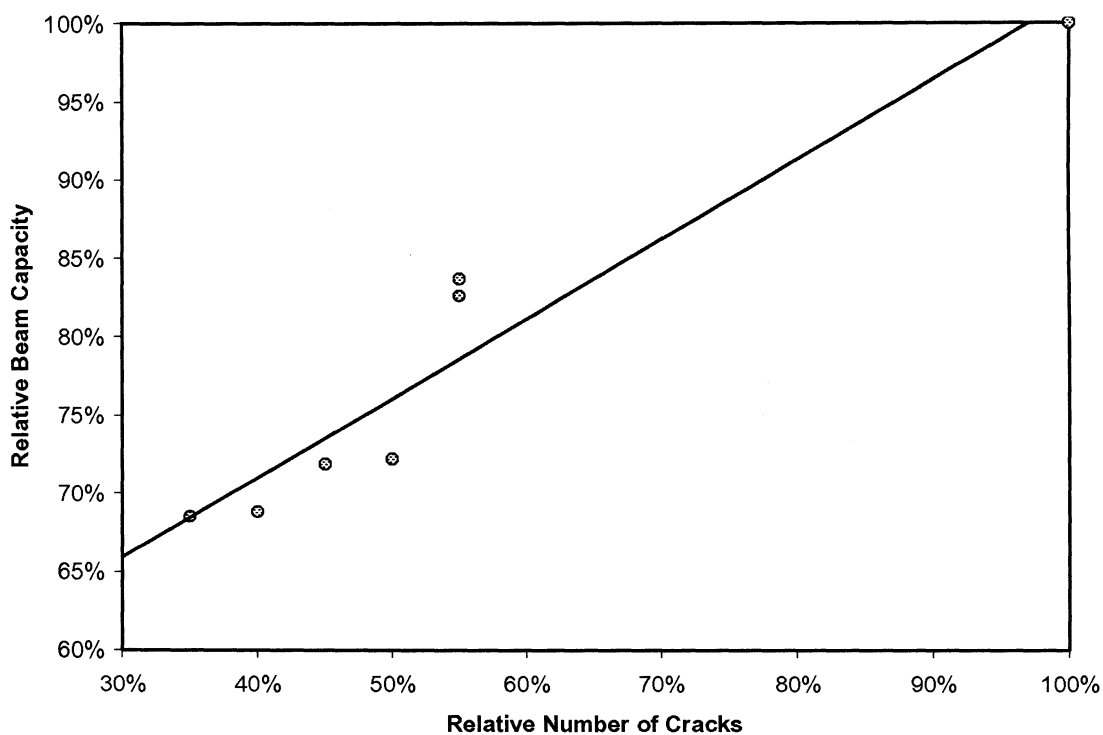
Figure 7-25: The relationship between the number of flexural cracks and beam capacity.

Equation 7-13 numerically expresses this relationship, which was obtained using regression analysis, where Cn is the relative number of flexural cracks, B is the relative beam capacity, and r^2 is the coefficient of determination.

Equation 7-13 $$B = 0.51Cn + 0.51 \qquad (r^2 = 0.92)$$

7.16.4 Beam Capacity and Flexural Crack Spacing

The reduction in beam capacity not only related to the number of flexural cracks, but also to their spacing. Figure 7-26 graphs this relationship between beam capacity and the spacing of flexural cracks. The Equation 7-14 of the best-fit line through the data is the numerical expression obtained using regression analysis, where Csp is the relative spacing of flexural cracks, B is the relative beam capacity, and r^2 is the coefficient of determination.
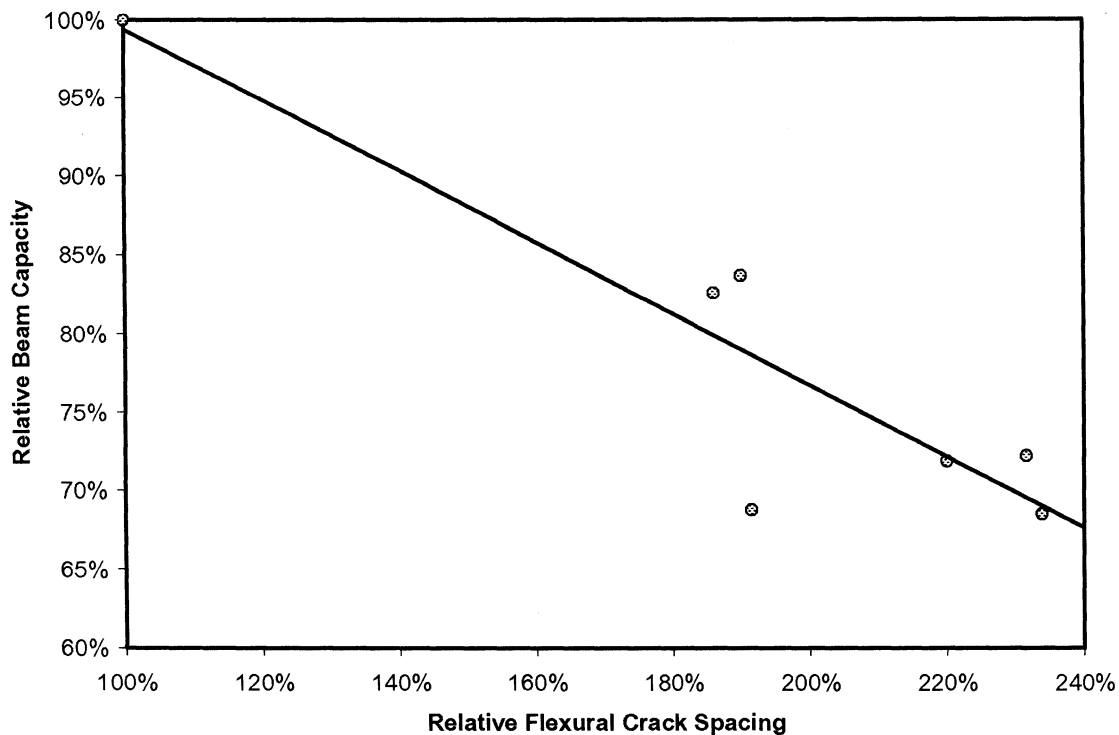
Figure 7-26: The relationship between the relative flexural capacity and the relative crack spacing.

Equation 7-14 $$B = -0.23Csp + 1.22 \qquad (r^2 = 0.83)$$

134

7.16.5 Beam Capacity and Deflection Ratio

In this study, beam capacity was also found to have a relationship with deflection ratio, as seen in Figure 7-23. This relationship was derived by adding Equation 7-7 (for beam capacity) to Equation 7-3 (for deflection ratio), which yields Equation 7-15, where B is the relative beam capacity, Dr is the deflection ratio, and r^2 is the coefficient of determination.

Equation 7-15 $B = -0.58 Dr + 1.61$
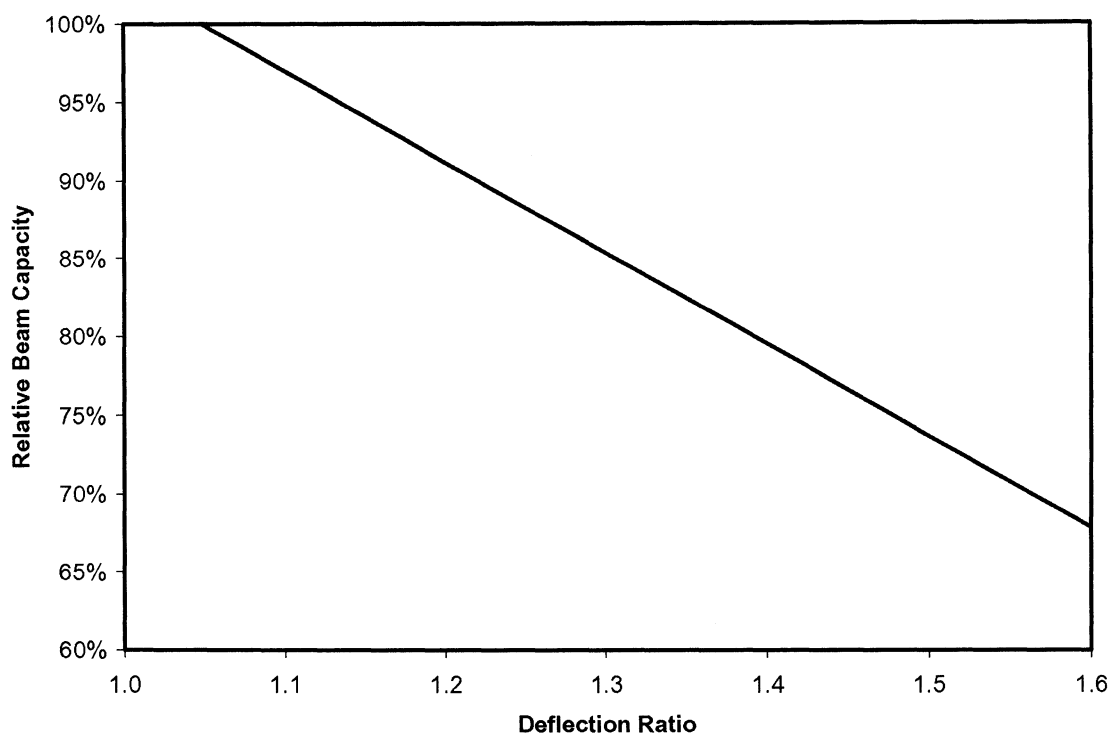
Figure 7-27: Relationship between beam capacity and deflection ratio.

7.16.6 Beam Capacity and Ductility

As mentioned previously, corrosion increases deflections while simultaneously reducing ductility. Data collected from the beam tests performed revealed that the reduction in ductility was nearly at par with the reduction in beam capacity, as illustrated in Figure 7-28.

Equation 7-16 provides the numerical expression of this relationship that was obtained by regression analysis, where Dc is the relative ductility, B is the relative beam capacity, and r^2 is the coefficient of determination.
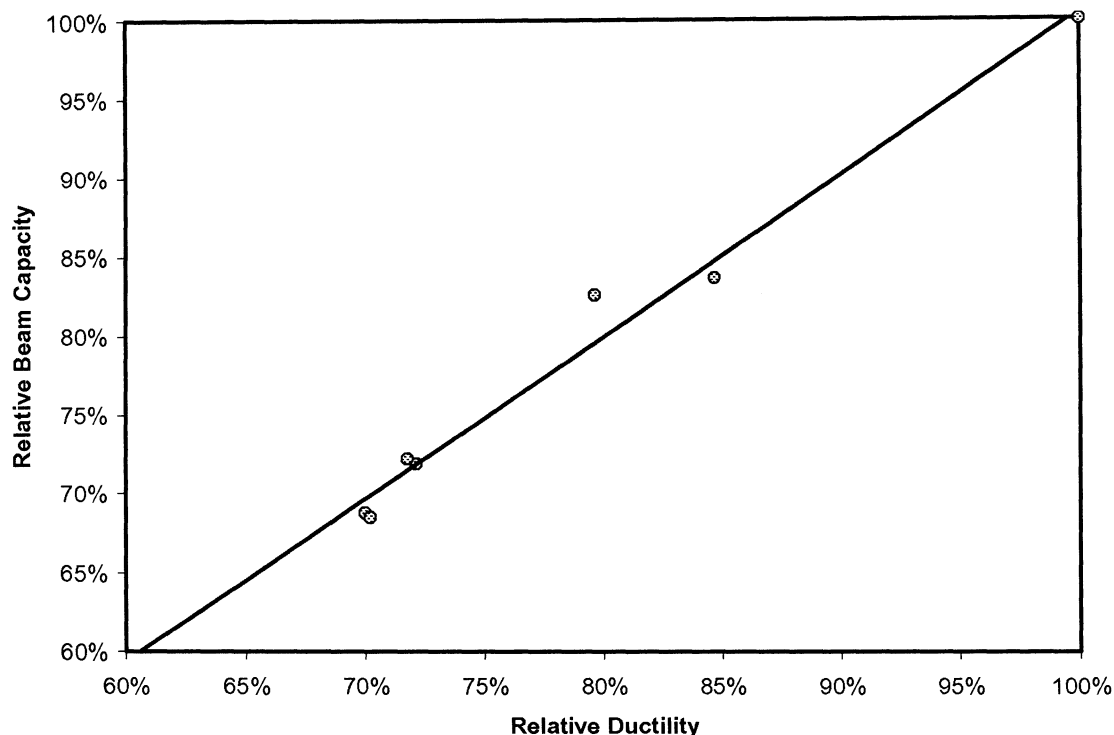
Figure 7-28: The relationship between the beam capacity and ductility.

Equation 7-16 $\qquad\qquad\qquad B = 1.03Dc - 0.022$ $\qquad\qquad\qquad (r^2 = 0.98)$

7.16.7 Beam Capacity and Stiffness

The stiffness of the beams tested was also related to a reduction in beam capacity. Equation 7-17 is the numerical expression of this relationship that was obtained by regression analysis, where k is the relative stiffness, B is the relative beam capacity, and r^2 is the coefficient of determination. Figure 7-29 graphs the data obtained from the beam tests and plots Equation 7-17, which is represented by the continuous line.

Equation 7-17 $\qquad\qquad B = 0.72 \ln k + 1.02 \qquad\qquad (\text{r}^2 = 0.86)$
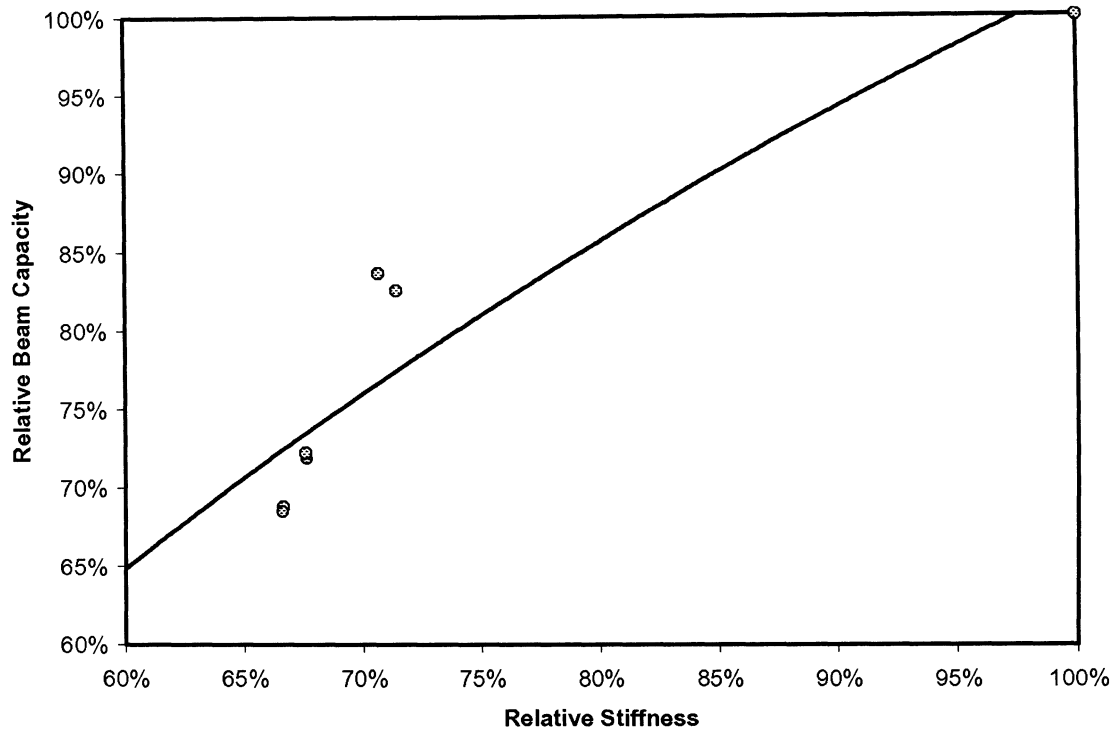
Figure 7-29: The relationship between beam capacity and stiffness.

The data in this figure suggests two distinct linear trends (represented by dashed lines in Figure 7-30), which intersect at (71.1%, 83.2%). The different slopes of these two lines imply that a considerable change in the behaviour of the beams occurred. Specifically, as the capacity of the beam was reduced to 83.2% of the control, the stiffness' rate of change decreased, as indicated by the sharp increase in the slope.

It is estimated that this change occurs at a corrosion level (mass loss) of 1.67%, which is the average mass loss between the two beam specimens that are located near the intersection of the proposed linear trend lines. Given this, it can be argued that the beam specimens were stiffened after their capacity fell below 83.2%, or the corrosion level passed 1.67%.
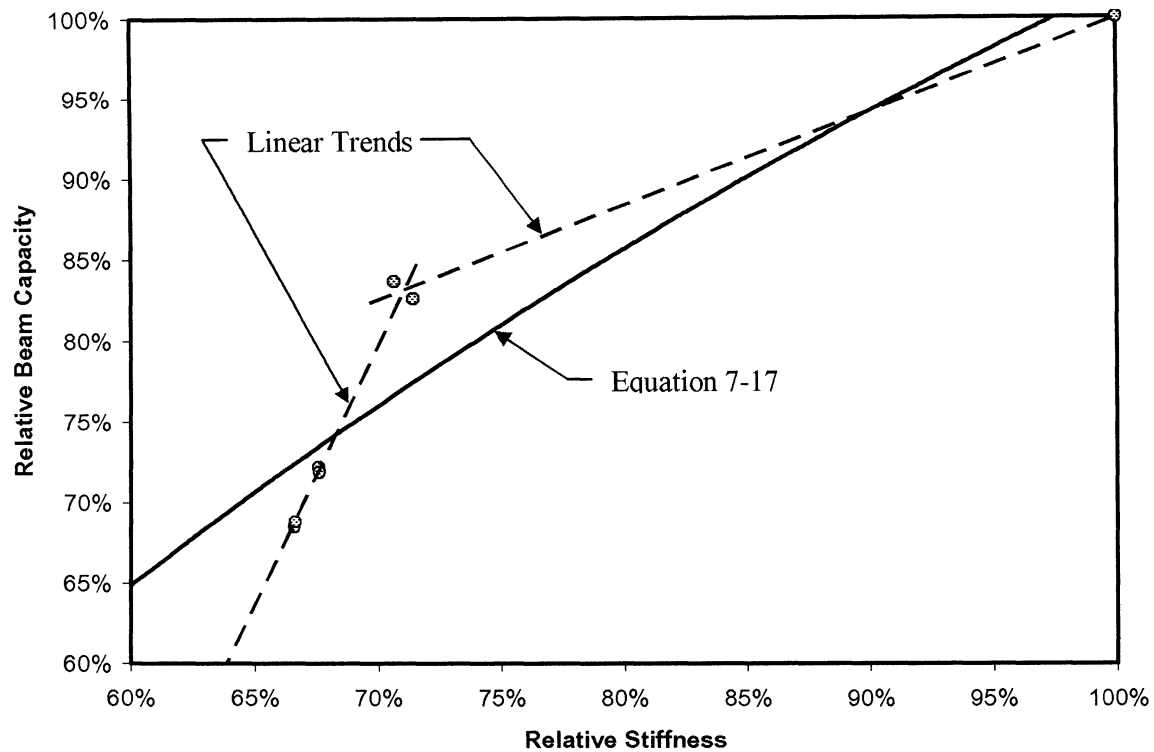
Figure 7-30: The relationship between beam capacity and stiffness

As previously discussed, the stiffness of RC beams tends to change whenever a redistribution of internal stresses occurs. Since redistributions of internal stresses accompany changes in the internal equilibrating mechanism, it can be hypothesized that in this study, beam action was replaced once the level of capacity fell below 83.2%. It can also be postulated that this replacement was due to a shift towards arch action, as this is permitted by both the support-induced confinement (as discussed in section 7.4) and the relatively short span. Moreover, according to Equation 7-11, a beam capacity of 83.2% corresponds to 54.5% bond strength. Thus, it can be inferred that this arch action was initiated when the bars lost 45.5% of their bond.

138

7.16.8 Beam Capacity and Toughness

Toughness is another beam property that relates well to the capacity loss of the beams tested. This relationship was found to have a remarkable correlation, as shown in Figure 7-31. Equation 7-18 is the numerical expression of the relationship between toughness and beam capacity that was obtained by logarithmic regression analysis[18], where B is the relative beam capacity, T is the relative toughness, and r^2 is the coefficient of determination.
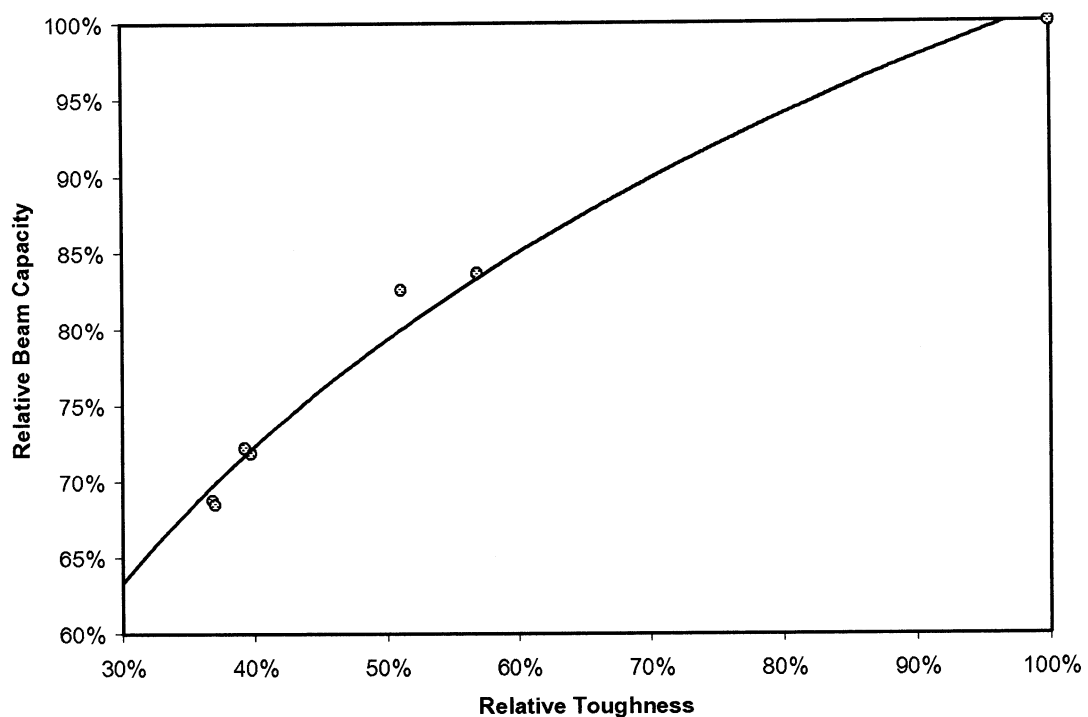
Figure 7-31: The relationship between beam capacity and toughness.

Equation 7-18 $$B = 0.31 \ln T + 1.01 \qquad (r^2 = 0.99)$$

---

[18] Since ln(0) is not possible, the regression analysis was conducted with the ML of the control beam taken as 0.0001.

Chapter 8

CONCLUSIONS AND RECOMMENDATIONS

8.1 Summary

In this experimental study, twelve reinforced concrete (RC) beams were constructed, corroded and tested using four-point loading. The results of these tests were used to examine the beams' various responses to corrosion, with respect to the initial cracking load, flexural crack development, evolution of the failure mode, deflection ratio, ductility, stiffness, toughness, and beam capacity. The data collected from the experimental work in this study enabled the proposal of several numerical relationships that describe the altered behaviour of corroded RC beams.

8.2 Conclusions

Based on the results of this research program, the following conclusions can be drawn:

The overall behaviour of the beam specimens tested conforms to that reported in the literature, with reductions in the ultimate capacity, deflection capacity and stiffness upon increasing corrosion.

The initial cracking load of the beams was observed to decrease at the onset of corrosion and remain constant until a mass loss of about 10%, with a final increase to above the original initial cracking load.

The beam tests revealed a change in flexural crack development with rising corrosion levels, in that there was a simultaneous increase in the average spacing and a decrease in the average number.

The results of this experiment clearly indicated a dramatic shift in the nature of the failure of corroded RC beams, which is confirmed by the literature reviewed. Specifically, it was observed in the present study that as corrosion increased, the failure mode of the beams shifted from predictable ductile flexure failures at mid-span, to more brittle failures near the support. In addition, severely corroded beams displayed sudden and extremely brittle failures at the support, having only one primary failure crack.

The results of this study indicate that there is a shift in the failure type of corroded beams, which is substantiated in the literature reviewed. This shift begins with the onset of corrosion and continues as corrosion propagates. Predicting the type of failure a corroded beam will experience at any given level of corrosion is clearly a topic that requires further research. This is important because knowing how a beam will likely fail can be used to direct measures taken to strengthen damaged beams and possibly prevent an impending failure.

In spite of precautionary measures taken, the accelerated corrosion intended for the tensile steel in the beams tested resulted in the corrosion of the stirrups as well. This caused cracking and delamination of the surrounding concrete, which contributed to the lowering of the residual strength and influenced the location of failure in at least one instance.

Based on the data collected, several new corrosion-dependant empirical relationships were established to model the altered responses of RC beams, including ones with beam stiffness, deflection ratio, ductility, and toughness.

It was found in this study that at a corrosion level of 10.25%, beam deflections increased by a factor of 1.54. Similarly, Cabrera (1996) reported that when the corrosion level reached 9%, beam deflections increased by a factor of 1.5. What distinguishes the present study from Cabrera's is the distribution of the results, indicating a logarithmic relationship rather than a simple linear one.

The data obtained in the current study testifies that ductility is reduced with increasing corrosion, with an exponential decrease followed by stabilization at approximately 75% of the original ductility. This observation is similar to the trend found by Castel et al. (2000b), who reported this stabilization as occurring at approximately 70% of the original ductility.

In this study, the slope of the load-deflection curve (LDC) was used to indicate the stiffness of the RC beams tested. As corrosion increased, their stiffness decreased exponentially and then stabilized at approximately 70% of the original, much like ductility loss.

The area under the LDC up to failure was used to determine the toughness of the RC beams tested. The data acquired showed a similar trend to that of the reduction in stiffness and ductility. Specifically, as corrosion increased, the energy absorbed decreased exponentially, followed by a levelling off. The difference in this case, however, is that the stabilization occurred at a lower value of approximately 40% of the original toughness.

The results obtained from the experimental study for relative ductility, stiffness, and toughness were all best numerically modelled (i.e. yielding the highest coefficient of determination) by power regression analysis. When these numerical relationships are compared, the relative stiffness is approximately equal to the relative ductility, which are both roughly twice the relative toughness.

For the purpose of this study, the results of over 100 corroded-beam tests conducted by other researchers were reviewed and a generalized equation for the capacity loss of RC beams in terms of steel mass loss was generated by way of logarithmic regression analysis.

Numerical relationships were identified between a reduced beam capacity and various phenomena. Namely, the total mass loss, maximum corrosion crack width, number and spacing of flexural cracks, toughness, deflection ratio, ductility, stiffness, and bond strength of the tensile steel were examined. These relationships are valuable in their potential for aiding in the development of an accurate prediction model of beam capacity.

The results of the beam tests indicated a redistribution of internal stresses and a shift in the manner in which the applied load was transferred to the supports. It is hypothesised that when the level of corrosion reached 1.67%, beam action was replaced with arch action, due to the following:

The capacity loss was relatively minor when compared to the bond loss. Since beam action cannot account for the capacities observed given such low bond strengths, it can be deduced that as corrosion progressed, beam action was replaced with an alternative such as arch action.

After considering the work of Coronelli and Gambarova (2004), Cairns and Zhao (1993), and Rodriguez et al. (1997), it can be concluded that the support-induced confinement of the beams tested was sufficient to allow for arch action.

The data acquired from the present experimental study showed that after the capacity dropped below 83.2%, the beams stiffened dramatically, indicating a redistribution of internal stresses. A distribution such as this can be explained by a change from beam to arch action.

This capacity of 83.2% corresponds to the corrosion level of 1.67% mentioned above, which was established using numerical relationships derived from the beam tests performed.

In sum, the results of this laboratory study have led to a better understanding, both qualitatively and quantitatively, of the impact of corrosion on various phenomena of reinforced concrete beams with corroded reinforcing steel. Moreover, several relationships involving the ultimate capacity and the level of corrosion were developed.

8.3   Recommendations for Future Research

Further research is required in order to gain a better understanding of the behavioural changes of RC beams due to corrosion. The following studies are recommended:

It is evident from the tests conducted that corrosion of the stirrups occurred. To investigate the effect that the corrosion of the stirrups had on the results of this experiment, similar beams should be tested without stirrups or with external stirrups. Such tests would also aid in the understanding of how the confinement of the concrete surrounding tensile bars affects the behaviour of corroded RC beams, particularly load-carrying capacity.

The results of the beam tests point to both the slipping and anchoring of the tensile bars; the lack of the widening of flexural cracks is symptomatic of the loss of anchorage, whereas the forces at the beam-ends suggest sufficient support-induced confinement to anchor the bars and allow for arch action. In order to learn more about this apparent contradiction, examining the anchorage of the bars of similar beams is recommended. This may be achieved through the measurement of bar slippage at the ends of the beams and the strains of both the tensile steel and concrete. This recommendation may also validate or refute the notion of the onset of arch action at the estimated corrosion level of 1.67%.

144

The measurement of the steel and concrete strains may also identify the manner in which the stresses were redistributed after the degradation of bond, and shed light on the unexpected failure modes of the corroded beams tested in this study.

Forcing anchorage of the tensile steel may affect the way in which the beams react to corrosion. This can be achieved by testing beams similar to those in this experiment, but with well-anchored bars (i.e. bars having hooks or bends at the beam-ends). A study of this nature can then be contrasted with the current findings in order to investigate the effects of anchorage on both the initiation of arch action and the evolution of the failure mode.

In closing, a great deal of testing is required before the nature and behaviour of corroded RC beams can be comprehended, as there are numerous variables to consider. These variables include the concrete cover thickness, bar size, reinforcement ratio, moment arm length, beam depth, and concrete permeability and compressive strength. A holistic understanding of RC beams with corroded reinforcing steel can only be achieved once each factor is understood individually. Moreover, the identification of cause and effect relationships between the variables and corroded RC beams is required to accurately model these elements and predict their residual strength and service life.

Finally, the development of practice-oriented equations for the evaluation of RC beams that consider the loss of both bond and steel cross-sectional area would contribute to the structural engineering community. However, the determination of the input parameters could pose a major limitation to these equations, which must be overcome before they can be used to facilitate the assessment of structures in the field. For instance, there are currently no methods available to conveniently determine either the cross-section reduction (location and distribution of pits) or the residual bond strength of corroded reinforcing steel. The

development of these methods would make the practice-oriented equations viable, which would undoubtedly prove to be a great asset to engineers in the field.

REFERENCES

Al-Negheimish, Abdulaziz I.; and Al-Zaid, Rajeh Z. "Effect of Manufacturing Process and Rusting on the Bond Behavior of Deformed Bars in Concrete." *Cement Concrete Composites* 26, no. 6 (2004): 735.

Al-Sulaimani, G.J.; Kaleemullah, M.; and Basunbul, I.A.; Rasheeduzzafar. "Influence of Corrosion and Cracking on Bond Behaviour and Strength of RC Members." *ACI Structural* Journal 87, no. 2 (1990): 220.

Amleh, Lamya. "Bond Deterioration of Reinforcing Steel in Concrete Due to Corrosion" Ph.D. diss, McGill University (Canada), 2000

Amleh, Lamya. Class Discussion. Ryerson University, Toronto. 13 April 2005.

Amleh, Lamya; and Mirza, Saeed. "Corrosion Influence on Bond between Steel and Concrete." *ACI Structural Journal* 96, no. 3 (1999): 415.

Azher, Syed Ayub. "A Prediction Model for the Residual Flexural Strength of Corroded Reinforced Concrete Beams." Ph.D. diss., King Fahd University of Petroleum and Minerals (Saudi Arabia), 2005.

Ballim, Y., J. C. Reid, and A. R. Kemp. "Deflection of RC Beams Under Simultaneous Load and Steel Corrosion." Magazine of Concrete Research 53, no. 3 (2001): 171-181.

Ballim, Y., and J.C. Reid. "Reinforcement Corrosion and the Deflection of RC Beams: An Experimental Critique of Current Test Methods." Cement and Concrete Composites 25 (2003): 625.

Bertolini, L., Elsener, B., and Polder, R.,"Corrosion of Steel in Concrete: Prevention, Diagnosis, Repair." Weinheim: Wiley-VCH, (2004).

Broomfield, John P. Corrosion of Steel in Concrete: Understand, Investigation and Repair. London: E & FN Spon, (1997).

Cabrera, J. G. "Deterioration of Concrete due to Reinforcement Steel Corrosion." *Cement Concrete Composites* 18, no. 1 (1996): 47.

Cabrera, J.G., and Ghoddoussi, P., "The Effect of Reinforcement Corrosion on the Strength of the Steel/Concrete Bond" International Conference on Bond in Concrete Riga, Latvia: CEB (1992): 10. Excerpted Under "Load Carrying Capacity of Concrete Structures with Corroded Reinforcement." Construction and Building Materials Construction and Building Materials 11.4 (1997): 239.

Cairns, J; Zhao, M.A. "Strength Assessment of Corrosion Damaged Reinforced Slabs and Beams." *Proceedings of the Institution of Civil Engineers, Structures and Buildings* 99, (1993): 141. Excerpted Under "Analytical Model to Predict Nonlinear Flexural Behaviour of Corroded RC Beams." ." *ACI Structural Journal* 102, no. 4 (2005): 550.

Capozucca, Roberto, and M. Nilde Cerri. "Influence of Reinforcement Corrosion-in the Compressive Zone-on the Behaviour of RC Beams." Engineering Structures 25, no. 13 (2003): 1575-1583.

Castel, A.; Francois, R.; and Arliguie, G. "Mechanical Behaviour of Corroded RC Beams - Part 1: Experimental Study of Corroded Beams." *Materials and Structures* 33, no. 233 (2000a): 539.

Castel, A.; Francois, R.; and Arliguie, G. "Mechanical Behaviour of Corroded RC Beams - Part 2: Bond and Notch Effects." *Materials and Structures* 33, no. 233 (2000b): 545.

Chung, Lan; Cho, Seung-Ho; Kim, Jang-Ho Jay; and Yi, Seong-Tae. "Correction Factor Suggestion for ACI Development Length Provisions Based on Flexural Testing of RC Slabs With Various Levels of Corroded Reinforcing Bars." *Engineering Structures* 26, (2004): 1013.

Coronelli, D; and Gambarova, P. "Structural Assessment of Corroded RC Beams: Modeling Guidelines." *Journal of Structural Engineering* 130, no. 8 (2004): 1214.

Dekoster, M., F. Buyle-Bodin, O. Maurel, and Y. Delmas. "Modelling of the Flexural Behaviour of RC Beams Subjected to Localised and Uniform Corrosion." Engineering Structures 25, no. 10 (2003): 1333-1341.

Eyre J.R. and Nokhasteh M-A., Strength assessment of corrosion damaged reinforced slabs and beams, *Proceedings Institution Civil Engineers, Structures & Buildings*, vol.94, (1992): 197-203.

Fan, Ying-Fang; Zhou, Jing; and Feng, Xin. "Prediction of Load-carrying Capacity of Corroded RC Beam." *China Ocean Engineering* 18, no. 1 (2004): 107.

Fang, Congqi; Lundgren, Karin; Chen, Liuguo; and Zhu, Chaoying. "Corrosion Influence on Bond in RC." *Cement and Concrete Research* 34, no. 11 (2004): 2159.

Feld, Jacob; and Carper, Kenneth L., Construction Failure 2nd Edition. New York: John Wiley & Sons, Inc. (1997).

Grimaldi, G.; Brevet, P.; Pannier, G.; and Raharinaivo, A. Br. Corros. J. 21 (1) (1986) 55.

Gu, Gordon Ping; Beaudoin, James J.; and Ramchandran, Vangi S. "Techniques for Corrosion Investigation in Rinforced Concrete." *Handbook of Analytical Techniques in Concrete Science and Technology.* New Jersey: Noyes Publications, (2001): 441.

Higgins, Christopher; Farrow III, William C.; Potisuk, Tanarat; Miller, Thomas H.; Yim, Solomon C.; Holcomb, Gordon R.; Cramer, Stephen D.; Covino, Bernard S.; Jr.; Bullard, Sophie J.; Ziomek-Moroz, Margaret; and Matthes, Steven A.. *Shear Capacity Assessment of Corrosion Damaged Reinforced Beams.* USA: Oregon Department of Transportation and Federal Highway Administration, (2003).

Higgins, Christopher, and William C. Farrow III. "Tests of Reinforced Concrete Beams with Corrosion-Damaged Stirrups." ACI Structural Journal 103, no. 1 (2006): 133-141.

Huang, R., and C.C. Yang. "Condition Assessment of RC Beams Relative to Reinforcement Corrosion." Cement and Concrete Composites 19 (1997): 131.

Hunkeler, F, "Corrosion in Rinforced Concrete: Processes and Mechanisms." *Corrosion in Rinforced Concrete Structures*, Cambridge, Woodhead Publishing Limited, (2005): 1

Illston, J.M.; and Domone, P.L.J., Construction Materials: Their nature and behaviour, London, Spon Press, (2001)

Koch G. H., M. H. P. Brongers, N. G. Thompson, Y. P. Virmani, and J. H. Payer (2002). *Corrosion Cost and Preventive Strategies in the United States.* Report no. FHWA-RD-01-156. Federal Highway Administration, U. S. Department of Transportation. Washington, DC. 773 pp.

Lee, Han-Seung; Noguchi, Takafumi; and Tomosawa, Fuminori. "Evaluation of the Bond Properties between Concrete and Reinforcement as a Function of the Degree of Reinforcement Corrosion." Cement and Concrete Research 32, no. 8 (2002): 1313.

Maaddawy, Tamer El; Soudki, Khaled; and Topper, Timothy. "Analytical Model to Predict Nonlinear Flexural Behaviour of Corroded RC Beams." *ACI Structural Journal* 102, no. 4 (2005a): 550.

Maaddawy, Tamer El; Soudki, Khaled; and Topper, Timothy. "Long-Term Performance of Corrosion-Damaged Reinforced Concrete Beams." *ACI Structural Journal* 102, no. 5 (2005b): 649-656.

MacGregor, James G.; and Bartlett, Michael F. RC: Mechanics and Design (1st Canadian Edition: Scarborough, Prentice Hall, (2000): 89-367.

Malhotra, V. M., and Carino, N. J., Handbook on Nondestructive Testing of Concrete Second Edition: Boca Raton, CRC Press LLC, (2004)

Mangat, P. S., and M. S. Elgarf. "Flexural Strength of Concrete Beams with Corroding Reinforcement." *ACI Structural Journal* 96, no. 1 (1999a): 149.

Mangat, P. S., and M. S. Elgarf. "Bond Characteristics of Corroding Reinforcement in Concrete Beams." *Materials and Structures/Materiaux Et Constructions* 32, no. 216 (1999b): 89-97.

Perno, S., Z. Rinaldi, C. Valente, and L. Pardi. "Experimental Evaluation of the Load Bearing Capacity of Corroded Beams." (2005): 508-516.

Plizzari, A, Giovanni, Deldossi A Massimo, and Massimo Stefano . "Experimental Study on Anchored Bars in R.C. Elements with Transverse Reinforcement." Materials and Structures/Materiaux Et Constructions 29, no. 193 (1996): 534-542.

Ramchandran, Vangi S. "Concrete Science." *Handbook of Analytical Techniques in Concrete Science and Technology.* New Jersey: Noyes Publications, (2001): 1.

RILEM TC 154-EMC, Mater. Struct. 36 (2003) 461.

Rodriguez, J.; Ortega, L. M.; and Casel, J. "Load-carrying Capacity of Concrete Structures with Corroded Reinforcement." *Construction Building Materials* 11, no. 4 (1997): 239.

Romagnoli, R.; Batic, R.O.; Vetere, V.F.; Sota, J.D.; Lucchini, I.T.; and Carbonari, R.O. "The Influence of the Cement Paste Microstructure on Corrosion and the Adherence of Reinforcing Bars as a Function of the Water-Cement Ratio." *Anti-Corrosion Methods and Materials* 49, no. 1 (2002): 11.

Roberge, Pierre R., Handbook of Corrosion Engineering: New York, McGraw Hill, (2000).

Stanish, Kyle; Hooton, R.D.; and Pantazopoulou, S.J. "Corrosion Effects on Bond Strength in RC." *ACI Structural Journal* 96, no. 6 (1999): 915.

Sarveswaran, V.; Roberts, M. B.; and Ward, J.A. "Reliability Assessment of Deteriorating Reinforced Concrete Beams." Proc. Instn Civ Engrs Structs & Blds, vol.140, (2000): 239-247

Uomoto, T., and Misra, S., "Behaviour of Concrete Beams and Columns in Marine Environment When Corrosion of Reinforcing Bars Take Place" ACI Special Publication SP-109 1988: 127-145. Excerpted Under "Load Carrying Capacity of Concrete Structures with Corroded Reinforcement." Construction and Building Materials Construction and Building Materials 11.4 (1997): 239.

Wang, Kejin, Yoon, Sanchun; Weiss, Jason W.; and Shah, Surendra P. "Combined Effect of Corrosion and Stresses in RC Beams." *ASCE-ME* (2000): 1.

Yoon, Sanchun; Wang, Kejin; Weiss, Jason W.; and Shah, Surendra P. "Interaction between Loading, Corrosion, and Serviceability of RC." ACI Materials Journal 97, no. 6 (2000): 637.

APPENDIX A: CURRENT AND VOLTAGE READINGS FROM THE ACCELERATED CORROSION PROGRAM

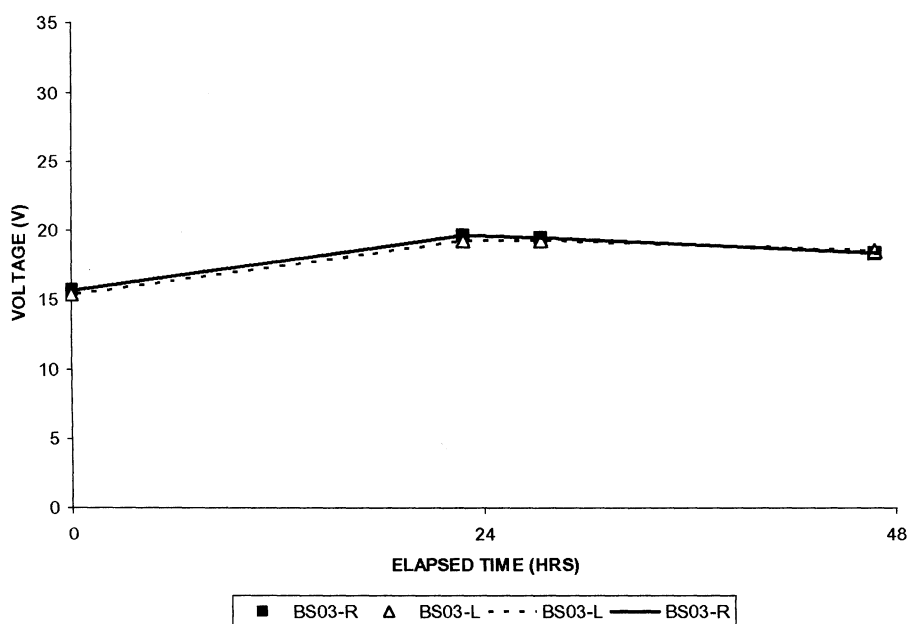N.B. Current was constant at 1.5 amp, unless otherwise shown.

Figure A-1: Voltage readings for BS03-R and BS03-L.

Figure A-2: Voltage readings for BS04-R and BS04-L.
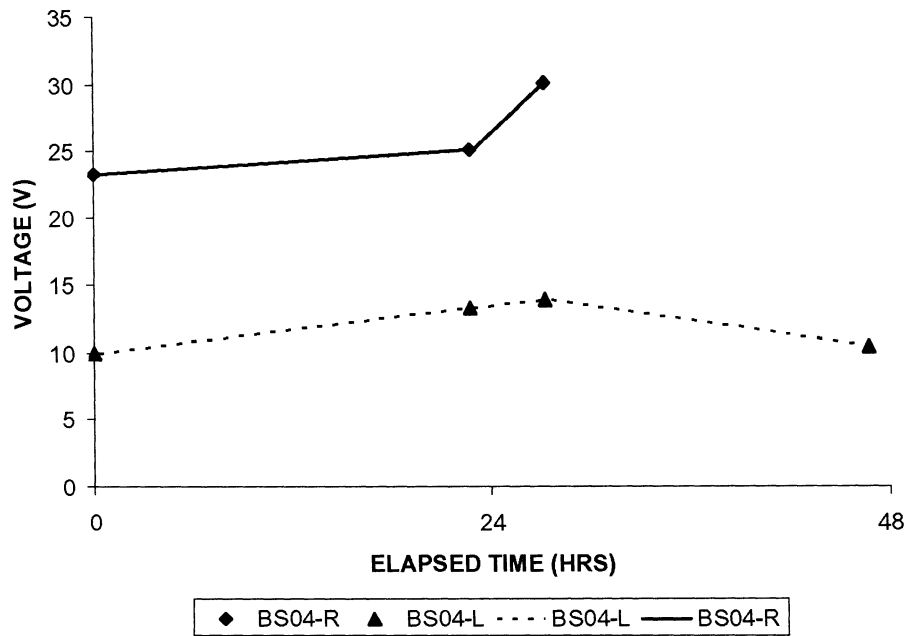

Figure A-3: Voltage readings for BS05-R and BS05-L.

Figure A-4: Voltage readings for BS06-R and BS06-L.

Figure A-5: Voltage readings for BS07-R and BS07-L.
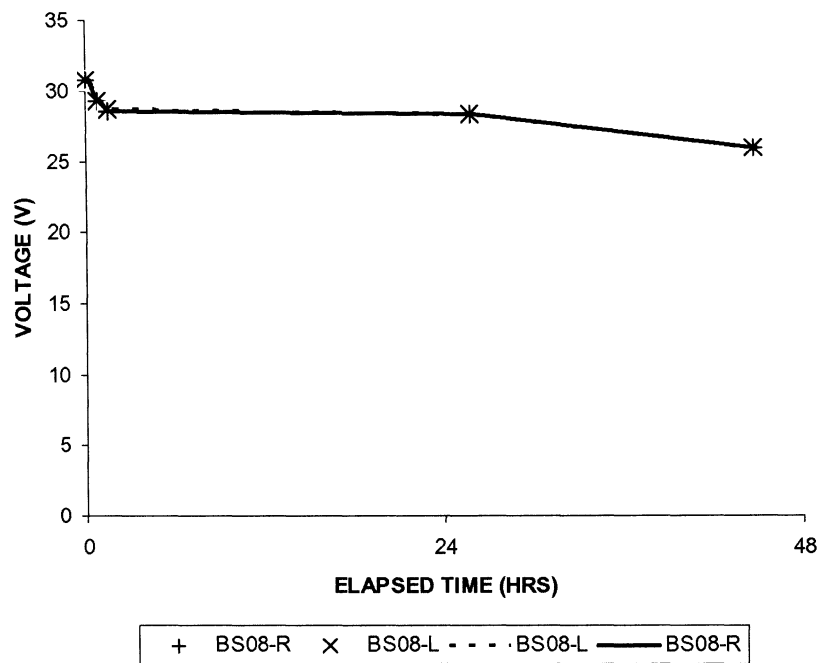
Figure A-6: Voltage readings for BS08-R and BS08-L.
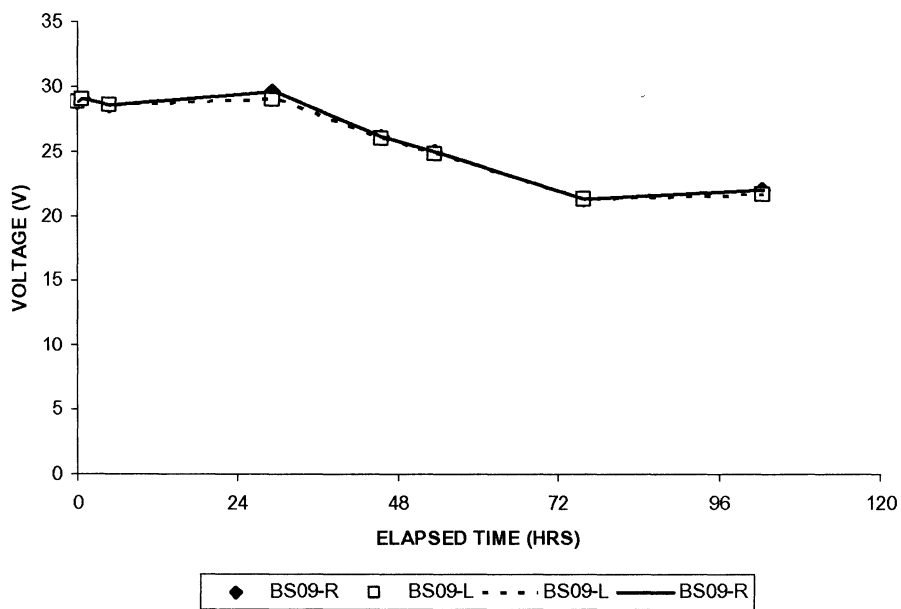
Figure A-7: Voltage readings for BS09-R and BS09-L.
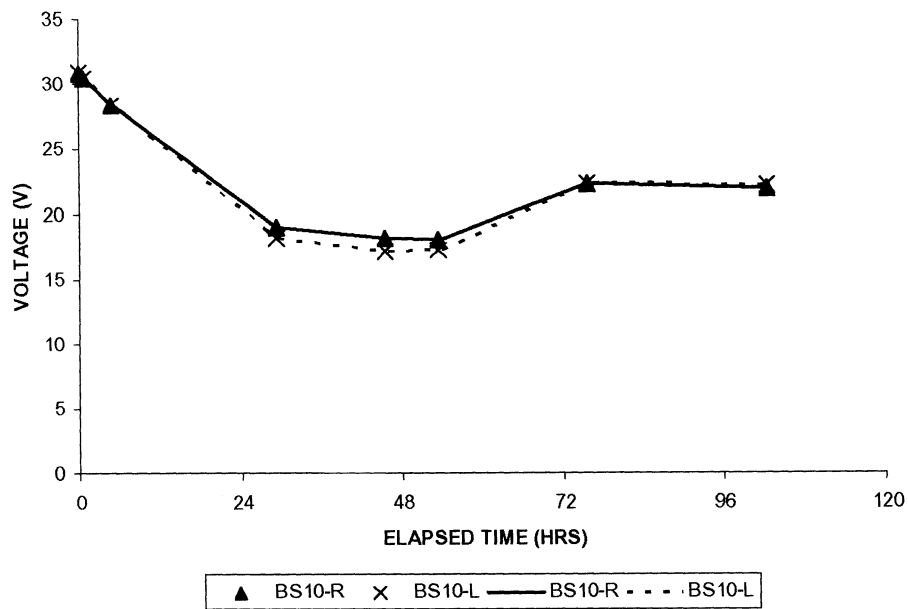
Figure A-8: Voltage readings for BS10-R and BS10-L.
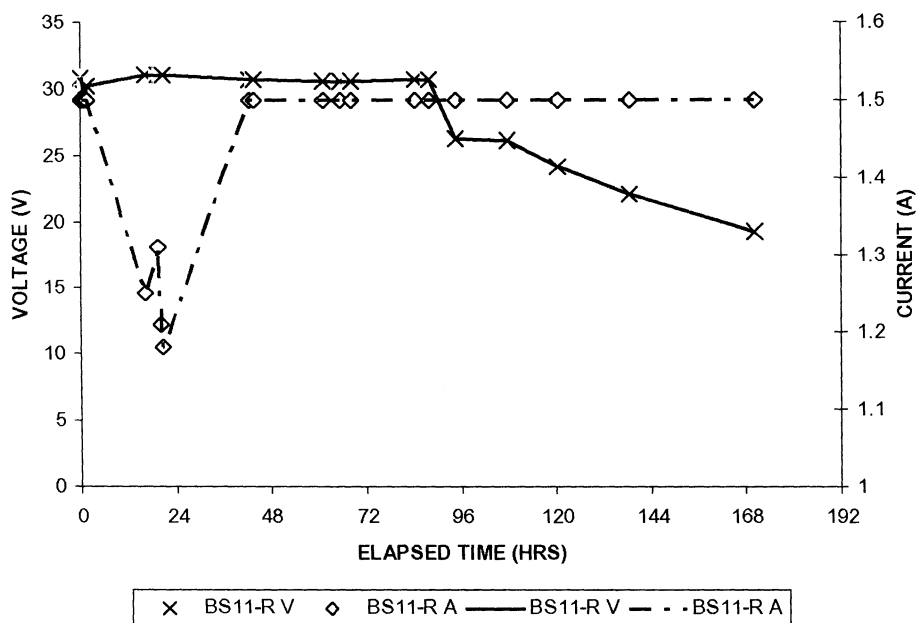
Figure A-9: Voltage and current readings for BS11-R.
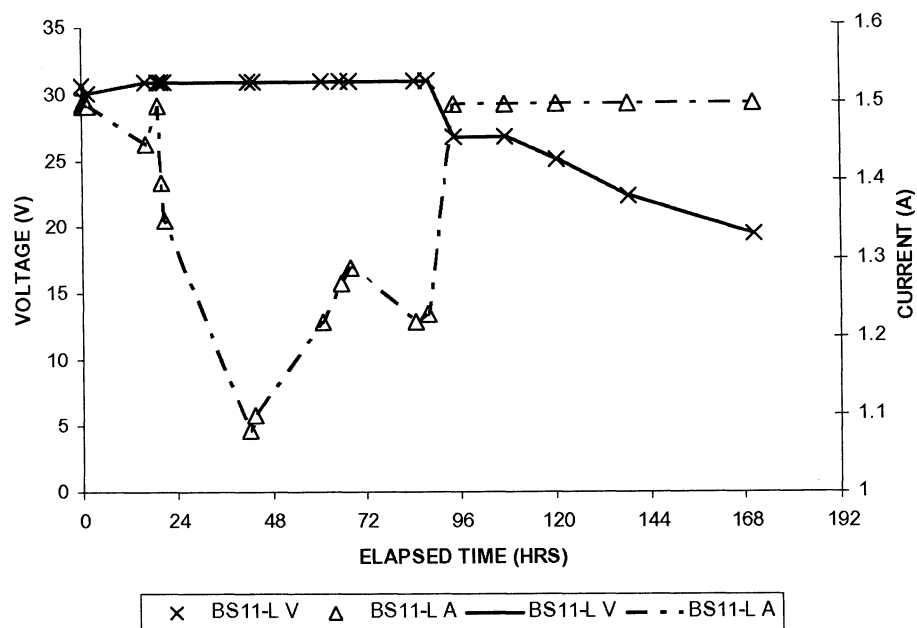
Figure A-10: Voltage and current readings for BS11-L.
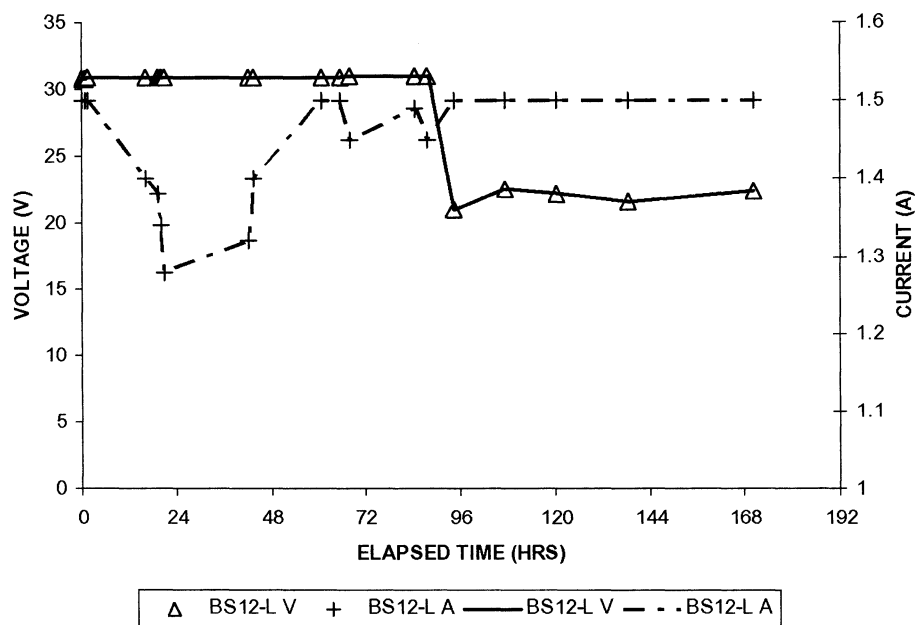
Figure A-11: Voltage and current readings for BS12-L.
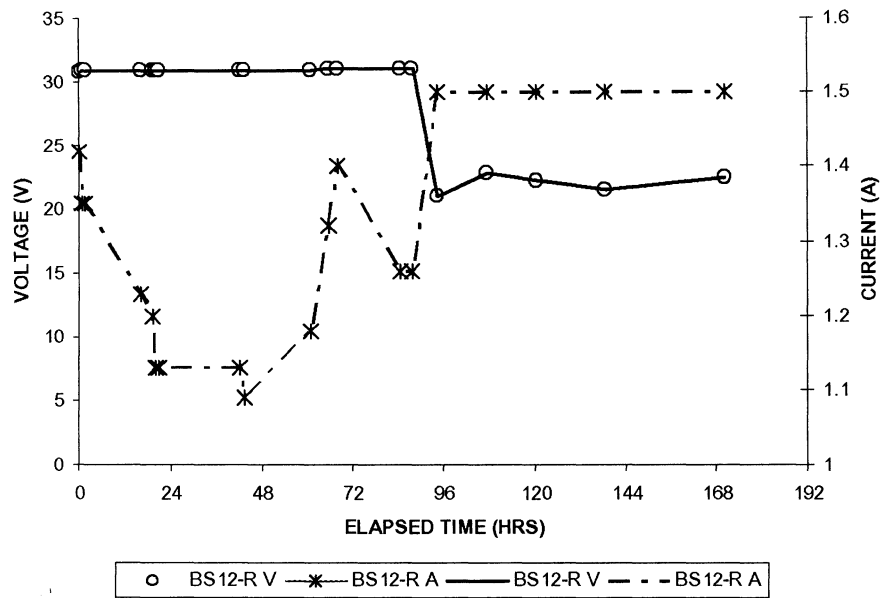
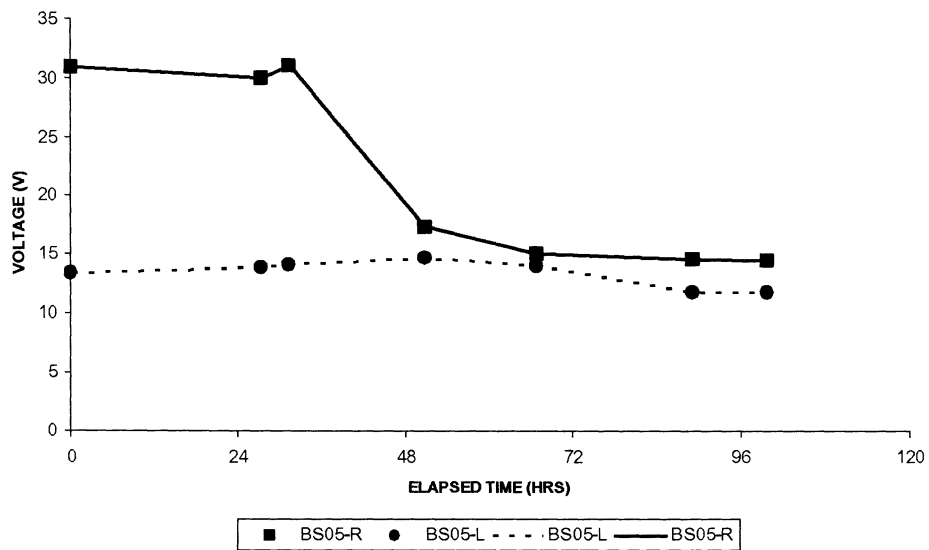Figure A-12: Voltage and current readings for BS12-R.
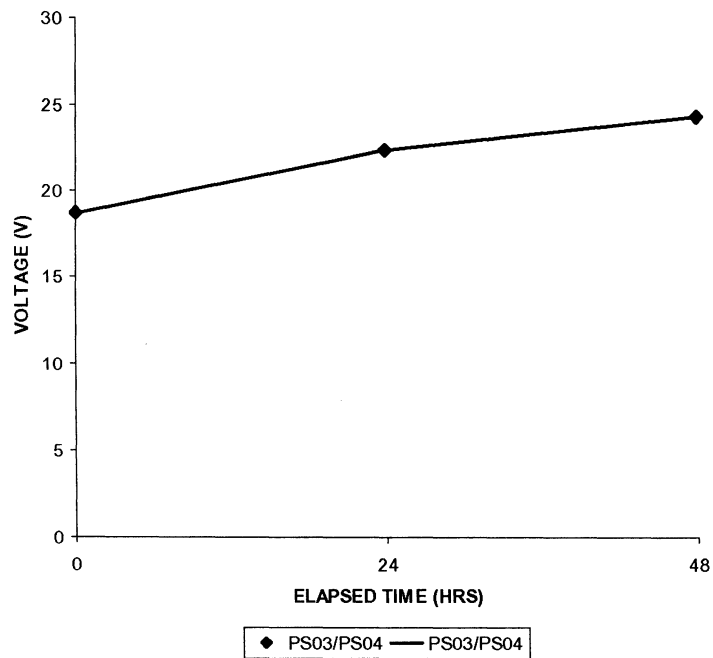
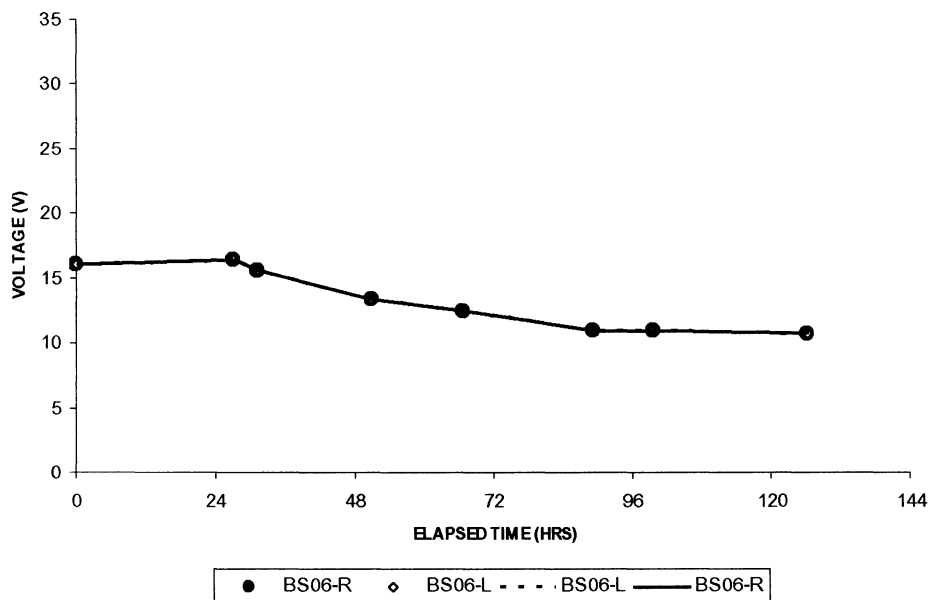Figure A-13: Voltage readings for PS03 and PS04.

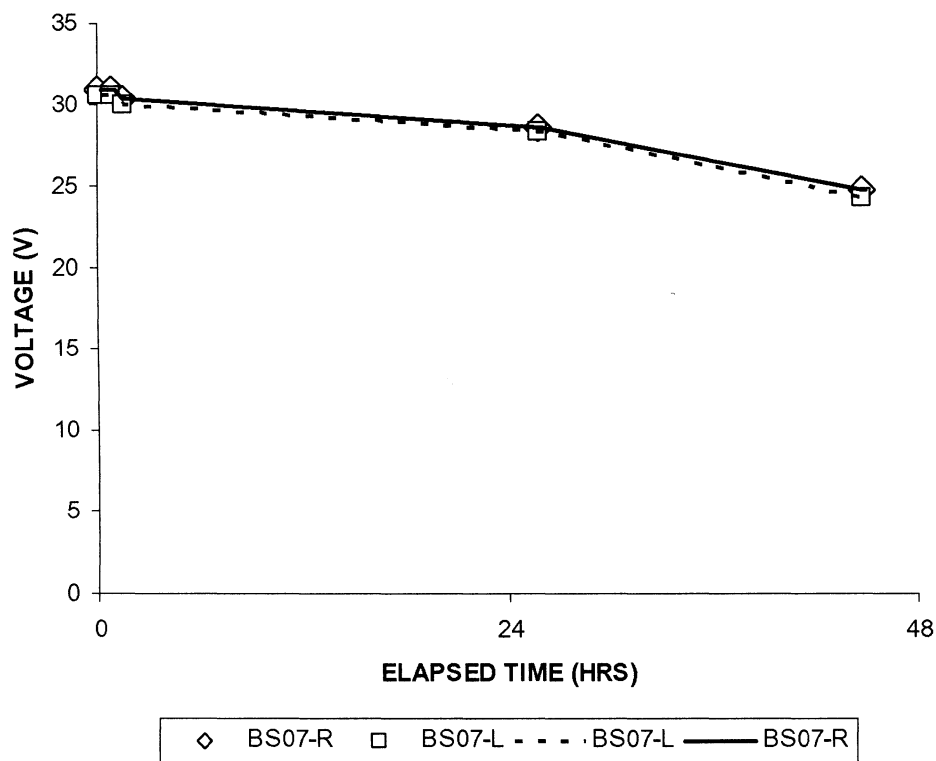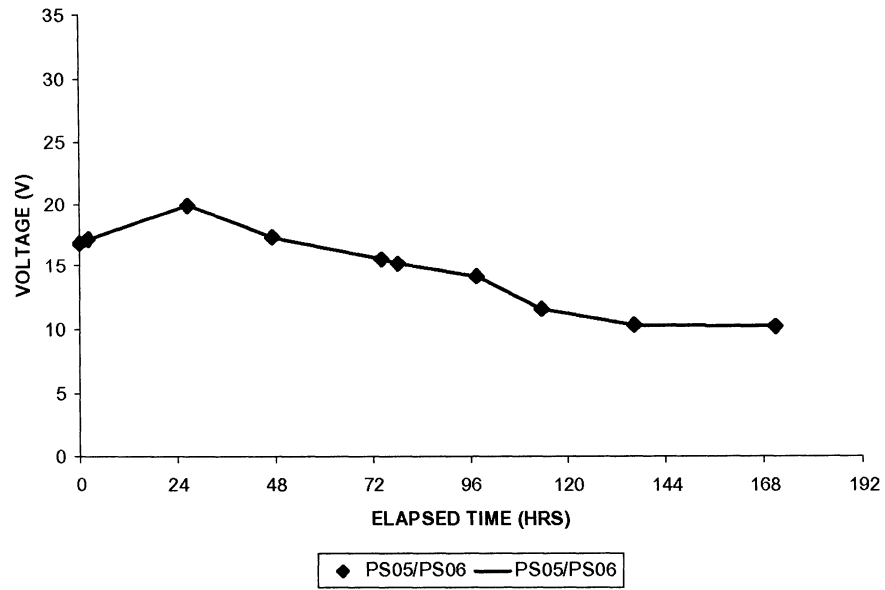**Figure A-14: Voltage readings for PS05 and PS06.**
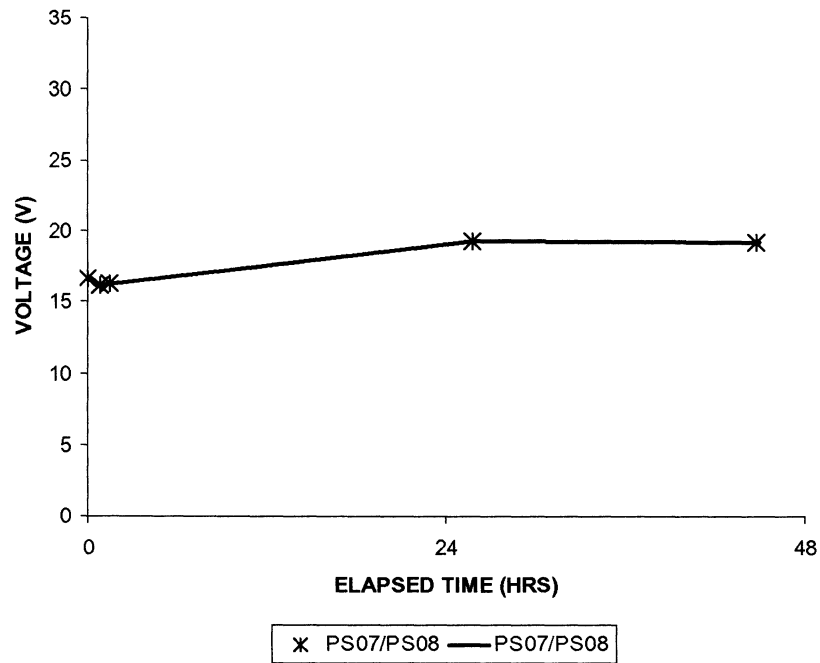
Figure A-15: Voltage readings for PS07 and PS08.

157
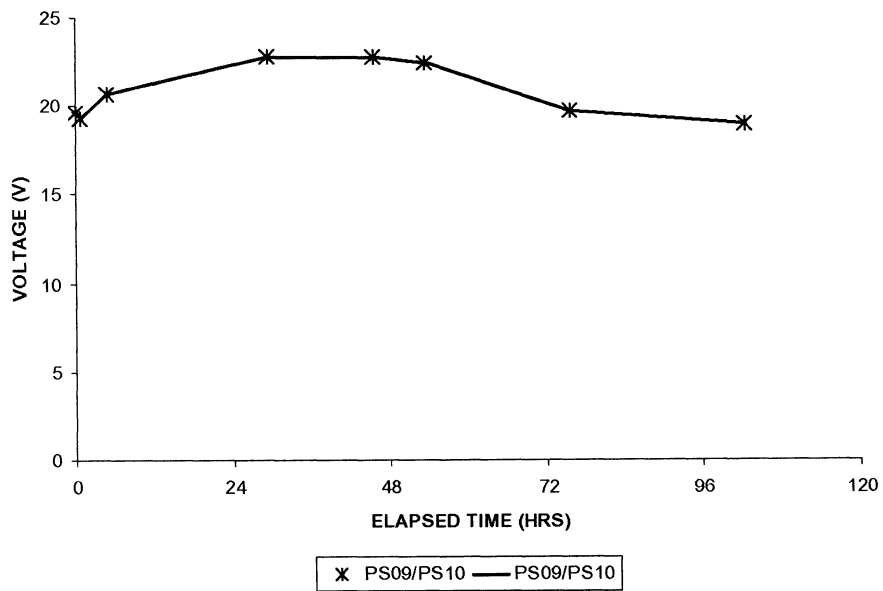
Figure A-16: Voltage readings for PS09 and PS10.
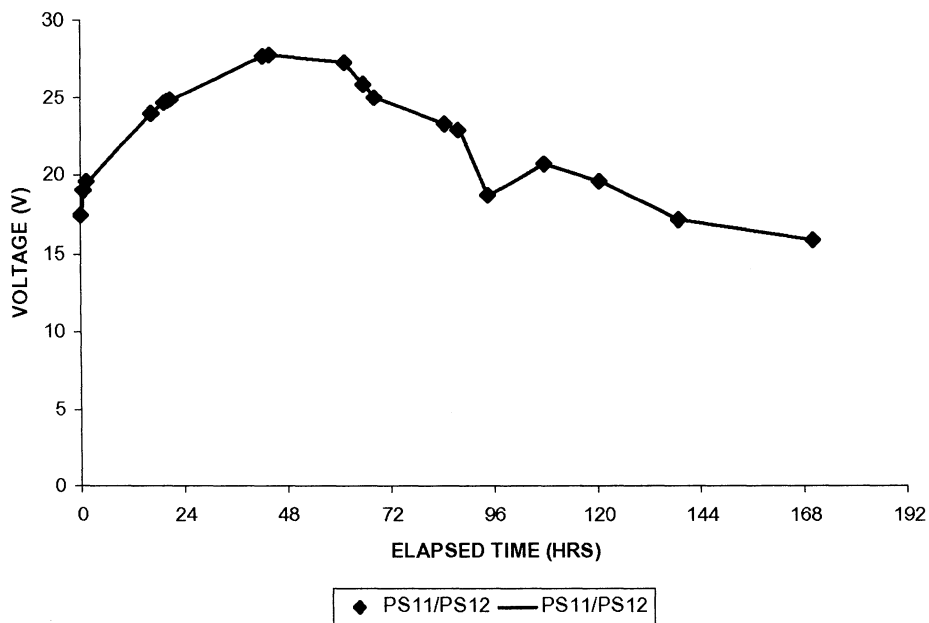
Figure A-17: Voltage readings for PS11 and PS12.

APPENDIX B: CORROSION CRACK MAPS
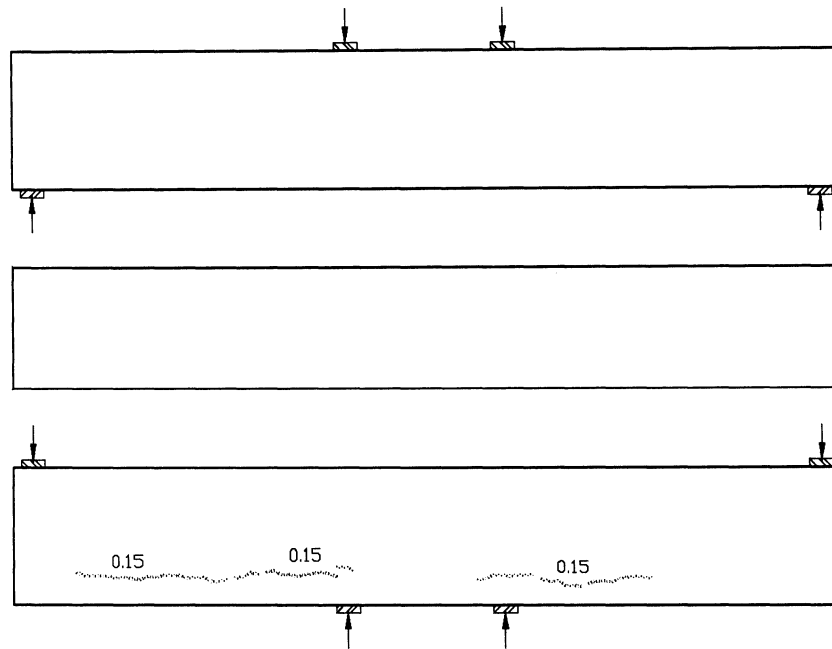
Figure B-1: Corrosion crack map for BS03
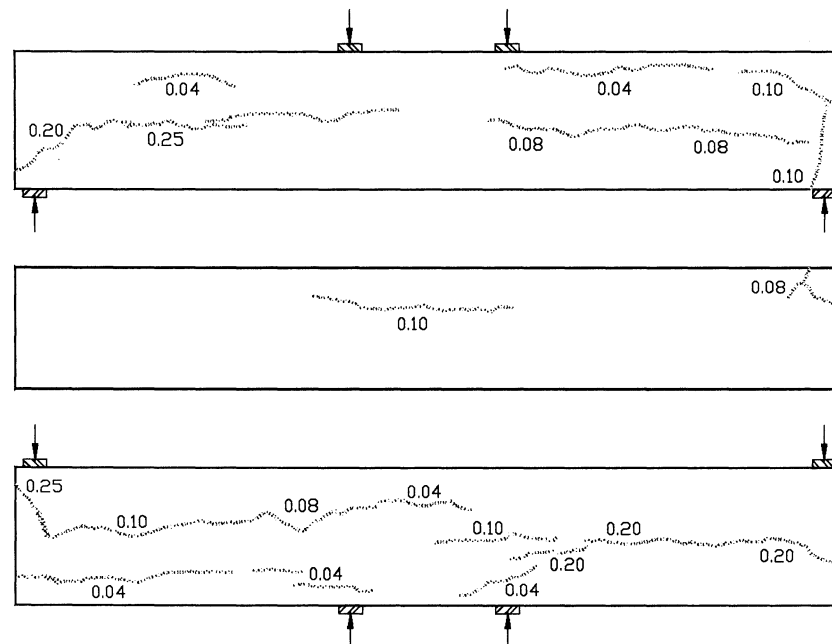
Figure B-2: Corrosion crack map for BS05
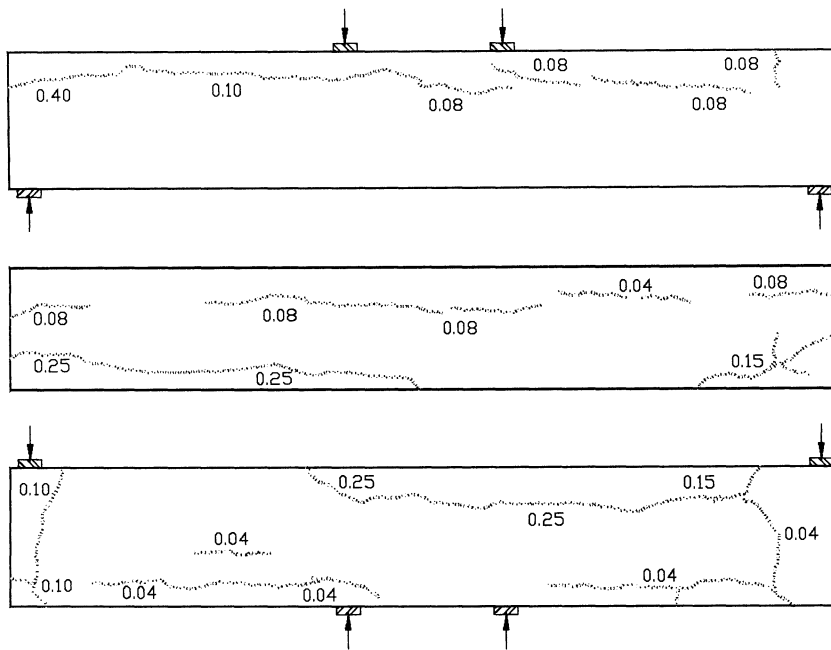
Figure B-3: Corrosion crack map for BS06
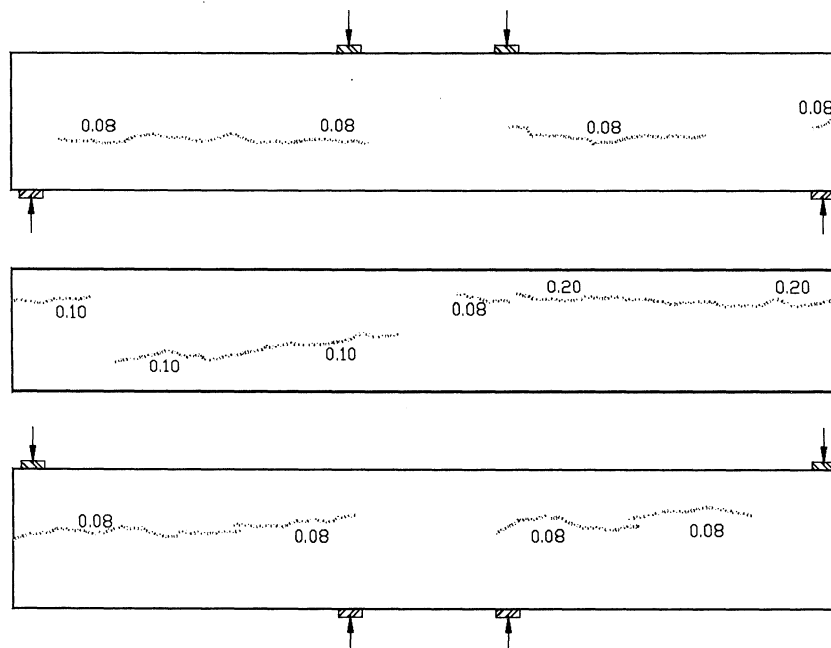
Figure B-4: Corrosion crack map for BS07
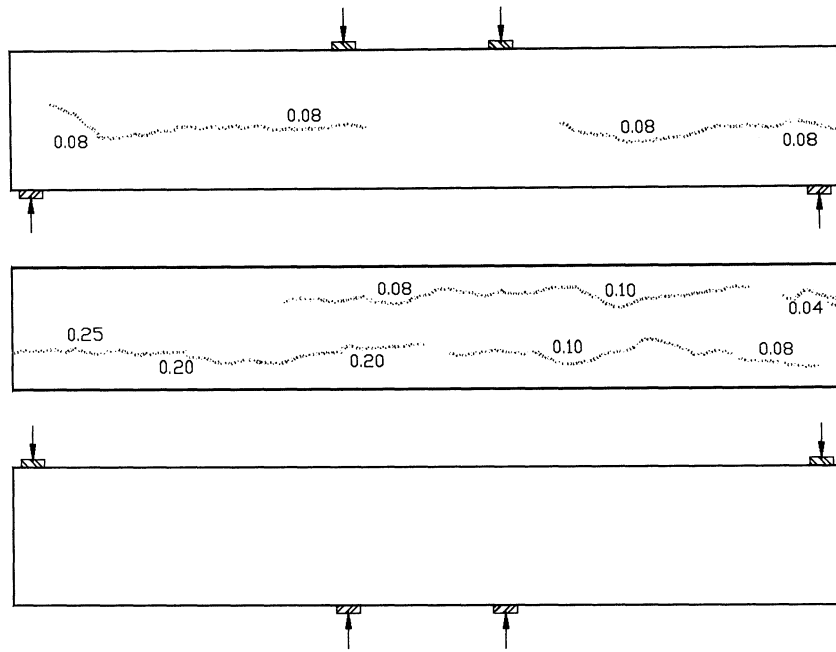
Figure B-5: Corrosion crack map for BS08
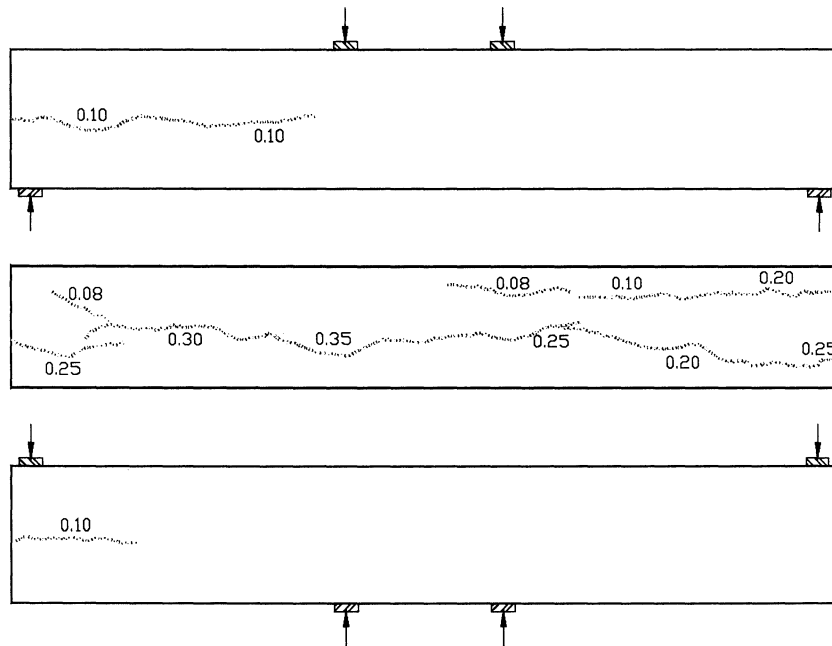
Figure B-6: Corrosion crack map for BS09

161
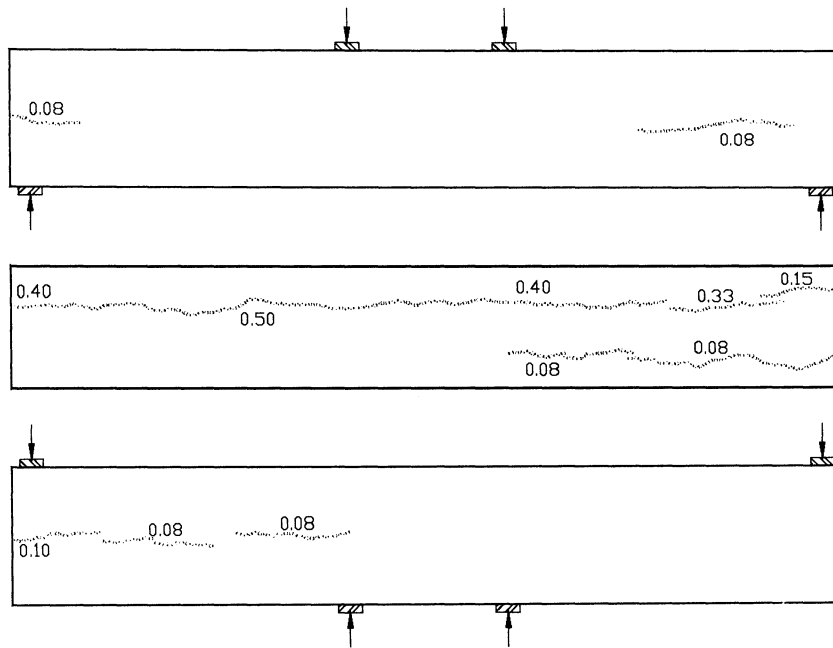
Figure B-7: Corrosion crack map for BS10
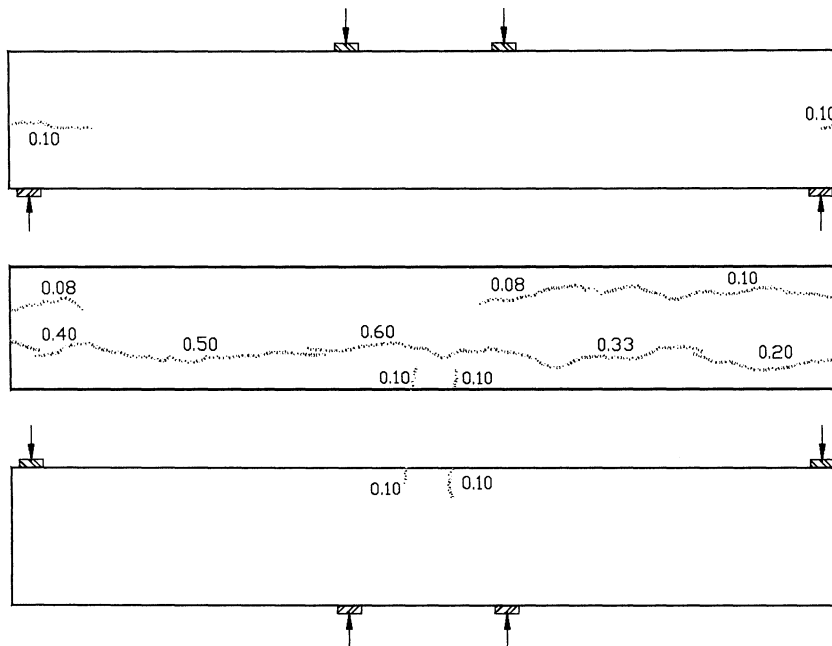
Figure B-8: Corrosion crack map for BS11

162
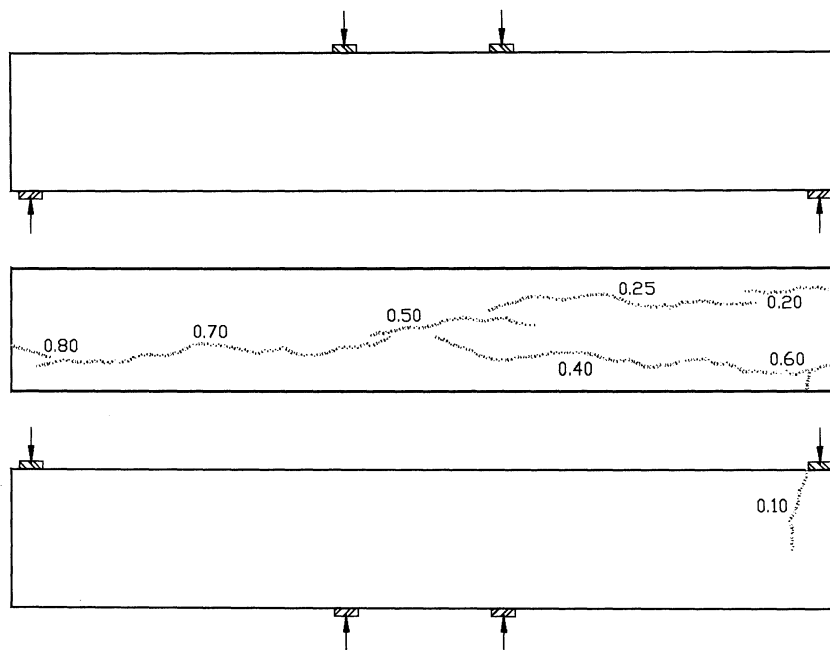
Figure B-9: Corrosion crack map for BS12

APPENDIX C: HALF-CELL POTENTIAL READINGS FOR BEAM SPECIMENS

Table C-1: Categories used to analyze the half-cell potential readings.

Designation	Readings Less Than	Legend
A	-0.42 mV	
B	-0.35 mV	
C	-0.28 mV	
D	-0.21 mV	
E	-0.14 mV	
F	-0.07 mV	
G	0.00 mV	

RIGHT												RIGHT
	-0.092	-0.095	-0.091	-0.089	-0.092	-0.077	-0.079	-0.088	-0.082	-0.081	-0.076	
BOTTOM	-0.085	-0.084	-0.097	-0.078	-0.078	-0.080	-0.079	-0.083	-0.079	-0.088	-0.087	BOTTOM
	-0.076	-0.086	-0.084	-0.081	-0.080	-0.093	-0.073	-0.080	-0.084	-0.077	-0.074	
LEFT	-0.078	-0.082	-0.076	-0.088	-0.089	-0.090	-0.088	-0.088	-0.075	-0.085	-0.076	LEFT

RIGHT												RIGHT
	F	F	F	F	F	F	F	F	F	F	F	
BOTTOM	F	F	F	F	F	F	F	F	F	F	F	BOTTOM
	F	F	F	F	F	F	F	F	F	F	F	
LEFT	F	F	F	F	F	F	F	F	F	F	F	LEFT

Figure C-1: Half-cell potential readings (mV) and their categories for BS01

164

RIGHT											RIGHT
	-0.120	-0.133	-0.135	-0.130	-0.132	-0.130	-0.134	-0.127	-0.133	-0.121	-0.119	
BOTTOM	-0.108	-0.112	-0.116	-0.122	-0.121	-0.119	-0.114	-0.109	-0.125	-0.112	-0.115	BOTTOM
	-0.107	-0.117	-0.117	-0.129	-0.119	-0.117	-0.107	-0.114	-0.123	-0.110	-0.123	
LEFT	-0.116	-0.114	-0.116	-0.112	-0.102	-0.115	-0.117	-0.120	-0.121	-0.131	-0.127	LEFT

RIGHT											RIGHT
	F	F	F	F	F	F	F	F	F	F	F	
BOTTOM	F	F	F	F	F	F	F	F	F	F	F	BOTTOM
	F	F	F	F	F	F	F	F	F	F	F	
LEFT	F	F	F	F	F	F	F	F	F	F	F	LEFT

Figure C-2: Half-cell potential readings (mV) and their categories for BS02

RIGHT											RIGHT
	-0.256	-0.275	-0.285	-0.288	-0.285	-0.278	-0.277	-0.277	-0.282	-0.270	-0.252	
BOTTOM	-0.251	-0.260	-0.263	-0.260	-0.262	-0.257	-0.262	-0.255	-0.258	-0.252	-0.251	BOTTOM
	-0.341	-0.347	-0.344	-0.344	-0.341	-0.366	-0.335	-0.332	-0.331	-0.330	-0.329	
LEFT	-0.342	-0.375	-0.369	-0.375	-0.361	-0.351	-0.350	-0.344	-0.341	-0.336	-0.330	LEFT

RIGHT											RIGHT
	D	D	C	C	C	D	D	D	C	D	D	
BOTTOM	D	D	D	D	D	B	D	D	D	D	D	BOTTOM
	C	C	C	C	C	C	B	C	C	C	C	
LEFT	C	B	B	B	B	B	B	C	C	C	C	LEFT

Figure C-3: Half-cell potential readings (mV) and their categories for BS03

RIGHT											RIGHT
	-0.297	-0.300	-0.289	-0.288	-0.268	-0.281	-0.301	-0.303	-0.297	-0.311	-0.335	
BOTTOM	-0.276	-0.291	-0.277	-0.287	-0.286	-0.289	-0.295	-0.297	-0.305	-0.311	-0.354	BOTTOM
	-0.136	-0.151	-0.133	-0.148	-0.149	-0.148	-0.153	-0.153	-0.165	-0.177	-0.204	
LEFT	-0.150	-0.157	-0.132	-0.126	-0.146	-0.140	-0.146	-0.151	-0.175	-0.180	-0.209	LEFT

RIGHT											RIGHT
	C	C	C	C	D	C	C	C	C	C	C	
BOTTOM	D	C	D	C	C	C	C	C	C	C	B	BOTTOM
	F	E	F	E	E	E	E	E	E	E	E	
LEFT	E	E	F	F	E	E	E	E	E	E	E	LEFT

Figure C-4: Half-cell potential readings (mV) and their categories for BS04

RIGHT	-0.390	-0.389	-0.434	-0.400	-0.384	-0.407	-0.411	-0.420	-0.411	-0.412	-0.368	RIGHT
BOTTOM	-0.434	-0.455	-0.445	-0.437	-0.451	-0.452	-0.438	-0.441	-0.433	-0.435	-0.425	BOTTOM
	-0.470	-0.481	-0.475	-0.469	-0.479	-0.461	-0.448	-0.461	-0.434	-0.418	-0.407	
LEFT	-0.484	-0.478	-0.495	-0.478	-0.485	-0.470	-0.463	-0.426	-0.434	-0.421	-0.379	LEFT

Figure C-5: Half-cell potential readings (mV) and their categories for BS05

RIGHT	-0.373	-0.393	-0.412	-0.393	-0.386	-0.407	-0.430	-0.447	-0.445	-0.430	-0.389	RIGHT
BOTTOM	-0.404	-0.419	-0.441	-0.445	-0.426	-0.420	-0.433	-0.441	-0.447	-0.452	-0.410	BOTTOM
	-0.400	-0.425	-0.414	-0.411	-0.409	-0.393	-0.409	-0.410	-0.403	-0.417	-0.395	
LEFT	-0.375	-0.374	-0.338	-0.361	-0.385	-0.392	-0.433	-0.428	-0.416	-0.398	-0.368	LEFT

Figure C-6: Half-cell potential readings (mV) and their categories for BS06

RIGHT	-0.398	-0.436	-0.434	-0.425	-0.434	-0.434	-0.478	-0.467	-0.457	-0.453	-0.392	RIGHT
BOTTOM	-0.375	-0.415	-0.417	-0.435	-0.420	-0.409	-0.430	-0.421	-0.428	-0.420	-0.367	BOTTOM
	-0.391	-0.419	-0.406	-0.409	-0.410	-0.440	-0.442	-0.439	-0.442	-0.420	-0.359	
LEFT	-0.378	-0.417	-0.428	-0.436	-0.441	-0.448	-0.456	-0.422	-0.422	-0.404	-0.383	LEFT

Figure C-7: Half-cell potential readings (mV) and their categories for BS07

RIGHT	-0.415	-0.450	-0.431	-0.431	-0.421	-0.420	-0.423	-0.434	-0.460	-0.449	-0.400	RIGHT
BOTTOM	-0.396	-0.442	-0.431	-0.433	-0.434	-0.423	-0.416	-0.428	-0.439	-0.419	-0.382	BOTTOM
	-0.407	-0.422	-0.438	-0.450	-0.439	-0.401	-0.422	-0.408	-0.430	-0.397	-0.374	
LEFT	-0.371	-0.415	-0.448	-0.453	-0.432	-0.388	-0.411	-0.422	-0.439	-0.426	-0.379	LEFT

RIGHT	B	A	A	A	A	A	A	A	A	A	B	RIGHT
BOTTOM	B	A	A	A	A	A	B	A	A	B	B	BOTTOM
	B	A	A	A	A	B	A	B	A	B	B	
LEFT	B	B	A	A	A	B	B	A	A	A	B	LEFT

Figure C-8: Half-cell potential readings (mV) and their categories for BS08

RIGHT	-0.517	-0.535	-0.537	-0.521	-0.547	-0.517	-0.547	-0.522	-0.548	-0.556	-0.496	RIGHT
BOTTOM	-0.556	-0.558	-0.545	-0.544	-0.554	-0.578	-0.550	-0.547	-0.553	-0.555	-0.519	BOTTOM
	-0.529	-0.535	-0.551	-0.573	-0.565	-0.570	-0.548	-0.543	-0.538	-0.542	-0.524	
LEFT	-0.495	-0.532	-0.533	-0.560	-0.549	-0.524	-0.539	-0.539	-0.521	-0.541	-0.486	LEFT

RIGHT	A	A	A	A	A	A	A	A	A	A	A	RIGHT
BOTTOM	A	A	A	A	A	A	A	A	A	A	A	BOTTOM
	A	A	A	A	A	A	A	A	A	A	A	
LEFT	A	A	A	A	A	A	A	A	A	A	A	LEFT

Figure C-9: Half-cell potential readings (mV) and their categories for BS09

RIGHT	-0.524	-0.550	-0.556	-0.552	-0.552	-0.531	-0.564	-0.545	-0.558	-0.539	-0.522	RIGHT
BOTTOM	-0.514	-0.546	-0.555	-0.546	-0.529	-0.502	-0.529	-0.556	-0.526	-0.536	-0.538	BOTTOM
	-0.501	-0.530	-0.550	-0.533	-0.512	-0.560	-0.532	-0.519	-0.531	-0.538	-0.537	
LEFT	-0.516	-0.485	-0.536	-0.525	-0.518	-0.515	-0.545	-0.515	-0.506	-0.521	-0.515	LEFT

RIGHT	A	A	A	A	A	A	A	A	A	A	A	RIGHT
BOTTOM	A	A	A	A	A	A	A	A	A	A	A	BOTTOM
	A	A	A	A	A	A	A	A	A	A	A	
LEFT	A	A	A	A	A	A	A	A	A	A	A	LEFT

Figure C-10: Half-cell potential readings (mV) and their categories for BS10

RIGHT	-0.672	-0.675	-0.695	-0.690	-0.691	-0.683	-0.673	-0.672	-0.655	-0.624	-0.602	RIGHT
BOTTOM	-0.628	-0.637	-0.636	-0.638	-0.633	-0.616	-0.628	-0.628	-0.626	-0.599	-0.604	BOTTOM
	-0.602	-0.604	-0.605	-0.594	-0.584	-0.593	-0.580	-0.590	-0.620	-0.597	-0.596	
LEFT	-0.606	-0.628	-0.633	-0.629	-0.607	-0.596	-0.613	-0.636	-0.640	-0.607	-0.591	LEFT

RIGHT	A	A	A	A	A	A	A	A	A	A	A	RIGHT
BOTTOM	A	A	A	A	A	A	A	A	A	A	A	BOTTOM
	A	A	A	A	A	A	A	A	A	A	A	
LEFT	A	A	A	A	A	A	A	A	A	A	A	LEFT

Figure C-11: Half-cell potential readings (mV) and their categories for BS11

RIGHT	-0.592	-0.561	-0.579	-0.604	-0.621	-0.610	-0.624	-0.619	-0.630	-0.641	-0.634	RIGHT
BOTTOM	-0.609	-0.594	-0.586	-0.597	-0.616	-0.633	-0.618	-0.601	-0.610	-0.626	-0.624	BOTTOM
	-0.585	-0.558	-0.580	-0.592	-0.604	-0.630	-0.611	-0.592	-0.590	-0.585	-0.607	
LEFT	-0.591	-0.598	-0.596	-0.614	-0.614	-0.622	-0.628	-0.609	-0.608	-0.608	-0.603	LEFT

RIGHT	A	A	A	A	A	A	A	A	A	A	A	RIGHT
BOTTOM	A	A	A	A	A	A	A	A	A	A	A	BOTTOM
	A	A	A	A	A	A	A	A	A	A	A	
LEFT	A	A	A	A	A	A	A	A	A	A	A	LEFT

Figure C-12: Half-cell potential readings (mV) and their categories for BS12.

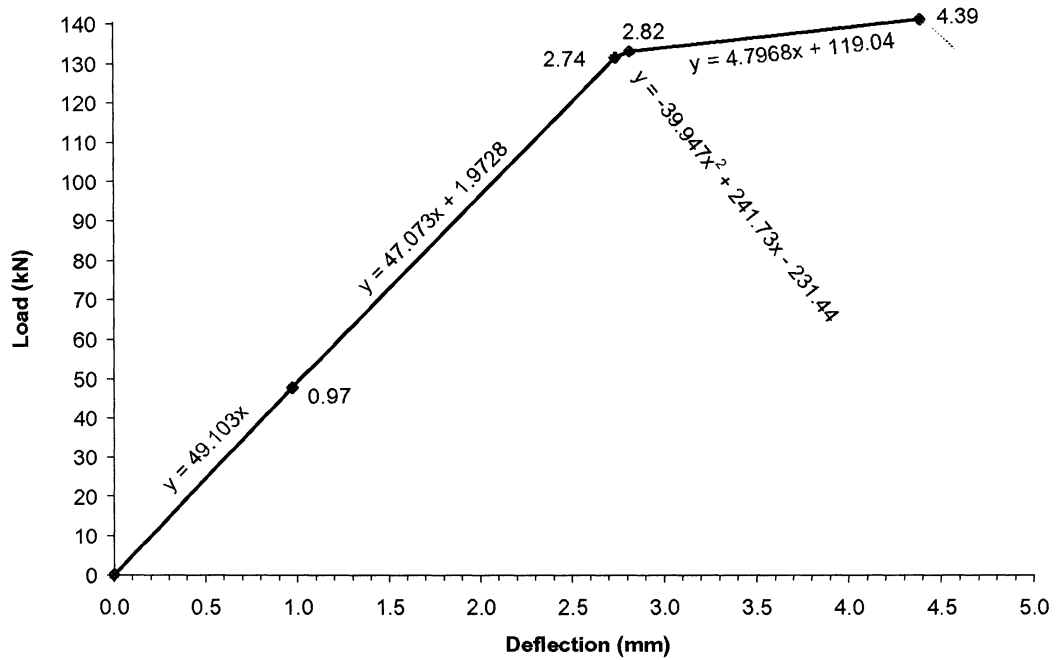# APPENDIX D: LOAD-DEFLECTION CURVE ANALYSIS

Figure D-1: LDC trend lines for BS01

Equation D-1

$$A_{BS01} = \int_{0.00}^{0.97}(49.103x)dx + \int_{0.00}^{2.74}(47.073x + 1.9728)dx$$

$$+ \int_{2.74}^{2.82}(-39.947x^2 + 241.73x - 231.44)dx + \int_{2.82}^{4.39}(4.7968x + 119.04)dx$$

$$\therefore A_{BS01} = 402.74\_kN \cdot mm$$

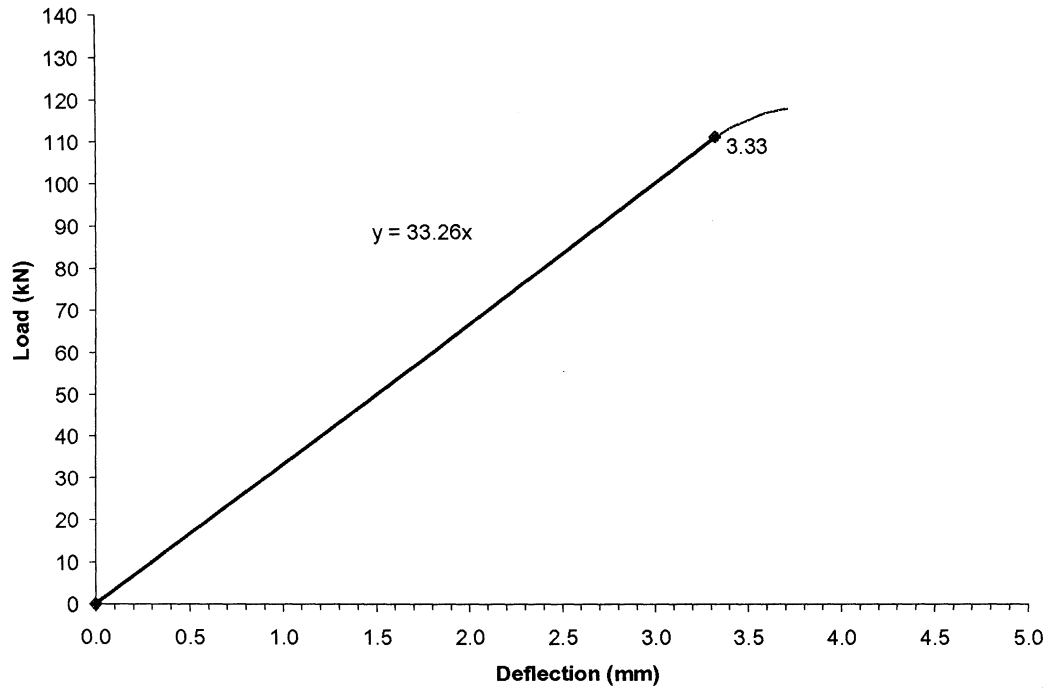Figure D-2: LDC trend line for BS07

Equation D-2

$$A_{BS07} = \int\limits_{0.00}^{3.33}(33.26x)dx + \int\limits_{3.33}^{3.72}(-25.446x^2 + 196.53x - 261.52)dx$$
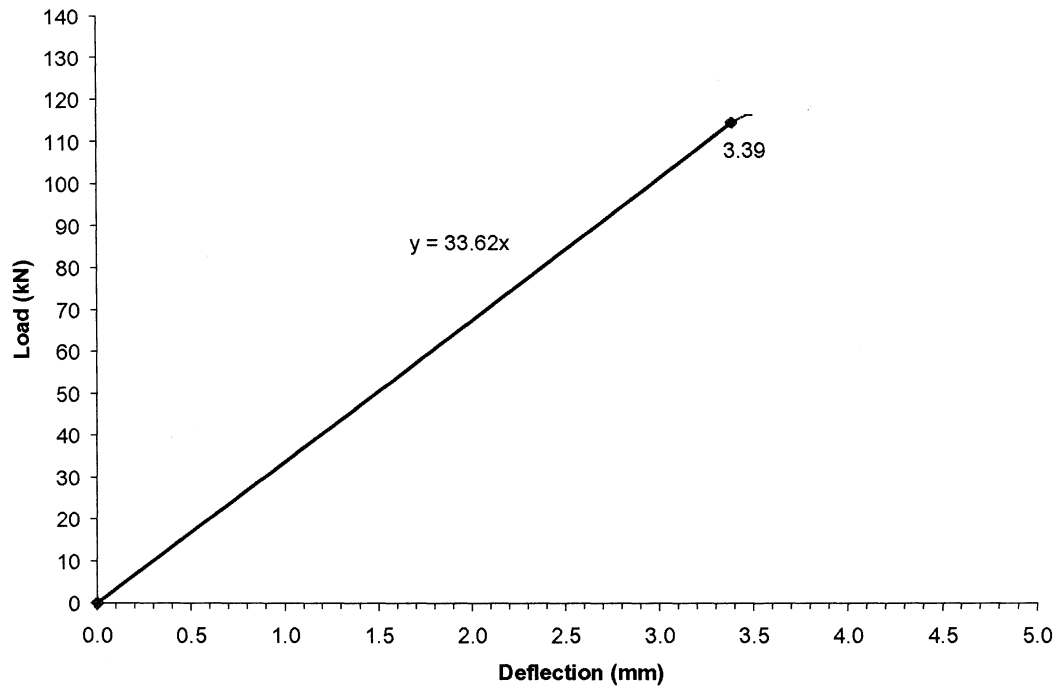
$$\therefore A_{BS07} = 229.06\_kN \cdot mm$$

Figure D-3: LDC trend line for BS08

Equation D-3

$$A_{BS08} = \int_{0.00}^{3.39}(33.62x)dx + \int_{3.39}^{3.50}(-209.74x^2 + 1460.4x - 2426.4)dx$$
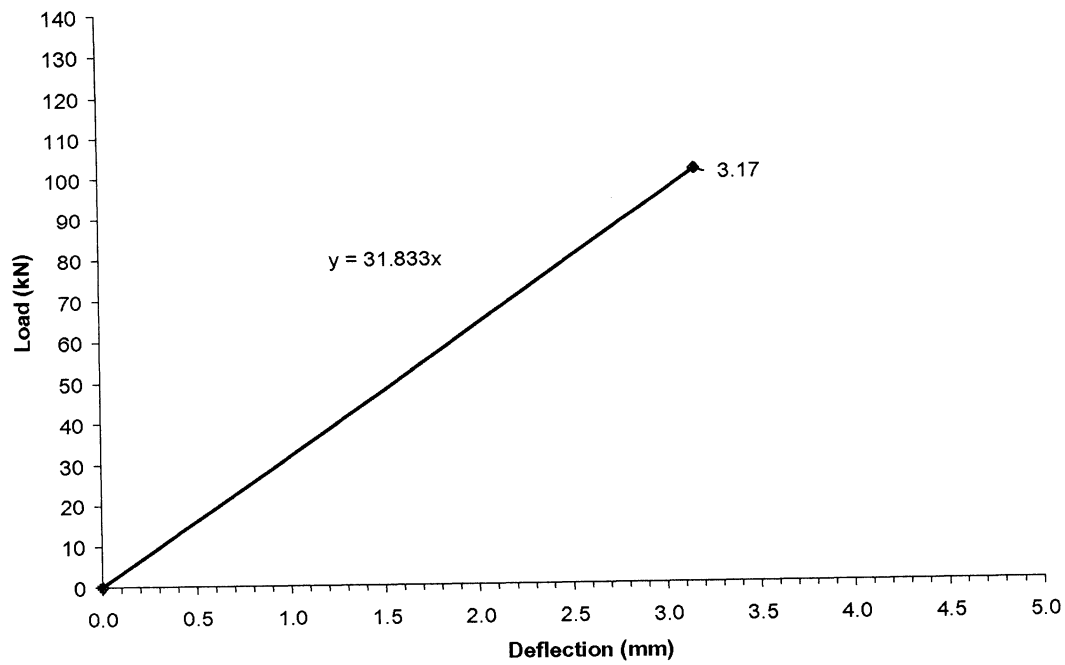
$$\therefore A_{BS08} = 205.69\_kN \cdot mm$$

171

Figure D-4: LDC trend line for BS09

Equation D-4

$$A_{BS09} = \int\limits_{0.00}^{3.17} (31.833x)dx$$
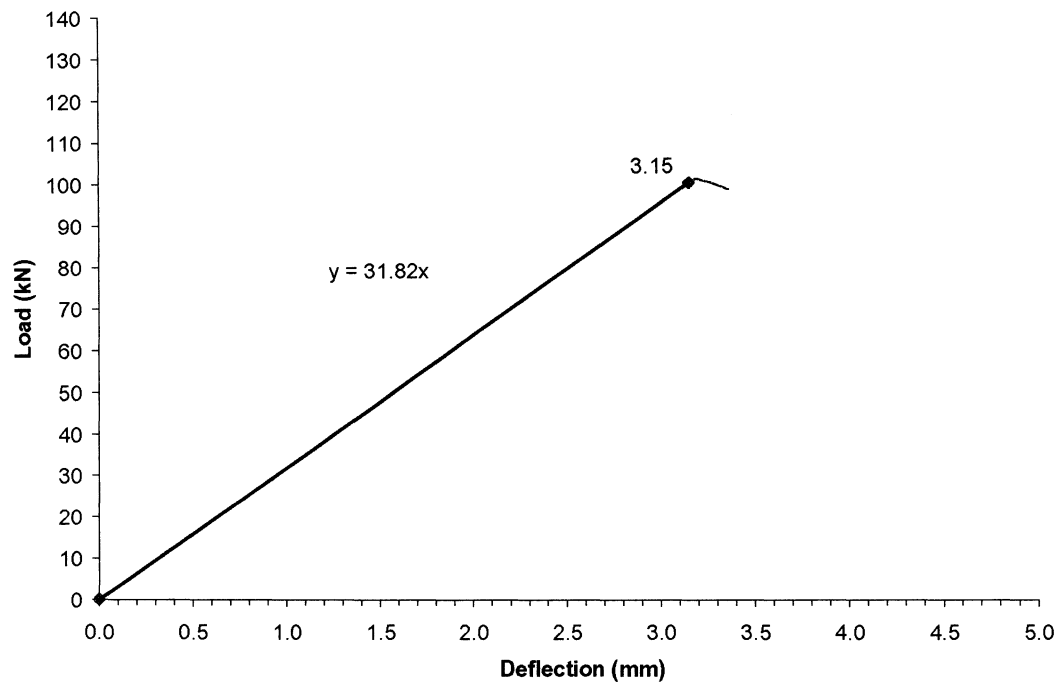
$$\therefore A_{BS09} = 159.99\_kN \cdot mm$$

Figure D-5: LDC trend line for BS10

Equation D-5

$$A_{BS10} = \int_{0.00}^{3.15} (31.82x)dx$$
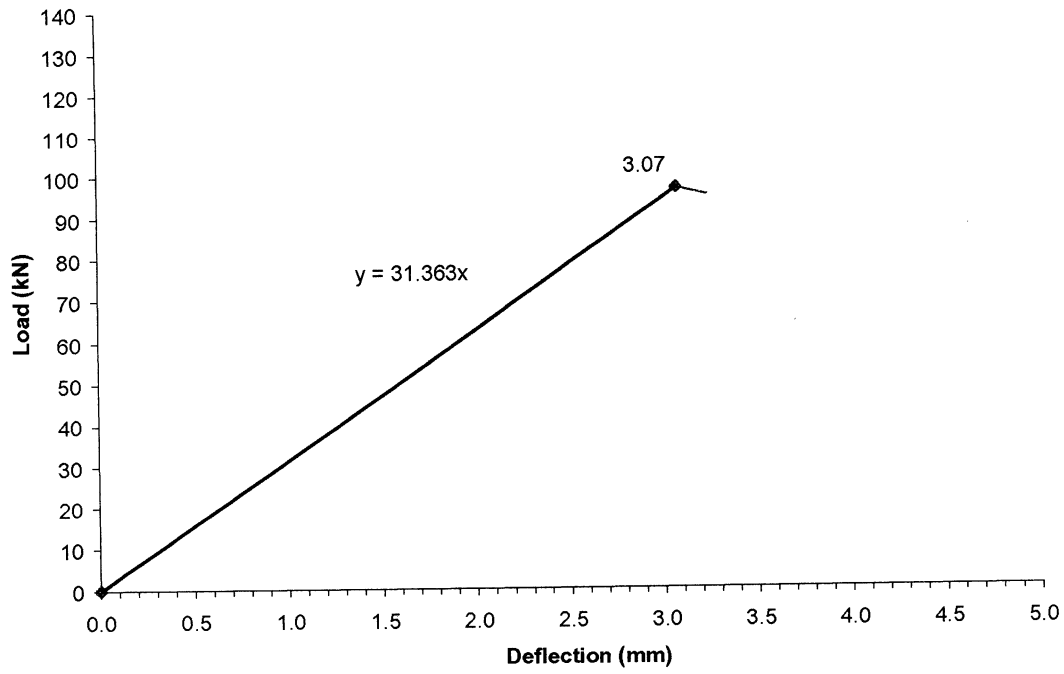
$$\therefore A_{BS10} = 158.00\_kN \cdot mm$$

Figure D-6: LDC trend line for BS11

Equation D-6

$$A_{BS11} = \int\limits_{0.00}^{3.07} (31.363x)dx$$
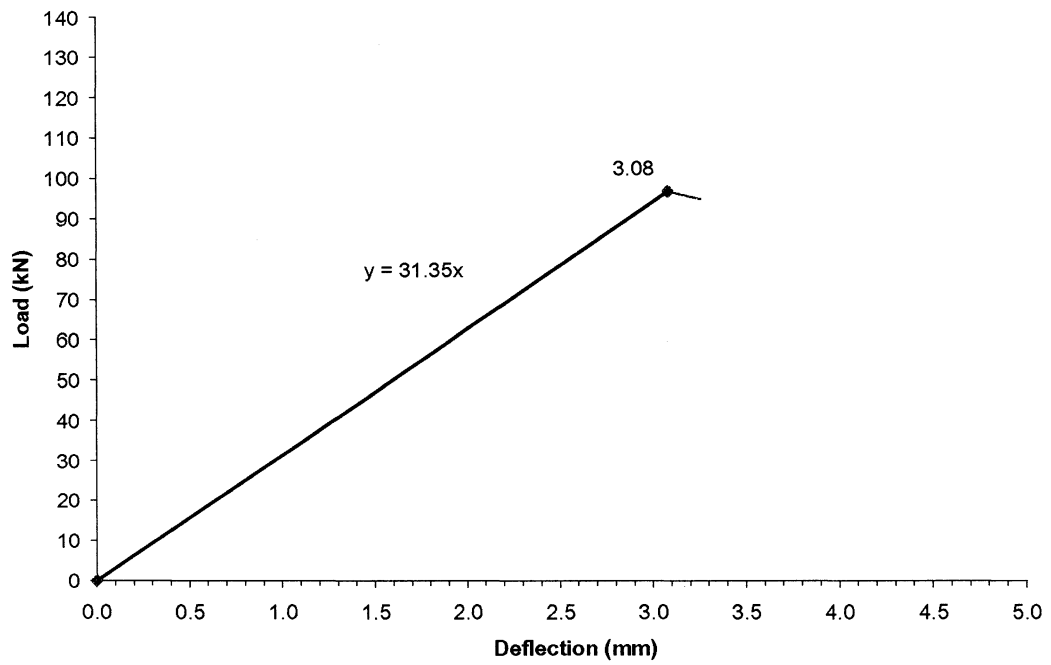
$$\therefore A_{BS11} = 148.21\_kN \cdot mm$$

Figure D-7: LDC trend line for BS12

Equation D-7

$$A_{BS12} = \int\limits_{0.00}^{3.08} (31.35x)dx$$

$$\therefore A_{BS12} = 149.01\_kN \cdot mm$$

APPENDIX E: FAILURE ZONE PICTURES

Figure E-1: Photograph showing the failure zone of BS01

Figure E-2: Photograph showing the failure zone of BS02

Figure E-3: Photograph showing the failure zone of BS03

Figure E-4: Photograph showing the failure zone of BS04

Figure E-5: Photograph showing the failure zone of BS05

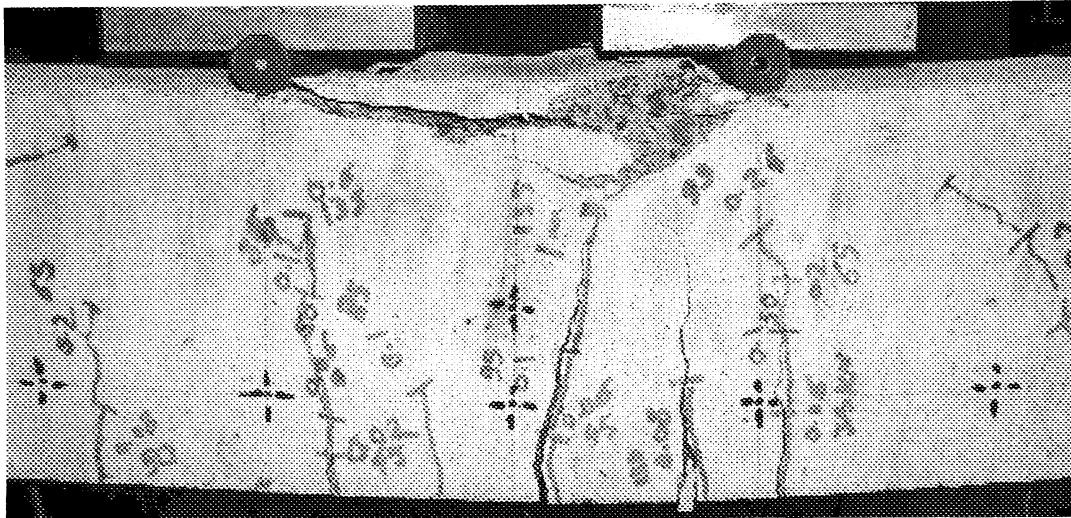Figure E-6: Photograph showing the failure zone of BS06

178
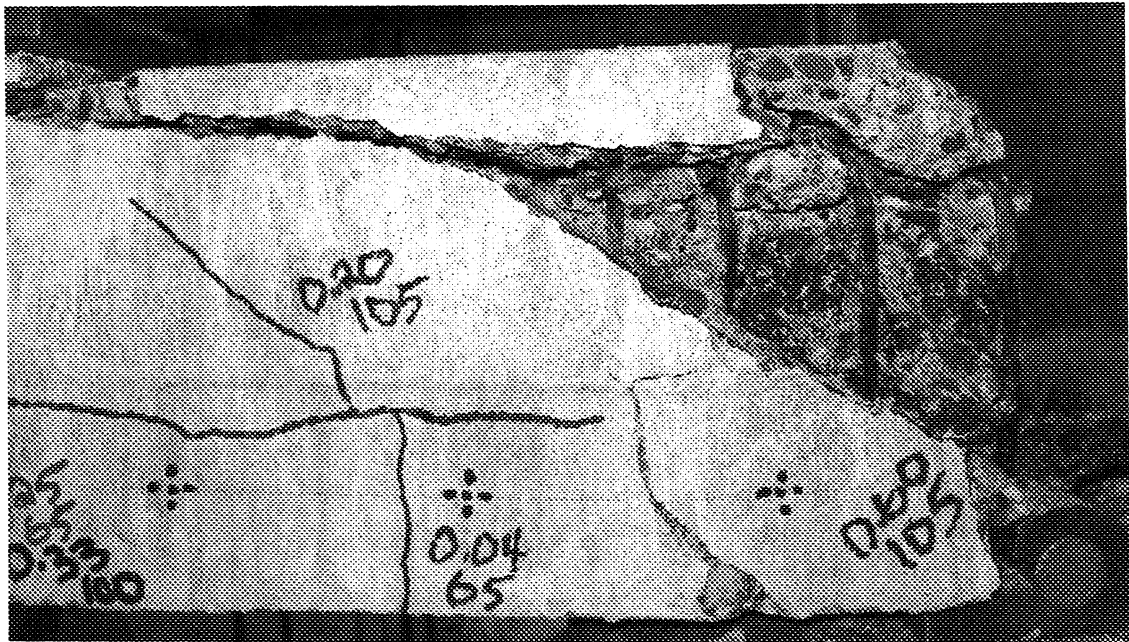
Figure E-7: Photograph showing the failure zone of BS07
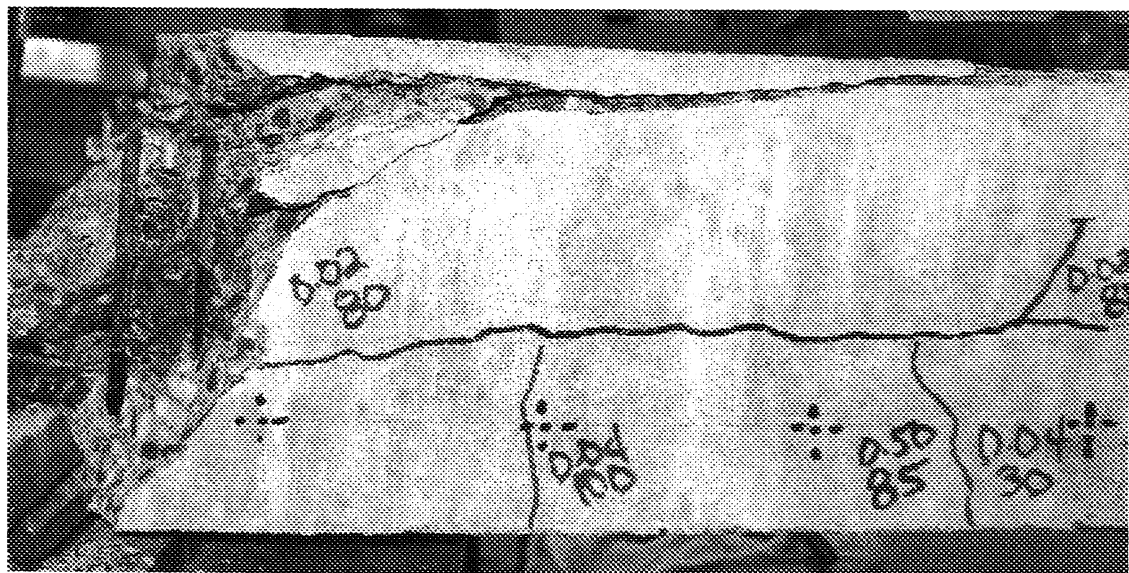
Figure E-8: Photograph showing the failure zone of BS08
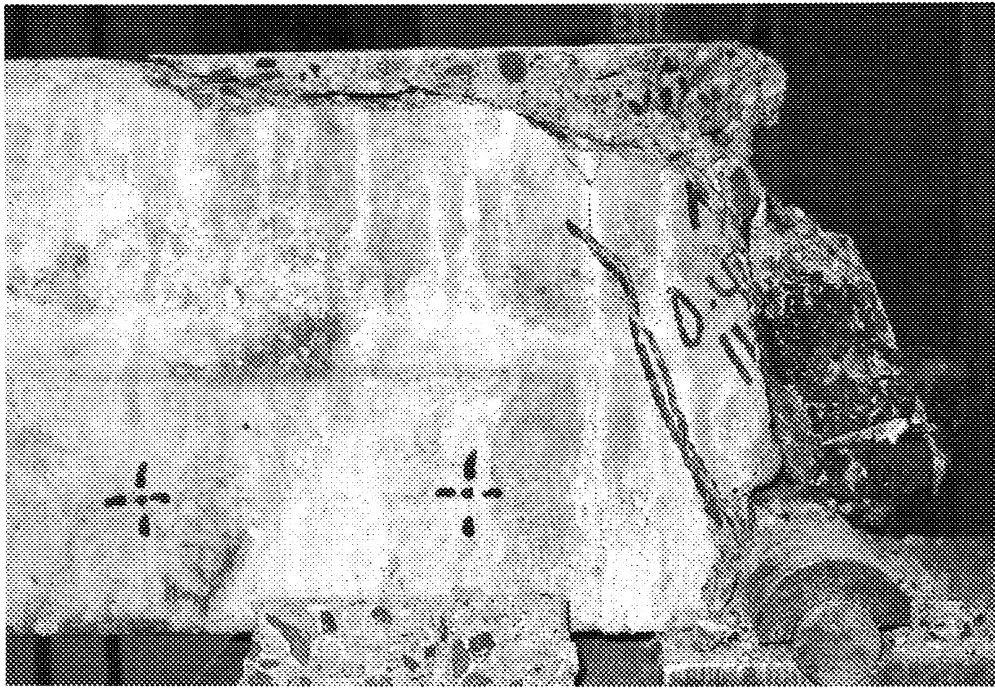
Figure E-9: Photograph showing the failure zone of BS09
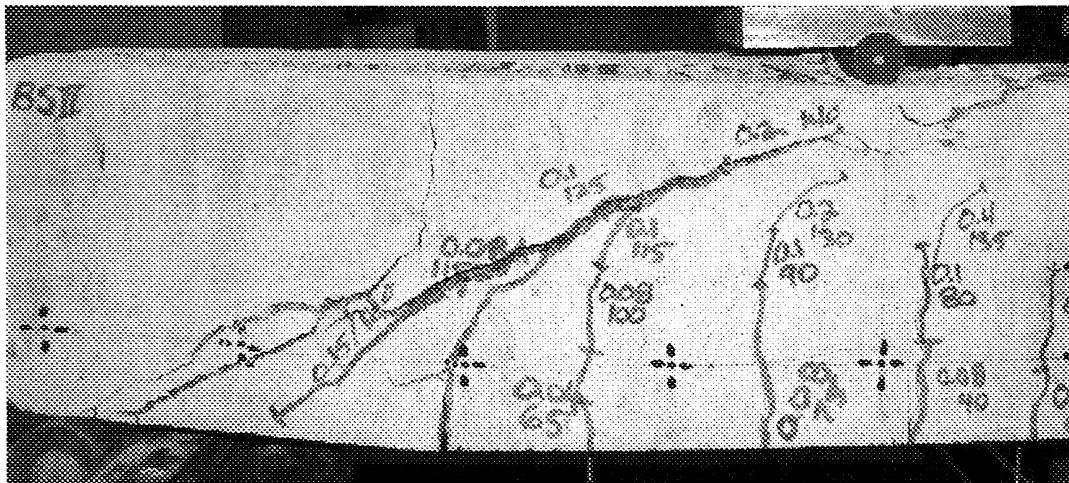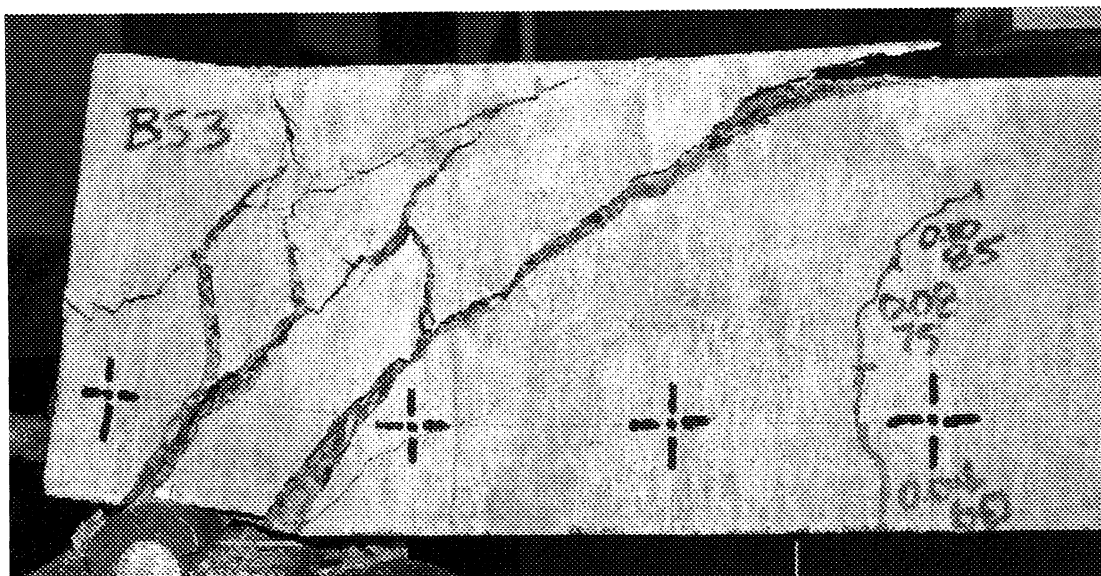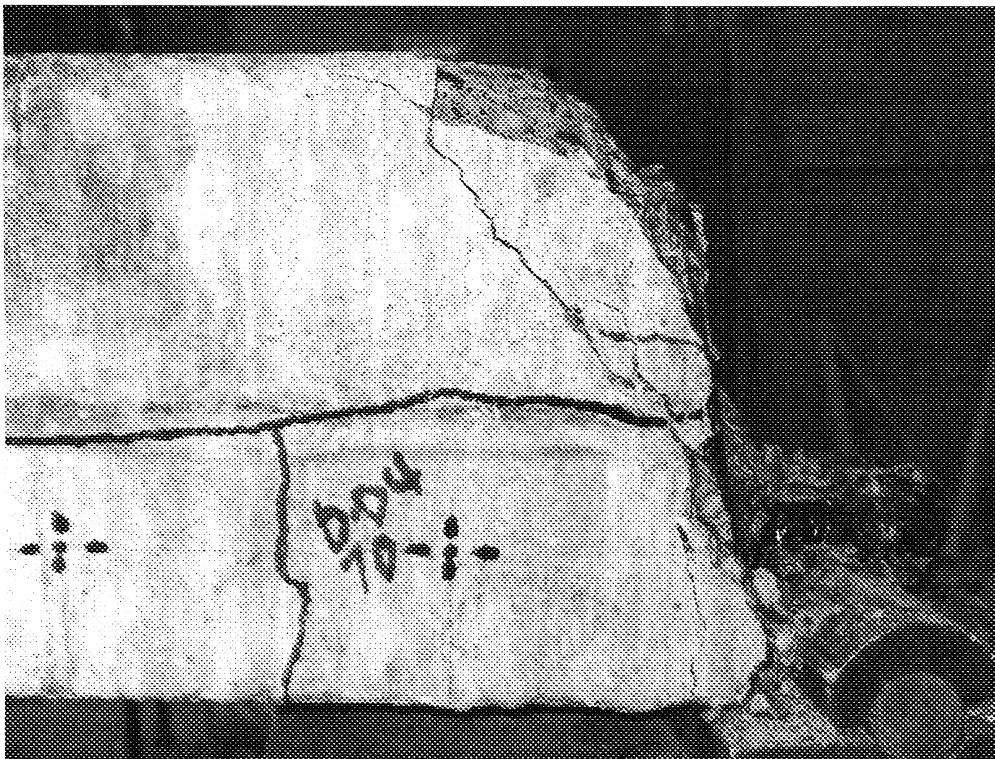

Figure E-10: Photograph showing the failure zone of BS10
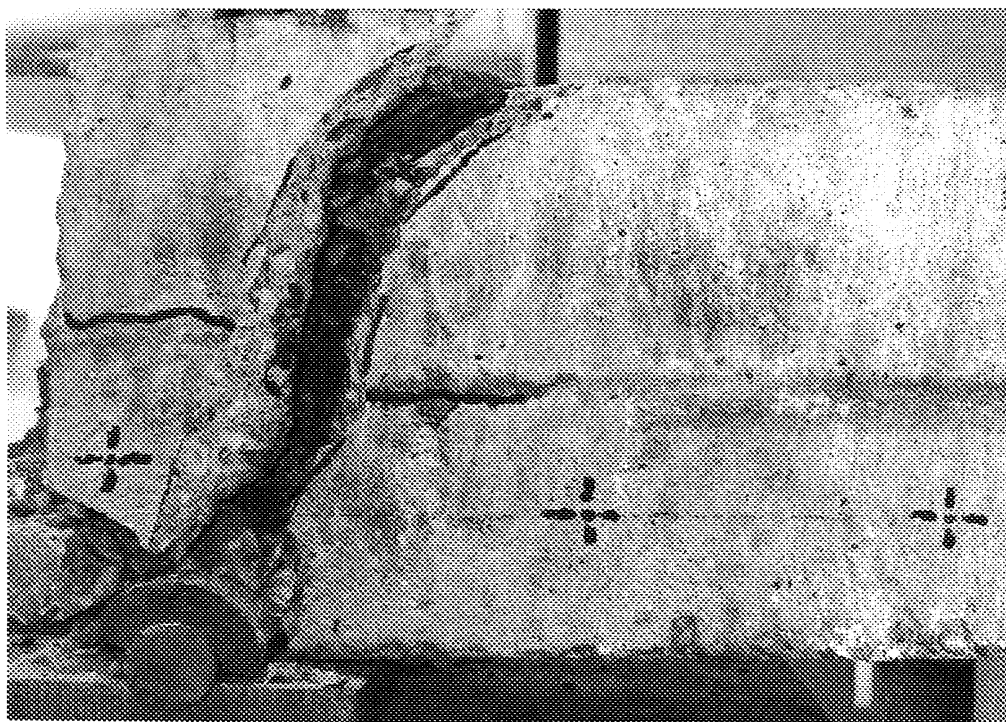
Figure E-11: Photograph showing the failure zone of BS11
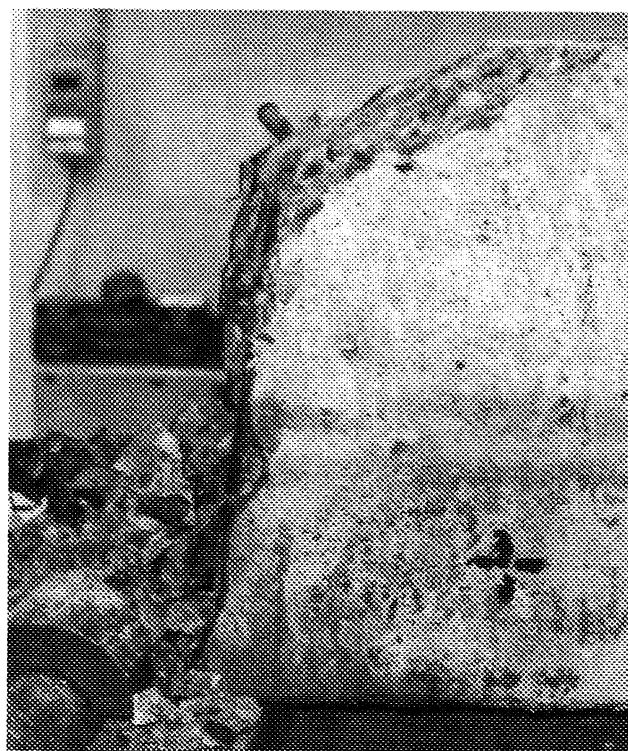
Figure E-12: Photograph showing the failure zone of BS12
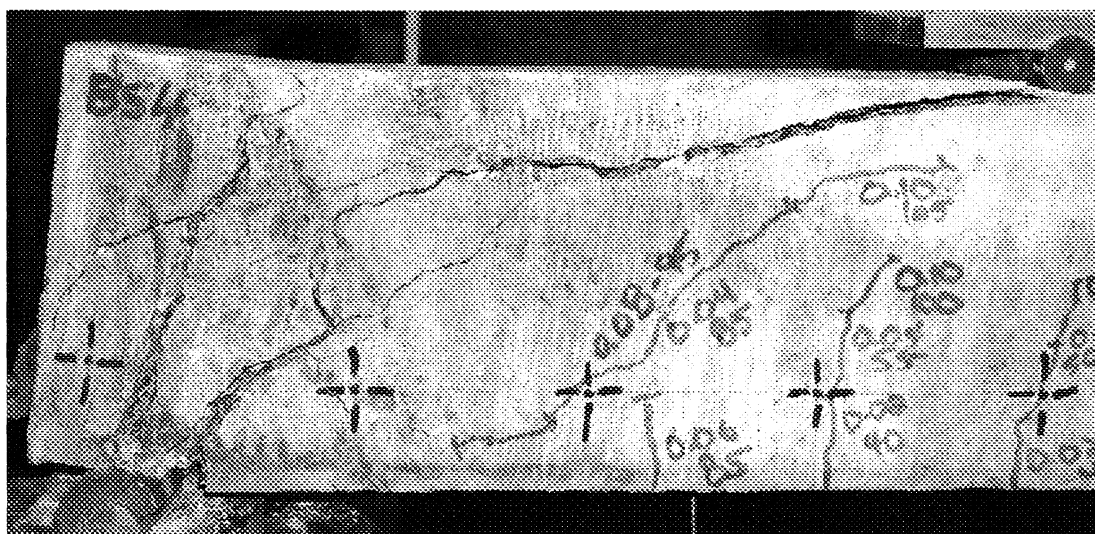
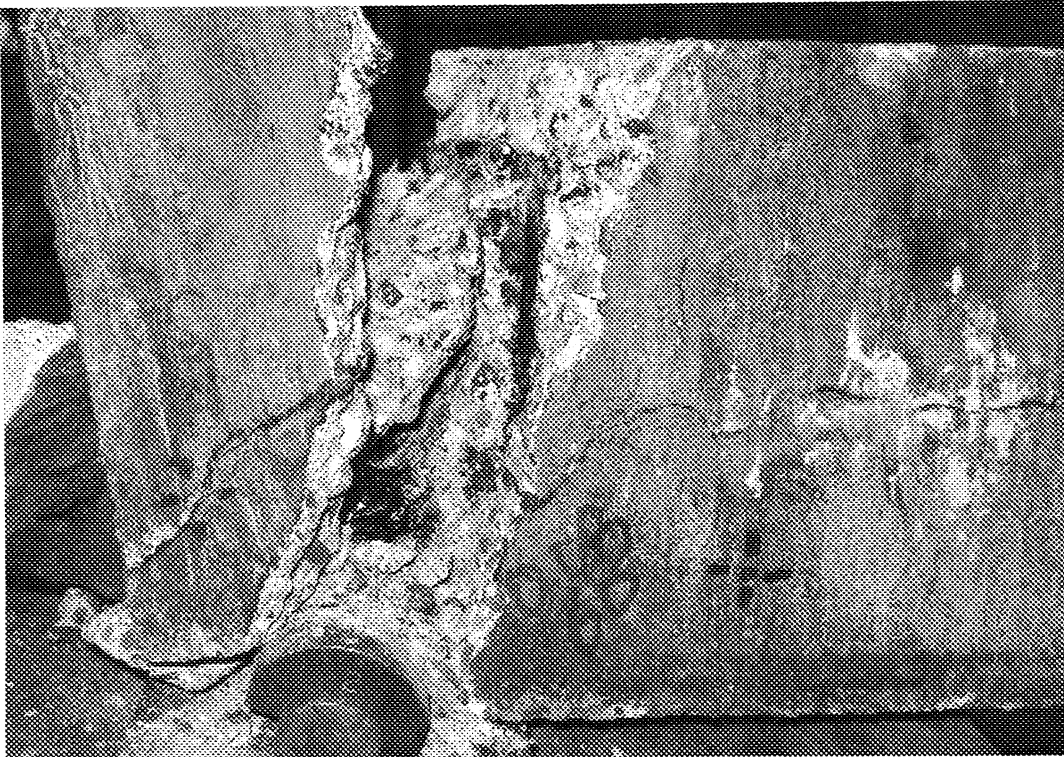# APPENDIX F: FLEXURAL CRACK SURVEY

———— FAILURE CRACK   ········ FLEXURE CRACK   ········ CORROSION CRACK

Figure F-1: Legend for the crack surveys below
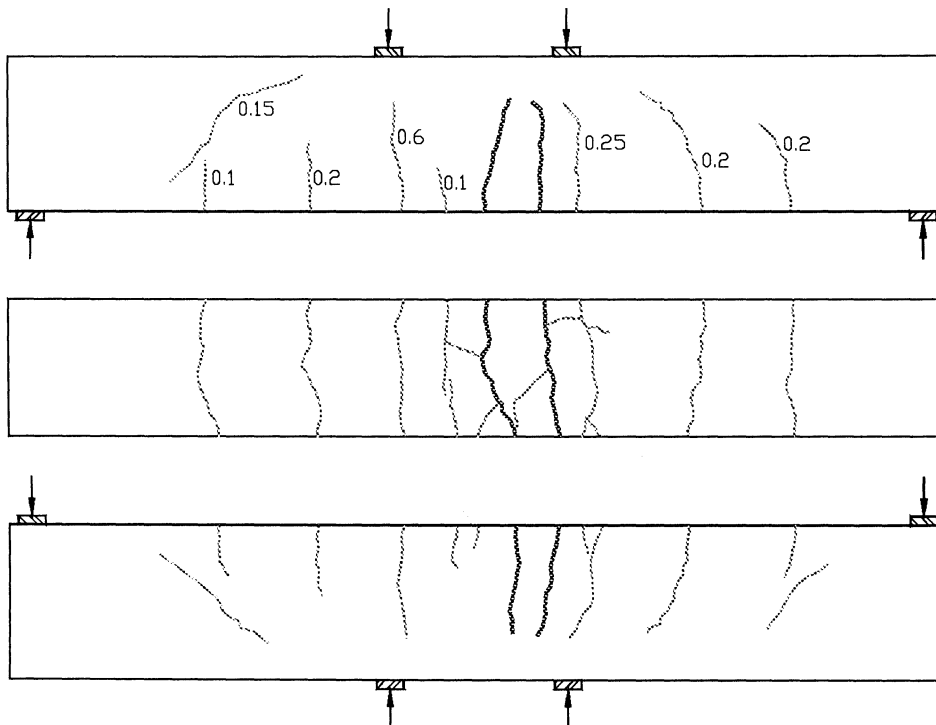
Figure F-2: Illustration showing the flexural crack development of BS01
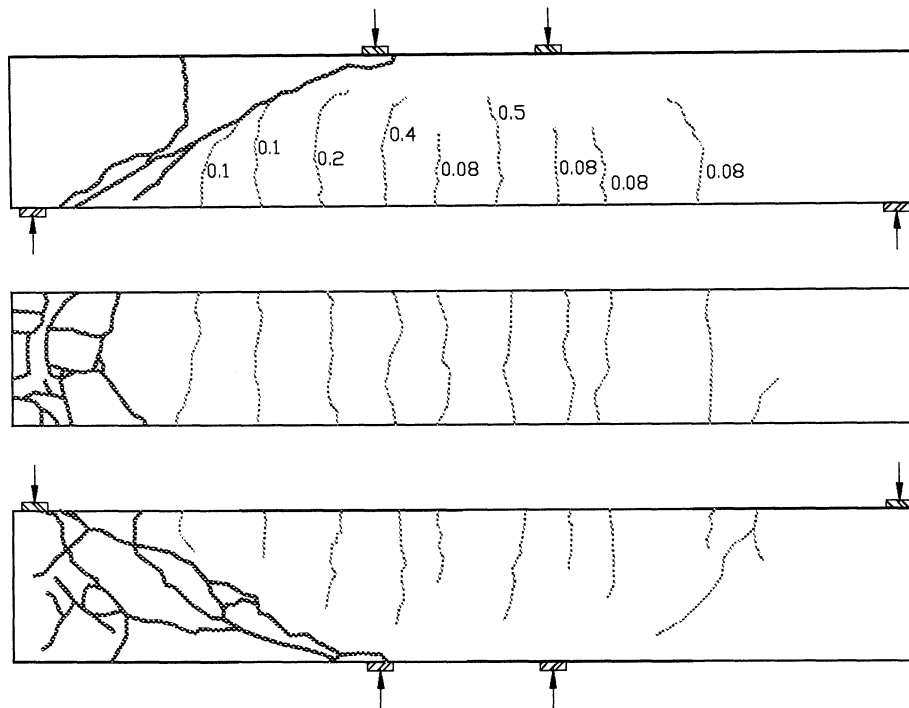
Figure F-3: Illustration showing the flexural crack development of BS02
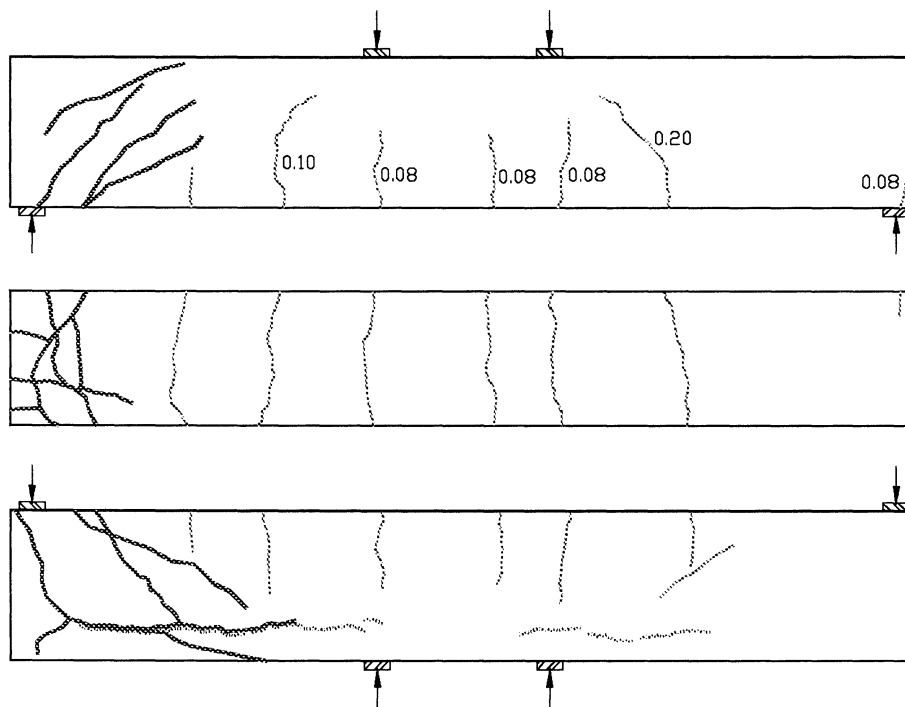
Figure F-4: Illustration showing the flexural crack development of BS03
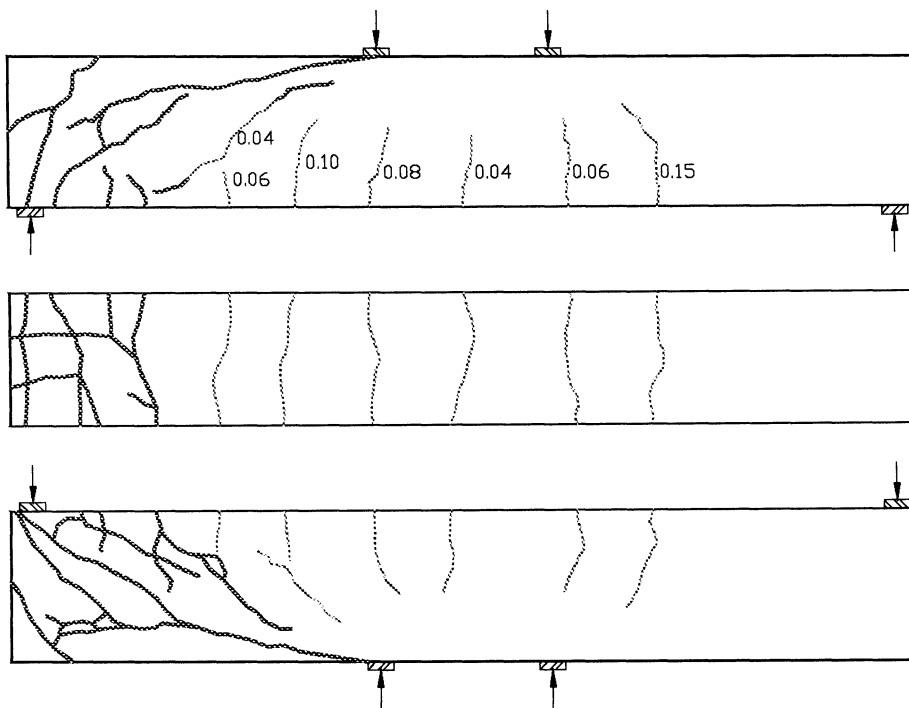
Figure F-5: Illustration showing the flexural crack development of BS04
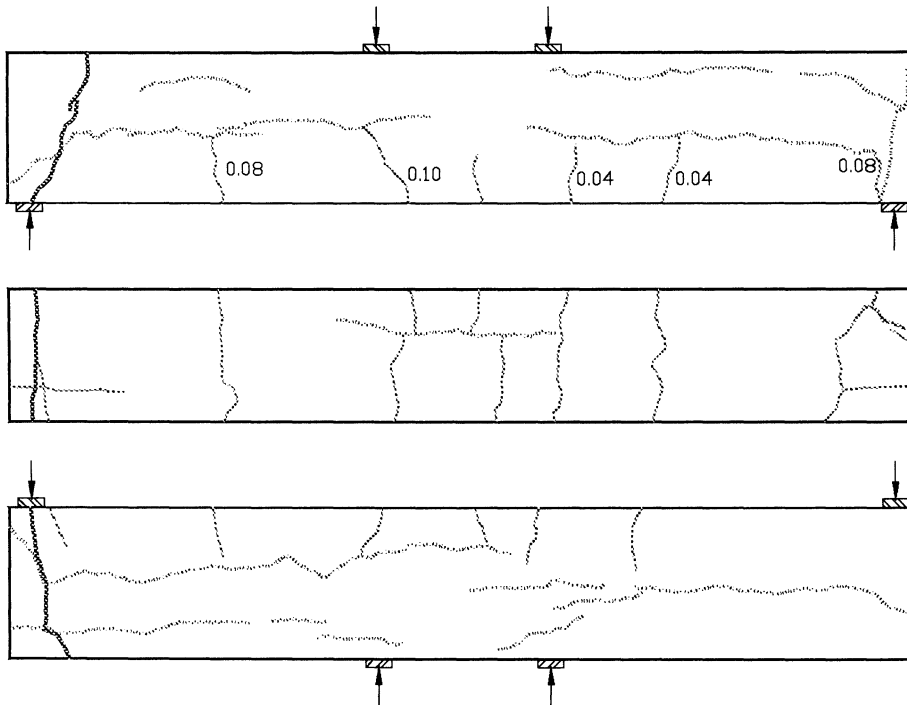
Figure F-6: Illustration showing the flexural crack development of BS05

184
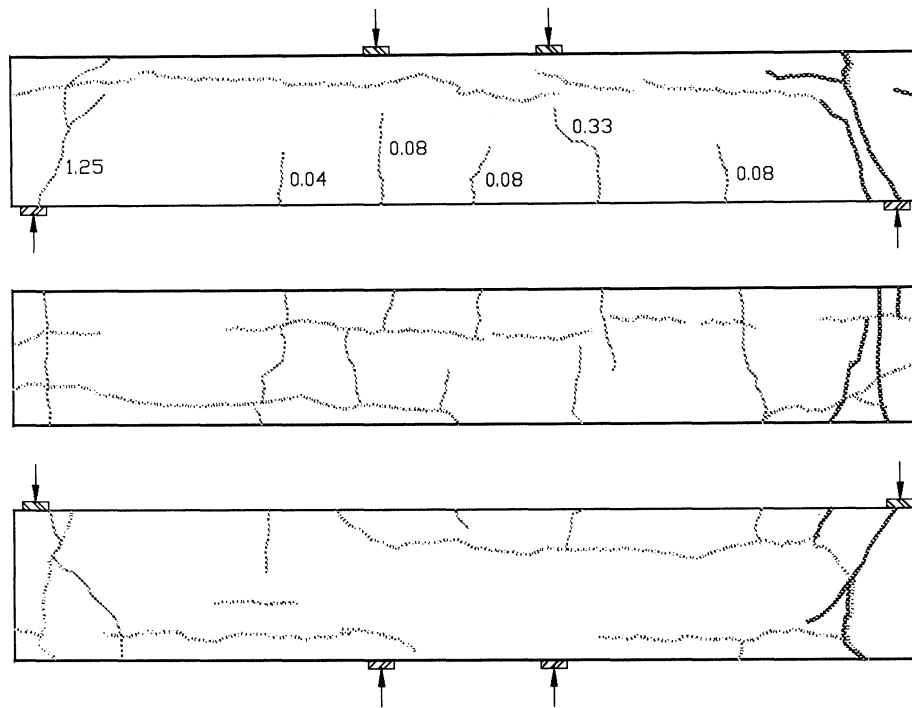
Figure F-7: Illustration showing the flexural crack development of BS06
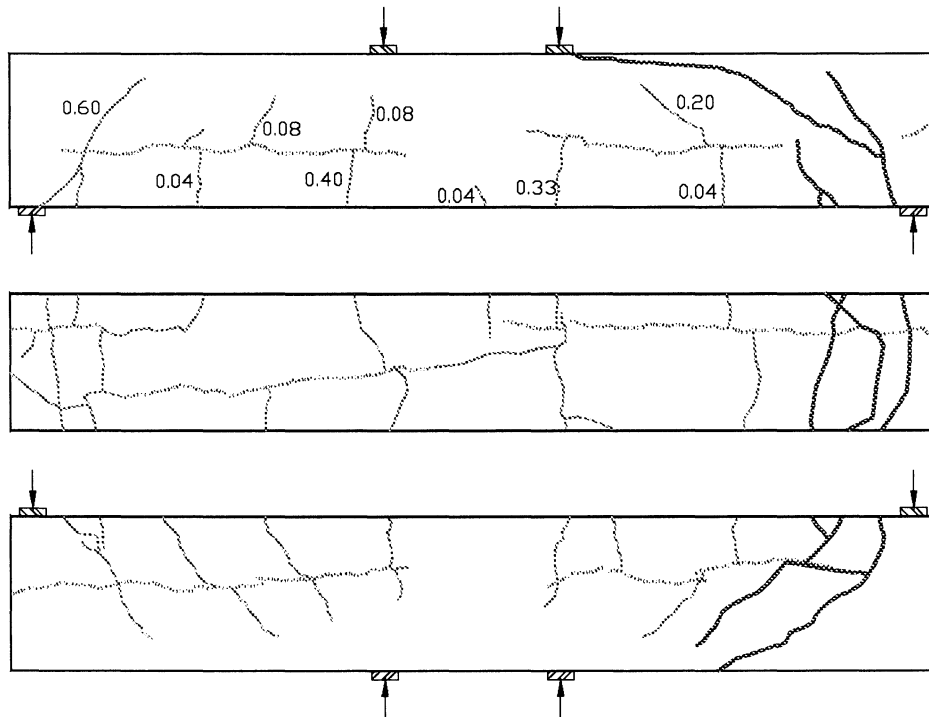
Figure F-8: Illustration showing the flexural crack development of BS07
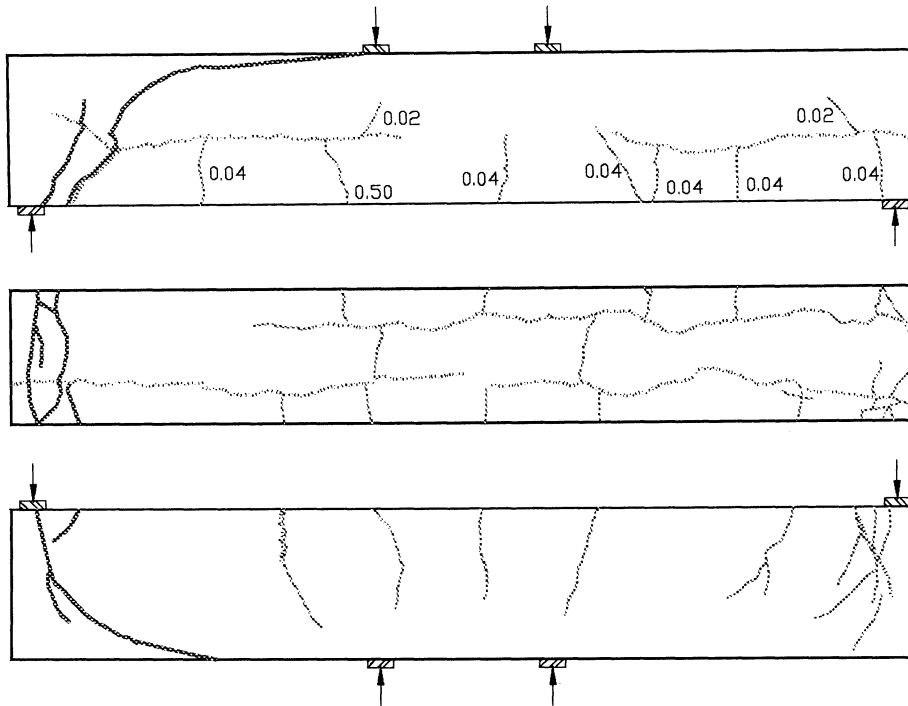
Figure F-9: Illustration showing the flexural crack development of BS08
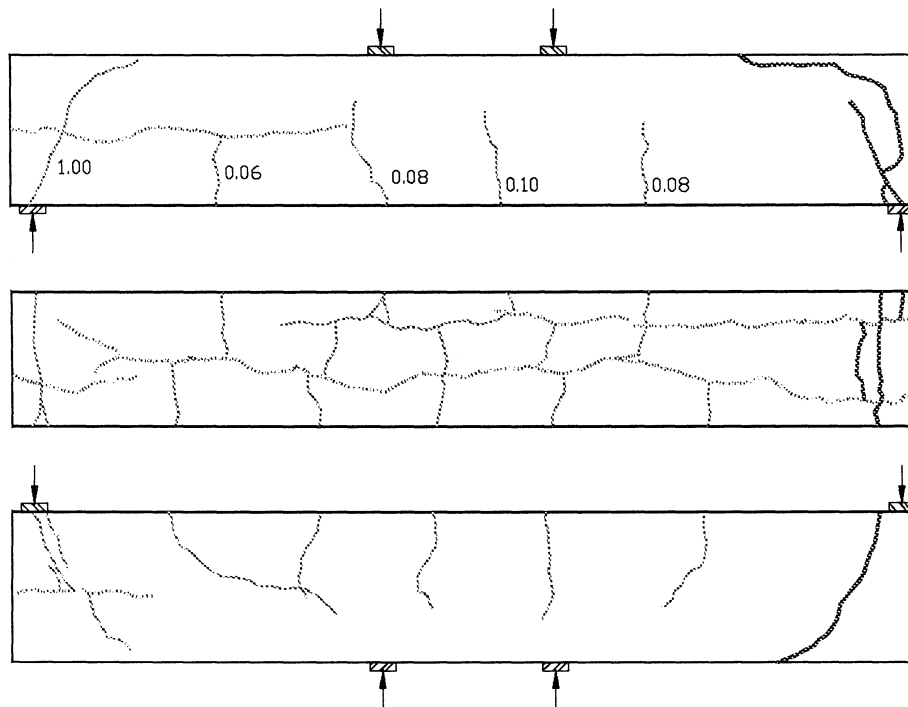
Figure F-10: Illustration showing the flexural crack development of BS09
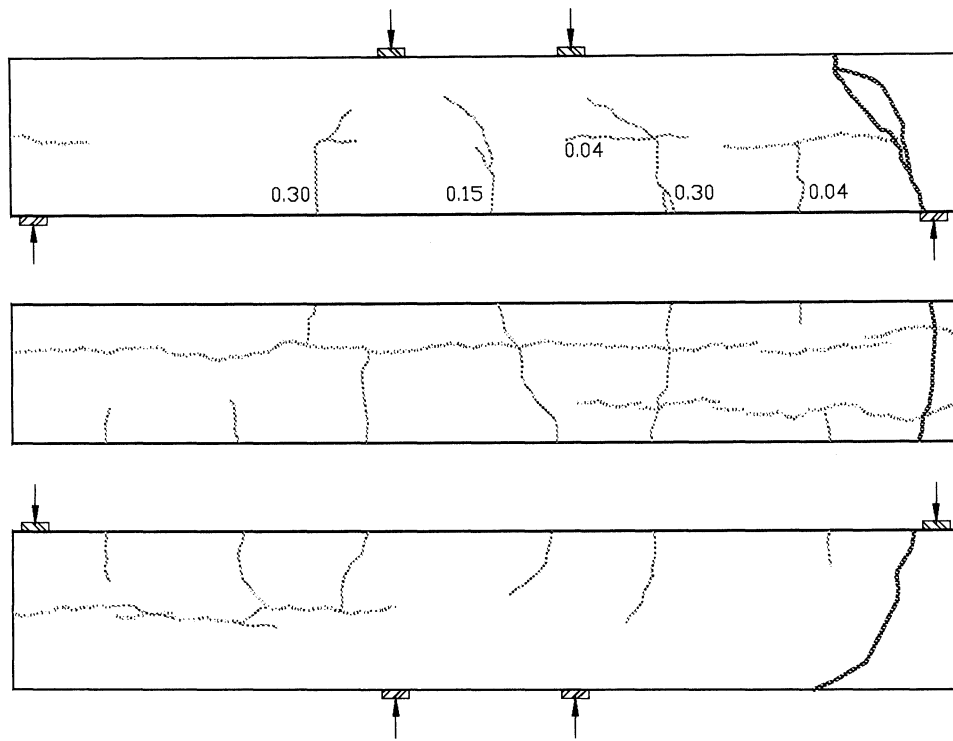
Figure F-11: Illustration showing the flexural crack development of BS10
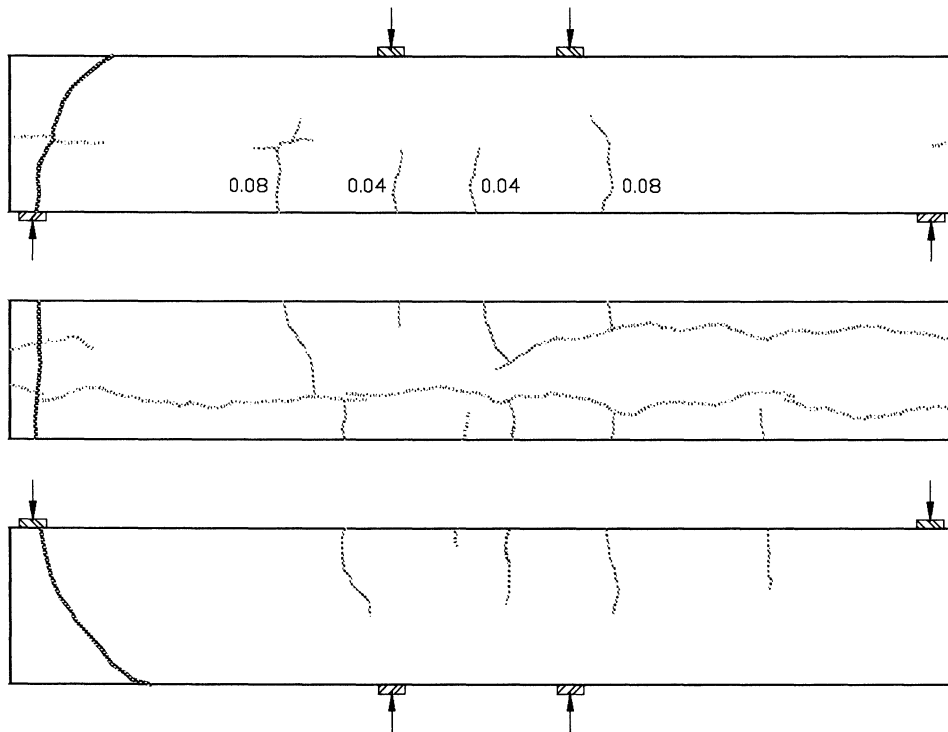
Figure F-12: Illustration showing the flexural crack development of BS11

187
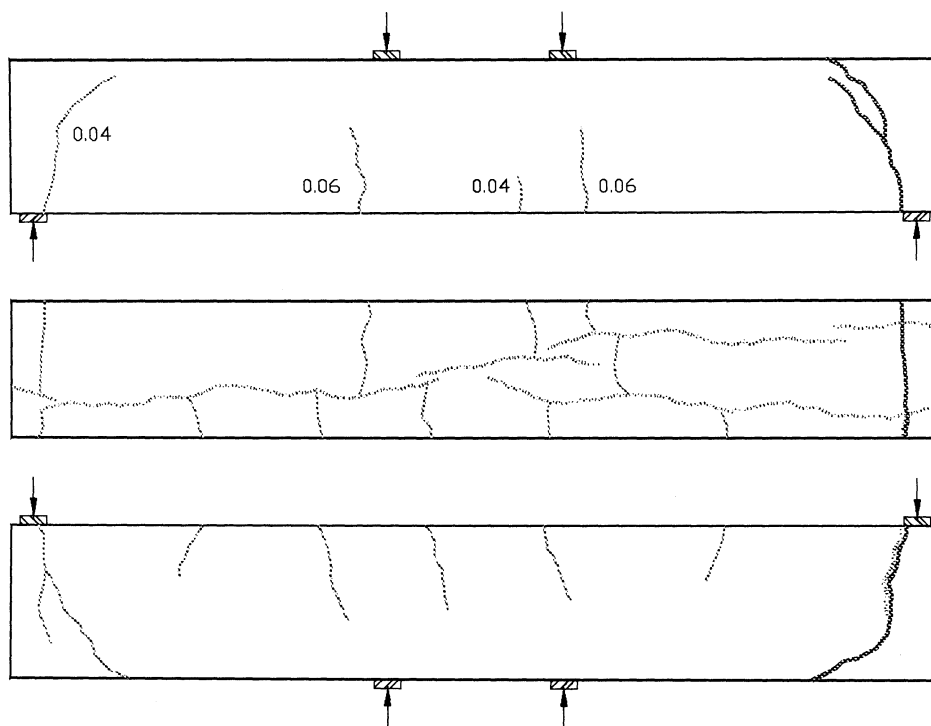
Figure F-13: Illustration showing the flexural crack development of BS12

APPENDIX G: PREVIOUS BEAM STUDIES

| Researchers	Width (mm)	Height (mm)	Span (mm)	Bar Dia. (mm)	# of Bars	Mass Loss	Capacity
Perno et al., 2005, 16 mm Bars	100	278		16	2	50.00%	69.00%
Perno et al., 2005, 16 mm Bars	100	278		16	2	30.00%	78.80%
Perno et al., 2005, 16 mm Bars	100	278		16	2	15.00%	85.80%
Perno et al., 2005, 16 mm Bars	100	278		16		50.00%	
Perno et al., 2005, 16 mm Bars	100	278		16		30.00%	
Perno et al., 2005, 16 mm Bars	100	278		16	2	15.00%	89.20%
Dekoster et al., 2003 (Toulouse)	150	280	2800	12			
Dekoster et al., 2003 (Lee)	200	250	2800	13			
Capozucca and Cerri, 2003	100	150	2250	8	3		
Higgins and Farrow, 2006 (Type I)	254	610	2400	8	5	6.11%	
Higgins and Farrow, 2006 (Type I)	254	610	2400	8	5	14.17%	
Higgins and Farrow, 2006 (Type I)	254	610	2400	8	5	30.31%	
Maaddawy et al., 2005b, 15 mm Bar, 33 mm Cover	152	254	3000	15	2	8.90%	93.50%
Maaddawy et al., 2005b, 15 mm Bar, 33 mm Cover	152	254	3000	15	2	14.20%	89.00%
Maaddawy et al., 2005b, 15 mm Bar, 33 mm Cover	152	254	3000	15	2	22.20%	80.00%
Maaddawy et al., 2005b, 15 mm Bar, 33 mm Cover	152	254	3000	15	2	31.60%	71.00%

Researchers	Width (mm)	Height (mm)	Span (mm)	Bar Dia. (mm)	# of Bars	Mass Loss	Capacity
Maaddawy et al., 2005b, 15 mm Bar, 33 mm Cover	152	254	3000	15	2	9.70%	88.11%
Maaddawy et al., 2005b, 15 mm Bar, 33 mm Cover	152	254	3000	15	2	15.40%	86.12%
Maaddawy et al., 2005b, 15 mm Bar, 33 mm Cover	152	254	3000	15	2	22.80%	85.57%
Maaddawy et al., 2005b, 15 mm Bar, 33 mm Cover	152	254	3000	15	2	30.00%	75.83%
Ballim, Reid and Kemp, 2001, 16 mm Bar, 20 mm Cover	100	160	1450	16	1	6.38%	72.00%
Ballim, Reid and Kemp, 2001, 16 mm Bar, 20 mm Cover	100	160	1450	16	1	5.88%	84.00%
Ballim, Reid and Kemp, 2001, 16 mm Bar, 20 mm Cover	100	160	1450	16	1	5.56%	84.00%
Ballim, Reid and Kemp, 2001, 16 mm Bar, 20 mm Cover	100	160	1450	16	1	8.47%	67.00%
Ballim, Reid and Kemp, 2001, 16 mm Bar, 20 mm Cover	100	160	1450	16	1	5.61%	95.00%
Ballim, Reid and Kemp, 2001, 16 mm Bar, 20 mm Cover	100	160	1450	16	1	7.98%	68.00%
Yan, Wang and Zhang, 2004	100	100		12	2		
Banic, Grandic and Bjegovic,	100	180	650	8	1		
Oyado, Hasegawa and Sato, 2003	100	200	1800	13	2		
Oyado, Hasegawa and Sato, 2003	100	200	1800	16	1		

Researchers	Width (mm)	Height (mm)	Span (mm)	Bar Dia. (mm)	# of Bars	Mass Loss	Capacity
Yoon et al. 2000 & Wang et al. 2000, (L), 19 mm Bar, 30 mm Cover	100	150	1050	19	1	4.00%	90.98%
Yoon et al. 2000 & Wang et al. 2000, (L), 19 mm Bar, 30 mm Cover	100	150	1050	19	1	6.00%	75.61%
Yoon et al. 2000 & Wang et al. 2000, (P), 19 mm Bar, 30 mm Cover	100	150	1050	19	1	3.80%	
Yoon et al. 2000 & Wang et al. 2000, (P), 19 mm Bar, 30 mm Cover	100	150	1050	19	1	3.20%	91.95%
Castel et al., 2000	150	280	2800	12	2		
Mangat and Elgarf 1999b	100	150		10	2		
Mangat and Elgarf 1999b	100	150		10	2		
Mangat and Elgarf 1999b	100	150		10	2		
Mangat and Elgarf 1999b	100	150		10	2		
Mangat and Elgarf 1999b	100	150		10	2		
Mangat and Elgarf 1999b	100	150		10	2		
Al-Sulaimani et al. (1990), 12 mm Bar, 29 mm Cover	150	150	900	12	1	0.17%	99.58%
Al-Sulaimani et al. (1990), 12 mm Bar, 29 mm Cover	150	150	900	12	1	0.72%	100.21%
Al-Sulaimani et al. (1990), 12 mm Bar, 29 mm Cover	150	150	900	12	1	1.50%	99.15%
Al-Sulaimani et al. (1990), 12 mm Bar, 29 mm Cover	150	150	900	12	1	1.75%	97.67%

Researchers	Width (mm)	Height (mm)	Span (mm)	Bar Dia. (mm)	# of Bars	Mass Loss	Capacity
Al-Sulaimani et al. (1990), 12 mm Bar, 29 mm Cover	150	150	900	12	1	1.86%	98.09%
Al-Sulaimani et al. (1990), 12 mm Bar, 29 mm Cover	150	150	900	12	1	1.96%	96.61%
Al-Sulaimani et al. (1990), 12 mm Bar, 29 mm Cover	150	150	900	12	1	2.75%	93.22%
Al-Sulaimani et al. (1990), 12 mm Bar, 29 mm Cover	150	150	900	12	1	3.75%	89.19%
Al-Sulaimani et al. (1990), 12 mm Bar, 29 mm Cover	150	150	900	12	1	3.89%	90.04%
Al-Sulaimani et al. (1990), 12 mm Bar, 29 mm Cover	150	150	900	12	1	4.10%	89.41%
Uomoto and Misra (1988)	100	200		16	2		
Huang and Yang (1997)	150	150		#4	2		
Mangat and Elgarf (1999a)	100	150		10	2		
Mangat and Elgarf (1999a)				8	2		
A A Torres-Acosta; 2004	100	150		9.5	1		
Azher (2005), 10 mm Bar, 25 mm Cover	150	150	900	10	2	5.40%	91.70%
Azher (2005), 10 mm Bar, 25 mm Cover	150	150	900	10	2	14.20%	87.20%
Azher (2005), 10 mm Bar, 25 mm Cover	150	150	900	10	2	15.20%	89.88%
Azher (2005), 10 mm Bar, 25 mm Cover	150	150	900	10	2	21.40%	78.62%
Azher (2005), 10 mm Bar, 25 mm Cover	150	150	900	10	2	21.50%	67.20%

Researchers	Width (mm)	Height (mm)	Span (mm)	Bar Dia. (mm)	# of Bars	Mass Loss	Capacity
Azher (2005), 10 mm Bar, 25 mm Cover	150	150	900	10	2	31.00%	55.65%
Azher (2005), 12 mm Bar, 25 mm Cover	150	150	900	12	2	5.50%	86.26%
Azher (2005), 12 mm Bar, 25 mm Cover	150	150	900	12	2	8.80%	80.89%
Azher (2005), 12 mm Bar, 25 mm Cover	150	150	900	12	2	20.10%	70.46%
Azher (2005), 12 mm Bar, 25 mm Cover	150	150	900	12	2	14.00%	71.30%
Azher (2005), 12 mm Bar, 25 mm Cover	150	150	900	12	2	22.90%	60.04%
Azher (2005), 12 mm Bar, 25 mm Cover	150	150	900	12	2	25.50%	57.37%
Azher (2005), 10 mm Bar, 40 mm Cover	150	150	900	10	2	8.00%	92.89%
Azher (2005), 10 mm Bar, 40 mm Cover	150	150	900	10	2	9.10%	86.67%
Azher (2005), 10 mm Bar, 40 mm Cover	150	150	900	10	2	10.10%	83.99%
Azher (2005), 10 mm Bar, 40 mm Cover	150	150	900	10	2	17.60%	78.94%
Azher (2005), 10 mm Bar, 40 mm Cover	150	150	900	10	2	21.40%	77.53%
Azher (2005), 10 mm Bar, 40 mm Cover	150	150	900	10	2	34.80%	56.10%
Azher (2005), 12 mm Bar, 40 mm Cover	150	150	900	12	2	7.90%	91.65%
Azher (2005), 12 mm Bar, 40 mm Cover	150	150	900	12	2	10.90%	83.30%
Azher (2005), 12 mm Bar, 40 mm Cover	150	150	900	12	2	13.40%	76.35%
Azher (2005), 12 mm Bar, 40 mm Cover	150	150	900	12	2	18.60%	68.40%

Researchers	Width (mm)	Height (mm)	Span (mm)	Bar Dia. (mm)	# of Bars	Mass Loss	Capacity
Azher (2005), 12 mm Bar, 40 mm Cover	150	150	900	12	2	18.00%	68.55%
Azher (2005), 12 mm Bar, 40 mm Cover	150	150	900	12	2	20.70%	57.65%
Rodriguez et al. (1997), 2-10 mm Bars, 2-8 mm Bars, 170 mm	150	200	2000	10	2	0.00%	
Rodriguez et al. (1997), 2-10 mm Bars, 2-8 mm Bars, 170 mm Stirrup Spacing	150	200	2000	10	2	0.00%	
Rodriguez et al. (1997), 2-10 mm Bars, 2-8 mm Bars, 170 mm Stirrup Spacing	150	200	2000	10	2	14.40%	75.32%
Rodriguez et al. (1997), 2-10 mm Bars, 2-8 mm Bars, 170 mm Stirrup Spacing	150	200	2000	10	2	18.00%	68.18%
Rodriguez et al. (1997), 2-10 mm Bars, 2-8 mm Bars, 170 mm Stirrup Spacing	150	200	2000	10	2	19.60%	65.58%
Rodriguez et al. (1997), 2-10 mm Bars, 2-8 mm Bars, 170 mm Stirrup Spacing	150	200	2000	10	2	28.40%	55.84%
Rodriguez et al. (1997), 4-12 mm Bars, 2-8 mm Bars, 170 mm Stirrup Spacing	150	200	2000	12	4	0.00%	
Rodriguez et al. (1997), 4-12 mm Bars, 2-8 mm Bars, 170 mm Stirrup Spacing	150	200	2000	12	4	0.00%	
Rodriguez et al. (1997), 4-12 mm Bars, 2-8 mm Bars, 170 mm Stirrup Spacing	150	200	2000	12	4	10.67%	77.96%

Researchers	Width (mm)	Height (mm)	Span (mm)	Bar Dia. (mm)	# of Bars	Mass Loss	Capacity
Rodriguez et al. (1997), 4-12 mm Bars, 2-8 mm Bars, 170 mm Stirrup Spacing	150	200	2000	12	4	11.67%	73.12%
Rodriguez et al. (1997), 4-12 mm Bars, 2-8 mm Bars, 170 mm Stirrup Spacing	150	200	2000	12	4	13.67%	54.84%
Rodriguez et al. (1997), 4-12 mm Bars, 2-8 mm Bars, 170 mm Stirrup Spacing	150	200	2000	12	4	13.33%	61.56%
Rodriguez et al. (1997), 2-12 mm Bars, 4-12 mm Bars @ mid-span, 2-8 mm Bars, 170 mm Stirrup Spacing	150	200	2000	12	2 +2 @mid	0.00%	
Rodriguez et al. (1997), 2-12 mm Bars, 4-12 mm Bars @ mid-span, 2-8 mm Bars, 170 mm Stirrup Spacing	150	200	2000	12	2 +2 @mid	0.00%	
Rodriguez et al. (1997), 2-12 mm Bars, 4-12 mm Bars @ mid-span, 2-8 mm Bars, 170 mm Stirrup Spacing	150	200	2000	12	2 +2 @mid	10.67%	67.38%
Rodriguez et al. (1997), 2-12 mm Bars, 4-12 mm Bars @ mid-span, 2-8 mm Bars, 170 mm Stirrup Spacing	150	200	2000	12	2 +2 @mid	11.67%	67.11%

Researchers	Width (mm)	Height (mm)	Span (mm)	Bar Dia. (mm)	# of Bars	Mass Loss	Capacity
Rodriguez et al. (1997), 2-12 mm Bars, 4-12 mm Bars @ mid-span, 2-8 mm Bars, 170 mm Stirrup Spacing	150	200	2000	12	2 +2 @mid	13.33%	56.19%
Rodriguez et al. (1997), 2-12 mm Bars, 4-12 mm Bars @ mid-span, 2-8 mm Bars, 170 mm Stirrup Spacing	150	200	2000	12	2 +2 @mid	13.00%	65.78%
Rodriguez et al. (1997), 4-12 mm Bars, 4-8 mm Top Bars, 170 mm Stirrup Spacing	150	200	2000	12	4	0.00%	
Rodriguez et al. (1997), 4-12 mm Bars, 4-8 mm Top Bars, 170 mm Stirrup Spacing	150	200	2000	12	4	0.00%	
Rodriguez et al. (1997), 4-12 mm Bars, 4-8 mm Top Bars, 170 mm Stirrup Spacing	150	200	2000	12	4	12.33%	72.49%
Rodriguez et al. (1997), 4-12 mm Bars, 4-8 mm Top Bars, 170 mm Stirrup Spacing	150	200	2000	12	4	10.33%	67.87%
Rodriguez et al. (1997), 4-12 mm Bars, 4-8 mm Top Bars, 170 mm Stirrup Spacing	150	200	2000	12	4	14.33%	49.87%

Researchers	Width (mm)	Height (mm)	Span (mm)	Bar Dia. (mm)	# of Bars	Mass Loss	Capacity
Rodriguez et al. (1997), 4-12 mm Bars, 4-8 mm Top Bars, 170 mm Stirrup Spacing	150	200	2000	12	4	17.67%	53.73%
Rodriguez et al. (1997), 4-12 mm Bars, 4-8 mm Top Bars, 85 mm Stirrup Spacing	150	200	2000	12	4	0.00%	
Rodriguez et al. (1997), 4-12 mm Bars, 4-8 mm Top Bars, 85 mm Stirrup Spacing	150	200	2000	12	4	0.00%	
Rodriguez et al. (1997), 4-12 mm Bars, 4-8 mm Top Bars, 85 mm Stirrup Spacing	150	200	2000	12	4	10.00%	73.34%
Rodriguez et al. (1997), 4-12 mm Bars, 4-8 mm Top Bars, 85 mm Stirrup Spacing	150	200	2000	12	4	16.00%	74.12%
Rodriguez et al. (1997), 4-12 mm Bars, 4-8 mm Top Bars, 85 mm Stirrup Spacing	150	200	2000	12	4	14.00%	71.52%
Rodriguez et al. (1997), 4-12 mm Bars, 4-8 mm Top Bars, 85 mm Stirrup Spacing	150	200	2000	12	4	17.00%	52.54%
Cabrera 1996; Cabrera and Ghoddoussi (1992)	125	160	968	12	2		
Cabrera 1996; Cabrera and Ghoddoussi (1992)	125	160	968	12	2		